2012

Mechanisms That Ensure the Proper Terminal Structure of Mammalian Telomeres

Peng Wu

MECHANISMS THAT ENSURE THE PROPER TERMINAL STRUCTURE OF MAMMALIAN TELOMERES

A Thesis Presented to the Faculty of

The Rockefeller University

in Partial Fulfillment of the Requirements for

the degree of Doctor of Philosophy

by

Peng Wu

June 2012

MECHANISMS THAT ENSURE THE PROPER TERMINAL STRUCTURE OF MAMMALIAN TELOMERES

Peng Wu, Ph.D.

The Rockefeller University 2012

The telomeric single-stranded 3' overhang, a conserved feature at the ends of linear chromosomes, is thought to contribute to the important functions of end protection and telomere length homeostasis. Here, I investigated the mechanism by which the overhang is generated and maintained at mammalian telomeres.

First, I evaluated the terminal chromatin structure of mouse telomeres using conventional micrococcal nuclease (MNase) assays and a novel method to examine the terminal nucleosomes adjacent to the telomeric overhang. In wild type mouse embryonic fibroblasts (MEFs), the telomeric overhang was protected from MNase digestion of chromatin in nuclei. In addition, the induction of various DNA damage responses at telomeres, through the deletion of shelterin components, had no apparent effect on the chromatin organization of telomeres and did not cause overt eviction of nucleosomes from the telomere terminus.

Next, I identified a role for the shelterin-associated Apollo nuclease in generating the telomeric overhang at ends synthesized by leading-strand DNA replication. Deletion of Apollo in mouse cells resulted in an overhang defect specifically at leading-end telomeres. Consistent with a requirement for the overhang in end protection, cells lacking Apollo activated an ATM-dependent DNA damage response at a subset of

telomeres in S phase and displayed fusions between a fraction of leading-end telomeres on metaphase spreads.

I next elucidated the mechanism by which the single-stranded telomere binding protein, POT1b, suppresses the accumulation of excessive telomeric overhangs in mouse cells. I found that POT1b inhibits 5' resection by Apollo at telomeres synthesized by both leading- and lagging-strand DNA replication while promoting the telomeric function of the Ctc1/Stn1/Ten1 (CST) complex. Though the role of CST is not well understood, Ctc1 and Stn1 were originally identified as accessory factors of DNA polymerase α/primase and may contribute to fill-in synthesis of the telomeric C-rich strand.

Finally, to identify additional factors that contribute to overhang dynamics, I tested the hypothesis that the factors involved in 5' end resection at a DNA double strand break also act at telomeres in wild type cells. I uncovered a role for exonuclease 1 in a transient telomere end-processing step that occurs at both newly-synthesized telomeres. The Exo1-mediated telomere end-processing step does not appear to require Nbs1 or BLM, and its physiologic role remains unknown.

This thesis supports a model in which leading- and lagging-end telomeres have different requirements for end-processing by the nucleases Apollo and Exo1. The binding of POT1b on appropriately generated single-stranded overhangs at both newly-synthesized telomeres limits overhang size and prevents accelerated telomere shortening by inhibiting Apollo and facilitating the activities of the CST complex.

In memory of –

my dear friend, James "Super" Song,
for watching over me from the other side of York Avenue,

and my dear lao ye,
for watching over me from the other side of the world.

ACKNOWLEDGEMENTS

I extend my utmost gratitude to my advisor, Titia de Lange. I will always value the rare privilege of having been mentored by a scientist with her level of intellect, acumen, and insight. I appreciate the extensive time and genuine effort she has dedicated to expanding my knowledge, hastening my experimental successes, and improving my communication skills. From her, I have learned to approach scientific experimentation carefully yet without hesitation, to interpret data more thoroughly and critically, and to present ideas with better clarity and precision. Beyond her scientific expertise, I am also grateful for her support and generosity in the face of unforeseen setbacks.

I would next like to thank all the lab members I have encountered throughout the years for making this experience enjoyable and educational. Among those who have taught me, I especially thank Rich Wang for guiding me through my first summer rotation, Nadya Dimitrova for passing along her rigorous approach to protocols, Dirk Hockemeyer for his mice, cell lines, and ideas about POT1, and Agnel Sfeir for her tireless enthusiasm and engagement in scientific discussions. I am grateful for having had the opportunity to collaborate with Megan van Overbeek and Hiro Takai on exciting and fruitful projects. I am indebted to Devon White, since so much depends upon his skill and devotion in maintaining our mouse colony. I thank the research assistants and lab helpers for making life easier. I also appreciate knowledge, reagents, and food provided by lab members as well as the solidarity among the students, especially the current ones: Teresa Davoli, Shaheen Kabir, and Michal Zimmermann.

I owe particular gratitude to Woodring Wright and Jerry Shay for hosting me in their lab at UT Southwestern in Dallas, and to Yong Zhao for teaching me the technique of separating leading- and lagging-end telomeres using CsCl density gradient equilibrium centrifugation. I thank Svetlana Mazel and her team at the RU Flow Cytometry Resource Center for their assistance. Many investigators, too numerous to name here but who are acknowledged within the text of this thesis, have shared mice, cell lines, constructs, antibodies, as well as personal communications, which have aided in my research.

I would like to thank my committee members, David Allis, Fred Cross, and Tom Kelly, for their time and thoughtful discussions of my work throughout my graduate career. I also appreciate Lorraine Symington for agreeing to be the outside examiner at my thesis defense.

I give warm thanks to the Tri-Institutional MD-PhD program, led by Olaf Andersen, and in particular my classmates in the entering class of 2004 for their support throughout what will be quite a memorable decade of my life. I have also benefited from the assistance of the RU Dean's Office and the unique environment of this graduate program that upholds student autonomy.

With much love, I thank my father, Zhijun Wu, for always expecting me to exceed my potential, and my mother, Qiying (Ann) Fu, for always supporting my choices. I salute my brother, Kevin Wu, for somehow having grown up and for not following too closely in my footsteps.

A few special words go to Ragu Vijaykumar, for staying young, hungry, and foolish with me for many years past and more to come.

TABLE OF CONTENTS

LIST OF FIGURES

LIST OF TABLES

CHAPTER 1:

INTRODUCTION

PART I: THE STRUCTURE AND FUNCTION OF MAMMALIAN TELOMERES

Sequence and structural features of chromosome ends

Linear chromosomes terminate in specialized nucleoprotein structures called telomeres. In humans, telomeric sequences consist of duplex TTAGGG repeats[1-4] and end in a single-stranded 3' overhang that protrudes ~30-500 nt beyond the complementary strand[5-7]. Lower eukaryotes including yeast and ciliates have short telomeres of a few hundred base pairs[8-11], while telomere length in mammals ranges from an average of 10-15 kb in primates, whales, and many large animals to 20-50 kb in rodents, rabbits, and bats (Table 1.1)[4,12,13].

Table 1.1. Sequence features of telomeres in different organisms.

Organism	Repeat sequence (5'-3' G-rich strand)	Telomere length	Overhang length
Oxytricha nova	TTTTGGGG	20 bp	16 nt
Euplotes aediculatus	TTTTGGGG	28 bp	14 nt
Tetrahymena	TTGGGG	250-300 bp	14-15 or 20-21 nt
S. cerevisiae	TG_{1-3}	~ 350 bp	~ 14 nt (G1) ~ 50 nt (S phase)
S. pombe	$GGTTACA_{0-1}C_{0-1}G_{0-6}$	~ 300 bp	n.d. (< 50 nt ?)
M. musculus	TTAGGG	20-50 kb	n.d.
H. sapiens	TTAGGG	2-10 kb	30-600 nt

Electron microscopy has revealed the presence of structures known as t-loops at telomeres in a number of vertebrates, including human, mouse, and chicken[14,15]. T-loops of heterogeneous size distribution form by strand invasion of the single-stranded telomeric overhang into the double-stranded telomeric repeats. In support of this model, incubation of *E. coli* single-stranded binding (SSB) protein with isolated telomeric DNA results in the detection of one to two SSB molecules bound to the displaced single-

stranded telomeric DNA (D-loop) at the base of the t-loop[14]. Importantly, telomeric 3' overhangs are required for *in vitro* t-loop formation[16].

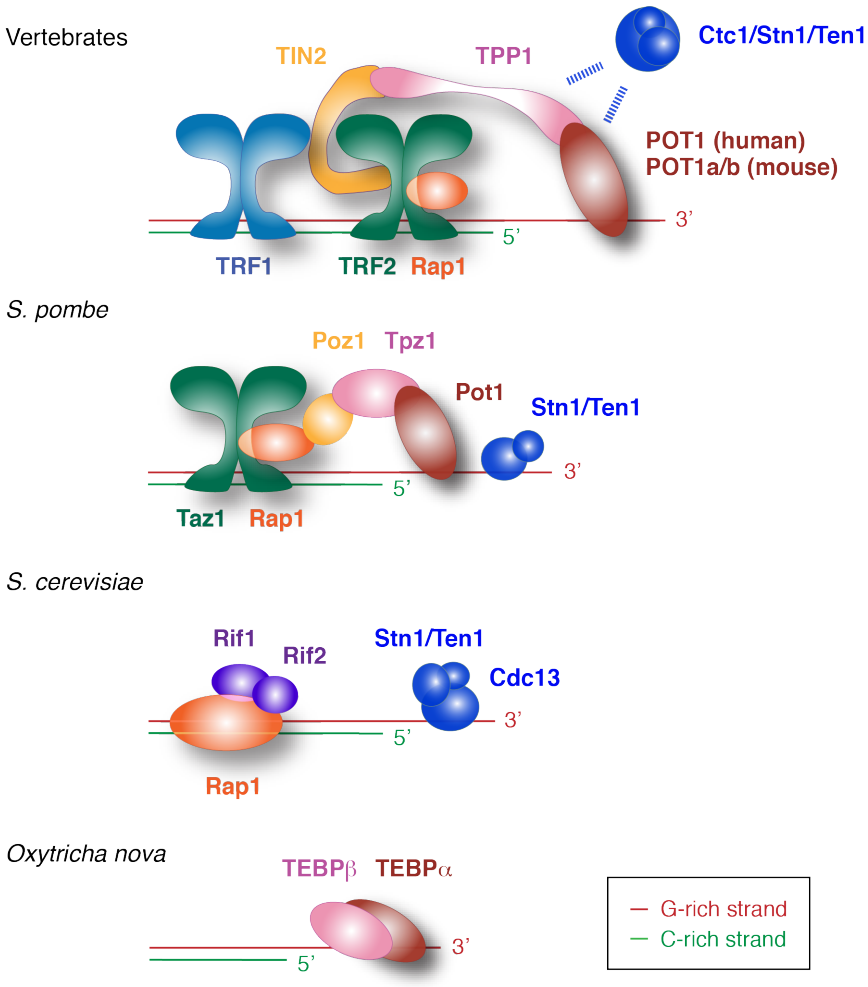

Figure 1.1. Telomere binding proteins. Telomeric complexes in vertebrates, yeast, and ciliates consist of duplex DNA binding proteins and single-stranded end binding proteins that are, in some organisms, connected through additional linking proteins. (adapted from ref. [28]).

The composition of telomeric protein complexes as well as the structure and function of individual telomere binding proteins exhibit considerable divergence across species (Figure 1.1). In mammalian cells, six proteins comprise the telomeric complex known as shelterin: TRF1, TRF2, Rap1, TIN2, TPP1, and POT1 (POT1a and b in rodents, Figure 1.2, reviewed in [17]). Among the members of shelterin, TRF1, TRF2, and

POT1 directly contact telomeric DNA. TRF1 and TRF2 are ubiquitously expressed, abundant, duplex telomeric binding proteins containing C-terminal Myb/SANT domains that recognize the half site 5'-YTAGGGTTR-3'[18-22]. The two proteins have similar homodimerization (TRFH) domains while differing in their N-termini, which is acidic in TRF1 and comprised of a basic glycine-arginine rich (GAR) domain in TRF2[23]. TRF2 has the ability to induce t-loop formation in model telomeric substrates *in vitro*[16]. A conserved region in TRF2 not present in TRF1, spanning amino acids 284 to 297 of the mouse protein, recruits Rap1 to telomeres[24] (Figure 1.2). This interaction between TRF2 and the RCT domain of Rap1 is required for the stability of the Rap1 protein[24,25]. TRF1 and TRF2/Rap1 have been reported to localize to chromosome internal sites containing telomeric sequences[26,27], though their functions at such sites are not well understood.

POT1 localizes to telomeres through its interaction with TPP1[29-31] and binds single-stranded telomeric DNA with its N-terminal oligonucleotide/oligosaccharide binding (OB) folds[32-34] (Figure 1.2). *In vitro*, POT1 can bind both internally and terminally placed telomeric repeats; its minimal binding site is the (TAGGGTTAG) nonamer while binding optimally to two telomeric repeats[34]. The *in vitro* binding of POT1 to single-stranded oligonucleotides shows some preference for the 3' end, which is modified when POT1 is in complex with TPP1[35]. Nonetheless, *in vivo*, POT1 is predicted to bind both the terminal overhang as well as the displaced D-loop that forms at the base of the t-loop. TPP1/POT1 complexes are less abundant than duplex DNA-binding shelterin components, but expected to be in excess of their single-stranded substrate[36]. Mouse POT1a and -b share approximately 70% sequence similarity with each other and

with human POT1[37,38] and have similar binding affinities for single-stranded telomeric DNA[39].

Finally, TIN2 bridges the entire shelterin complex through interactions with TRF1, TRF2, and TPP1 (Figure 1.2)[31,40-43]. TIN2 can simultaneously interact with the TRFH domain of TRF1 and a region in TRF2 just C-terminal of the Rap1-binding domain (Figure 1.2)[40,44,45]. TIN2 also interacts with the C-terminus of TPP1[31,41,45]. The entire six-subunit shelterin complex as well as subcomplexes containing TRF2/Rap1, TIN2, and TPP1/POT1 but not TRF1 have been isolated from HeLa cells, but the *in vivo* significance of shelterin subcomplexes has not been determined[40].

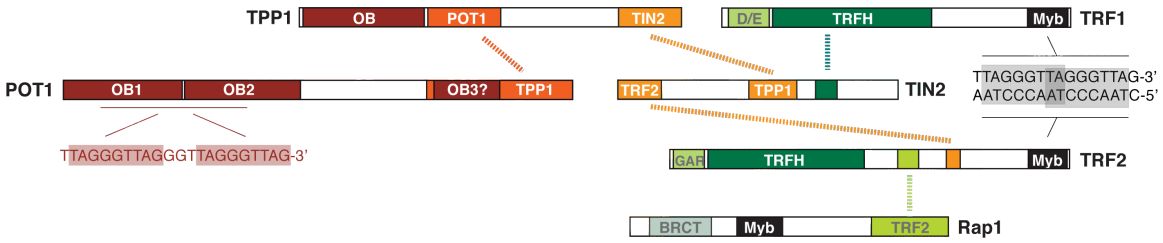

Figure 1.2. Interactions between the components of human shelterin. The domain organizations of the six shelterin components, and their interactions with each other and with DNA. (adapted from [28]).

The core components of shelterin also interact with a number of accessory factors that perform diverse functions at telomeres. TRF1-interacting factors include tankyrase 1[46], BLM[47], Ku[48], and PinX1[44] while TRF2 interacts with Nbs1[49], ERCC1/XPF[50], Apollo/SNM1b[51-53], Fen1[54]), and Mus81[55], among others. In contrast to shelterin, these accessory factors are not found at all telomeres, their localization to telomeres can be transient, and they generally have non-telomeric functions. Structural studies of interactions between peptides of TRF1 and TIN2 and between peptides of TRF2 and Apollo have led to the proposal that a common docking site in the TRFH domains of

TRF1 and TRF2 can interact with a F/YxLxP motif found in a number of binding partners[44].

In addition to binding shelterin and being organized in t-loops, mammalian telomeres are nucleosomal[12,56,57], in contrast to the telomeres of yeast and ciliates[58-60]. In mammalian cells, telomeric chromatin resembles bulk chromatin in its composition, consisting of the canonical core histone components, but the nucleosomal repeat length is short, and the nucleosomal core particle shows hypersensitivity to MNase[12,56,57]. In addition, telomeric chromatin is enriched for heterochromatic marks, such as trimethylation of H3K9 and H4K20, and the results of studies in mice have shown that the loss of such marks correlates with abnormally elongated telomeres[61-63]. Short human telomeres show evidence of an unusual chromatin structure, as deduced from the more diffuse nature of micrococcal nuclease (MNase) digestion patterns[57], but the molecular basis of this change is not known.

Mechanisms of telomere length maintenance

The end-replication problem

Telomeres across species have evolved to solve two major problems that threaten the viability of cells with linear chromosomes: the end-replication problem and the end-protection problem. The former, recognized by Watson[64] and Olovnikov[65], refers to the inability to completely duplicate linear DNA, a problem intrinsic to DNA replication due to the 5' to 3' directionality of DNA polymerases and their requirement for a 3' OH provided by an RNA primer. The biochemical requirements for eukaryotic replication were deduced from *in vitro* experiments reconstituting replication on DNA containing a

simian virus 40 (SV40) origin of replication[66-69], which depends on cellular factors as well as the viral SV40 T antigen[70-72]. In this system, the initiation of DNA synthesis requires the four-subunit DNA polymerase α/primase complex, replication protein A (RPA), and SV40 T antigen[71,73]. With regards to the end-replication problem, both the inability of DNA polymerase α/primase to initiate DNA synthesis starting from the very end of a template and the removal of the terminal RNA primer would be expected to result in the loss of sequence information.

An *in vitro* reconstitution system using SV40 T antigen and human 293T cellular extracts to replicate linear DNA containing an SV40 origin of replication has further corroborated the existence of the end-replication problem[74]. Though SV40-based replication is most efficient on circular templates[67], this system was optimized for linear DNA and was used to show that leading-strand DNA synthesis can proceed to the ends, leaving blunt duplex termini[74]. On the other hand, lagging-strand DNA synthesis was unable to replicate an average of 200 nt of the terminal DNA and left 3' overhangs as predicted by the end-replication problem[74]. This was shown for linear DNA containing either telomeric or nontelomeric sequences at their termini, though this system could not address the contribution of additional factors at telomeres *in vivo* that could affect the ability for leading or lagging strand replication to proceed to chromosome ends.

The recognition that most telomeres end in a single-stranded overhang extended the end-replication problem to chromosome ends synthesized by leading strand replication. Continuous leading-strand synthesis to the end of a linear chromosome would result in either a blunt end or, if the template is not copied entirely, a recessed 3' end. The presence of a 3' overhang at telomeres predicted the existence of helicases and

nucleases that would resect the template strand of leading-end telomeres, causing newly synthesized leading-ends to shorten with every round of replication[75].

Telomerase

In most eukaryotic organisms, the end-replication problem is solved by the telomerase ribonucleoprotein, which uses its RNA component, TERC/TR, to template the synthesis of telomeric G-rich sequences by the catalytic reverse transcriptase subunit, TERT. Exceptions to telomerase-dependent telomere maintenance include a retrotransposon-based mechanism used by *Drosophila melanogaster*[76-78] and the Alternative Lengthening of Telomeres (ALT) pathway employed by telomerase-negative cancer cells comprising ~10% of all classified cancers[79]. ALT has been proposed to involve recombination-based mechanisms but the details have not been elucidated[80].

A terminal transferase-like activity that extends the ends of chromosomes was predicted based on the finding that linearized plasmids containing the *Tetrahymena* telomeric sequence could be maintained in yeast through the addition of repetitive G-rich sequences[11,81]. The responsible enzymatic activity was isolated from *Tetrahymena* and attributed to a ribonucleoprotein, named telomerase[82,83]. The RNA component was cloned and introduction of mutant alleles into the macronuclei of *T. thermophila* resulted in the addition of mutant telomeric sequences to chromosome ends, defects in cell division, and morphological abnormalities associated with senescence[84,85]. The importance of the telomerase RNA component extends across species; its deletion in mouse results in the loss of 5 kb of telomeric sequence in every generation that results in compromised organ function and organismal viability after 4-5 generations[86].

A genetic screen for *S. cerevisiae* mutants unable to add telomeric repeats to linearized plasmids allowed the further identification of genes important for telomerase activity and supported the hypothesis that telomere shortening during successive cell divisions ultimately compromises cell viability[87]. Years later, the catalytic subunit of telomerase was purified from *Euplotes aediculatus* and found to contain a reverse transcriptase domain[88]. Sequence analyses revealed homology with the *S. cerevisiae* Est2 gene, which had previously been implicated in telomere function through genetic analysis of telomere maintenance mutants[89] and was now identified to encode the catalytic subunit of telomerase[88,90,91].

Assembly of a catalytically active telomerase holoenzyme in human cells requires several steps involving distinct nuclear compartments. TERT, TERC, and dyskerin comprise the major components of the telomerase holoenzyme isolated from human cells[92], though a number of additional telomerase-associated factors have been identified in recent years. The trafficking of telomerase through nuclear structures known as Cajal bodies is thought to be important for complex assembly and potentially for the recruitment of telomerase to telomeres. Cajal bodies have been described as important sites for post-transcriptional RNA modification and biogenesis of RNPs. Telomerase RNA co-localizes with Cajal bodies throughout the cell cycle[93]. Dyskerin, in complex with NHP2, NOP10, and GAR1, binds the H/ACA domain of telomerase RNA, also found in small nucleolar RNAs (snoRNAs) and small Cajal body RNAs (scaRNAs). Mutations in TERC-binding proteins compromise RNA stability and RNP assembly. In addition, the ATPases pontin and reptin interact with TERT and dyskerin during S phase and facilitate telomerase RNP accumulation in human cells[94]. A newly identified

member of the telomerase complex, TCAB1, appears to be required for the accumulation of TERC in Cajal bodies and affects telomere elongation *in vivo* without affecting telomerase activity[95]. How the trafficking of catalytically active telomerase RNP through Cajal bodies contributes to its action at telomeres remains to be determined.

The regulation of telomerase expression and its mode of action vary depending on the organism. In humans, telomerase activity has been demonstrated in the germline, primary tumor samples, and cancer cell lines but is suppressed in somatic tissues[96]. In contrast, primary cells from rodents and other small mammals show constitutive telomerase activity and correspondingly longer telomeres, suggesting that the regulation of cellular lifespan by telomere shortening might not apply for these small animals[13]. Whereas yeast telomerase acts in G2[97,98] and preferentially elongates the shortest telomeres in a cell[99,100], telomerase in human cancer cells appears to act indiscriminately at most chromosome ends immediately following their synthesis in mid-S phase[101].

In addition to the synthesis of G-rich repeats by telomerase, telomere maintenance also requires coordinated synthesis of the C-rich strand. In ciliates and budding yeast, C-strand synthesis is coupled to the action of telomerase and involves lagging-strand DNA polymerases[97,102,103]. On the other hand, in human cells where telomerase acts throughout S phase, fill-in synthesis does not occur until late in G2 through incremental steps distinct from the conventional process of lagging strand DNA replication[101].

In the absence of telomerase, human cells lacking telomerase undergo terminal sequence loss at a rate of 50 bp per end per cell division[104]. While most mouse cells constitutively express telomerase, primary *Mus spretus* cells lacking detectable telomerase activity lose 75 bp per end per cell division[105], which is consistent with the

rate of telomere shortening observed in successive generations of *Mus musculus* deficient for telomerase RNA[86]. Mammals and other vertebrates exhibit faster telomere shortening than yeast, which lose only 3-5 bp/end/cell division in the absence of telomerase[87,89].

Telomere length regulation

In cells that express telomerase, proteins that bind the telomeric duplex array act as a counting mechanism to inhibit telomerase in *cis* as telomeres become long. The basis for this model came from studies in *S. cerevisiae* showing that the extent of telomerase-mediated repeat addition to an induced short telomeric seed sequence was limited by the insertion of Rap1-binding sites[106]. In human cells, shelterin components negatively regulate telomere elongation (Figure 1.3). When wild type TRF1 is overexpressed in the human telomerase-positive HT1080 cancer cell line, telomeres progressively shorten at a rate of 3 to 11 bp per population doubling while telomerase activity is unaffected[107]. Conversely, expression of a dominant negative truncated form of TRF1 results in telomere elongation[107]. The information about telomere length conveyed by TRF1 bound to duplex repeats is transduced to the telomere terminus by POT1. A dominant negative allele of POT1 lacking its OB fold can still localize to telomeres, presumably through its interaction with TPP1, but results in telomere elongation when introduced into telomerase-positive human cells[108]. Consistent with their role in mediating POT1 recruitment to telomeres, TIN2 and TPP1 have also been implicated in the *cis*-inhibition of telomerase[30,31,42,109]. To date, no component of mouse shelterin has been assigned a role in the negative regulation of telomerase.

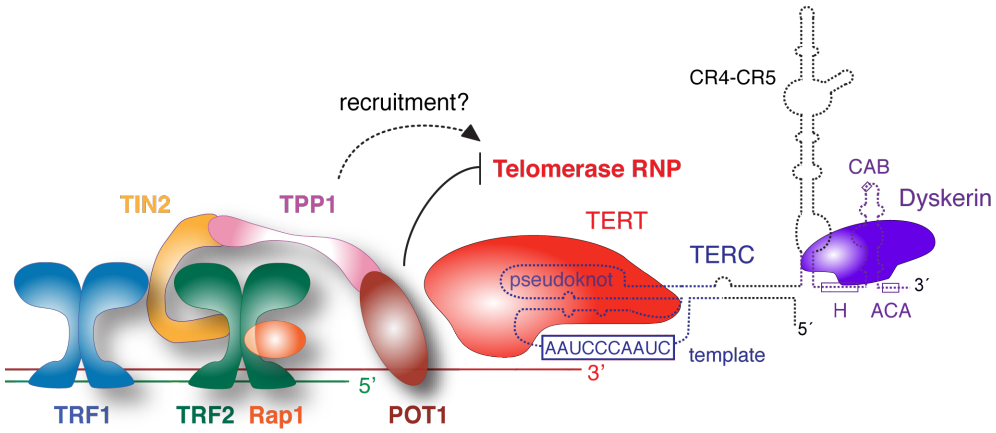

Figure 1.3. Human telomerase and its regulation by shelterin. The main components of the human telomerase ribonucleoprotein are shown in association with the 3' terminus of the telomeric overhang. Shelterin negatively regulates TERT through POT1 binding of the terminal overhang, while TPP1 has been proposed to recruit telomerase and increase its processivity. (adapted from [28])

The estimated number of telomerase molecules in a single human cell does not substantially exceed the number of telomeres[92], suggesting that telomerase must be recruited to its site of action. In yeast, two pathways dependent on Ku and Cdc13 regulate the accumulation of Est2p at telomeres. Chromatin immunoprecipitation has shown a bimodal association of Est2p with telomeres in late G1/early S and again in late S/G2 when telomere elongation occurs[110]. Ku interacts with the telomerase RNA component TLC and promotes the association of telomerase at telomeres in late G1/late S[111,112]. The second phase of telomerase association at telomeres involves the single-stranded telomere binding protein Cdc13p. Est1p connects Cdc13 to Est2 by interacting with both proteins; fusing Cdc13 directly to Est2 bypasses the requirement for Est1p in telomerase recruitment[113].

Telomerase recruitment in mammalian cells is less well characterized. While POT1 negatively regulates telomerase *in vivo*, *in vitro* studies have suggested that TPP1, in complex with POT1, can interact with telomerase, enhance its processivity, and facilitate telomere elongation[35,114]. The interaction between TPP1 and telomerase requires

its OB fold[114]. Several studies have attributed TPP1 to the recruitment of telomerase *in vivo*[115,116], but it has so far been difficult to dissociate the role of TPP1 in telomerase recruitment from its function in end protection. Expression of a TPP1 mutant lacking its OB fold impairs telomerase recruitment in human cells but is also unable to suppress the telomere dysfunction phenotypes associated with TPP1 depletion[115]. In addition, the low abundance of telomerase makes it difficult to detect endogenous TERT. So far, immunofluorescence for TERT and FISH for TERC have been the only methods used to evaluate the recruitment of endogenous telomerase in human cells[117,118].

Telomere length homeostasis in physiological settings depends not only on the recruitment and modulation of telomerase activity but also on the regulation of processing events that occur during telomere replication. In theory, the rate of telomere shortening in the absence of telomerase depends on the balance between telomeric C-strand synthesis and nucleolytic degradation of telomeres (at leading-ends), processes that are not well-characterized but likely to be regulated. Telomere maintenance also requires the suppression of aberrant processes that can drastically alter telomere length. In cases of telomere dysfunction, discussed in the next section, aberrant telomere recombination or nucleolytic degradation might be predicted to induce rapid telomere shortening.

Mechanisms of chromosome end-protection

The end-protection problem

The end-protection problem refers to the ability for natural chromosome ends to be distinguished from sites of DNA damage. Nearly 80 years ago, McClintock

recognized that broken chromosome ends were unstable, prone to fusion and breakage cycles[119], while the analysis of chromosome rearrangements occurring in *Drosophila* after X-ray irradiation revealed the absence of chromosomes with terminal deletions[120]. Natural chromosome ends were thus proposed to possess specific features that protect them from behaving like broken chromosome ends, and the term "telomere" was coined, from the Greek "telos" for "end" and "meros" for "part"[120]. While many features of telomeres could in principle predispose them to being recognized as sites of DNA damage, the end-protection problem as it is now defined primarily concerns the ability for telomeres to evade detection as a DNA double strand break. The methods used by different organisms to solve the end protection problem are likely to reflect the DNA damage response pathways to which chromosome ends are vulnerable in different species.

The mammalian DNA damage response

The cellular response to a DSB generally involves the activation of cell cycle checkpoints and repair of the break through pathways that differ depending on the context of the damage (reviewed in [121,122]). In mammalian cells, DNA damage in different phases of the cell cycle activate the G1/S, intra-S, or G2/M checkpoints, which promote cell cycle arrest through the ATR (ataxia telangiectasia and Rad3 related) and ATM (ataxia telangiectasia mutated) kinase pathways. An additional replication checkpoint refers to the mechanism that prevents premature mitotic entry when DNA replication is slowed or stalled.

Activation of the ATM and/or ATR kinases results in a rapid response mediated by post-translational protein modifications and a slow transcription-dependent maintenance of cell cycle arrest. The rapid signaling cascade initiated by ATM and/or ATR results in the activation of the transducing kinases, Chk1and/or Chk2, which in turn phosphorylate Cdc25 phosphatases and target them for ubiquitin-mediated degradation123-128. Cdc25 phosphatases activate different cyclin/Cdk complexes that promote cell cycle progression. When ATM is activated in G1 or S phase, degradation of Cdc25A leads to the accumulation of inactive phosphorylated Cdk2 in complex with cyclin E or A[129]; the resultant inability for Cdk2 to activate Cdc45 blocks the firing of replication origins[130,131]. Rapid proteolysis of cyclin D1 upon DNA damage has also been reported to contribute to the inhibition of Cdk2, which mediates G1 arrest[132]. Meanwhile, the slower transcription-mediated response to DNA damage involves phosphorylation of p53 by ATM/ATR and Chk1/Chk2[133-136], which promotes transcription of the CDK inhibitor p21[137]. The binding of p21 to cyclin-Cdk2 and -Cdk4 complexes prevents the phosphorylation of Rb, thus inhibiting the transcription of S-phase genes[138,139]. Finally, the activation of ATM and/or ATR in G2 results in the degradation of Cdc25 and upregulation of Wee1, which together cause the accumulation of inactive cyclin B/Cdc2 complexes that are unable to promote mitotic entry[123,125].

One mode by which natural chromosome ends could prevent the activation of cell cycle checkpoints is to evade initial sensing by the DNA damage machinery. Activation of the ATM kinase pathway requires the Mre11/Rad50/Nbs1 sensor complex[140-142]. Structurally, the MRN complex consists of a globular domain that contacts DNA and an extended coiled-coil formed by Rad50, which also contains a conserved hook domain

thought to mediate dimerization[143,144]. Mre11 dimers bind DNA and facilitate the bridging of two ends[145], while Nbs1 regulates both the DNA-binding and nuclease activities of Mre11[146]. Nbs1 contains adjacent FHA and BRCT domains that interact with other DNA damage factors[146,147]. All three components of MRN are essential in mice while hypomorphic mutants exhibit a range of cellular phenotypes including S/G2 cell cycle checkpoint defects, reduced ATM activity, and chromosome instability (reviewed in [148]).

The ATR kinase pathway is activated by the cooperative binding of RPA to long stretches of exposed single-stranded DNA, which promotes the recruitment of ATRIP[149]. Interactions between TopBP1 and ATRIP as well as the clamp loader Rad17 and the Rad9/Hus1/Rad1 (9-1-1) clamp at the 5' end of the single stranded DNA promote ATR activation and the subsequent phosphorylation of downstream targets[150-155]

The signaling cascade initiated by activated ATM and/or ATR involves the recruitment and post-translation modification of a number of DNA damage factors. These include the MRN complex[156,157], the histone variant H2A.X[158,159], 53BP1[160], and MDC1[161-163] which localize to DSBs induced by IR and spread to cover several hundred kilobases surrounding the site[164], forming large foci detectable by immunofluorescence. The interplay between kinases, ubiquitin ligases, and deubiquitinating enzymes that alter the binding and signaling capabilities of various DNA damage factors is thought to modulate the response[165-171].

The two major pathways that repair a DNA double strand break are non-homologous end joining and homology directed repair. The non-homologous end joining pathway is an error-prone mechanism of repairing DSBs that has been most extensively

studied in the context of V(D)J recombination during immune cell maturation. Factors involved in classical non-homologous end-joining include the end-binding factor Ku70/86[172,173], Artemis[174], DNA-PKcs[175], and DNA ligase IV/XRCC4[176-178]. In the absence of Ku70/86 or DNA ligase IV, alternative end joining pathways can mediate repair in various contexts[179-181]. These pathways appear to utilize alternate ligases and end-binding factors, though many details remain unclear.

In contrast to nonhomologous end joining, the more accurate homology directed repair pathway occurs during S/G2 phase in the presence of a homologous sister chromatid. Homology directed repair is initiated by extensive 5' resection exposing long single-stranded DNA ends that are coated by Rad51 filaments in a BRCA2-dependent process[182-184]. The ensuing sequence of events involve strand invasion into the homologous duplex region, second end capture and DNA synthesis, and ultimately dissolution or resolution of Holliday junction intermediates. Additional genetic requirements for efficient HDR in mammalian cells include BRCA1, Rad54[185,186]. The mechanisms by which nucleases mediate initial 5' resection and final HJ resolution will be discussed in more detail in a later section.

End protection by shelterin

The role of shelterin in suppressing DNA damage signaling and aberrant repair events at mammalian telomeres has been revealed by conditional gene deletion in mice (Figure 1.4). Of the shelterin components, only Rap1 and POT1b are non-essential for mouse embryogenesis, though their deletion still gives rise to pathological outcomes[24,37,187].

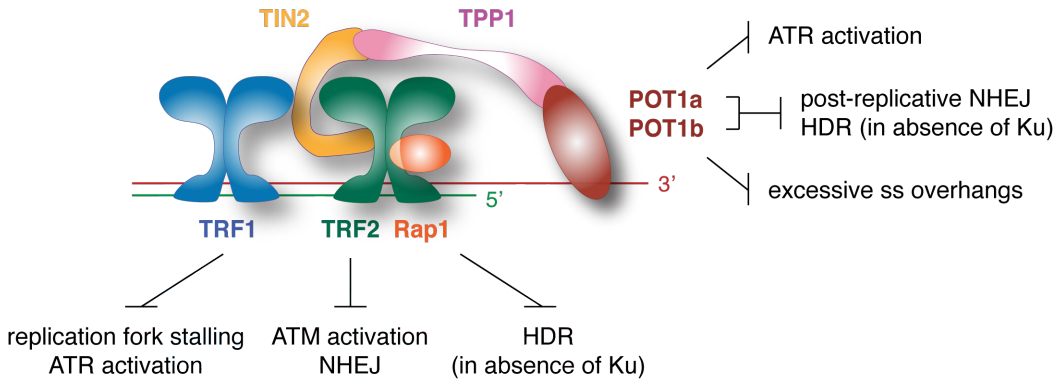

Figure 1.4. End protection by shelterin. Functions of mouse shelterin components deduced from conditional deletion of individual genes. TPP1 deficiency phenocopies the deletion of both POT1a and POT1b[188], while TIN2 deletion results in a range of phenotypes including activation of both ATM and ATR and phenotypes associated with POT1a/b deletion[189]. It has not been ruled out that TPP1 and TIN2 can directly regulate aspects of the DNA damage response.

Repression of the ATM kinase is mediated by TRF2[190]. Inhibition of TRF2 by the introduction of dominant negative alleles in human cells or conditional gene deletion in mouse embryonic fibroblasts activates an ATM-dependent DNA damage response[190,191]. Early events in this response include the localization of DNA damage factors such as 53BP1 and γ-H2AX to telomeres, forming telomere-dysfunction induced foci (TIFs) at a majority of telomeres in nearly all cells[192,193]. Activated ATM phosphorylates Chk2 and p53, resulting in transcriptional upregulation of p21, and apoptosis or cell cycle arrest[191]. Both the formation of TIFs and the phosphorylation of downstream effectors depend on Nbs1, consistent with the proposed role of the MRN complex as the sensor that activates ATM[194,195]. Other DNA damage response factors, such as MDC1 and H2AX, also contribute to robust formation of TIFs at telomeres lacking TRF2, but are not absolutely required to activate ATM and execute the checkpoint[194,196]. Removal of TRF2 from telomeres in any phase of the cell cycle results in similar DNA damage responses[197].

In addition to activating an ATM-dependent DNA damage signal, telomeres lacking TRF2 engage in fusions that depend on Ku and Ligase IV (as well as the

XPF/ERCC1 in human but not mouse cells)[193,198]. In cells lacking TRF2, telomeric NHEJ occurs primarily in G1 phase, while NHEJ of telomeres in S phase is repressed by a Cdk-dependent mechanism[197]. ATM signaling is required for NHEJ of deprotected telomeres in G1[194], while factors that are not required for ATM signaling nevertheless contribute to NHEJ. Depletion of MDC1 or deletion of 53BP1 in the context of TRF2 deficiency respectively slow or abolish telomere fusions despite little effect on ATM activation or downstream phosphorylation events[196,199]. 53BP1 increases the chromatin mobility of deprotected telomeres[199]. Whereas 53BP1 deficiency does not affect V(D)J recombination involving NHEJ between ends in close physical proximity[200,201], the requirement for 53BP1 to promote fusions of deprotected telomeres[199] and of distant ends in V(D)J recombination and class switch recombination[202,203] led to the proposal that 53BP1-mediated chromatin mobility becomes critical specifically between ends separated by a significant distance.

One proposed model to explain the suppression of ATM and NHEJ by TRF2 is that t-loop formation promoted by TRF2 prevents the loading of Ku and MRN on DNA ends in G1[194]. Interestingly, co-deletion of TRF2 and Nbs1 repressed chromosome fusions in G1 but resulted in the appearance of a low level of chromatid-type fusions on metaphase spreads, between telomeres synthesized by leading strand DNA replication[194,195]. In the absence of Nbs1-mediated DNA damage signaling, TRF2 deletion still induces significant overhang loss, even though telomeric NHEJ events are infrequent and limited to leading-end telomeres[194]. These observations led to the proposal that TRF2 recruits or activates a nuclease that generates the 3' overhang at leading end telomeres. In the absence of TRF2, the MRN/ATM pathway promotes resection at the

unprotected ends, thereby providing an alternative means of generating overhangs at the leading-end telomeres. Consistent with this proposal, the fusion of leading-end telomeres is a highly specific phenotype associated with TRF2 deletion or depletion from MRN- or ATM-deficient cells[194,195,204]. In this model, suppression of telomere NHEJ in S/G2 requires the presence of telomeric overhangs, which are presumably constitutive at chromosome ends synthesized by lagging strand DNA replication while leading-ends require processing by either TRF2-associated or MRN-dependent nucleases.

In addition to suppressing DNA damage signaling and NHEJ at telomeres, TRF2 also has a role in preventing aberrant homology directed repair. The N-terminal GAR domain of TRF2 can stabilize Holliday junctions *in vitro*[205,206], and human cells expressing a dominant negative form of TRF2 lacking this basic region undergo aberrant t-loop HDR whereby the HJ at the base of the t-loop is resolved, generating an extrachromosomal telomeric circle[207]. Such extrachromosomal telomeric circles have been detected in human ALT cell lines that presumably maintain telomeres through recombination[208]. In addition, TRF2 stabilizes and recruits its binding partner Rap1 to telomeres, where Rap1 and Ku act in parallel to repress telomeric sister chromatid exchanges (T-SCEs), an indication of elevated HR at telomeres[24,26,198]. The mechanism by which Rap1 represses homology directed repair remains to be elucidated.

While TRF2 suppresses ATM signaling at telomeres, POT1 suppresses ATR[190,209]. Depletion of POT1 by shRNA in human cells results in a transient telomere damage response[210,211]. Deletion of POT1a and POT1b in mouse cells leads to ATR-dependent TIF formation and phosphorylation of the Chk1 kinase as well as the accumulation of extensive single-stranded telomeric overhangs[37,38,190]. The DNA damage response is

abolished by the re-introduction of POT1a but not POT1b[37]. On the other hand, POT1b, but not POT1a, represses excessive overhang formation[37], a function that will be discussed in the next section, which focuses on the regulation of terminal telomere structure. The DNA damage response induced by POT1a/b deletion results in endoreduplication, whereby a long G2 phase is followed by re-entry into a second replication cycle without an intervening mitosis[37,212]. Telomeres lacking POT1a and –b also engage in sister telomere fusions, suggesting a role for the POT1 proteins in suppressing postreplicative end joining events[37]. Finally, co-deletion of POT1a/b and Ku results in a low level of T-SCEs, suggesting that the POT1 proteins also repress homology directed repair at telomeres[39].

POT1a has been proposed to repress ATR activation by excluding RPA from telomeres[190,213], despite evidence that RPA is more abundant than POT1a/b, and the *in vitro* binding affinities of POT1a, POT1b, and RPA for telomeric substrates are similar[39]. The observation that TIN2 deletion results in similar phenotypes as the loss of POT1a/b has led to the proposal that RPA exclusion is achieved through the tethering of TPP1/POT1 to telomeres by TIN2[189]. An alternative model has invoked a role for the recently discovered transcribed telomeric RNAs (TERRA) in promoting the ability for POT1 to exclude RPA[214].

More recently, shelterin has been implicated in solving a problem not directly associated with end protection *per se* but rather with the semi-conservative replication of telomeric repeats. When challenged with low levels of the DNA polymerase inhibitor aphidicolin, telomeres behave similarly to common fragile sites elsewhere in the genome and become susceptible to fork stalling and chromosome decondensation and/or

breakage[215,216]. Deletion of the shelterin factor TRF1 greatly exacerbates the appearance of fragile telomeres and TRF1-associated helicases, such as BLM, have been proposed to stabilize aberrant G-quadruplex structures that could arise during replication, thereby facilitating fork progression through telomeric repeats[215,216]. The fragile telomere phenotype has now been observed in a number of settings, though its repression may slightly differ in human and mouse cells. A role for TRF2/Apollo in facilitating the replication of telomeric repeats has been described in human cells whereas gene deletion in mouse cells has revealed no such role[217]. This may be attributed to mechanistic differences in the recovery from replication fork stalling in mouse and human cells, since human cells appear to be more sensitive to drug treatments that stall forks. Following treatment with a prolonged (24 hour) pulse of hydroxyurea, mouse embryonic cells are able to restart replication while similarly treated human cells exhibit inefficient recovery[218,219].

Consequences of telomere shortening

Replicative senescence

Human fibroblasts have a finite lifespan in culture[220]. After ~50 population doublings, cells enter a state of replicative senescence characterized by growth arrest in G1, changes in cell morphology, positive β-galactosidase staining[221], and other alterations in gene expression. The discovery that introducing telomerase into normal human epithelial cells and fibroblasts can indefinitely extend their *in vitro* lifespan established the contribution of telomere shortening to replicative senescence[222].

The *in vitro* growth behavior of cultured human fibroblasts has been described as a two-stage process[223]. When telomerase-deficient normal human fibroblasts arrest at the G1/S transition after a fixed number of population doublings (senescence, also known as M1 stage), inactivation of both p53 and Rb by the introduction of SV40-LT allows the cells to bypass arrest and proliferate for ~20 additional PDs[223,224]. Nevertheless, these cells enter a stage known as crisis (M2) during which the rate of cell division balances that of cell death. Immortalized cells that emerge from crisis have either reactivated telomerase or an alternative lengthening of telomeres (ALT) pathway but display marked cytogenetic abnormalities and aneuploidy that presumably confer transformation potential[225].

Telomere dysfunction and cancer

Depending on the context, telomere shortening can either act in a tumor suppressive capacity or promote cancer development by increasing genome instability. Progressive telomere shortening is predicted to limit the proliferative capacity of hyperplastic cells *in vivo* by the activation of cell cycle checkpoints in response to telomere dysfunction. Indeed, the inactivation of telomerase has been shown to impair tumorigenesis in several mouse models of cancer[226,227].

However, telomere dysfunction can promote genome instability by instigating breakage-fusion-bridge cycles that generate extensive chromosome rearrangements or by inducing endoreduplication that results in an unstable polyploid state. In fact, mice null for the telomerase RNA component show an increased incidence of spontaneous tumors in later generations, which has been linked to the increasing appearance of chromosome

fusions and aneuploidy[228]. In p53-deficient mice with a high incidence of lymphomas, loss of telomerase increases the rate of tumorigenesis and shifts the tumor spectrum to epithelial carcinomas that have more commonly been attributed to aging in humans[229,230].

Evidence of telomere dysfunction and fusions during the progression of human cancer has been demonstrated for chronic lymphocytic leukemia[231]. Measuring the telomere length distribution of the XpYp telomere in different CLL patients showed that shorter telomeres correlated with poorer prognoses, with patients in stage A, B, and C of disease having respective mean telomere lengths of 5, 3.5, and 2 kb[231]. PCR-based assays to detect specific fusion events between the XpYp and 17p telomeres demonstrated a high fusion rate in patients, especially those with poor prognosis disease, compared to control subjects[231]. The telomere dysfunction observed *in vivo* was suggested to be a driving factor in genome instability and clonal evolution of advanced disease.

Inherited disorders of telomere dysfunction

A number of inherited disorders exemplify the consequences of telomere dysfunction in humans[232]. The most well-studied is dyskeratosis congenita, a rare syndrome characterized by skin and mucous membrane abnormalities including hyperpigmentation, nail dystrophy, and leukoplakia[233]. Patients with this disease succumb to bone marrow failure and exhibit predisposition for certain cancers. Genetic anticipation, whereby the disease manifests at a younger age in later generations, reflects progressive telomere shortening in the germline. Autosomal recessive, X-linked, and autosomal dominant forms of the disease have been identified and attributed to mutations in various components of the telomerase RNP, including TERT[234,235], TERC[236],

dyskerin[237,238], Nop10[239], Nhp2[240], as well as the shelterin protein, TIN2[241,242]. Recently, a patient with a severe form of DC known as Hoyeraal-Hreidarsson syndrome was found to express a splice variant of the telomere-associated Apollo nuclease that abolishes its ability to function at telomeres, though the disease-causing mutation was not identified[243]. In addition to DC, familial forms of idiopathic pulmonary fibrosis[244] and aplastic anemia[245,246] have also been attributed to mutations in telomerase components. Although accelerated telomere shortening has been correlated with a multitude of other disorders associated with aging, in most cases a causal relationship remains to be established.

The contribution of the single-stranded overhang to telomere function

Functions of the telomeric overhang

A conserved feature of terminal telomere structure is the presence of a single-stranded 3' overhang of variable length (refer to Table 1.1). Found at nearly all chromosome ends in a cell[5], the telomeric overhang contributes to the solutions of both the end-replication and end-protection problems, as outlined in previous sections. A 3' single-stranded overhang is required for repeat synthesis by telomerase, which does not display activity on a blunt duplex end[247]. The single-stranded telomeric repeats also serve as the docking site for telomere binding proteins that regulate and/or recruit telomerase [32,33,108]. Importantly, the length of the telomeric overhang correlates with the rate of telomere shortening in human cells lacking telomerase[248]. Overhang generation at newly synthesized telomeres is thus thought to be tightly regulated since insufficient overhangs might compromise telomerase function, while excessive 5' end resection could accelerate telomere shortening in the absence of telomerase.

The telomeric overhang is presumed to contribute to end protection in mammalian cells both by mediating t-loop formation and by binding POT1 proteins. Electron microscopy has been used to detect t-loops formed *in vitro* by incubating TRF2 with 500 bp duplex telomeric substrates containing variable terminal structures. In the presence of substrates containing 3' telomeric overhangs, t-loops were detected at ~11-19% of DNA molecules[16]. On the other hand, <3% of the detected molecules formed t-loops in the presence of substrates with blunt ends, 5' overhangs, or 3' overhangs consisting of non-telomeric sequences[16]. Removal of the overhang by ERCC1/XPF is required for NHEJ of telomeres lacking TRF2[50], suggesting that the presence of an overhang may suppress telomere fusions even when t-loop formation is abolished. The observation that deletion of POT1a and POT1b results in post-replicative sister telomere fusions suggests that an overhang unbound by POT1 proteins is specifically vulnerable to fusions in S phase[37]. In POT1a/b-deficient cells, the absence of chromosome-type fusions could be explained by the ability to re-sequester the telomere terminus in t-loops as cells progress through G2/M, thereby suppressing NHEJ in G1.

There has been no formal demonstration that overhang loss directly activates the DNA damage response, partly because there has been no way to abolish the overhang without compromising shelterin function. In fact, when NHEJ of telomeres lacking TRF2 is inhibited by co-deletion of Ku, Ligase IV, or 53BP1, ATM activation persists in the absence of detectable overhang loss, suggesting that overhang loss is not necessary for persistent DNA damage signaling[193,198,199]. It may be that the ability to form t-loops depends on the presence of both TRF2 and the telomeric overhang, thus loss of either TRF2 or the overhang is sufficient to activate DNA damage responses. Though it was

proposed that short overhangs could trigger replicative senescence, it has since been shown that the telomeric overhangs in several primary human cell lines remain stable in length through senescence[249].

Overhang length dynamics in different organisms

A long-standing question in the telomere field concerns the generation and regulation of the telomeric overhang. Studies of terminal telomere structure in a number of organisms have yielded extensive information about overhang dynamics in different settings and have identified factors that modulate overhang length. However, the nucleases involved in generating the telomeric overhang in mammalian cells (particularly at leading-end telomeres) had not been identified when this thesis work was begun.

Several end-processing steps modify overhang length in S phase (Figure 1.5). The 3' overhang at leading-end telomeres is thought to be generated by nucleases and helicases[75], while lagging-end telomeres constitutively terminate in 3' overhangs due to both the inability to begin synthesis at the very end of the template as well as degradation of the last RNA primer. Telomerase can extend overhangs either immediately upon completion of replication in human cancer cells[101], or in late S phase in budding yeast[97]. Telomerase-independent processing can also result in the transient generation of long overhangs in late S/G2[250]. As cells progress through G2/M, overhangs once again become short through a poorly understood process thought to involve fill-in synthesis of the C-rich strand[101,250].

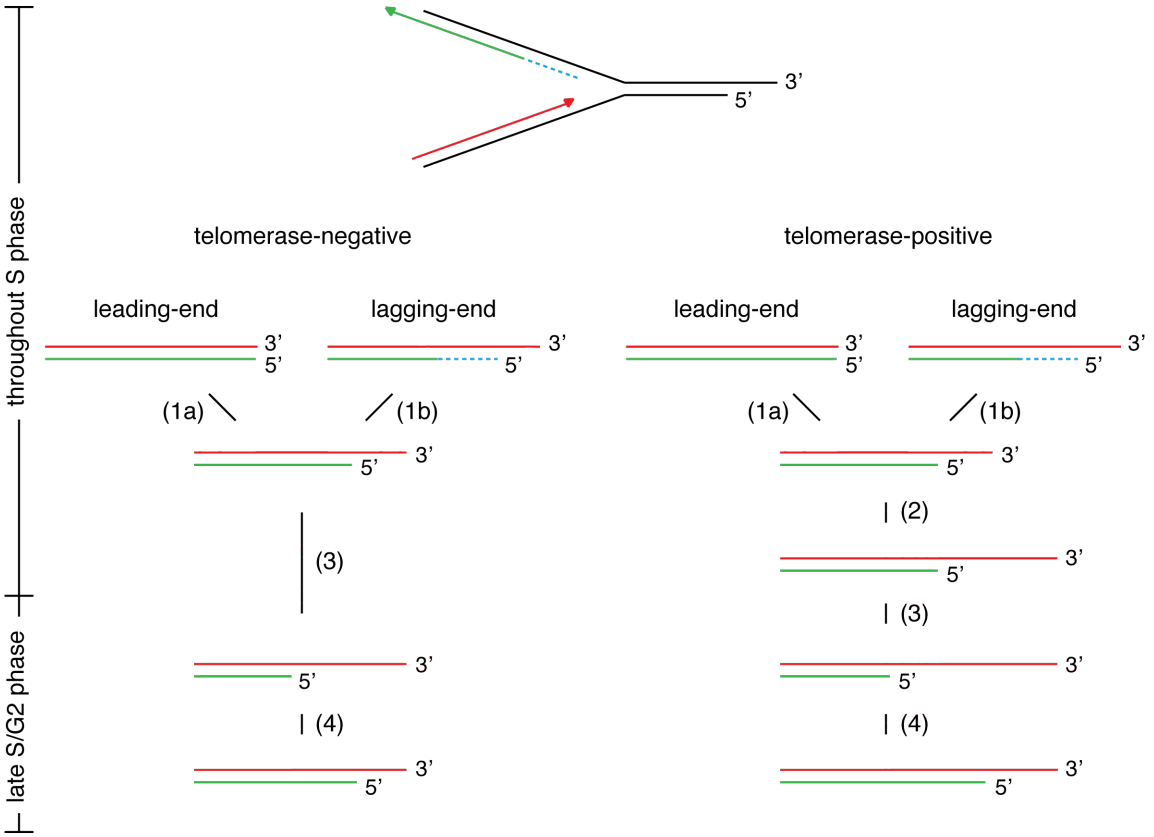

Figure 1.5. Overhang dynamics during S phase. In human cells, telomeres replicate throughout S phase and undergo changes in overhang length corresponding to different processing steps. In step (1), overhangs are generated at newly synthesized telomeres by degradation of the template strand at the leading-end telomere (1a) or degradation of the RNA primer at the lagging-end telomeres (1b). Next, in telomerase-positive cells, the telomeres are elongated by telomerase throughout S phase (2). In step (3), further degradation of the C-rich strand can occur, resulting in the appearance of long overhangs in late S/G2 phase. In step (4), which occurs as cells progress through G2/M, overhangs return to the short length found in G1, through fill-in synthesis of the C-rich strand.

Evidence for the strict regulation of overhang generation and telomere end processing first emerged from studies revealing precise sequences at the extreme terminus of ciliate telomeres. In the mature macronuclei of *Oxytricha* and *Euplotes crassus*, the last nucleotides on both the telomeric G-rich and C-rich strands are precisely defined[9,10], though more heterogeneous structures appear transiently during the period of active telomere synthesis in the sexual stage of the ciliate life cycle when macronuclei are formed[251]. In *Tetrahymena*, the G-rich telomeric strand ends with a 14-15 or 20-21 nt overhang terminating in 5'-T_2G_4T-3', while the sequence of the recessed C-rich strand is

3'-AACC-5' or 3'-AACCC-5'[102]. Analyses of overhang generation in *Tetrahymena* suggested that both the G and C rich strands undergo processing by nucleases that are not sequence-specific, since altering the telomeric sequence by mutating the telomerase RNA template does not abolish the specificity of cleavage[102]. Thus, the properties of single-stranded telomeric binding proteins, rather than intrinsic sequence specificity of nucleases, were proposed to define the boundaries of end processing.

In *S. cerevisiae*, short ~14 nt overhangs are present at telomeres in G1 and additional processing generates long overhangs in S phase[252-254]. This transient overhang elongation requires the passage of the replication fork but is independent of telomerase[255]. Constitutive overhang generation depends upon Mre11, which is also required for telomerase-mediated extension[256,257], whereas the generation of transiently long overhangs does not require Mre11[258]. Instead, the appearance of transient overhangs in S phase is abolished only when both the Sae2 and Sgs1 are deleted, suggesting that redundant pathways can generate the transiently elongated overhangs[259].

Telomeric overhangs of 30-500 nt have been detected at >80% of human telomeres by a number of techniques, including a primer extension based method and DNA length analysis after complete digestion of duplex genomic DNA, which leaves the overhang intact[5,7,260]. In telomerase-negative human cells, overhangs at leading-end telomeres appear to be shorter than those at lagging-end telomeres, while the presence of telomerase equalizes the size distribution of overhangs between the two newly-synthesized telomeres[7]. While the last nucleotides of the G-rich strand are variable, the terminal nucleotides on the C-rich strand end in 3'-CCAATC-5' at >80% of telomeres, suggesting that 5' end-processing of both newly synthesized telomeres in human cells is

well regulated[261]. Depleting MRN components transiently reduces the overhang by ~20-30 nt in telomerase-positive human cells but not in telomerase-negative settings, thus MRN was proposed to have a role in modulating telomerase action at human telomeres[262]. Altered telomeric overhangs have been documented in some human diseases[263-265], though whether they are a cause or consequence of disease has not been well established.

Role of single-stranded DNA binding proteins in overhang regulation

Across species, different single-stranded DNA binding proteins bind the overhang, modulate its length, and have roles in end protection (refer to Figure 1.1). The common structural feature of these telomeric end-binding proteins is the presence of OB folds that bind single stranded telomeric sequences with subnanomolar affinity[266]. The first end-binding proteins isolated were the ciliate TEBPα/β proteins that form a heterodimer in *Euplotes* and *Oxytricha*[267-270]. Though a role in end protection was proposed, the lack of genetic tools precluded further investigation into their *in vivo* functions.

The development of budding yeast as a model system provided powerful genetic tools to gain insight into the *in vivo* functions of end-binding proteins, despite significant divergence of the telomeric binding proteins from those found in other yeasts. As previously noted, the *S. cerevisiae* Cdc13-Stn1-Ten1 complex binds to the single-stranded telomeric overhangs[271] and is required for telomerase recruitment and end protection[272-275]. Temperature sensitive cdc13 mutants undergo extensive resection of the C-rich strand and activation of a RAD9-dependent cell cycle checkpoint[276]. The requirement for CST in end protection is specific to S phase and is primarily

accomplished by Stn1/Ten1, since expression of a chimeric protein comprised of the DNA-binding domain of Cdc13 fused with Stn1 is sufficient to suppress the end-capping defects of cdc13 mutants[277]. Interactions between CST and DNA polymerase alpha contribute to its telomere capping function[278]. Structural comparisons between yeast Stn1/Ten1 and human RPA2/3 have recently led to the proposal that CST functions as a telomere-specific RPA complex[279,280].

In addition to CST, the Rap1-associated Rif1 and Rif2 factors, as well as Ku, also protect telomeres from increased resection of the C-rich strand. In yeast, like mammalian cells, Ku binds to DNA ends without sequence preference. Deletion of Ku in any cell cycle phase leads to the accumulation of single stranded telomeric DNA due to 5' end resection by the Exo1 nuclease[281-285]. While the deletion of either Rif1 or Rif2 alone does not lead to significant resection, co-deletion of Rif1 in cdc13-1 mutants results in increased temperature sensitivity due to excessive MRX-dependent resection[286]. Thus, Rif1 appears to protect telomeres from degradation in a redundant manner with CST.

Single-stranded telomeric DNA binding proteins in *S. pombe* and human were identified based on limited sequence similarity to *Oxytricha* TEBPα and named POT1 for protection of telomeres[32,108]. Besides containing OB folds, the POT1 proteins lack sequence and structural similarities with Cdc13 but perform some similar functions. Deletion of *pot1+* in *S. pombe* results in a severe end protection defect reflected by C-rich strand degradation in the S phase immediately following inactivation of pot1 in synchronized G1 cells followed by ~5 kb of rapid telomere loss and growth arrest after approximately 10 generations[32,287]. Depletion of POT1 in human cells does not produce such a dramatic overhang phenotype; however, a role for POT1 in regulating terminal

telomere structure was suggested by the fact that POT1 depletion abolished the specification of the last 5' nucleotide of the C-rich telomeric strand[210].

The two POT1 proteins found in mouse cells act in distinct ways to protect the telomere terminus. As mentioned previously, POT1a specifically suppresses ATR signaling while POT1b regulates terminal telomere structure[37]. Deletion of POT1b in mouse cells results in the telomerase-independent accumulation of long single-stranded telomeric overhangs, and accelerated telomere shortening[187]. POT1b-deficient mice survive embryogenesis, but display pathologic features resembling the human disease dyskeratosis congenita, such as hyperpigmentation, nail dystrophy, testicular atrophy, and bone marrow failure, which are exacerbated by telomerase haploinsufficiency[187]. Thus, POT1b was proposed to limit degradation of the telomeric C-rich strand. The nuclease(s) responsible for aberrant processing have not been identified, though Exonuclease 1 was ruled out based on the observation that co-deletion of POT1b and Exo1 did not mitigate the phenotype[187].

Recently, a mammalian complex, composed of the OB-fold containing proteins Ctc1, Stn1, and Ten1, has been proposed to be the ortholog of the yeast CST complex based on structural similarities[288,289]. Ctc1 and Stn1 were originally identified as accessory factors of DNA polymerase alpha/primase, which stimulate *de novo* RNA primer synthesis as well as primer-dependent elongation in reconstituted systems[290]. Mammalian CST has been reported to localize to a subset of telomeres as well as replication foci elsewhere in the genome[288,290]. The telomeric localization of human Stn1 has been reported to be independent of POT1, while an interaction between Stn1 and TPP1 has been identified[288,291]. Depletion of Ctc1 or Stn1 in human cells results in the

accumulation of single stranded telomeric DNA at both terminal and internal sites, potentially reflecting distinct roles. Functions proposed for mammalian CST include C-rich strand fill-in synthesis following telomerase action at the telomere terminus and recovery from fork stalling[288,289], though no direct evidence for such roles has so far emerged. CST has also recently been implicated in the negative regulation of telomerase[292]. Whether shelterin cooperates with or promotes the function of CST in order to inhibit the action of telomerase in *cis* is an interesting question to be answered.

It is noteworthy that in the cases of telomere deprotection induced by deletion of shelterin components, the phenotype with respect to C-strand degradation and telomere shortening is much milder than that observed in end-binding mutants from other model organisms. Such relatively low rates of degradation could suggest that, in diseases related to telomere dysfunction, unregulated nucleolytic activities at telomeres contribute relatively less to genome instability compared to aberrancies in cell cycle progression and/or fusion events. Nonetheless, the recent identification of additional factors that can protect mammalian telomeres from extensive resection in a redundant manner with shelterin has revealed that chromosome ends are protected from degradation in more ways than previously imagined[293]. Indeed, the nucleases that act at protected and deprotected telomeres may yet prove to contribute significantly in the pathogenesis of telomere dysfunction related disorders.

Candidates for overhang generation in mammalian cells

In this thesis, the following general categories were considered as candidates in generating the telomeric overhang at leading end telomeres (and/or additional 5'

resection at lagging end telomeres): 1) novel telomere-specific nuclease(s), 2) known shelterin-associated nucleases that also have non-telomeric functions, 3) nucleases involved in DSB resection that localize to telomeres due to the transient recognition of chromosome ends as DNA damage during replication.

The identification of a novel telomere-specific nuclease with a dedicated function in 5' end processing at telomeres was considered possible but unlikely. In theory, the final nucleotide could be specified by an endonuclease that localizes to telomeres and mediates specific cleavage between the two 5' cytosines of 5'-(AATCCC)n-3' repeats. Studies on the terminal structure of ciliate telomeres have suggested that end-binding proteins rather than sequence-specific nucleases regulate the sequence specificity of the telomere terminus[102]. A 100 kDa protein with *in vitro* nuclease activity that specifically cleaves telomeric C-rich strands ending in 3'-AA-5' or 3'-CA-5' has been isolated from *Tetrahymena*, though the *in vivo* function of this activity is not known[294]. Extensive mass spectrometry approaches to isolate shelterin-associated factors have yielded a number of nucleases, but none appear to be telomere specific. The failure to isolate such a factor suggests that if a novel telomeric nuclease does exist, its association with telomeres is likely to be weak and/or transient. Thus, biochemical approaches to isolate a novel telomeric nuclease were not attempted here.

Another possibility is that nucleases and/or helicases with non-telomeric roles are recruited by shelterin to mediate 5' end processing at telomeres. The members of shelterin are known to interact with nucleases (Apollo/SNM1b[51,52,295], FEN1[54], ERCC1/XPF[50]), helicases (BLM[47,296], WRN[296,297]), and factors that modulate nuclease/helicase activity (Nbs1[49], ATM[298], SLX4[299]). Since TRF2 has been proposed to

recruit a factor that generates overhangs at leading-end telomeres[194], nucleases known to associate with TRF2, including Apollo/SNM1b and Fen1, as well as nucleases recruited by the scaffolding protein SLX4, were particularly attractive candidates.

Finally, a third hypothesis is that telomeres are transiently recognized as DNA damage, in which case factors involved in DNA DSB resection might be recruited and resect the 5' ends. This hypothesis stems from chromatin immunoprecipitation experiments that have detected DNA damage factors at telomeres in cells progressing synchronously through S phase following cell cycle arrest by double thymidine or aphidicolin[300,301]. The associations of ATM, ATR, and other components of these pathways with telomeres occur at two points in S phase, once in early/mid S and again in late S/G2[300,301]. The recombination proteins Rad51, Rad52 and XRCC3 also appeared to localize to telomeric DNA during late S phase[300]. While the first peak of association between DNA damage factors and telomeres was attributed to fork stalling during telomere replication, the late S phase association was attributed to end processing events that occur after the completion of replication. The caveat of this interpretation is that the experiments involved drug treatments that can induce low levels of DNA damage, and the telomeric localization of various DNA damage factors could reflect distinct repair activities rather than physiologic processes.

A largely genetic approach was undertaken to identify factors involved in overhang generation and dynamics. The expectation that the nucleases and/or helicases involved in telomere end processing might be redundant led to the choice of *Mus musculus* as the preferred organism for genetic manipulations. A large number of nucleases, helicases, and associated factors were considered as potential candidates

(Table 1.2), thus the next section of this introduction concerns the general properties and mechanisms of the DNA nucleases that may function at telomeres.

Table 1.2. Candidates for overhang generation

	Nucleases	Helicases	Other factors
Shelterin-associated	Apollo/SNM1b (Fen1) (Mus81)	BLM (WRN)	Mre11/Rad50/Nbs1 (ATM) SLX4
No confirmed association with shelterin	CtIP Exo1 (Dna2) Artemis SNM1a	(RecQL4) (RecQL5) RecQL1 (Pif1)	Cdk (non-specific) SIRT6 (Msh2) (Mlh1)

Listed are all candidates considered for a role in overhang generation and/or dynamics, with tested candidates listed in black (in parentheses are those candidates that were tested but not discussed here) and untested factors listed in gray. Candidates are grouped based on whether they have been reported to interact with shelterin (in any context).

PART II: NUCLEASES IN EUKARYOTIC DNA REPLICATION AND REPAIR

General classes and properties of eukaryotic structure-specific DNA nucleases

Deoxyribonucleases that hydrolyze the phosphodiester backbone of DNA contribute to a multitude of important cellular transactions. Nucleolytic activities associated with DNA replication ensure the fidelity of DNA polymerases and the appropriate processing of Okazaki fragments generated during lagging strand replication. In addition, nucleases mediate the repair of different kinds of DNA damage arising from both spontaneous reactions within the cell (eg. deamination, alkylation, oxidation) and exogenous sources (e.g. UV, X-ray irradiation, chemicals). Endonucleases and exonucleases cleave their substrates upon recognition of specific sequences or structures.

Whereas a diverse collection of bacterial sequence-specific restriction endonucleaseshave been identified[302], sequence-specific nucleases are less common in eukaryotes. Some examples include the *S. cerevisiae* HO[303-305] and I-SceI nucleases[306,307] that belong to the LAGLIDADG family of homing endonucleases. The sequence specificity of bacterial restriction enzymes is conferred by the ability to distort specific bases in the center of cognate palindromic sequences[302]. In comparison, eukaryotic homing endonucleases recognize longer sequences and tolerate more degeneracy[302].

Since a telomere sequence-specific nuclease was considered an unlikely candidate for overhang generation, I will focus here on the eukaryotic structure-specific nucleases and their roles in various contexts of DNA replication and repair. Structure-specific nucleases are grouped primarily based on their conserved catalytic domains and include the flap endonucleases, the XPF/ERCC4 family, and the UvrC class of nucleases. Despite their diverse *in vitro* and *in vivo* activities on various DNA substrates, many of

these enzymes share common structural motifs involved in DNA binding and catalyze hydrolysis using divalent metal cations as cofactors.

Members of the flap endonuclease family include FEN-1, EXO-1, GEN-1, and XPG (reviewed in [308]). FEN-1 has 5' to 3' exonuclease and endonucleolytic activity, preferentially acting on 5' single-stranded DNA termini[309,310]. Purified human Exo1 also has 5' to 3' exonucleolytic and flap endonuclease activity *in vitro*, preferentially at blunt-ended or 5' recessed DNA[311]. XPG and GEN-1 are thought to act via endonucleolytic activities at DNA bubbles and four-way junctions, respectively[312,313], though *in vitro* 5' to 3' exonucleolytic activity has also been reported for XPG[314].

Structural studies of archaeal and bacterial FEN nucleases[309,315], and more recently, human FEN-1[316] and EXO-1[317] have lent insight into the common mechanisms by which these nucleases bind and cleave DNA while maintaining specificity for different substrates. Members of this family contain conserved N- and C-terminal domains that contact DNA and are separated by a variable length intermediate (I) domain thought to form a helical arch or clamp[308]. The catalytic site is located in the N-terminal portion of the I-domain and consists of seven positionally conserved aspartates and glutamates that coordinate metal ion cofactors[317]. A helix-two-turn-helix motif in the C-terminus of the protein binds duplex DNA upstream of the cleavage site, while the N-terminus binds to the downstream DNA segment[317]. These interactions bend DNA near the cleavage site at a 90-100 degree angle, which can only be achieved in DNA with a gap or flap[316,317]. This sharp bend exposes the scissile bond and causes fraying of two nucleotides at the 5' end, which provides a common intermediate for apparent endo- and exonucleolytic actions[316,317]. Elements specific to the individual nucleases confer

preferences for different structures while factors that interact with the C-terminal domain of the nucleases have been proposed to further regulate nuclease activity[317]. For instance, a positively charged groove near the active site of EXO1 accomodates the binding of 3' overhangs and gapped structures[317].

The XPF family members XPF/ERCC4 and Mus81 compose another class of divalent metal cation dependent endonucleases. XPF consists of a catalytic domain (also known as the ERCC4 domain) with the active site motif GDX_nERKX_3D, followed by a DNA-binding domain containing two helix-hairpin-helix (HhH) motifs[318]. Mus81 contains a similar catalytic domain flanked by single HhH motifs[319,320]. The activities of both XPF and Mus81 require their interactions with structurally related protein partners, ERCC1 and Eme1, respectively, which contain similar ERCC4 and HhH motifs but lack critical residues for catalytic activity[321-323]. XPF/ERCC1 cleaves the 5' end of bubble structures as well as within the duplex regions next to a 3' or 5' single-stranded overhang[324,325]. RPA specifically stimulates the binding of XPF/ERCC1 to the double-stranded/single-stranded DNA junction next to a 5' protruding end[326,327]. Mus81/Eme1 has been implicated in Holliday junction resolution and has *in vitro* activity at branched duplex DNA, replication fork substrates, and synthetic HJ intermediates[322,323,328].

Eukaryotic SLX1 typifies the UvrC family of endonucleases, which were first identified as prokaryotic NER factors. An N-terminal GIY domain contains several conserved residues important for catalysis, including a glutamate and several tyrosine or histidine residues involved directly or indirectly in coordinating the active site metal cation and an arginine that may stabilize the phosphate group at the scissile bond. While UvrC contains a C-terminal helix-hairpin-helix motif for DNA binding, SLX1 orthologs

contain a C-terminal cysteine-rich PHD zinc finger-like domain[329]. Like the XPF family nucleases that require a partner for activity, the nucleolytic activity of yeast SLX1 is stimulated by SLX4[330]. Mammalian SLX4 appears to interact with a number of other nucleases and repair proteins including Mus81, Msh2-3 as well as the shelterin component TRF2, suggestive of a telomeric role[299,331,332]. SLX1-SLX4 acts at branched DNA containing a ds-ss junction, including 5' flaps, 3' and replication fork structures, and symmetrically cleaves Holliday junctions[299,331,332].

A final class of nucleases considered here is the β-CASP family of metallo- β -lactamases, which includes the CPSF, Artemis, SNM1 and PSO2 (CASP) nucleases[333]. This family is thusly named due to a common structural motif shared with the β-lactamases expressed by bacteria to counteract antibiotics. This common metallo-β-lactamase (MBL) fold consists of two anti-parallel β-sheets between two α helices, with the metal-binding site on one edge[334]. The MBL domain contains a characteristic HxHxDH motif that comprises the active site of PSO2/SNM1 family members, with the first histidine and aspartate being conserved in all MBL proteins[333]. A second C-terminal domain found specifically in the β-CASP family contains additional conserved carboxylates and a histidine involved in coordinating the zinc cation in the active site[333]. While no structural information is yet available for DNA-processing β-CASP proteins, structures of prokaryotic and eukaryotic RNA processing β-CASP family members have suggested that the β-CASP domain forms a lid-like structure on the edge of the MBL that limits substrate access to the active site[335,336].

The *in vitro* activities of the β-CASP family members are diverse. Purified Artemis alone acts as a 5' to 3' exonuclease[337]. However, when complexed with the

DNA-dependent protein kinase, DNA-PKcs, Artemis exhibits endonucleolytic activity that cleaves 5' and 3' overhangs as well as hairpins[337]. Apollo also possesses 5' to 3' exonuclease activity on single stranded DNA as well as double stranded blunt and recessed ends[52]. In addition, Apollo purified from insect cells has been found to exhibit endonucleolytic activity on branched, bubble, and hairpin substrates *in vitro*[338]. The exonucleolytic activity of Apollo has been reported to be modified by its binding with TRF2[217]. Whether Apollo is modified or complexed with proteins other than TRF2 is not known, but such *in vivo* interactions could also modulate its function.

Involvement of nucleases in DNA replication and repair pathways

Okazaki fragment maturation

The removal of initiator RNA primers during Okazaki fragment maturation has been proposed to occur via a number of possible mechanisms that involve the FEN1 and/or Dna2 nucleases as well as RNase H (reviewed in [339]). During replication, DNA polymerase α/primase synthesizes RNA primers, initiates low-processivity, low-fidelity synthesis, after which polymerase switching occurs whereby more processive polymerases extend the newly-synthesized strand[340-343]. *In vitro* reconstitution experiments had originally demonstrated the ability for DNA polymerase δ to act at both strands at a replication fork[344]. However, more recent genetic experiments in *S. cerevisiae* investigating the strand-specific mutation rates caused by DNA polymerase mutants with higher error rates have assigned DNA polymerase δ primarily to lagging-strand synthesis[345], while polymerase ε replicates the leading-strand[346]. RNA primers used in lagging strand synthesis can be digested by RNase H or via polymerase-

dependent strand displacement and flap cleavage by DNA nucleases. The FEN1 nuclease was isolated from a number of mammalian sources and found to be required for the removal of initiator RNA and ligation of Okazaki fragments in several systems of *in vitro* reconstituted replication[347-350]. While FEN1 can act within RNA via its endonucleolytic activity[351], eukaryotic RNase H has also been implicated in lagging strand synthesis[352]. In *S. cerevisiae*, overexpression of RNase H partially suppresses the growth defect of Rad27 (Fen1 ortholog) mutants[352].

Though the presence of RNase H and FEN1 are sufficient for Okazaki fragment maturation using *in vitro* reconstituted systems, genetic studies have led to a model that also involves DNA2, which is essential in *S. cerevisiae*[353]. DNA2p interacts physically and genetically with Rad27p[354]. In addition, *in vitro* reconstituted systems using yeast proteins have suggested that polymerase-dependent displacement of downstream Okazaki fragments generates a flap of variable length[355]. While short 5' flaps can be cleaved by FEN1, stable binding of RPA to flaps of 30 nt or longer can inhibit the activity of FEN1, while stimulating the nuclease activity of DNA2[356]. Thus, a revised model proposes that while Okazaki fragment maturation largely involves short flaps that are cleaved by FEN1 (with or without RNase H), strand displacement synthesis nevertheless generates some long flaps, which are lethal if unresolved, accounting for the essential role of DNA2.

Base excision repair

The base excision repair pathway responds to modified bases that do not induce significant distortion of the DNA backbone (reviewed in [122,357]). In brief, specific DNA glycosylases recognize and remove various modifications to generate an abasic (AP) site.

Subsequently, an AP endonuclease introduces an incision 5' to the AP site[358,359], and the area can be excised by one of two mechanisms. Short-patch BER occurs through the removal of the abasic sugar to leave a 1-nt gap that is filled by DNA polymerase beta in conjunction with DNA ligase III-XRCC1[360]. On the other hand, long-patch repair occurs when DNA synthesis mediated by DNA polymerase delta/epsilon and PCNA cause strand-displacement, producing a 2-10 nt flap cleaved by FEN1[361]. In this case, DNA ligase I seals the nick[362]. The choice of repair pathway appears to depend on the tissue type and the mechanism by which the AP site is generated.

Nucleotide excision repair

Bulky adducts induced by UV damage or chemical agents are recognized and resolved by nucleotide excision repair. NER involves a complex sequence of events accomplished by over 30 proteins that assemble at the lesion, excise a 24-32 nt long segment to generate a single-stranded gap, and finally re-synthesize DNA across the gap using the undamaged strand as a template[363]. This mode of repair can occur via either a transcription-coupled pathway in which the lesion is sensed by the stalling of RNA polymerase II or a global genome pathway that depends on DNA binding proteins, RPA, XPA, and XPC, which recognize damaged duplex DNA and initiates the recruitment of other NER factors[364-366]. Two nucleases, XPG and XPF (heterodimerized with ERCC1), make incisions 3' and 5' to the damaged site, respectively[312,367].

Mismatch repair

The mechanism of eukaryotic mismatch repair has mostly been elucidated through biochemical reconstitution of mismatch or nick- directed repair, which requires the MutS complex (predominantly MutSα composed of Msh2/6 or, in some cases, MutSβ composed of Msh2/3), the MutL complex (Mlh1/Pms2 or Mlh1/Mlh3), PCNA, RFC, and exonuclease 1[368] (reviewed in [369]). The paradox that either a 5' or 3' nick can direct excision by the 5'-3' exonuclease 1[370] was resolved by the identification of endonucleolytic activity of MutL, which is thought to generate two nicks flanking the mismatch[371]. The intervening sequence is excised by exonuclease-1 and can be resynthesized by DNA polymerase δ[368]. While Msh2-deficient mice have significantly compromised mismatch repair[372,373], the Exo1-deficient mouse exhibits only mild mutator phenotypes suggesting the existence of Exo1-independent repair pathways[374].

DSB repair

The non-homologous end-joining and homology directed repair pathways that respond to DNA double strand breaks have been outlined previously, so here I will focus on the nucleases associated with these pathways. The primary nucleolytic activity in the NHEJ pathway is that of the 5' to 3' nuclease Artemis, which has mainly been studied in the context of V(D)J recombination[174,375,376]. Artemis is required to cleave the hairpins generated on coding ends following the initial cleavage by the lymphoid specific RAG1 and RAG2 endonucleases[337]. Artemis interacts with the catalytic subunit of the DNA-dependent protein kinase, DNA-PKcs, which phosphorylates several C-terminal S/TQ

sites in Artemis that modify its *in vitro* nucleolytic activity, though these modifications do not appear to be required for *in vivo* activation[377].

Two steps in homology-directed repair require the activity of nucleases: initiation of 5' end resection and HJ resolution. Resection at a double strand break has been genetically dissected in yeast and appears to involve sequential steps performed by several partly redundant nucleases. MRX acts in conjunction with Sae2 endonuclease to initiate a cut, while two pathways dependent on either Exo1 or Sgs1/Dna2 mediate more extensive resection[378-380]. Deletion of Sae2 slows the rate of resection after DSB induction by HO, though a subset of breaks still undergo efficient resection that is dependent on Exo1[378,379]. Similarly, in the absence of either Rad50 or Mre11, ~20% of DSBs do not initiate resection, while resection beyond 25 kb from the initial break site still occurs at a majority of breaks[378,379]. Co-deletion of Exo1 and Sae2 impairs but does not abolish resection and subsequent homology-directed repair, and the remaining activity that allows resection has been attributed to the Sgs1 helicase acting with the Dna2 nuclease[378,379]. Interestingly, 5' resection has been reconstituted *in vitro* with Dna2, Sgs1, and RPA[381,382]. In this *in vitro* reaction, RPA stimulates Sgs1 unwinding of a duplex as well as the 5' to 3' nucleolytic activity of Dna2, while inhibiting the 3' to 5' nuclease activity of Dna2[381,382].

In mammalian cells, extensive resection at a DSB has been attributed to Exo1 and BLM[380]. The induction of DSBs in replicating human cells by the topoisomerase inhibitor camptothecin resulted in reduced cell survival and RPA foci formation when both Exo1 and BLM were depleted, compared to depleting either factor alone[380]. Initial resection by CtIP appears to promote the recruitment of Exo1 and further resection[380].

Resection by CtIP is modulated by a number of modifications including phosphorylation by Cdk and acetylation by SIRT6[383,384].

Following strand invasion and second end capture, the double Holliday junction can either be dissolved by the BLM/Top3/Rmi complex or resolved by a number of structure-specific endonucleases. Resolvase activity has been attributed to Mus81, GEN1/YEN1, and SLX1-SLX4[313,322,328,331,332,385]. GEN1/YEN1 behaves similar to classical bacterial resolvases that incise symmetrically on opposite sides of the four-way junction, while Mus81 cleaves asymmetrically[313,322,328]. The differential contributions of the different nucleases to dHJ resolution *in vivo* are not easily explained by their *in vitro* activities. Depletion of SLX1-SLX4 or GEN1 in human cells compromises repair in response to the interstrand crosslink inducing agent mitomycin C and camptothecin, while depletion of Mus81 has little effect[385]. In BLM-deficient human cells that exhibit increased sister-chromatid exchanges, it appears that Mus81 and SLX1-SLX4 have a significant role in the resolving double Holliday junctions, while the role of GEN1/YEN1 appears to become important when either Mus81 or SLX1-SLX4 is depleted[386]. The relative contribution of these nucleases *in vivo* may depend on other interacting factors that are important for their recruitment to HJs.

Interstrand crosslink repair

The interstrand crosslink repair pathway responds to crosslinks that can occur between complementary strands of DNA treated with various chemical agents, including mitomycin C (MMC) and cisplatin. Compared to the other repair pathways described in this section, ICL repair is less well-understood. Replication-coupled ICL repair is

thought to be the dominant pathway and its mechanism has been elucidated through *in vitro* systems reconstituted with Xenopus egg extracts[387]. The recognition of interstrand crosslinks during replication involves the NER factor ERCC1-XPF. Incisions are made flanking the break site[387]. A multiprotein complex composed of members of the FANC complementation group localizes to the site and is required for processing that results in a one-ended DSB, which is presumably repaired by HDR[387]. ICL repair thus requires the nucleases that perform incisions surrounding the lesions as well as nucleases involved in HDR. Recently, the novel nuclease FAN1 and the human orthologs of the yeast Slx1/Slx4 complex have been implicated in ICL repair, though the steps at which they act are not well elucidated[388-391].

Known telomeric roles of nucleases

A number of mammalian nucleases have been documented to contribute to telomeric function, though it has often been difficult to distinguish between global repair functions and telomere-specific roles. Telomere-related phenotypes reported in cells deficient for various repair factors can sometimes be nonspecific, such as in the case of Artemis deficiency, where telomere fusions have been reported to occur at a very low frequency. Nucleases that interact with shelterin may likely have important telomeric functions. However, the absence of detectable telomeric localization of a candidate nuclease does not preclude a telomeric role. Telomere end-processing may involve only transient telomeric localization of nucleases and is not expected to occur synchronously at all telomeres in a cell. Thus, cases in which compromised nuclease function has

produced aberrant telomere phenotypes warrant a re-evaluation of the telomeric overhang.

Nucleases known to interact with shelterin include Apollo/SNM1b, Mre11, XPF/ERCC4, FEN1, and Mus81. The interaction between SLX4 and TRF2 may also mediate the localization of additional nucleases to telomeres. Human Apollo was identified as a member of the TRF2/Rap1 complex by mass spectrometry[51,52]. Though the inability to generate an adequate antibody has precluded the detection of endogenous Apollo, exogenously expressed Apollo appears to colocalize with a subset of telomeres[51-53]. A C-terminal YxLxP motif in Apollo interacts with the TRFH domain of TRF2[44]. This interaction is abolished by mutating phenylalanine 120 of TRF2 or by deleting the YxLxP motif of Apollo[44]. Depletion of Apollo by shRNA in human cells results in a transient DNA damage response in S phase cells and the appearance of multiple telomeric FISH signals at a low percentage (<5%) of chromosome ends in metaphase[51]. These results suggested a role for Apollo in telomere replication. Recent evidence has indicated that human TRF2/Apollo may have a role in the replication of interstitial telomeric sequences, though no such role has been ascribed in mouse[217].

The interaction of the MRN complex with TRF2 in human cells is also suggestive of a role during telomere replication. The association of Nbs1 with telomeres appears specific to S phase cells, while the other components of the complex, Mre11 and Rad50, localize to telomeres throughout interphase[49]. Depleting MRN components transiently reduces the overhang by ~20-30 nt in telomerase-positive human cells but not in telomerase-negative settings, thus MRN was proposed to have a role in modulation telomerase action at human telomeres[262]. In mouse cells, compromising MRN function

does not lead to any telomere-specific phenotypes, suggesting that the complex is not absolutely required for telomere function and that other factors may act redundantly[194]. Only in the absence of TRF2 does the MRN complex appear to have a function in promoting NHEJ in G1 and generating the overhang at leading ends in S phase[194,195].

A telomeric role for FEN1 has been described, but the challenge is in dissociating this function from its general role in lagging strand DNA replication. Depletion of FEN1 in human cells results in a low level of γ-H2AX detected in telomeric ChIP and loss of lagging-end telomeres on metaphase[54]. FEN1 appears to contribute to the stability of the telomeric replication fork while not being essential for general S phase progression[54]. On the other hand, depleting FEN1 in mouse cells does not result in phenotypes associated with fork instability, but results in a low level of fusions between newly-synthesized lagging-end telomeres[392]. Though this role of FEN1 required its nuclease activity, its depletion had no apparent effect on the telomeric overhang[392].

The telomeric roles of other shelterin-associated nucleases make them less likely candidates for physiologic overhang generation. XPF/ERCC1 has been proposed to protect telomere from recombining with interstitial (TTAGGG) repeats[50]. Human cells depleted for XPF or ERCC1-deficient mouse cells do not have reduced overhangs[50]. However, XPF/ERCC1 is involved in the removal of 3' overhangs and subsequent NHEJ when TRF2 is inhibited in human cells[50]. In mouse, other nucleases can perform this role[393].

Mus81 interacts with TRF2 specifically in human telomerase-negative ALT cells, and localizes to telomeres by ChIP, an association that could not be detected in non-ALT immortalized human cell lines[299]. In this setting, the interaction between TRF2 and

Mus81 was found to inhibit the *in vitro* nuclease activity[299]. These findings support a function for Mus81 at telomeres specifically in ALT cells.

Finally, though Exonuclease 1 has not been documented to interact with shelterin components, its deficiency ameliorates the organ dysfunction associated in late generations of mice lacking the telomerase RNA component[394]. This was attributed to the role of Exo1-mediated resection in the DNA damage response to dysfunctional telomeres, rather than a direct function of Exo1 in altering telomere structure[394]. Nonetheless, subtle effects of Exo1 deficiency on telomere structure or function may have been missed in the gross characterizations performed in this study that focused largely on *in vivo* phenotypes.

PART III: OBJECTIVES

The objective of this thesis was to elucidate the mechanism by which the single-stranded 3' overhang at the telomere terminus is generated and regulated. First, I examined the chromatin structure of the telomere terminus through a combination of conventional micrococcal nuclease digestion and a novel assay to determine the chromatin organization adjacent to the telomeric overhang (Chapter 2 and [395]). These assays were also used to determine whether terminal chromatin organization is altered at deprotected telomeres. Next, I identified a role for the TRF2-associated nuclease Apollo in the generation of overhangs at telomeres synthesized by leading strand DNA replication in mouse cells (Chapter 3 and [396]). Through subsequent studies on the mechanism by which POT1b limits overhang size at mouse telomeres, I determined that POT1b inhibits 5' resection by Apollo while promoting the function of the mammalian

Ctc1/Stn1/Ten1 complex (Chapter 4). Finally, to identify additional nucleases that might contribute to overhang generation, I tested the hypothesis that telomeres are transiently recognized as sites of DNA damage and processed by the same factors that perform resection at a DNA double strand break (Chapter 5). Through these studies, I uncovered a role for Exonuclease 1 in the generation of transiently extended telomeric overhangs in late S phase. However, the processing of telomeres by Exonuclease 1 did not appear to recapitulate previously proposed models for resection at a DNA double strand break, and the mechanism by which Exo1 is recruited to telomeres remains unknown.

CHAPTER 2:

THE TERMINAL CHROMATIN ORGANIZATION

OF MAMMALIAN TELOMERES

INTRODUCTION

Whereas the telomeric overhangs in yeast and ciliates are protected by end-binding proteins arranged in non-nucleosomal complexes[58-60] the results of electron microscopy and micrococcal nuclease (MNase) digestion studies have demonstrated the presence of nucleosomes at telomeres in a number of vertebrates[12,15,56,57]. The chromatin organization of the telomere terminus could be one way by which changes in the state of telomere protection are signaled to the DNA damage response machinery.

The cellular machinery that responds to DNA damage executes its functions within the context of chromatin, and several studies have suggested that chromatin remodeling and modifications contribute to the recognition and repair of DSBs. Chromatin decondensation at DSBs has been suggested to occur in living cells subjected to DNA damaging agents, and such conformational changes have been proposed to activate the ATM kinase[397,398]. In addition, nucleosome loss has been observed at sites of induced DSBs in several model systems. In yeast, the induction of a single DSB by HO-endonuclease leads to histone displacement that depends on the DNA damage sensor MRX and the chromatin remodeling complex, INO80[399,400]. In human cells, break sites introduced by the I-PpoI nuclease exhibit nucleosome disruption that requires NBS1 and ATM[401]. Furthermore, several steps in NHEJ or HDR are stimulated by one or more of the three major ATP-dependent chromatin remodeling complexes, INO80, Swi/Snf, and RSC[399,402-406].

Given that telomere dysfunction activates the canonical response to DSBs, exploring the role of chromatin remodeling at damaged telomeres may lend insight into the mechanisms by which shelterin protects telomeres from being recognized as DNA

damage. Here, I investigated the terminal chromatin organization of native and deprotected telomeres to determine whether the DNA damage signaling and repair processes at damaged telomeres involve chromatin remodeling at the terminus.

RESULTS

The telomere terminus has a nucleosomal organization similar to bulk telomeres

A standard method to examine nucleosomal organization involves the partial digesting of chromatin in nuclei with micrococcal nuclease (MNase), after which fractionation of the DNA on agarose gels results in a periodic ladder of fragments corresponding to the mononucleosomes, dinucleosomes, and higher order oligonucleosomes[407]. Genomic loci of interest, such as telomeres, can be detected after Southern blot and hybridization with a specific probe.

I devised a novel method for detecting the nucleosomal organization at the telomere terminus based on the fact that mammalian telomeres end in a 30-500 nt single-stranded tract of TTAGGG repeats, termed the 3' overhang[5,6,260,408]. Although the 3' overhang is removed from telomeres undergoing NHEJ, the single-stranded TTAGGG repeats are retained when TRF2 is deleted from DNA ligase IV-deficient cells[193] and also persist in POT1-deficient cells[37]. Therefore, the last nucleosome of the dysfunctional telomeres in these settings is expected to be adjacent to the 3' overhang, and an assay detecting chromatin organization of the terminus can be used to determine whether telomere deprotection induces changes in the terminal chromatin structure.

A concern with using the 3' overhang as a marker for the last nucleosome is that MNase is known to rapidly degrade single-stranded DNA[409]. Indeed, when agarose-embedded protein-free genomic DNA was digested with MNase, the single-stranded overhang signal decreased rapidly and at a much faster rate than the total TTAGGG signal representing the duplex telomeric repeats (Figure 2.1A). In contrast, the telomeric overhang remains largely intact during the MNase treatment of nuclei from wild type

cells, as well as in nuclei lacking POT1a and –b (Figure 2.1B), indicating that the single-stranded DNA is protected from the nuclease. As discussed below, this protection could be due to strand-invasion of the 3' overhang in the t-loop configuration and/or coating with POT1a and -b.

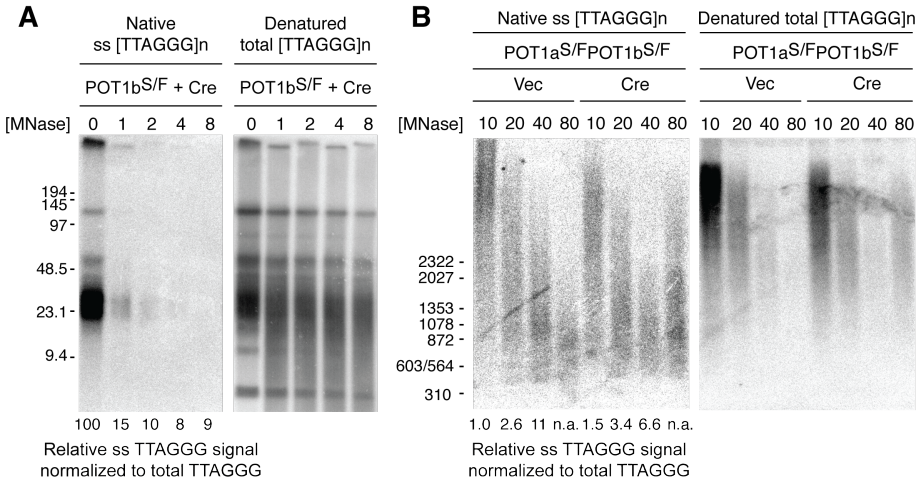

Figure 2.1. The single-stranded telomeric overhang is protected in chromatin from MNase digestion. In gel overhang assay of DNA fragments recovered from MNase digestion of (A) agarose-embedded genomic DNA and (B) nuclei from POT1a$^{S/F}$ POT1b$^{S/F}$ cells infected with pWzl vector (left panel) or pWzl-Cre (right panel) at 5 days post-selection with hygromycin. MNase concentrations are given as U/mL. Agarose plugs were digested overnight with *Mbo*I and fractionated on a 1% agarose gel in 0.5x TBE by pulse field electrophoresis. Fragments in solution were treated with *Alu*I/*Mbo*I and fractionated on a 0.7% agarose gel. Gels were dried by vacuum suction and hybridized with [^{32}P](CCCTAA)$_4$. The gel was denatured *in situ* and rehybridized with the same probe. The relative G-strand signal in the native gel was normalized to the total telomeric signal detected in the denatured gel. The numbers below each lane correspond to the ratio relative to the value in the first lane of that panel. n.a.: not applicable. The relative overhang signal at [MNase] = 80 U/mL in (B) was not quantified because the duplex signal was at background level making the ratio between ss overhang signal and duplex TTAGGG repeats unreliable.

The resistance of the telomeric overhang to MNase digestion of chromatin in nuclei suggested that it should be possible to detect the most terminal nucleosome abutting the 3' overhang. However, the standard method of detecting DNA fragments bearing a 3' overhang – in-gel hybridization to native DNA – is not applicable to fragments smaller than ~500 bp due to their loss during the gel-drying step required for this protocol. I therefore developed an alternative method of detecting the MNase product representing the last nucleosome next to the single-stranded TTAGGG repeats

(Figure 2.2A). Biotinylated oligonucleotides complementary to the 3' overhang were annealed to the DNA fragments recovered from MNase-treated nuclei; the last nucleosomal fragments could then be precipitated with streptavidin beads. The DNA fragments in the supernatant and precipitate were fractionated on an agarose gel, transferred onto a nitrocellulose membrane, and the telomeric signal was detected with a $[^{32}P](CCCTAA)_4$ probe.

To verify that this assay could efficiently isolate telomeric fragments containing a G-rich overhang, I constructed a model telomeric fragment by annealing and ligating a *Bgl*II/*Kpn*I restriction fragment (dsTel) excised from a plasmid with 25 tandem TTAGGG repeats (pSXneo.25T_2AG_3)[410] to a single-stranded $(TTAGGG)_{12}$ oligonucleotide (ssTelG) containing a *Bgl*II protrusion at the 5' end (Figure 2.2B). When the products of the ligation reaction were detected by Southern blot for telomeric signal, the major product was a 270 to 280 bp fragment that was absent when either dsTel or ssTelG was excluded from the reaction (Figure 2.2C). When this model telomeric fragment was annealed to biotin-$(CCCTAA)_6$ and isolated with streptavidin beads, nearly all of the DNA was pulled down (Figure 2.2D). On the other hand, dsTel lacking the 3' overhang remained in the supernatant, confirming that only the fragments containing a G-rich overhang can be isolated by the assay.

Figure 2.2. Assay to detect nucleosomes near the telomere terminus. (A) Scheme of the last nucleosome assay. Nuclei are treated with MNase and the isolated DNA fragments are incubated with a biotinylated oligonucleotide representing the C-rich telomeric DNA strand, biotin-$(CCCTAA)_6$. Magnetic streptavidin beads are used to pull down DNA fragments containing a telomeric [TTAGGG]n 3' overhang. The supernatant contains fragments of bulk nucleosomes while the pull down contains nucleosomal fragments ending at the telomere terminus. Fragments were fractionated on a 1% agarose gel and subjected to southern blot hybridization with a $[^{32}P](CCCTAA)_4$ probe. (B) Scheme for the construction of a model telomeric fragment to test the last nucleosome assay. A *Bgl*II/*Kpn*I fragment excised from pSXneo.25(T_2AG_3) (dsTel) was annealed and ligated to a single stranded telomeric oligonucleotide (ssTel) containing the complementary *Bgl*II recognition sequence at its 5' end. (C) Southern blot detection of the telomeric signal ligation products of dsTel and ssTel (lane 1), dsTel only (lane 2), or ssTel only (lane 3). (D) Southern blot detection of the telomeric signal after annealing the DNA products from lanes 1 and 2 in (C) with biotin-$(CCCTAA)_6$ and separating the supernatant (sup) and pull-down (ppt) following incubation with streptavidin beads. 2% of the supernatant was loaded next to 50% of the total pulldown. (E) Detection of the telomeric signal associated with the last nucleosomes in wild type MEFs. The last nucleosomal assay was performed as described, and the supernatant (2% of total fraction) containing the bulk nucleosomes were loaded in the first eight lanes, while nucleosomal fragments containing the telomeric overhang (50% of total pulldown) were loaded in the last eight lanes. MNase concentrations are given as U/ml. (F) Detection of the telomeric signal pulled down by the last nucleosomal assay following ExoI treatment of DNA from MNase-digested nuclei. DNA fragments isolated after MNase digestion were mixed and treated with ExoI (300 U in 300 μl), removing the 3' overhang. ExoI-treated and untreated samples were then subjected to the last nucleosome assay. 2% of the supernatant (bulk nucleosomes) was loaded next to 50% of the total pull down (last nucleosomes). Percent of total TTAGGG signal pulled down was calculated by the equation: (2 x pulled down signal) / (2 x pulled down signal + 50 x supernatant signal).

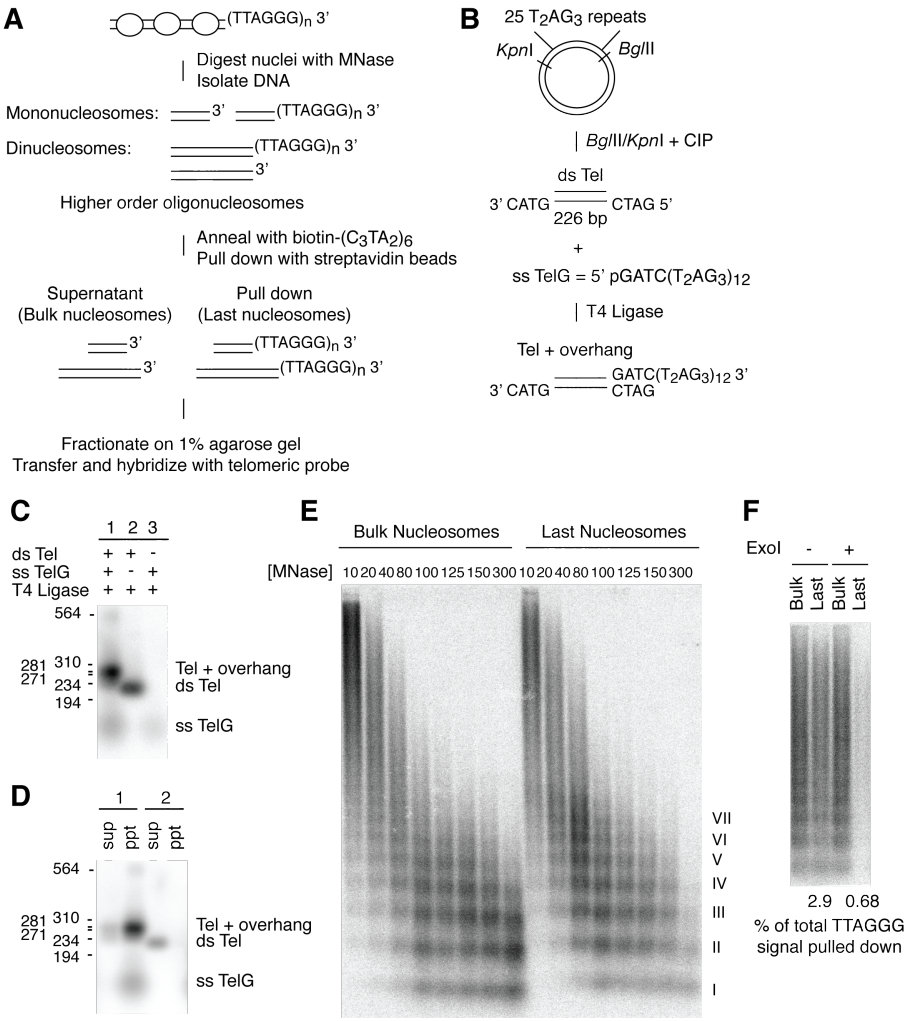
A
(TTAGGG)n 3'
Digest nuclei with MNase
Isolate DNA
Mononucleosomes:
3'
(TTAGGG)n 3'
Dinucleosomes:
(TTAGGG)n 3'
3'
Higher order oligonucleosomes
Anneal with biotin-(C3TA2)6
Pull down with streptavidin beads
Supernatant
(Bulk nucleosomes)
Pull down
(Last nucleosomes)
3'
(TTAGGG)n 3'
Fractionate on 1% agarose gel
Transfer and hybridize with telomeric probe
B
25 T2AG3 repeats
KpnI
BglII
BglII/KpnI + CIP
ds Tel
3' CATG
CTAG 5'
226 bp
+
ss TelG = 5' pGATC(T2AG3)12
T4 Ligase
Tel + overhang
GATC(T2AG3)12 3'
3' CATG
CTAG
C
1 2 3
ds Tel + + -
ss TelG + - +
T4 Ligase + + +
564
281
271
310
234
194
Tel + overhang
ds Tel
ss TelG
D
1 2
sup ppt sup ppt
564
281
271
310
234
194
Tel + overhang
ds Tel
ss TelG
E
Bulk Nucleosomes
Last Nucleosomes
[MNase] 10 20 40 80 100 125 150 300 10 20 40 80 100 125 150 300
VII
VI
V
IV
III
II
I
F
ExoI - +
Bulk Last Bulk Last
2.9 0.68
% of total TTAGGG
signal pulled down

I tested this assay for nucleosomes associated with the 3' overhang in wild type cells. The pattern of MNase digestion at the terminus largely resembled that of bulk telomeric chromatin (Figure 2.2E). Partially digested oligomers of up to 7-8 nucleosomes could be visualized. Quantitatively, after normalizing for the relative volumes loaded, the signal intensity of the DNA associated with the last nucleosome accounted for approximately 2 to 4% of the total telomeric signal at low MNase concentrations (Figure 2.3B) when the median size of the MNase products is ~0.9 kb. A maximal yield of ~3% is expected upon isolation of the terminal fragments from a 30 kb telomere digested into fragments of 1 kb. The observed yield in the last nucleosome assay is therefore within the expected range.

The results of additional control experiments confirmed the specificity of the assay for the 3' overhang. When DNA fragments recovered from MNase digestion were treated with the *E. coli* 3' to 5' exonuclease ExoI prior to annealing with the biotinylated oligonucleotide, the percentage of total telomeric signal pulled down by the assay decreased by 50 to 70% (Figure 2.2F). Furthermore, when the assay was performed with a biotin-$(TTAGGG)_6$ oligonucleotide instead of the C-rich oligonucleotide, and the telomeric signal was probed with $[^{32}P](TTAGGG)_4$, no telomeric signal was detected in the pull down.

Finally, I applied the last nucleosome assay to a setting in which telomeres become fused and are therefore expected to lose their 3' overhang. For this control, I used Cre-mediated deletion of TRF2 from DNA ligase IV proficient cells, focusing on a late time point when ~30% of chromosome ends have undergone NHEJ[193]. TRF2 deletion from these cells resulted in a 20 to 40% reduction in the percentage of total telomeric

signal pulled down in the last nucleosome assay compared to the percentage for the control (Figure 2.3A-B). The difference between Cre-infected cells and the controls became less pronounced with increasing MNase concentration (Figure 2.3B), suggesting that the optimal range for interpreting results from the last nucleosome assay was at MNase concentrations less than 80 U/ml.

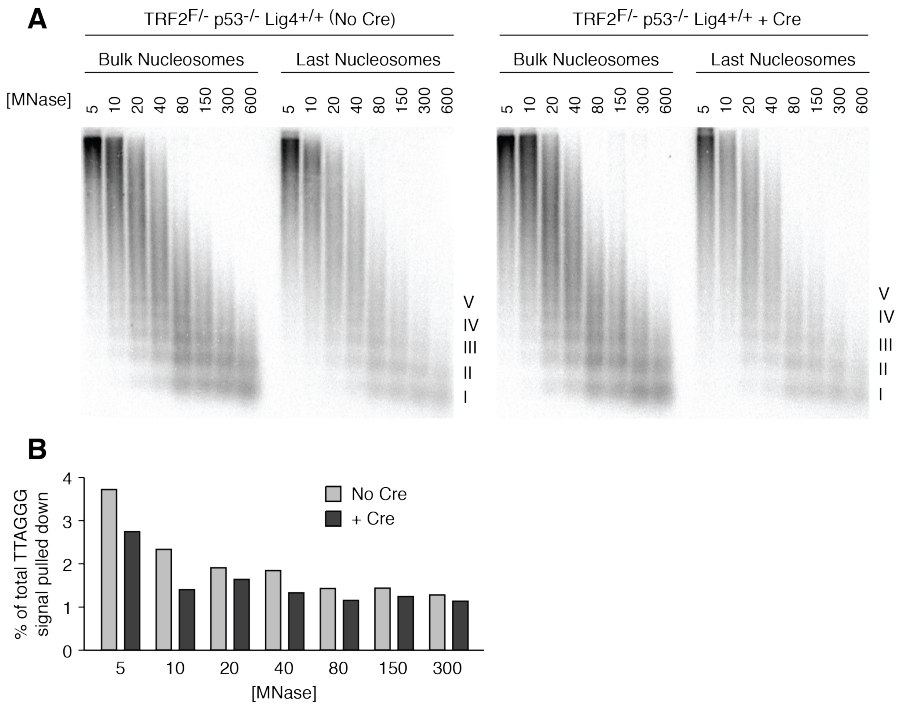

Figure 2.3. Telomere fusion reduces the signal in the last nucleosome assay. (A) MNase sensitivity of bulk and last telomeric nucleosomes assessed by the last nucleosomal assay, performed as previously described in *TRF2$^{F/-}$p53$^{-/-}$Lig4$^{+/+}$* cells not infected with Cre (top) or at 120 hrs following Cre-mediated TRF2 deletion (bottom). MNase concentrations are given as U/ml. (B) Quantitation of the percentage of total TTAGGG signal pulled down in (A).

Deletion of TRF2 does not disrupt the organization of telomeric chromatin or result in overt nucleosome eviction

To explore the possibility of chromatin remodeling at telomeres in the setting of ATM kinase activation, I first examined bulk telomeric nucleosomes following Cre-mediated deletion of TRF2 in *TRF2$^{F/-}$p53$^{-/-}$Lig4$^{-/-}$* MEFs. Due to the absence of p53 and

DNA ligase IV, these cells do not undergo cell cycle arrest nor do they accumulate telomeric fusions, thus allowing the assessment of the nucleosomal organization of free dysfunctional telomeres. Nucleosomal chromatin was examined in this and other experiments by digesting nuclei with MNase. Cells were harvested at 90 hr after Cre infection, and immunoblots confirmed the loss of TRF2 and its interacting partner Rap1 (Figure 2.4A). Furthermore, as expected, the cells showed evidence of ATM kinase signaling based on the phosphorylation of Chk2 (Figure 2.4A).

Nuclei from these cells lacking TRF2 were digested with MNase, and the resulting DNA products were fractionated on agarose gels to visualize bulk and telomeric chromatin fragments. The deletion of TRF2 resulted in no obvious change in the MNase sensitivity of bulk nucleosomes, as seen by the results of ethidium bromide staining (Figure 2.4B). In cells with and without TRF2, MNase digestion generated the typical nucleosomal ladder with regular periodicity. DNA fragments representing partial digestion products of up to 7-8 nucleosomes were seen at low MNase concentrations. In comparison to bulk nucleosomes, telomeric nucleosomes showed a more diffuse ladder of oligonucleosomes (Figure 2.4C), as reported previously[57]. However, when wild type and TRF2-deficient cells were compared, no obvious difference in the sensitivity of telomeric chromatin to MNase was observed. The telomeric chromatin maintained the same nucleosomal periodicity in the presence and absence of TRF2. Furthermore, in both cases, the formation of partial products correlated similarly with the MNase concentration, suggesting no difference in the rate of MNase digestion of the dysfunctional telomeres.

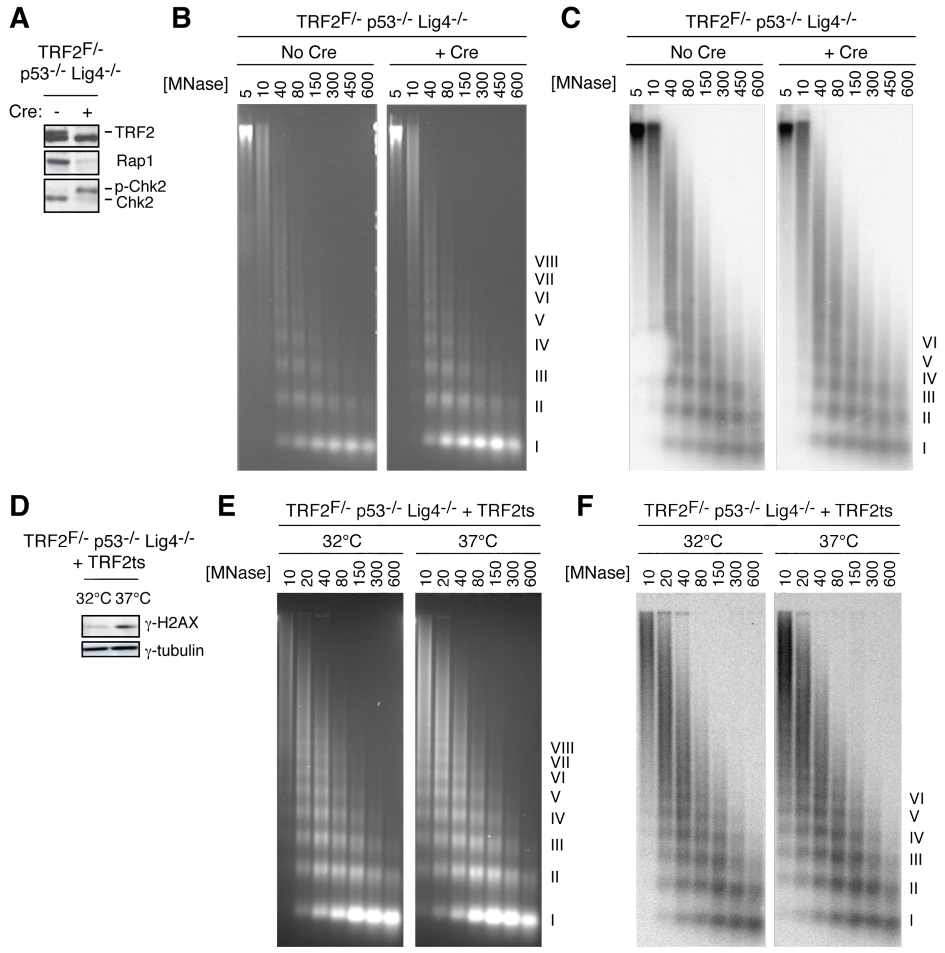

Figure 2.4. No disruption of telomeric chromatin after TRF2 depletion. (A) Immunoblot confirming loss of TRF2 and Rap1, and phosphorylation of Chk2 at 90h after retroviral-mediated Hit&Run-Cre expression in *TRF2$^{F/-}$p53$^{-/-}$Lig4$^{-/-}$* MEFs. The non-specific band on the TRF2 blot served as a loading control. (B) Bulk nucleosomes in cells with and without TRF2 detected by ethidium bromide staining of DNA from nuclei digested with MNase and fractionated on a 1% agarose gel. (C) Telomeric nucleosomes detected by Southern blot hybridization with a [^{32}P](CCCTAA)$_4$ probe. Roman numerals represent oligonucleosomes formed by partial digestion. (D) Immunoblot for γ-H2AX, confirming activation of DNA damage signaling after 6 h shift of TRF2ts cells from the permissive temperature (32°C) to the non-permissive temperature (37°C). γ-tubulin is shown as a loading control. (E) Bulk nucleosomes in cells with and without TRF2 detected by ethidium bromide staining of DNA from nuclei digested with MNase and electrophoresed on a 1% agarose gel. (F) Telomeric nucleosomes detected by Southern blot hybridization with a [^{32}P](CCCTAA)$_4$ probe. MNase concentrations are given as U/ml. Roman numerals represent oligonucleosomes formed by partial digestion.

While Cre-mediated deletion of TRF2 requires several days before the consequences of telomere dysfunction can be assayed, a recently characterized temperature-sensitive allele of TRF2 allowed me to examine chromatin organization within a shorter time frame after telomere deprotection[197]. The TRF2ts allele has a point

mutation in the Myb/SANT DNA binding domain (I468A in mouse TRF2) that affects the ability of TRF2 to stably associate with telomeric DNA at the non-permissive temperature. A DNA ligase IV-deficient cell line carrying TRF2ts was generated by expressing the mouse TRF2ts allele in *TRF2*$^{F/-}$*p53*$^{-/-}$*Lig4*$^{-/-}$ MEFs and removing the endogenous TRF2 through Cre-mediated deletion[197]. These cells retain telomere protection at 32°C, while incubation at 37°C dislodges TRF2ts from telomeres, leading to a telomere damage response within hours. I compared the MNase sensitivity of telomeric chromatin in TRF2ts cells growing at 32°C to that of cells shifted to 37°C for 3 or 6 h. Immunoblotting confirmed that the temperature shift induced γ-H2AX at 6 h (Figure 2.4D). Consistent with the data obtained after Cre-mediated deletion of TRF2, the MNase digestion patterns of telomeric chromatin remained unchanged within 3-6 h after removal of TRF2ts from telomeres (Figure 2.4E-F). Thus, there is no overt alteration in the nucleosomal structure of dysfunctional telomeres despite ongoing ATM kinase signaling.

Since the 3' overhang remains intact following deletion of TRF2 in cells deficient for DNA ligase IV[193], the assay for the last nucleosome could be used to examine whether terminal nucleosomes are evicted following telomere deprotection in this setting. Thus, I isolated the DNA fragments associated with the last nucleosome in *TRF2*$^{F/-}$*p53*$^{-/-}$*Lig4*$^{-/-}$ MEFs infected with Cre. Whereas degradation of the overhang would decrease the yield of the terminal DNA, thereby reducing the signal intensity of the ladder representing the last nucleosomes, Iobserved no change in the signal intensity of last nucleosomal DNA from cells infected with Cre compared to those that were uninfected (Figure 2.5A). Upon longer exposure, the signal due to the last nucleosome appeared similar with and without

TRF2 and quantification indicated a comparable percentage of total telomeric signal pulled down by the assay in both cases (Figure 2.5B). Furthermore, no significant shift in the last nucleosome was observed, further supporting the absence of nucleosome eviction from telomere ends lacking TRF2.

I further assayed the MNase sensitivity of the last nucleosome following telomere deprotection in the TRF2ts system. After 6 h of incubation at 37°C, there was no change in the MNase digestion pattern in the last nucleosome compared to that in cells maintained at the permissive temperature (Figure 2.5C). The relative telomeric signal pulled down by the assay also remained roughly similar before and after removal of TRF2 (Figure 2.5D).

Deletion of POT1a and –b leads to increased MNase susceptibility of the overhang, but no overt nucleosome eviction

Next, I evaluated nucleosomal organization at telomeres deprotected by POT1 deletion to determine whether chromatin remodeling accompanies activation of the ATR kinase. The introduction of Cre into $POT1a^{STOP/FLOX}POT1b^{STOP/FLOX}$ MEFs resulted in the expected loss of both POT1a and POT1b proteins, as confirmed by immunoblots (Figure 2.6A). The loss of the POT1 proteins did not affect the MNase sensitivity of the bulk nucleosomes (Figure 2.6B) or the telomeric nucleosomes (Figure 2.6B-C). Furthermore, similar to the result with TRF2, deletion of both POT1 genes or either POT1a or POT1b alone also did not lead to an obvious change in MNase digestion patterns (Figure 2.6D-E).

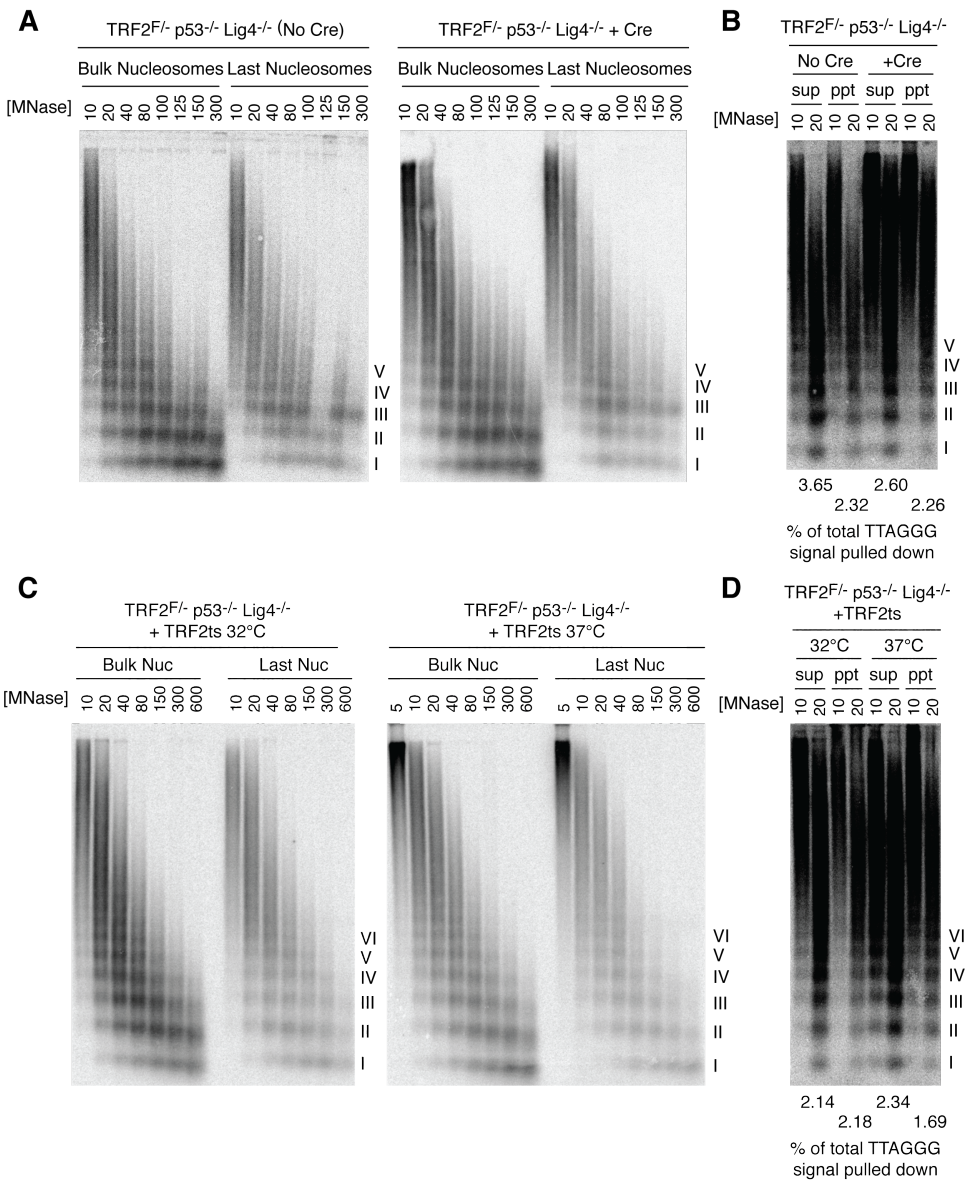

Figure 2.5. No eviction of terminal nucleosomes following TRF2 depletion. MNase sensitivity of bulk and last telomeric nucleosomes assessed by the last nucleosomal assay in (A) *TRF2$^{F/-}$p53$^{-/-}$Lig4$^{-/-}$* cells not infected with Cre (left) or at 90 hrs following Cre-mediated TRF2 deletion (right) and (C) TRF2ts cells at 32°C (left) or after 6 hours of incubation at 37°C (right). MNase concentrations are given as U/ml. Roman numerals represent oligonucleosomes formed by partial digestion. (B) and (D) Longer exposure of the telomere blots for the last nucleosome assay in TRF2-deficient cells by Cre-mediated deletion or temperature shift, respectively, with 4% of total supernatant and 100% of total pull down loaded onto the gel. Quantitation of the percentage of total TTAGGG signal pulled down is provided below the blot. Percent of total TTAGGG signal pulled down was calculated by the equation: (pulled down signal) / (pulled down signal + 25 x supernatant signal).

I next determined whether the DNA damage response associated with POT1 deficiency involves nucleosome eviction from the chromosome end. Although POT1 DKO cells show a two- to three-fold excess of single-stranded overhang signal, the amount of single-stranded telomeric signal in the fragments recovered after MNase digestion was comparable to that from control cells following the same treatment (Figure 2.1B). This suggested that MNase digestion of POT1 DKO nuclei led to some degradation of the excess single-stranded DNA, although the last nucleosome assay could still be used to detect chromatin organization at the telomere ends with intact overhangs.

I used the last nucleosome assay to compare the MNase digestion pattern of the last nucleosomes in Cre-infected *POT1a*$^{STOP/FLOX}$*POT1b*$^{STOP/FLOX}$ cells to that in vector-infected control cells. First, I found that the percentage of total telomeric signal pulled down in POT1 DKO cells was significantly less than that in control cells, corroborating the data showing that some of the overhangs were degraded (Figure 2.7A). However, POT1 deletion did not significantly alter the MNase pattern of the detectable last nucleosomes (Figure 2.7B). Partial digestion products representing 6 to 7 nucleosomes from the chromosome end were seen in cells with and without POT1a and -b. Furthermore, deletion of either POT1a or POT1b alone also did not affect the MNase digestion pattern of the terminal nucleosomes (Figure 2.7C,E). In addition, deletion of POT1b led to no change in the fraction of last nucleosomal fragments pulled down in the assay (Figure 2.7D,F). On the other hand, deletion of POT1a alone resulted in a reduction in the percentage of total telomeric signal pulled down, suggesting some degradation of the single-stranded overhang by MNase (Figure 2.7E-F).

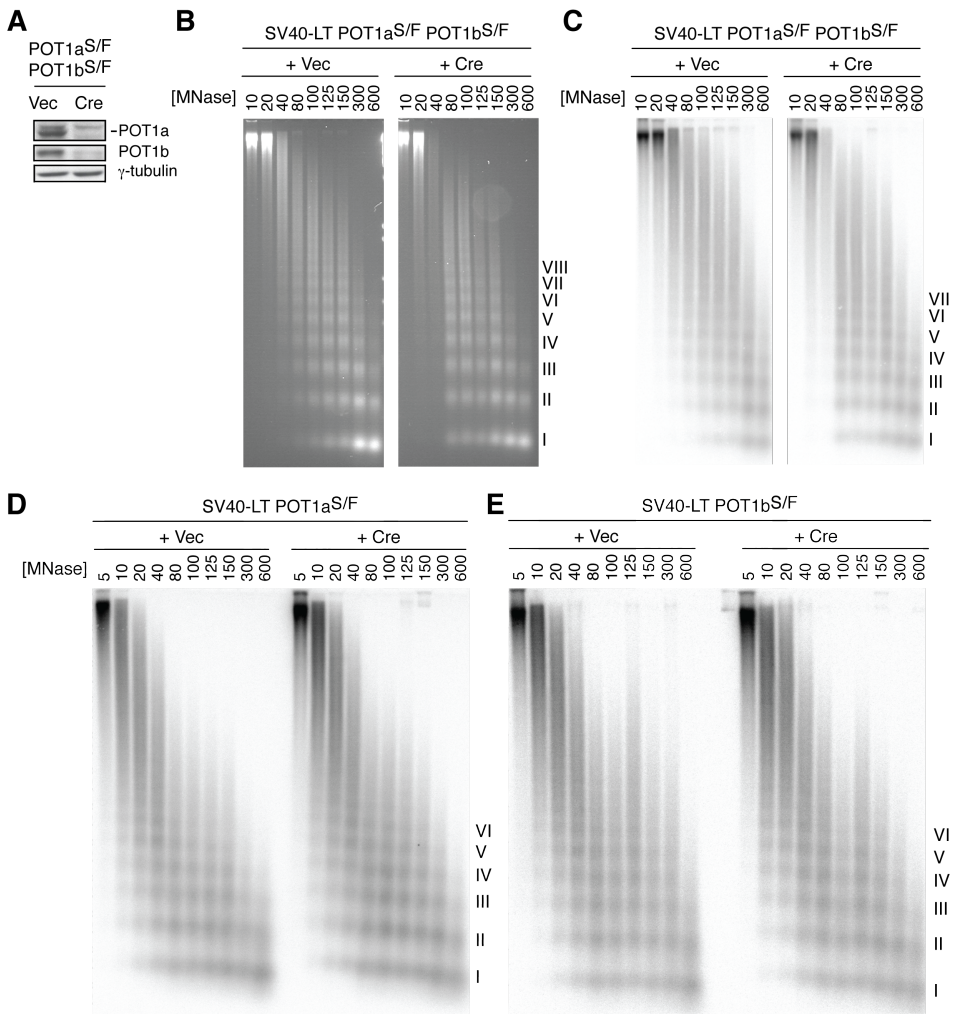

Figure 2.6. No disruption of telomeric chromatin after deletion of POT1a and POT1b. (A) Immunoblot confirming deletion of POT1a and POT1b after retroviral infection of *POT1a*$^{S/F}$*POT1b*$^{S/F}$ cells with pWzl-Cre followed by 5 days selection with hygromycin. γ-tubulin is shown as a loading control. (B) Bulk nucleosomes in cells with and without POT1a and -b detected by ethidium bromide staining of DNA from nuclei digested with MNase and fractionated on 1% agarose gels. (C) Telomeric nucleosomes detected by Southern blot hybridization with a [^{32}P](CCCTAA)$_4$ probe. Roman numerals represent oligonucleosomes formed by partial digestion. Southern blot detection of telomeric nucleosomes by hybridization of a [^{32}P](CCCTAA)$_4$ probe to DNA fragments isolated and fractionated following MNase digestion of nuclei in (D) *POT1a*$^{S/F}$ cells infected with pWzl vector or pWzl-Cre at 5 days post-selection with hygromycin and (E) *POT1b*$^{S/F}$ cells infected with pWzl vector or pWzl-Cre at 5 days post-selection with hygromycin. MNase concentrations are given as U/mL. Roman numerals represent oligonucleosomes formed by partial digestion.

TRF2 deletion in Ku-deficient cells does not affect nucleosome organization, while deletion of POT1 and Ku leads to increased MNase susceptibility of the overhang.

Since nucleosome displacement appears particularly important in DSB repair by homology directed repair[399,400,402], I further explored the possibility that nucleosome eviction occurs in the absence of factors that protect telomeres from HDR. Recombination between sister telomeres is frequent in cells that lack both Ku70 and TRF2[198] and increased T-SCEs have been observed in cells triply deficient in Ku70, and both POT1a and POT1b[39]. Therefore, I examined the MNase digestion pattern of bulk telomeric chromatin as well as that of the last nucleosomes, in cells deficient in Ku70 and either TRF2 or POT1a and -b. Ku70 deficiency alone led to a typical MNase digestion pattern of the bulk and last nucleosomes (Figure 2.8A and C, left panels). Further removal of TRF2 did not alter the MNase digestion pattern of either the bulk telomeric chromatin or terminal nucleosomes (Figure 2.8A, right panel). Furthermore, there was no change in the signal intensity of the MNase digestion ladder for the last nucleosomes, indicating no degradation of the overhang (Figure 2.8B). On the other hand, deletion of POT1a and -b in Ku deficient cells did not affect the MNase digestion pattern of the telomeric nucleosomes but reduced the percentage of total telomeric signal that could be isolated with the last nucleosome assay, suggesting an increased susceptibility of the overhang to MNase (Figure 2.8C-D). The results seen in the absence of POT1 and Ku appeared similar to those observed with POT1 deletion alone.

Figure 2.7. No eviction of terminal nucleosomes following POT1a and POT1b deletion. MNase sensitivity of bulk and last telomeric nucleosomes assessed by the last nucleosomal assay in (A) POT1aS/F POT1bS/F cells infected with pWzl vector (left) or pWzl-Cre (right) at 5 days post-selection with hygromycin. MNase concentrations are given as U/ml. MNase sensitivity of bulk and last telomeric nucleosomes assessed by the last nucleosomal assay in (A) POT1a$^{S/F}$ cells infected with pWzl vector (left) or pWzl-Cre (right) at 5 days post-selection with hygromycin and C) POT1b$^{S/F}$ cells infected with pWzl vector (left) or pWzl-Cre (right) at 5 days post-selection with hygromycin. MNase concentrations are given as U/mL. Roman numerals represent oligonucleosomes formed by partial digestion. (B) and (D) Longer exposure of the telomere blots for the last nucleosome assay in POT1a and POT1b deleted cells, respectively, with 4% of total supernatant and 100% of total pull down loaded onto the gel. Quantitation of the percentage of total TTAGGG signal pulled down is provided below the blot. Roman numerals represent oligonucleosomes formed by partial digestion. (B) Longer exposure of the telomere blots for the last nucleosome assay in POT1-deleted cells, respectively, with 4% of total supernatant and 100% of total pull down loaded onto the gel. Quantitation of the percentage of total TTAGGG signal pulled down is provided below the blot. Percent of total TTAGGG signal pulled down was calculated by the equation: (pulled down signal) / (pulled down signal + 25 x supernatant signal).

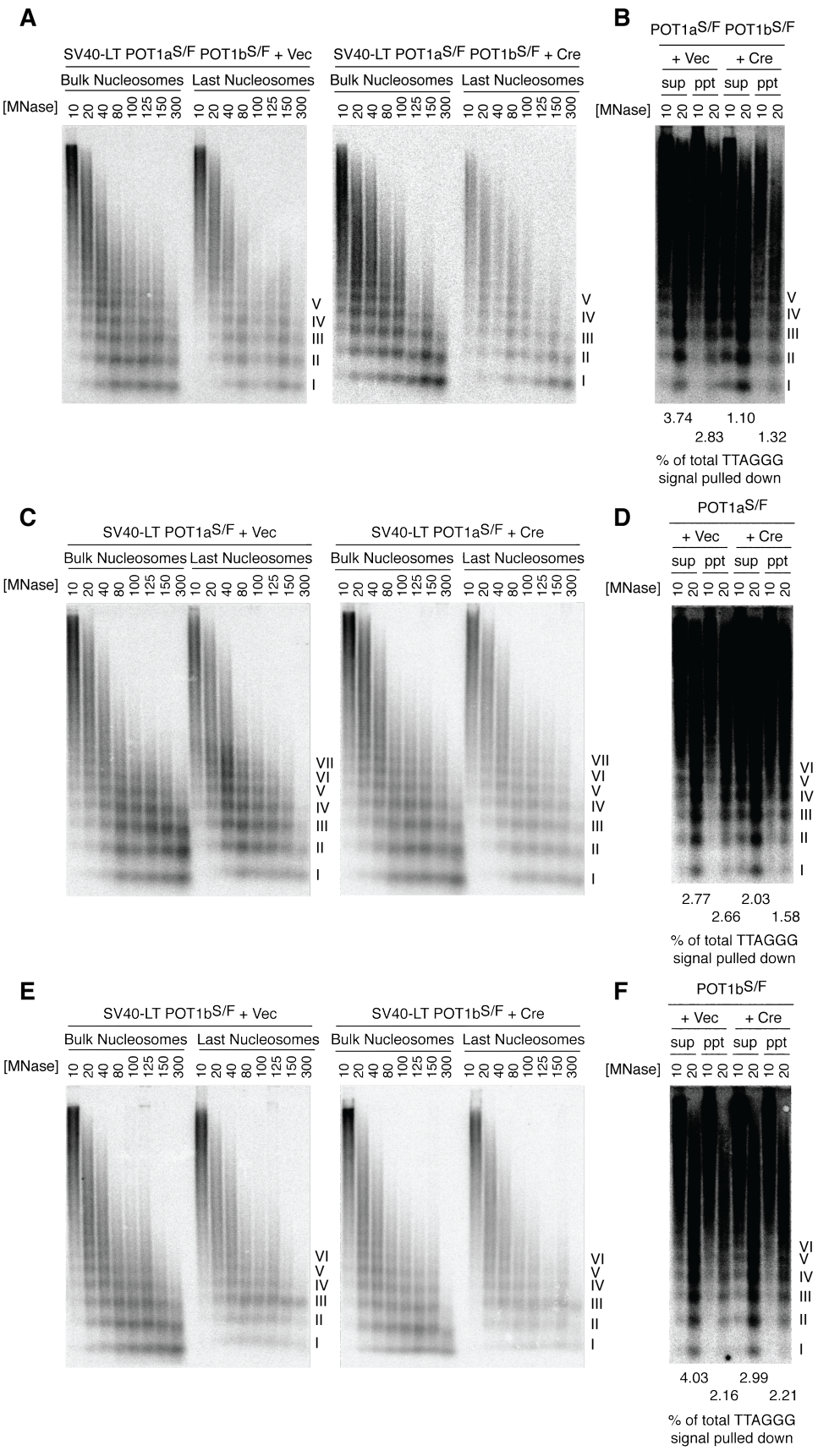
A
SV40-LT POT1a$^{S/F}$ POT1b$^{S/F}$ + Vec
SV40-LT POT1a$^{S/F}$ POT1b$^{S/F}$ + Cre
Bulk Nucleosomes
Last Nucleosomes
[MNase]
10 20 40 80 100 125 150 300
V IV III II I
B
POT1a$^{S/F}$ POT1b$^{S/F}$
+ Vec
+ Cre
sup ppt sup ppt
[MNase]
10 20 10 20 10 20 10 20
V IV III II I
3.74 1.10
2.83 1.32
% of total TTAGGG signal pulled down
C
SV40-LT POT1a$^{S/F}$ + Vec
SV40-LT POT1a$^{S/F}$ + Cre
Bulk Nucleosomes
Last Nucleosomes
[MNase]
10 20 40 80 100 125 150 300
VII VI V IV III II I
D
POT1a$^{S/F}$
+ Vec
+ Cre
sup ppt sup ppt
[MNase]
10 20 10 20 10 20 10 20
VI V IV III II I
2.77 2.03
2.66 1.58
% of total TTAGGG signal pulled down
E
SV40-LT POT1b$^{S/F}$ + Vec
SV40-LT POT1b$^{S/F}$ + Cre
Bulk Nucleosomes
Last Nucleosomes
[MNase]
10 20 40 80 100 125 150 300
VI V IV III II I
F
POT1b$^{S/F}$
+ Vec
+ Cre
sup ppt sup ppt
[MNase]
10 20 10 20 10 20 10 20
VI V IV III II I
4.03 2.99
2.16 2.21
% of total TTAGGG signal pulled down

SUMMARY OF FINDINGS

The results described in this chapter suggest that the telomeric terminus in mammalian cells is organized in a protected chromatin state that resists digestion when nuclei are treated with MNase. I found that MNase treatment left the single-stranded overhang largely intact in wild type and TRF2-deficient cells but led to some degradation following deletion of POT1a or POT1a and –b. The absence of the NHEJ factor Ku70 did not affect the protection of the overhang from MNase. As MNase rapidly degrades the single-stranded telomeric DNA in naked DNA, the results suggest that POT1 proteins, in particular POT1a, block MNase from digesting the telomeric overhang in chromatin. Nevertheless, even in POT1a-deficient cells, DNA fragments recovered after MNase digestion retained a significant fraction of the overhang, suggesting an alternative mode of protection, potentially involved other single-stranded DNA binding proteins, such as replication protein A, or the strand invasion of the overhang into duplex telomeric DNA as it occurs in the t-loop.

My results revealed that the organization of terminal nucleosomes in wild type cells resembles that of bulk telomeric chromatin. The results of previous work have shown that short telomeres yield a more diffuse MNase pattern than long telomeres, which led to the proposal that telomere ends may exhibit an unusual chromatin organization that would appear more prominently in cells with short telomeres[57]. However, this previous study did not examine the terminal telomeric chromatin directly. Alternative explanations for the altered chromatin of short telomeres may be a difference in shelterin loading or a change in the histone modification state of shorter versus longer telomeres[61-63].

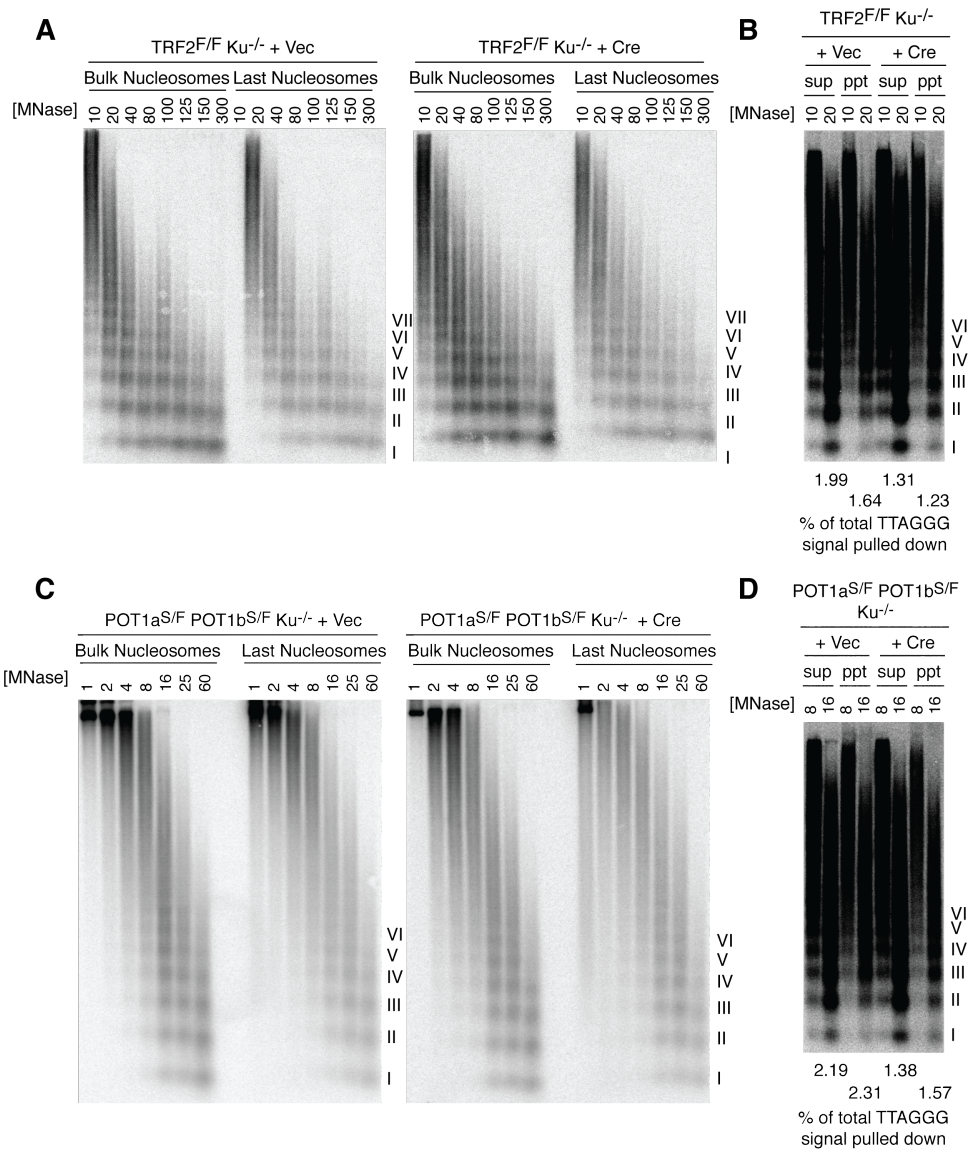

Figure 2.8. No eviction of terminal nucleosomes in cells doubly deficient for Ku70 and TRF2 or POT1a and -b. MNase sensitivity of bulk and last telomeric nucleosomes in (A) *TRF2$^{F/-}$Ku$^{-/-}$* cells without Cre infection (left) or at 96 hr after Cre-mediated TRF2 deletion (right) and (C) *POT1a$^{S/F}$POT1b$^{S/F}$Ku$^{-/-}$* cells not infected with Cre (left) or at 96 hr after Cre (right). MNase concentrations are given as U/ml. Roman numerals represent oligonucleosomes formed by partial digestion. (B) and (D) High exposure of the telomere blots for the last nucleosome assay in TRF2/Ku-deficient and POT1/Ku-deficient cells, respectively, with 4% of total supernatant and 100% of total pull down loaded onto the gel. Quantitation of the percentage of total TTAGGG signal pulled down is provided below the blot.

The results of my studies on cells with deprotected telomeres suggest that a number of DNA damage signaling and repair pathways can occur at damaged telomeres without detectable changes in the organization of the bulk telomeric chromatin or overt

nucleosome eviction. The absence of any observable change in the sensitivity of telomeric chromatin to MNase following the conditional deletion of shelterin components demonstrates that damaged telomeres retain their nucleosomal organization while eliciting an ongoing DNA damage signal. Specifically, since no overt chromatin remodeling occurs at either bulk or terminal telomeric nucleosomes at timepoints when TIFs have previously been observed[37,193], the maintenance of the DNA damage signal at dysfunctional telomeres, as evident from the phosphorylation of H2AX and the recruitment of 53BP1, does not appear to require persistent nucleosome eviction.

Importantly, my work contributes to an understanding of the mechanisms by which the sensing of DNA damage and subsequent activation of ATM signaling occur at dysfunctional telomeres. The Mre11/Rad50/Nbs1 complex has been implicated as a DNA damage sensor that promotes ATM activity[142], but the molecular event sensed by the Mre11 complex remains undefined. It has been suggested that chromatin changes directly activate ATM, based on the results of studies in which ATM activation occurred in the presence of chromatin relaxation without DSBs[397]. In contrast, the absence of changes in telomeric chromatin following the deletion of TRF2 excludes the requirement of nucleosome eviction for DNA damage sensing and signaling by ATM at damaged telomeres.

My results further suggest that signaling through the ATR pathway can also occur without overt nucleosome eviction, since cells lacking POT1a and POT1b, which accumulate ATR-dependent TIFs, maintain their nucleosomal organization at the telomeres. In POT1a and –b DKO and POT1a knockout cells, MNase degraded some, but not all, of the single-stranded overhang and hindered the isolation of the last

nucleosomal DNA. Nonetheless, the assay retrieved a fraction of ends, whose chromatin organization appeared unchanged following POT1 deletion. In cases where MNase significantly degrades the single-stranded overhang, it remains a possibility that my assay detects a subset of terminal nucleosomes that maintain protection and are not involved in the DNA damage signaling or repair processes.

Finally, my results suggest that NHEJ and HDR at damaged telomeres do not require nucleosome eviction, since the telomeric chromatin did not show obvious changes in settings that make telomeres highly susceptible to these repair pathways. It is interesting that no chromatin rearrangements were observed under conditions where T-SCEs occur, since nucleosome displacement has been posited to be particularly important for HDR[399,400,402].

What accounts for the finding that damaged telomeres do not appear to experience nucleosome eviction whereas DSBs elsewhere in the genome undergo extensive chromatin remodeling? One explanation may be that the kinetics of DNA damage signaling and repair processes at damaged telomeres differ from those found in other models of the response to DSBs. In my system, distinct steps in signaling by ATM or ATR and in repair by NHEJ or HDR may indeed involve nucleosome displacement at damaged telomeres, but may occur transiently or too early to be detected by these methods. The results of my studies using the TRF2ts allele, which allows the assessment of chromatin organization within a shorter time frame, argue against the likelihood of this explanation, since I demonstrate the absence of nucleosome eviction as early as 3 to 6 h after the removal of TRF2. Alternatively, nucleosome rearrangement may not be required at chromosome ends lacking TRF2 or POT1 because intrinsic properties of

telomeric chromatin render it more accessible to DNA damage factors. For instance, the shelterin component TRF1, which can bind telomeric DNA within a nucleosomal context, has been shown to modulate nucleosome structure[411]. It is also interesting to note that nucleosomes assembled on telomeric sequences under physiologic conditions appear intrinsically more mobile than those assembled on average DNA[412] and that the telomeric core particles appear highly sensitive to nucleases. Perhaps these unusual features of telomeric nucleosomes obviate the need for chromatin remodeling, permitting access to DNA repair and signaling factors in the native telomeric chromatin state. Such a model would be consistent with the view that numerous DNA repair factors are present at telomeres, where they presumably act to promote the protective function of telomeres.

The finding that telomeric chromatin does not undergo remodeling in the presence of a persistent and robust DNA damage signal has implications for how shelterin protects the telomere. It has previously been proposed that shelterin may create an alternative nucleosomal organization that prevents the end from being recognized as a DSB. My findings argue against this possibility, as there appears to be no difference between the organization of telomeric chromatin in protected and deprotected states. Nonetheless, these results do not preclude contributions of chromatin remodeling and modifications to shelterin function in other ways that remain to be elucidated.

CHAPTER 3:

THE ROLE OF THE SHELTERIN-ASSOCIATED NUCLEASE APOLLO AT TELOMERES SYNTHESIZED BY LEADING-STRAND DNA REPLICATION

INTRODUCTION

In this chapter, I investigated the role of the TRF2-associated nuclease Apollo in overhang generation. It had been previously proposed that TRF2 recruits a nuclease required for overhang generation and protection of newly synthesized leading-end telomeres[194,195,204]. Apollo was an attractive candidate based on previous work showing that its depletion in human cells activates a DNA damage response at telomeres in S phase[51].

Apollo belongs to the mammalian SNM1/Pso2 family of nucleases, which also includes SNM1A and Artemis/SNM1C. SNM1A contributes to the repair of DNA interstrand crosslinks (ICLs)[413,414], lesions that block DNA replication and transcription (reviewed in [415]). Similarly, knockdown of Apollo/SNM1B in human cells results in hypersensitivity to ICL-inducing agents[413,416]. In contrast, Artemis/SNM1C functions as an endonuclease to remove hairpins from coding ends during V(D)J recombination[174,337,375] and has been suggested to contribute to HDR and NHEJ of a subset of DSBs by removing structures that block repair reactions[376,417,418]. Apollo is the only member of the SNM1/Pso2 family known to function as a shelterin accessory factor. Here, the function of mouse Apollo was determined using Cre-mediated gene deletion, complementation with Apollo mutants, and the TRF2-F120A mutant that cannot bind Apollo.

RESULTS

Conditional gene deletion of Apollo in mouse embryonic fibroblasts

A conditional gene deletion system was developed using gene targeting to modify the mouse Apollo gene (*Dclre1b*, chr. 3), yielding a floxed allele ($Apollo^{F}$) that contained loxP Cre recombinase target sites flanking exons 2 and 3 (generated by S. Rooney, Figure 3.1A). Deletion of exons 2 and 3 is predicted to result in out-of-frame splicing of exon 1 to exon 4, interrupting the Apollo ORF at amino acid position 67. This strategy was favored over conditional deletion of exon 1, which might affect the neighboring Ap4b1 gene (Figure 3.1A). $Apollo^{F/F}$ embryos (E13.5) derived from $Apollo^{F/+}$ mouse intercrosses were used to establish SV40 large T antigen (SV40-LT) immortalized MEFs. Transient expression of Cre recombinase in these cells resulted in the expected deletion of the Apollo gene and concomitant loss of the full-length Apollo mRNA whereas the Ap4b1 transcript was not affected (Figure 3.1B,C).

Cre treatment of $Apollo^{F/F}$ MEFs resulted in a slight proliferation defect that was due to the absence of Apollo since it was largely rescued by expression of the wild type protein (Figure 3.1D). The cell cycle profile of SV40-LT $Apollo^{F/F}$ MEFs showed an elevated 4N peak due to a high basal level of tetraploid cells, which is a common phenomenon in immortalized MEFs. Cre-mediated deletion of Apollo caused a slight increase in tetraploid cells reflected in an increase in the 8N peak, but did not significantly alter the cell cycle profile or S phase index, as measured by BrdU incorporation (Figure 3.1E). Thus, deleting Apollo does not immediately block proliferation of immortalized cells, allowing the evaluation of Apollo function in these cells.

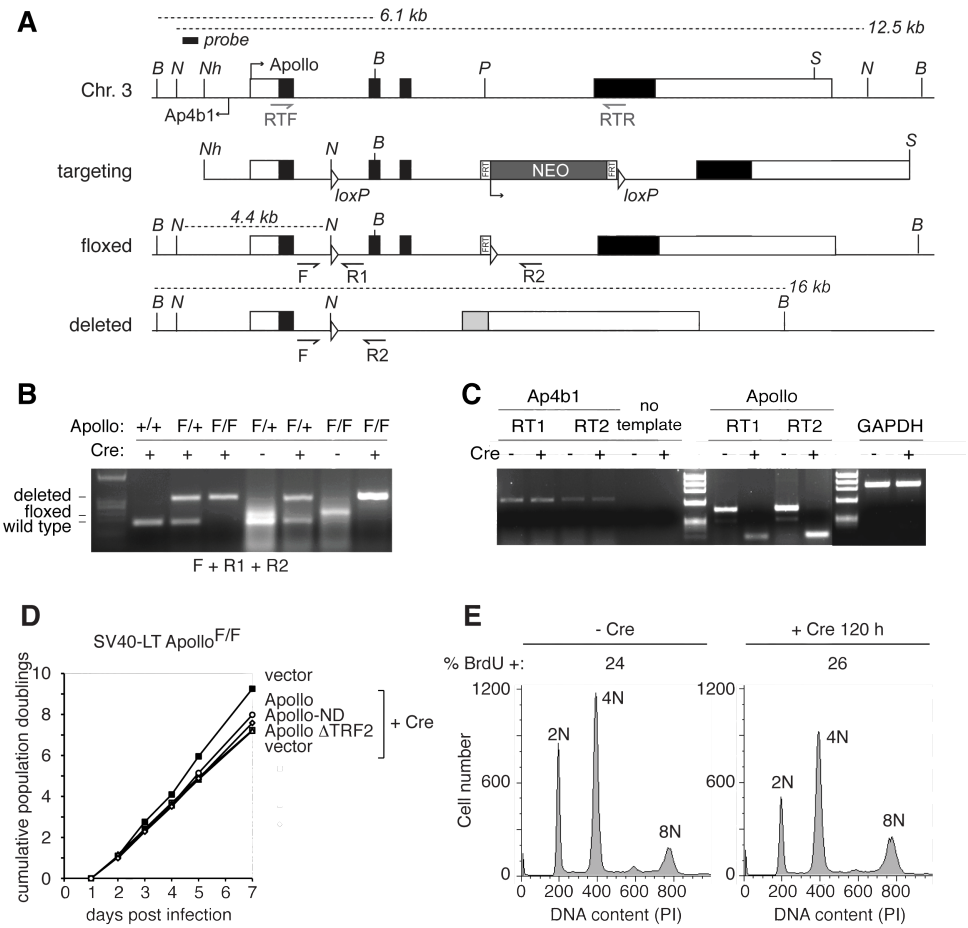

Figure 3.1. Conditional gene deletion of mouse Apollo. (A) Targeting of the mouse Apollo locus. The structure of the genomic locus, the targeting construct, the floxed allele and the deleted allele are shown. loxP sites are represented as triangles; FRT sites surrounding the neo gene are shown as rectangles. Approximate positions of the PCR primers for genomic analysis (F and R1 and R2) and RT-PCR mRNA analysis (RTF and RTR) are shown. Restriction endonucleases and the probe used for analysis of genomic DNA: *B, BamHI, N, NsiI, Nh, NheI, P, PacI, S, ScaI*. (B) Genotyping PCR for Apollo using DNA from MEFs. (C) RT-PCR with two independent sets of primers for both Apollo and Ap4b1 using RNA purified from cells treated with or without Cre. GAPDH was used as a control. (D) Growth curve of SV40LT-immortalized *Apollo*$^{F/F}$ MEFs expressing different Apollo alleles. Filled squares: vector (no cre). Open squares: vector +Cre. Open circles: Apollo +Cre. Open diamonds: Apollo-ND +Cre. Open triangles: ApolloΔTRF2 +Cre. (E) Cell cycle profile of SV40-LT *Apollo*$^{F/F}$ MEFs 120h after Cre. Cells were pulsed for 30 minutes with BrdU, fixed, and stained with PI for DNA content and FITC-anti-BrdU to determine %BrdU-positive cells.

Apollo mutants

An Apollo allele deficient for binding to telomeres (ApolloΔTRF2) was generated to assess the telomere-specific functions of Apollo (M. van Overbeek, S. Rooney, Figure 3.2A-C). Despite a previous report documenting that Apollo is unstable when not bound

to TRF2[295], mouse ApolloΔTRF2 was expressed at the same level as the wild type protein (Figure 3.2B). Deletion of the YLLTP TRF2 binding site abolished the interaction of Apollo with TRF2 and generated a protein that was incapable of accumulating at telomeres (Figure 3.2C-D).

Two nuclease-deficient alleles of Apollo were generated to evaluate whether the function of Apollo depends on its nuclease activity. The Apollo-ND allele contained mutations in the HxHxDH motif in the metallo β-lactamase domain as well as a highly conserved histidine in the β-CASP domain (M. van Overbeek, S. Rooney, Figure 3.2A-C). Both the HxHxDH motif and histidine 230 are conserved in Artemis and required for the endonucleolytic activity of this closely-related SNM1 nuclease[333,419,420]. Consistent with the preservation of the TRF2-interacting site in Apollo-ND, the nuclease-deficient protein associated with TRF2 and localized to telomeres (Figure 3.2C-D). Based on IF analysis (n>100 nuclei), both the wild type and Apollo-ND alleles were detectable at approximately half the telomeres in the cells. Since Apollo is not as abundant at telomeres as the shelterin components, it is possible that both wild type Apollo and Apollo-ND localize to all telomeres but escape detection because of their low abundance. I generated an additional nuclease-deficient allele, ApolloΔ31-37, that removes the HxHxDH motif in the metallo-β-lactamase domain and also contains the H230A mutation. This mutant was expressed at similar levels as wild type Apollo and retained its interaction with TRF2 (Figure 3.2E).

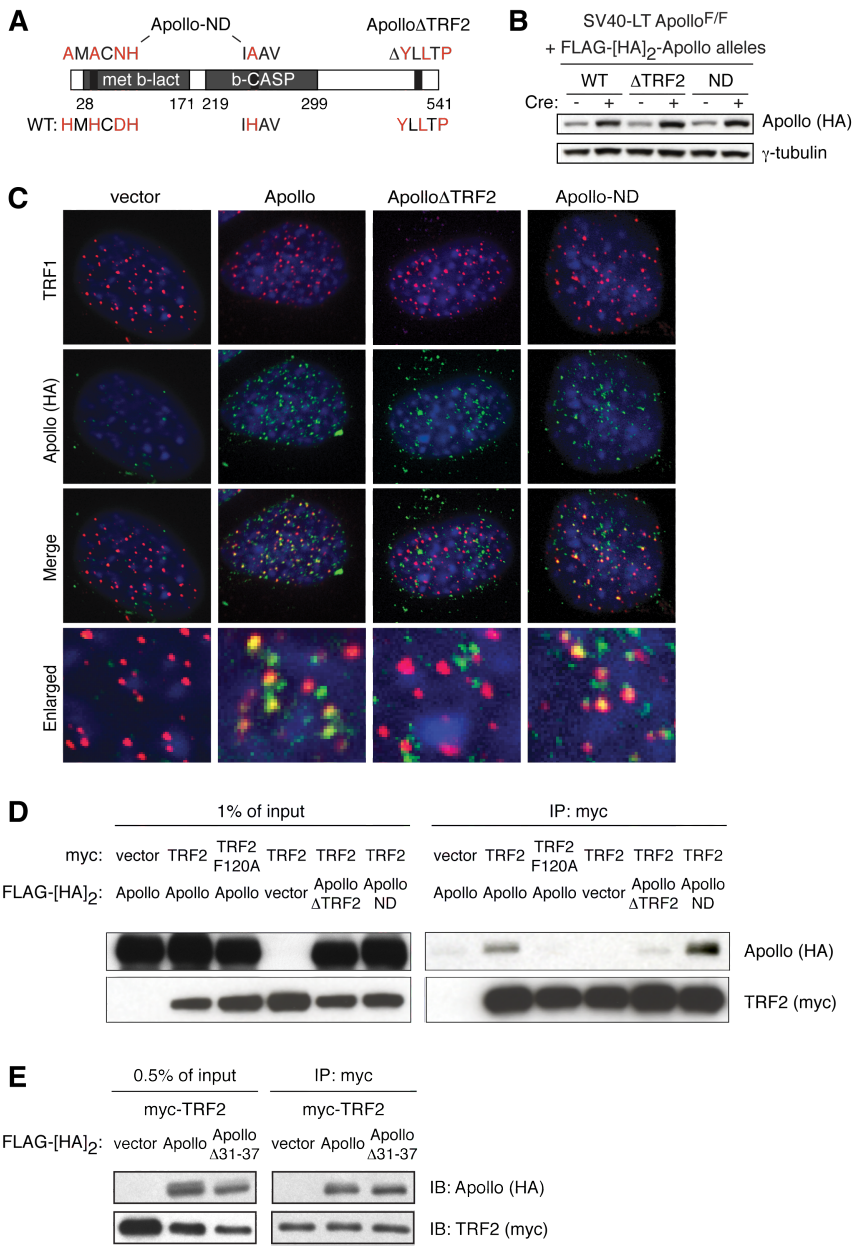

Figure 3.2. Expression and localization of Apollo mutants. (A) Schematic of the mouse Apollo protein indicating regions that are altered in Apollo rescue alleles. Amino acids in red indicate important residues for nuclease activity and TRF2 interaction. (B) Immunoblotting analysis of *Apollo*$^{F/F}$ MEFs expressing the indicated Apollo alleles in the absence of Cre and at 120h after Cre. Apollo is detected with the HA.11 antibody. (C) Immunofluorescence showing the localization of the indicated Apollo alleles (detected with HA.11 Ab) in *Apollo*$^{F/F}$ MEFs at 72h after Cre infection. Telomeric loci are detected with Ab 644 to the shelterin component TRF1. DNA is stained with DAPI. (D) Co-immunoprecipitation of Apollo and TRF2 alleles. 293T cells were transiently transfected with the indicated myc-tagged TRF2 alleles and FLAG-[HA]$_2$-tagged Apollo alleles and IPs were performed with the myc (9E10) antibody. Input (left) and IPs (right) were analyzed by immunoblotting for tagged-Apollo (HA.11, top panels) and tagged-TRF2 (myc 9B11, bottom panels). (E) Co-immunoprecipitation of ApolloΔ31-37 and TRF2. 293T cells were co-transfected with myc-TRF2 and FLAG-[HA]$_2$-tagged Apollo alleles. IPs were performed with the myc (9E10) antibody. Input (left) and IPs (right) were analyzed by immunoblotting for tagged-Apollo (HA.11, top panels) and tagged-TRF2 (myc 9B11, bottom panels).

The TRF2-F120A mutant

In an alternative approach to assess the role of Apollo at telomeres, I analyzed MEFs expressing the mouse TRF2-F120A mutant (generated by S. Kabir) containing a phenylalanine-to-alanine point mutation at amino acid 120, the conserved residue required for the interaction between human TRF2 and Apollo[44]. Co-immunoprecipitation of mouse Apollo and TRF2-F120A co-transfected in 293T cells confirmed that the F120A mutation abolished the interaction between the proteins, as previously reported for the human orthologs (Figure 3.2D).

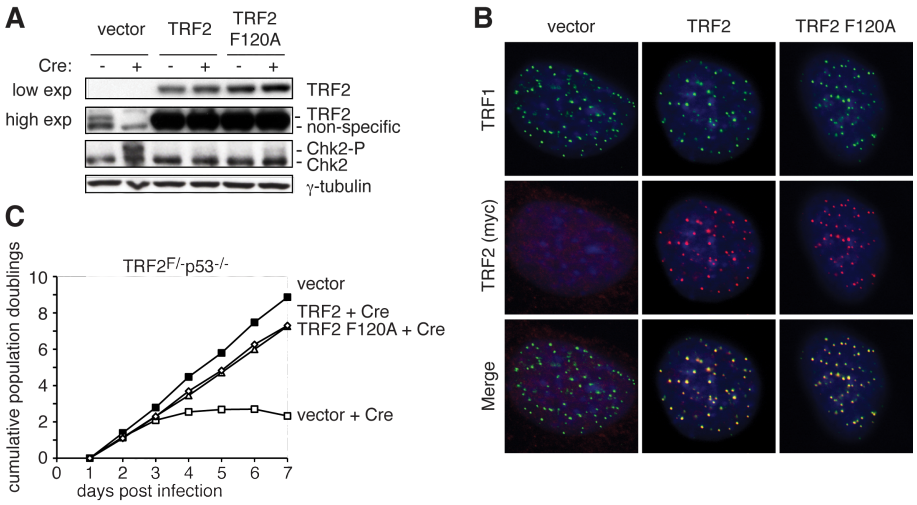

Figure 3.3. The TRF2-F120A mutant localizes to telomeres and rescues the growth defect associated with TRF2 deletion. (A) Immunoblot for TRF2 in *TRF2$^{F/-}$p53$^{-/-}$* MEFs expressing the indicated rescuing alleles without Cre and at 144 hours after Hit&Run Cre. (B) IF showing localization of TRF2 alleles in *TRF2$^{F/-}$p53$^{-/-}$* MEFs at 72h after Cre. TRF2 alleles are detected with the myc antibody 9B11. Telomeres are detected with the TRF1 antibody #644. (C) Growth curve showing cumulative population doublings after infection with Cre. Filled squares: vector (no Cre). Open squares: vector +Cre. Open circles: TRF2 +Cre. Open triangles: TRF2-F120A +Cre.

TRF2-F120A or wild type TRF2 were introduced into *TRF2$^{F/-}$p53$^{-/-}$* MEFs and the endogenous TRF2 was deleted with Cre. TRF2-F120A was overexpressed to the same level as the exogenous wild type TRF2 (Figure 3.3A) and co-localized with TRF1 at telomeres (Figure 3.3B). While cells lacking TRF2 exhibited a severe defect in

proliferation, TRF2-F120A rescued this growth defect to a similar extent as wild type TRF2 (Figure 3.3C). This result is consistent with the ability of TRF2-F120A to largely suppress the ATM-mediated DNA damage response and frequent telomere fusions associated with TRF2 deletion (discussed later).

TRF2-bound Apollo contributes to overhang generation at leading-end telomeres

To evaluate the role of Apollo in generating the proper terminal structure of telomeres, I used native in-gel hybridization to detect the telomeric overhang in cells lacking Apollo. At five days after Cre-mediated deletion of Apollo, I observed a 30-40% reduction in the relative telomeric overhang signal (Figure 3.4A-B). The overhang phenotype was rescued by full-length wild type Apollo but not by ApolloΔTRF2 or Apollo-ND (Figure 3.4A-B). Similar results were observed in cells expressing TRF2-F120A in place of endogenous TRF2. When TRF2 is deleted in MEFs, the telomeric overhang is lost due to extensive NHEJ-mediated chromosome fusions, which can be visualized as a smear of high molecular weight signal in the denatured gel. Expression of the TRF2-F120A mutant in TRF2-deficient cells suppressed the appearance of such signals in the denatured gel. However, the relative telomeric overhang signal was approximately 30% less than in the presence of wild type TRF2 (Figure 3.4C-D). As will be shown later, telomeric FISH on metaphase spreads further confirmed that TRF2-F120A represses most of the telomere fusions resulting from *TRF2* deletion (Figure 3.11C-E). Thus, the disproportionate loss in overhang signal cannot be ascribed to processing by NHEJ; more likely, the diminished overhang signal in the TRF2-F120A setting is due to the lack of recruitment of Apollo to telomeres.

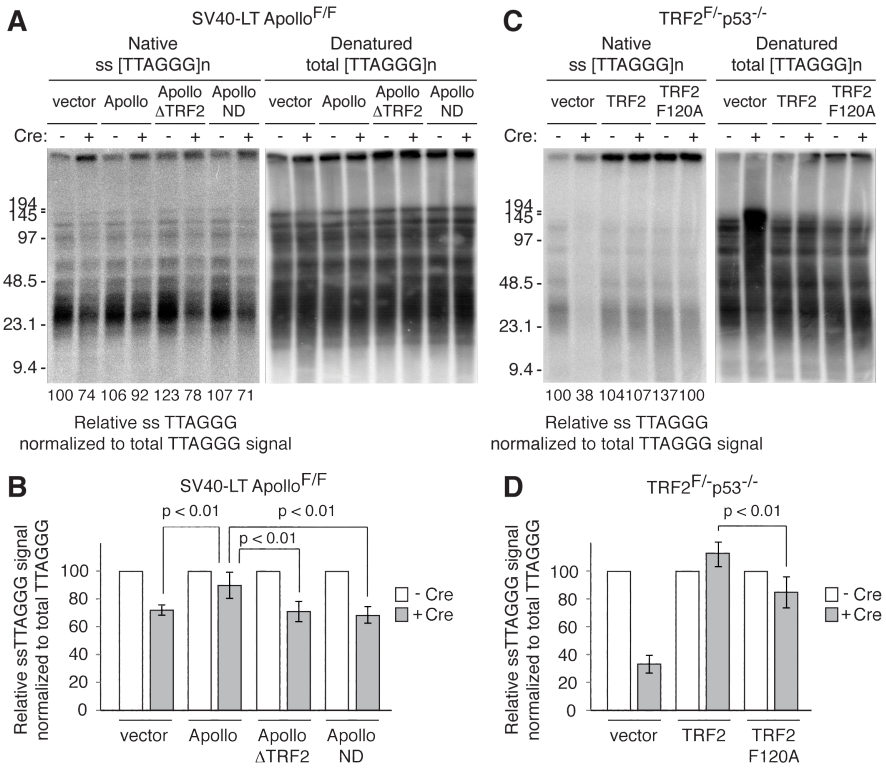

Figure 3.4. TRF2-bound Apollo maintains the telomeric overhang. (A) Representative telomeric overhang analysis of *Apollo*$^{F/F}$ MEFs expressing the indicated rescuing alleles without Cre and 120 h after pWzl-Cre infection. The single-stranded telomeric signal was determined by in-gel hybridization (left) of an end-labeled ^{32}P-(AACCCT)$_4$ telomeric oligonucleotide to native *Mbo*I-digested genomic DNA. After capture of the signal, the DNA was denatured *in situ* and the gel was rehybridized with the same probe to determine the total telomeric DNA signal (right). The single-stranded telomeric signal between ~9-100kb in each lane was normalized to the total telomeric DNA signal in the same region of that lane. (B) Quantification of relative single-stranded telomeric overhang signal with *Apollo*$^{F/F}$ MEFs. Values represent means for five independent experiments with SDs. (C) Representative telomeric overhang analysis of *TRF2*$^{F/-}$*p53*$^{-/-}$ MEFs expressing the indicated alleles without Cre and at 120h post Cre-infection, assayed as in (A). (D) Quantification of relative single-stranded telomeric signal with *TRF2*$^{F/-}$*p53*$^{-/-}$ MEFs. Values represent means for three independent experiments with SDs. For each rescuing allele (or cells infected with the empty vector) the normalized value was set at 100 for cells not treated with Cre and the post-Cre values are given as a percentage of this value. p-values were determined using paired student t-test.

In the presence of telomerase, telomeric overhangs can be elongated transiently due to the uncoupling of telomerase action, which occurs throughout S phase, and C-strand fill-in, which is delayed until late S/G2[260]. To exclude the possibility that the change in overhang signal was due to an effect of Apollo on telomerase, I generated *TRF2*$^{F/F}$*mTR*$^{-/-}$ MEFs in order to assess the phenotype of the TRF2-F120A mutant in a telomerase-deficient setting. *Apollo*$^{F/F}$ *mTR*$^{-/-}$ MEFs could not be generated due to the

proximity of the genes encoding Apollo and telomerase RNA on mouse chromosome 3. Cre treatment of SV40-LT immortalized *TRF2*$^{F/F}$*mTR*$^{-/-}$ MEFs expressing TRF2-F120A resulted in a ~30% reduction in overhang signal (Figure 3.5A-D). This result indicates that Apollo regulates the telomeric overhang in a manner independent of telomerase.

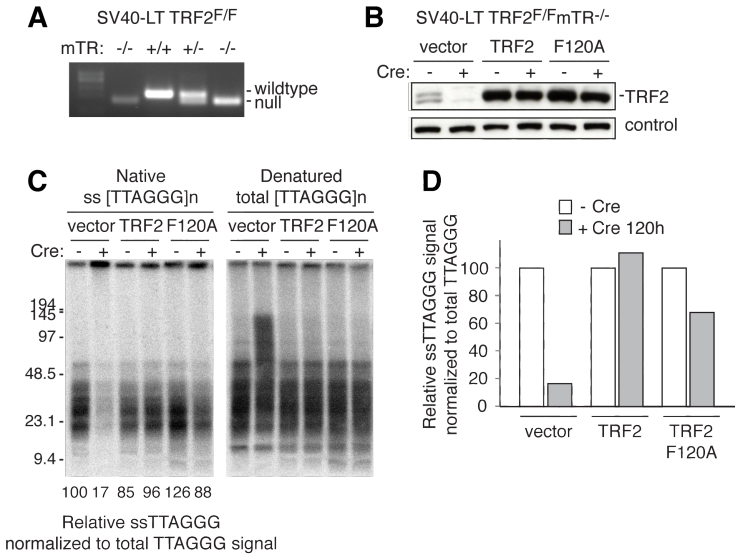

Figure 3.5. The overhang defect in cells expressing TRF2-F120A is independent of telomerase. (A) Genotyping PCR for mTR status of MEFs generated from a *TRF2*$^{F/F}$*mTR*$^{+/-}$ intercross. *TRF2*$^{F/F}$*mTR*$^{-/-}$ MEFs analyzed in the fourth lane were used in subsequent experiments. (B) Immunoblot for TRF2 in SV40-LT *TRF2*$^{F/F}$*mTR*$^{-/-}$ MEFs expressing the indicated TRF2 alleles, at 120 hours after Hit&Run Cre. (C) Representative telomeric overhang analysis of SV40-LT *TRF2*$^{F/F}$*mTR*$^{-/-}$ MEFs expressing the indicated alleles before and after Cre. The relative single-stranded signal was determined with the first lane set to 100. (D) Quantification of the telomeric overhang signal. Values represent the mean of two independent experiments. For each rescuing allele, the normalized value in the absence of Cre was set to 100.

I next analyzed the overhang signal in Apollo null cells in different phases of the cell cycle using a method for isolating G1, S, and late S/G2 cells based on the FUCCI (fluorescence ubiquitination-based cell-cycle indicator) system[421] (Figure 3.6A-D). FUCCI uses fluorescently-tagged Cdt1 (expressed in G1 and degraded in early S phase) and Geminin (expressed in S/G2 and degraded in mitosis) to mark cells in different phases of the cell cycle. With this approach, G1, S, and S/G2 populations are isolated by FACS sorting, avoiding the disadvantages of synchronizing cells with drug treatments.

For the FUCCI-sorting method, I introduced red/orange-fluorescent Cdt1 and green-fluorescent Geminin into immortalized *Apollo*$^{F/F}$ MEFs and used FACS for both Cdt1 and Geminin to select cells that had incorporated both constructs into their genomes. The cells, which were in early S phase at the time of the FACS-sorting, were re-plated and infected with Hit&Run Cre to delete *Apollo*. At 120 h after Cre, wild type and Apollo-deficient cells were harvested and sorted again by FACS to isolate Cdt1^{+}Gem^{-} G1 and Cdt1^{-}Gem^{+} late S/G2 populations, which were immediately embedded in agarose plugs to assess the telomeric overhang (Figure 3.6C). In addition, in order to collect cells in early-mid S phase, Cdt1^{+}Gem^{-} G1 cells were plated and harvested at different time points. All cells were pulsed for 30 minutes with BrdU to evaluate their S phase index.

The cell cycle profile of the Cdt1^{+}Gem^{-} cells, analyzed immediately after sorting, showed distinct 2N and 4N peaks with few cells containing intermediate DNA content (Figure 3.6D). The low percentage of BrdU-positive cells confirmed that most cells were not in S phase. Given the high incidence of tetraploid cells in the asynchronous *Apollo*$^{F/F}$ MEFs (Figure 3.1E), the 4N peak of the Cdt1^{+}Gem^{-} G1 cells likely reflects tetraploid cells in G1 rather than diploid G2 cells. Meanwhile, Cdt1^{+}Gem^{+} cells analyzed upon sorting showed a majority of cells with an intermediate DNA content between 2N and 4N or 4N and 8N, while ~80% of cells incorporated BrdU (Figure 3.6D). Thus, these cells were likely in early/mid S phase. Finally, the cell cycle profiles of Cdt1^{-}Gem^{+} cells immediately after sorting showed a large number of cells nearing either a 4N or an 8N DNA content and ~80% BrdU-positive cells (Figure 3.6D), confirming that these cells were in late S/G2. The different sorted populations exhibited similar cell cycle profiles in the presence and absence of Apollo.

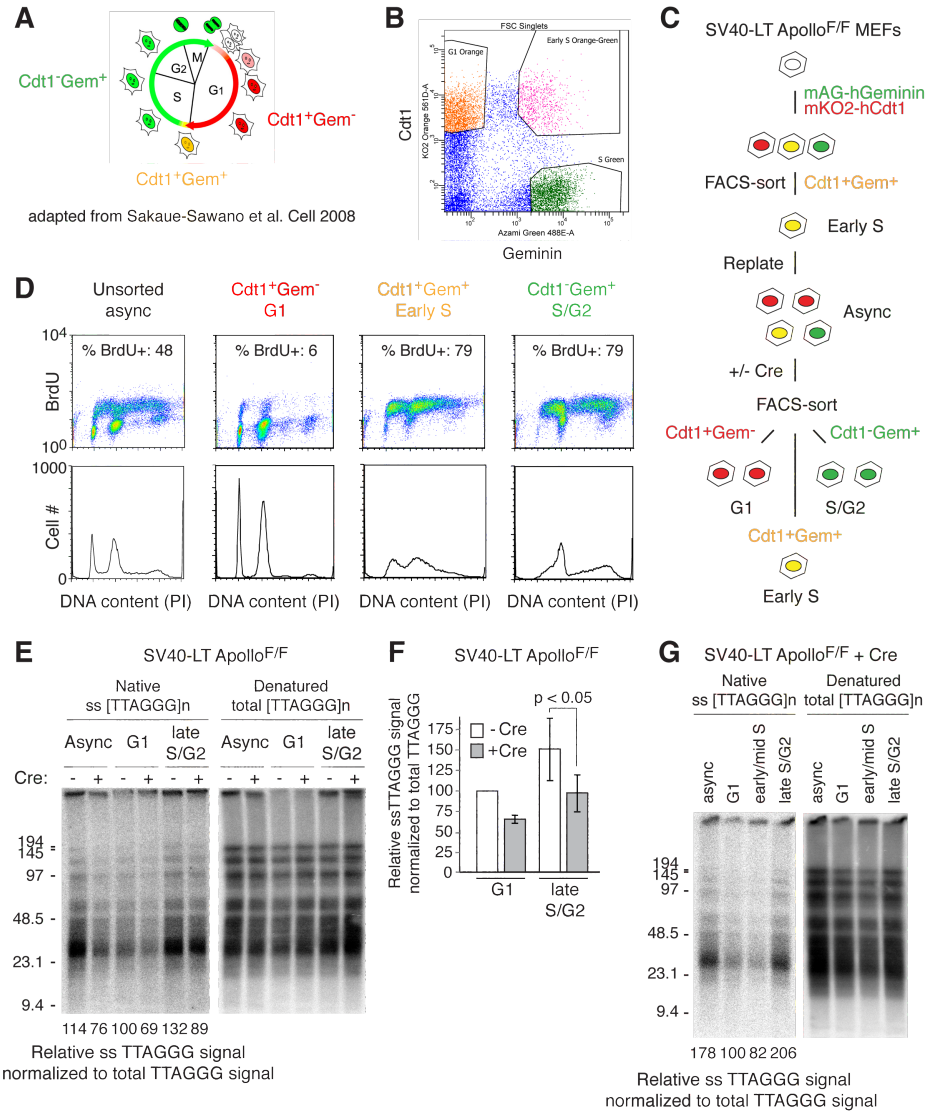

Figure 3.6. Apollo deficiency results in reduced telomeric overhangs in G1 and S phase. (A) Schematic showing cell cycle expression of FUCCI markers. (B) Representative FACS sort of cells expressing the FUCCI markers. Wild type MEFs transduced with mKO2-Cdt1 (red) and mAG-Geminin (green) were excited with 561nm and 488nm lasers, and gates are shown for the three sorted populations: Cdt1^{+}Gem^{-}, Cdt1^{+}Gem^{+}, and Cdt1^{-}Gem^{+}. (C) Schematic of the procedure for isolating cells in G1, early S, and late S/G2 phases by FUCCI-FACS. SV40-LT *Apollo*$^{F/F}$ MEFs transduced with the FUCCI vectors were selected by FACS for integration of both plasmids, replated, and infected with Hit&Run Cre. Cells were harvest at the desired time after Cre, sorted for different populations, and embedded in agarose for overhang analyses. (D) Cell cycle profiles of unsorted and sorted populations. Cells were pulsed with BrdU for 30 minutes prior to sorting. After sorting, cells were immediately fixed, stained with FITC-anti-BrdU and PI for DNA content, then analyzed by flow cytometry. (E) Representative telomeric overhang analysis of G1 and late S/G2 *Apollo*$^{F/F}$ MEFs at 120 h after Cre. The relative single-stranded signal was normalized to total TTAGGG signal and determined as a percentage of the signal in the lane containing G1 cells without Cre (set at 100). (F) Quantification of relative single-stranded telomeric signal in G1 and late S/G2 as assayed in (E). The single-stranded telomeric signal was normalized to the total TTAGGG signal and determined as a percentage of the signal in G1 cells without Cre (set at 100). Values are the mean of three independent experiments and SDs. p-values were determined by paired student's t-test. (G) In-gel detection of relative overhang signal in early/mid S phase in SV40-LT *Apollo*$^{F/F}$ MEFs at 120 h post Cre.

When the telomeric overhangs of cells in different cell cycle phases were analyzed by in-gel hybridization, Apollo-deficient cells in G1 and late S/G2 showed a 40% reduction in telomeric overhang signal compared to wild type cells in the same phase of the cell cycle. Interestingly, the telomeric overhangs in both wild type and Apollo-deficient cells were increased in late S phase compared to G1 (Figure 3.6E-G). This Apollo-independent increase in overhang signal during progression from G1/early S to late S phase could arise due to extension of the G-rich overhang by telomerase (which in mammalian cells is uncoupled from complementary strand synthesis) and/or resection of the C-rich strand by other nucleases. As will be shown later (Chapter 5), this increase in overhang signal occurs in telomerase-deficient MEFs, suggesting that this step in telomere end-processing is telomerase-independent.

In order to determine whether Apollo acts differentially at leading- and lagging-end telomeres, I adapted an approach for separating newly synthesized telomeres of human cells[7] to analyze the overhangs at leading- and lagging-end telomeres in MEFs. This approach is based on sequence differences between the complementary strands of telomeric DNA. For every 6 bp of telomeric sequence, the G- and C-rich strands respectively contain two and one thymidine that can be replaced with the heavier BrdU. Incorporating BrdU into replicating telomeres yields leading-end telomeres (containing the newly-synthesized G-rich strand) that are heavier than lagging-end telomeres (containing the newly-synthesized C-rich strand), permitting their separation by CsCl density gradient equilibrium centrifugation (Figure 3.7A). For this procedure, MEFs were grown in the presence of 100 μM BrdU for one round of replication (16 hours). Genomic DNA was isolated and digested with *Mbo*I and *Alu*I to retain telomeric

restriction fragments. The DNA was fractionated by CsCl density gradient equilibrium centrifugation and the telomeric signal in each fraction was determined by slot blot with a ^{32}P-labeled G-rich telomeric probe. When the telomeric signal intensities were plotted as a function of the CsCl density calculated based on the measured refractive index of each fraction, distinct peaks of telomeric signal appeared, corresponding to the unreplicated, lagging-end, leading-end, and doubly replicated telomeres. Between three to five fractions spanning each peak were pooled, and the telomeric overhangs were detected by native in-gel hybridization.

To confirm the density of unreplicated and doubly substituted telomeric DNA, DNA was also isolated from cells that were not treated with BrdU (Figure 3.7C) or cells that had been incubated with BrdU for 48 hours. (Figure 3.7D). CsCl density gradient equilibrium centrifugation of unlabeled telomeres followed by slot blot detection of the telomeric signal in each collected fraction resulted in the appearance of a single peak of telomeric signal at 1.74 g/ml. Meanwhile, the same protocol performed on telomeres that had undergone two rounds of replication yielded a major peak at 1.87 g/ml, two minor peaks at 1.78 and 1.82 g/ml, corresponding to those telomeres that had only completed one round of replication, and no peak at 1.74 g/ml, since presumably all cells had replicated within the 48 hours of the BrdU pulse.

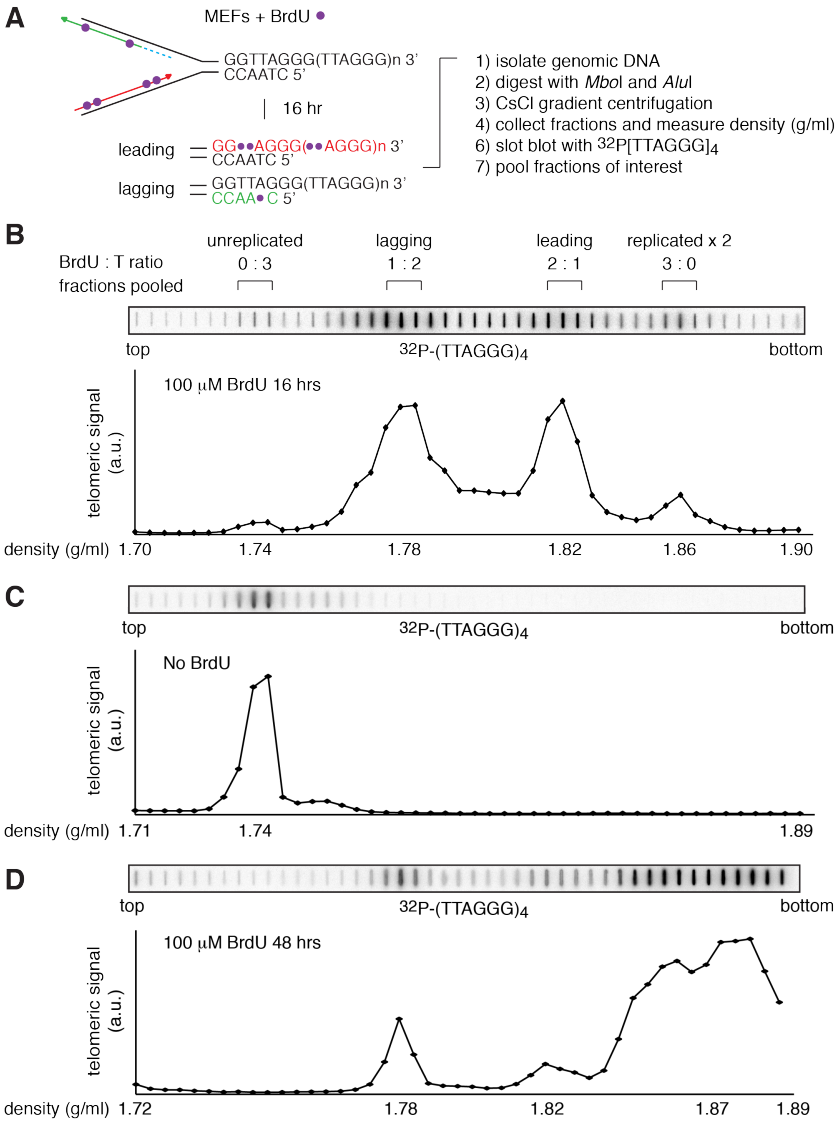

Figure 3.7. Separation of newly synthesized leading- and lagging-end telomeres. (A) Schematic of the separation of newly synthesized telomeres, as described in the text. (B) Representative slot blot of telomeric signal in each fraction collected from CsCl density gradient equilibrium centrifugation of telomeric DNA labeled with BrdU for one round of replication. The density of each fraction corresponding to peaks in telomeric signal was calculated based on the measured refractive index. (C) Slot blot of telomeric signal in fractions collected from CsCl gradient using telomeric DNA not labeled with BrdU. (D) Slot blot of telomeric signal in fractions collected from CsCl gradient using telomeric DNA isolated from cells incubated for >2 PDs with BrdU.

In-gel hybridization was used to detect the relative overhang signal at newly synthesized leading- and lagging-end telomeres in the presence and absence of Apollo. In wild type MEFs, the relative overhang signal at leading-end telomeres was either

approximately equal to or slightly greater than that at lagging-end telomeres (3.8C-D). This is in contrast to published studies on absolute overhang length in telomerase-negative human cells, which is greater at lagging-end telomeres compared to leading-end telomeres. In human cells, expression of telomerase reduces the difference in overhang length between leading- and lagging-end telomeres, though the lagging-end overhangs still remain longer[7]. Evaluation of the relative overhang signal at leading- and lagging-end telomeres in telomerase-negative MEFs revealed no reproducible differences compared to telomerase-positive MEFs (see Chapter 4). This result may be indicative of differences in telomere-end processing between MEFs and human fibroblasts, and should be kept in mind when making interspecies comparisons.

When this method was used to separate the newly synthesized leading- and lagging-end telomeres from Apollo-deficient cells, slot blot detection of the telomeric signal in each fraction showed similar peaks of intensity corresponding to the leading-, lagging-end, and unreplicated telomeres (Figure 3.8A-B). No aberrant intermediate peaks of telomeric signal intensity were observed, suggesting that telomeres lacking Apollo were able to complete replication. Detection of the telomeric overhang signal by in-gel hybridization revealed that the overhangs at leading-end telomeres were reduced by ~50% while lagging-end overhangs were unaffected (Figure 8C-D). On the native gel, the single stranded overhang of telomeres lacking Apollo appeared as a smeared signal, which may be indicative of secondary structures that occur as leading end telomeres lacking an overhang are recognized and processed as DNA damage. The severity of the overhang defect at leading end telomeres in the absence of any defect in lagging-end overhangs is consistent with the 25-35% reduction in overhang signal

detected in bulk DNA isolated from Apollo-deficient cells. Thus, Apollo contributes to the size of overhangs generated specifically at newly synthesized leading-end telomeres.

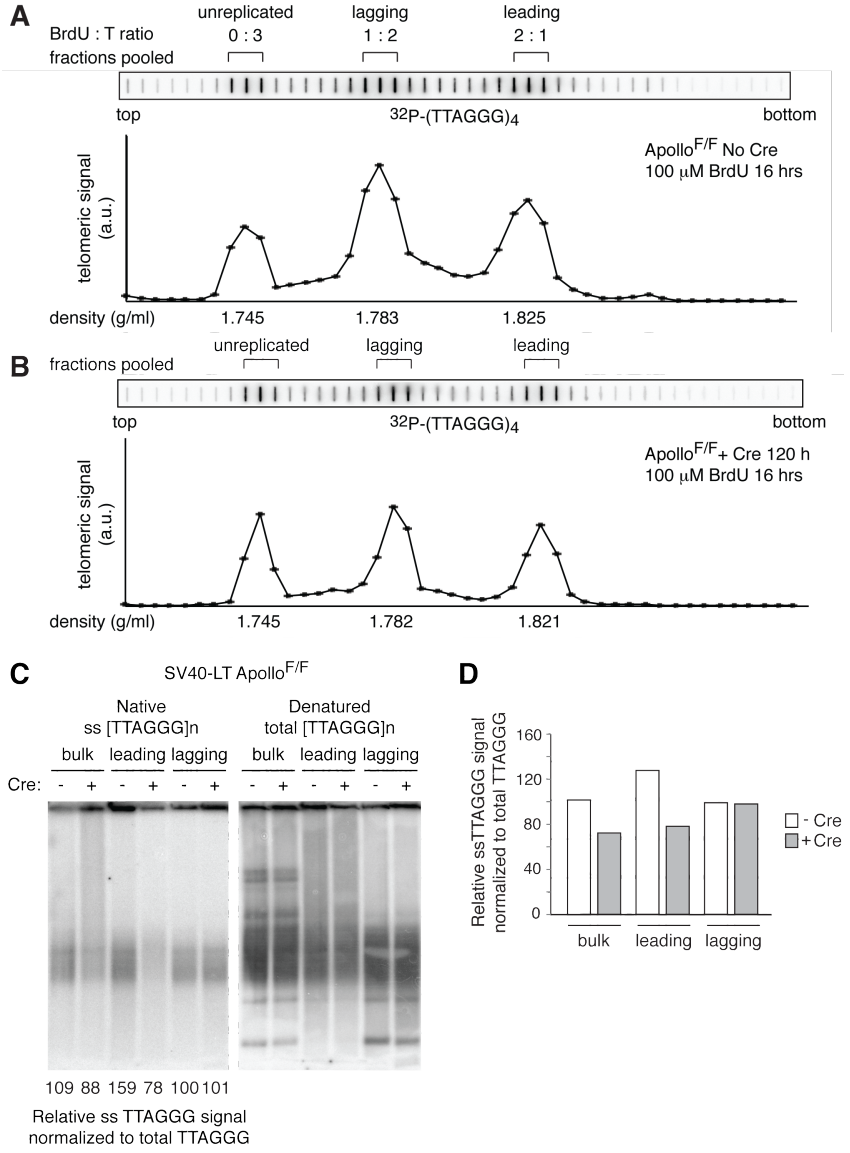

Figure 3.8. Apollo contributes to overhang generation at newly synthesized leading-end telomeres. (A) Representative slot blot of telomeric signal in each fraction collected from CsCl density gradient equilibrium centrifugation of telomeric DNA from Apollo$^{F/F}$ MEFs labeled with BrdU for one round of replication. The fractions pooled for overhang analyses are shown. (C) Representative overhang analysis of bulk telomeres (prior to CsCl density gradient equilibrium centrifugation), and separated leading, and lagging-end telomeres from Apollo$^{F/F}$ MEFs in the absence of Cre and 120 hours post-Cre. (D) Quantification of relative overhang signal as detected in (C). Values represent the mean of two independent experiments.

Apollo protects a subset of telomeres from activating the ATM kinase in S phase

The effect of Apollo deletion on the repression of DNA damage signaling at telomeres was next investigated to determine whether an overhang defect can compromise end protection. Following deletion of Apollo, approximately one-third of cells exhibited Telomere dysfunction-Induced Foci (TIFs; [192]) at a subset (~10%) of the telomeres (Figure 3.9A,E). The TIF response was accompanied by phosphorylation of Chk2, a target of the ATM kinase (Figure 3.9B). Consistent with the Chk2 phosphorylation, the TIF response was ablated when cells were treated with an shRNA to the ATM kinase but unaffected by knockdown of ATR (M. van Overbeek, Figure 3.9C-G). Thus, deletion of Apollo elicits ATM kinase signaling at a subset of the telomeres in a fraction of the cells.

Whereas wild type Apollo effectively repressed TIF formation and Chk2 phosphorylation in Cre-treated *Apollo*$^{F/F}$ MEFs, ApolloΔTRF2 was unable to prevent the DNA damage response associated with Apollo loss (Figure 3.9A-B,E). In addition, Apollo-ND failed to prevent activation of ATM signaling at telomeres. Both mutant forms of Apollo induced a level of Chk2 phosphorylation similar to that in the absence of Apollo (Figure 3.9B). Therefore, repression of ATM signaling at telomeres appears to require an Apollo that is both nuclease-proficient and localizes to telomeres.

Figure 3.9. Apollo is required to repress telomeric ATM signaling. (A) TIF assay on *Apollo*$^{F/F}$ MEFs expressing the indicated Apollo alleles to detect telomeric DNA damage signaling before (left) and after (right) deletion of the endogenous Apollo with Cre. Telomeres are detected using a FISH probe (green). DNA damage sites are marked with 53BP1 (red). DNA is counterstained with DAPI (blue). Circled TIFs in the enlarged images highlight the prevalence of TIF occurrence at two closely positioned telomeres or in cells with paired telomeres, indicative of DNA damage signaling during or after telomere replication. (B) Immunoblotting for the phosphorylation state of Chk2 at 6 days after Cre treatment. (C) Immunoblot showing depletion of ATM (Mat3-Sigma) 6 days after shRNA treatment and 3 days after the start of puromycin selection in *Apollo*$^{F/F}$ MEFs expressing the indicated Apollo alleles. Apollo-ND* is identical to Apollo-ND, except without the mutation of H230. (D) Effect of ATM kinase knockdown on the TIF response in Apollo deficient cells. TIF analysis as in (A) but with cells expressing an shRNA to the ATM kinase. (E) Quantification of TIF responses as assayed in (A) and (D). TIFs were scored on the basis of co-localization of 53BP1 foci with 5 or more telomeres per cell. Values for alleles +Cre indicate the mean of 3 independent experiments (> 100 nuclei per experiment), and SDs. * indicates the use of the Apollo-ND* allele in the ATM shRNA experiment. (F) Immunoblot showing depletion of ATR (FRP-Santa Cruz) 6 days after shRNA treatment and 3 days after start of puromycin selection in SV40-LT *Apollo*$^{F/F}$ MEFs expressing the indicated Apollo alleles. (G) TIFs after ATR shRNA. The % of cells with ≥5 TIFs is noted below the images. Apollo-ND* is identical to Apollo-ND, except without the mutation of H230. (H) Immunoblot for TRF2 and Chk2 in *TRF2*$^{F/-}$*p53*$^{-/-}$ MEFs expressing the indicated TRF2 alleles without Cre and at 144 hours after Hit&Run Cre. (I) TIF assay on *TRF2*$^{F/-}$*p53*$^{-/-}$ MEFs expressing the indicated TRF2 alleles to detect telomeric DNA damage signaling before (left) and after (right) deletion of the endogenous TRF2 with Cre. Telomeres are detected using a FISH probe (green). DNA damage sites are marked with 53BP1 (red). DNA is counterstained with DAPI (blue). (J) Quantification of TIF response as assayed in (I). TIFs were scored on the basis of co-localization of 53BP1 foci with 5 or more telomeres per cell. Values indicate the mean of 3 independent experiments (>100 nuclei per experiment) and SDs. p-values were determined based on paired student's t-test.

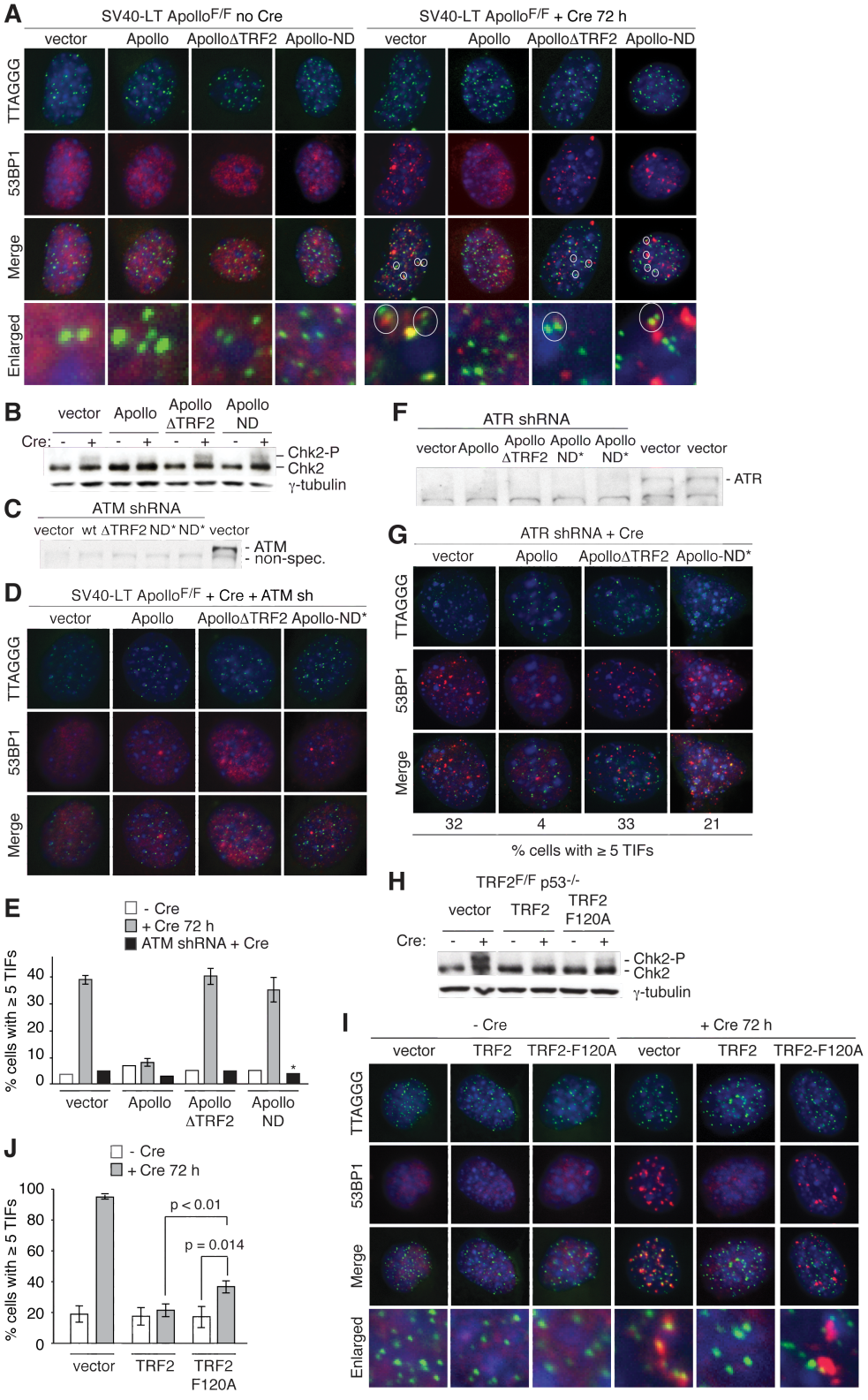
A
SV40-LT Apollo F/F no Cre
SV40-LT Apollo F/F + Cre 72 h
vector
Apollo
ApolloΔTRF2
Apollo-ND
TTAGGG
53BP1
Merge
Enlarged
B
vector
Apollo
Apollo ΔTRF2
Apollo ND
Cre:
Chk2-P
Chk2
γ-tubulin
C
ATM shRNA
vector
wt ΔTRF2
ND*
ND*
vector
- ATM
- non-spec.
D
SV40-LT Apollo F/F + Cre + ATM sh
Apollo-ND*
E
- Cre
+ Cre 72 h
ATM shRNA + Cre
% cells with ≥ 5 TIFs
F
ATR shRNA
- ATR
G
ATR shRNA + Cre
32
4
33
21
% cells with ≥ 5 TIFs
H
TRF2 F/F p53 -/-
TRF2
TRF2 F120A
I
- Cre
+ Cre 72 h
TRF2-F120A
J
p < 0.01
p = 0.014

I also examined the ability of TRF2-F120A to suppress the ATM-mediated DNA damage response induced in the absence of TRF2. Whereas TRF2 deletion resulted in 80-90% cells with TIFs at most telomeres, expression of the TRF2-F120A mutant reduced the percentage of TIF-positive cells by approximately 2-fold and the remaining TIF-positive cells had fewer TIFs/cell (Figure 3.9I-J). Expression of TRF2-F120A also diminished the level of Chk2 phosphorylation elicited by TRF2 deletion (Figure 9H). Notably, however, the fraction of cells with ≥ 5 TIFs in the presence of TRF2-F120A remained significantly greater than when TRF2-deficient cells were complemented with wild type TRF2 (Figure 3.9I-J). As was observed for Apollo deletion, 30-40% of the cells were TIF positive (Figure 3.9I-J). Furthermore, like cells lacking Apollo, the TRF2-F120A cells showed a low level of Chk2 phosphorylation (Figure 3.9H). Thus, disrupting the Apollo binding site of TRF2 elicits a DNA damage response that resembles the phenotype of Apollo deletion.

Since the TIF response was observed in approximately one third of the Apollo-deficient cells, and these cells often contained paired TTAGGG repeat FISH signals indicative of recent replication (Figure 3.9A), I investigated the cell cycle dependence of this DNA damage response. Using the FUCCI sorting method, I isolated Apollo-deficient cells in G1 and late S/G2 phase, which were plated on coverslips, and fixed for immunofluorescence either 1.5 h or 6-8 h later. Prior to fixation, cells were treated with a 30 min pulse of BrdU in order to evaluate their S phase index. At 1.5 h after plating, the cell cycle profile of MEFs that were $Cdt1^{+}Gem^{-}$ at the time of sorting was almost identical to cells analyzed immediately upon sorting (Figure 3.10A). In addition, only ~10% of cells were positive for BrdU incorporation, indicating that these cells remained in G1

phase. On the other hand, by 6-8 h after plating, a significant fraction of cells that were in G1 upon sorting had progressed into early/mid S phase based on their DNA content, with ~40% having incorporated BrdU (Figure 3.10A). Finally, when cells sorted based on Cdt1-Gem+ staining were analyzed at 1.5 h after plating, cell cycle profiles showed a large number of cells nearing a 4N or an 8N DNA content while ~70% of the cells were BrdU-positive, indicating that the majority of these cells remained in late S/G2.

Immunofluorescence detection of DNA damage markers in cells at different cell cycle phases revealed that the TIFs seen in the absence of Apollo occurred in early/mid S phase (Figure 3.10B). Whereas the percentage of TIF positive G1 or late S/G2 cells did not increase, Apollo-deficient cells in mid-S phase had a strikingly higher TIF response than the controls (Figure 3.10C). Thus, the absence of Apollo results in a telomeric DNA damage signal in early/mid S phase.

TRF2-bound Apollo prevents fusion of leading-end telomeres

In addition to activating ATM at a subset of telomeres, Apollo deletion was associated with aberrant DNA repair at telomeres. Apollo-deficient MEFs showed a distinctive telomere fusion phenotype on metaphase spreads (M. van Overbeek, Figure 3.11A). Although the telomere fusions were 5-10 times less frequent compared to when TRF2 is deleted, the fusion phenotype of Apollo-deficient cells was highly significant. Strikingly, the telomere fusions observed between 84-120 hours after introduction of Cre were nearly all of the chromatid-type, indicating a post-replicative fusion event (M. van Overbeek, Figure 3.11B). Later time points included chromosome-type fusions that were most likely due to duplication of chromatid-type fusions after their segregation into

daughter cells. These secondary chromosome-type fusions were not likely to reflect the function of Apollo, and their incidence was affected by the proliferation rate of the cells. Therefore, later time-points after Apollo deletion were not analyzed.

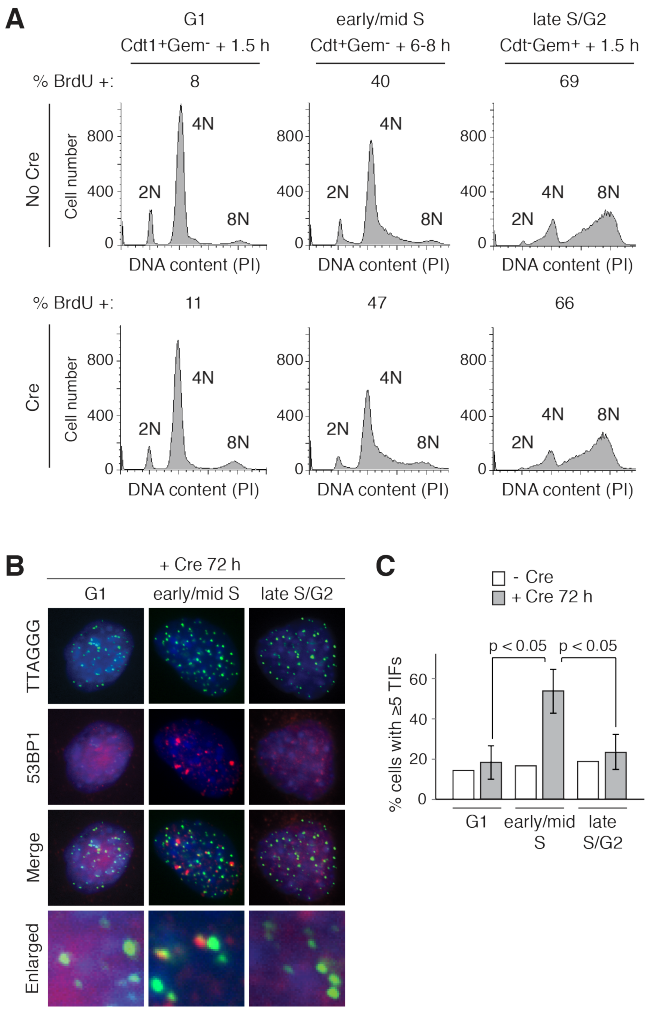

Figure 3.10. Cell cycle dependence of telomere dysfunction in the absence of Apollo. (A) Cell cycle profile and S phase index for different FUCCI-sorted population at 1.5 h or 6-8 h after plating on coverslips for immunofluorescence. Cells were pulsed for 30 min with BrdU before harvesting and fixing for cell cycle analysis. Cells were stained with FITC-anti-BrdU and propidium iodide (PI) for DNA content, and analyzed by flow cytometry. (B) TIF assay of G1, early/mid S, and late S/G2 *Apollo*$^{F/F}$ MEFs at 72 h post Cre. G1 and late S/G2 cells were obtained by sorting Cdt1^{+}Gem^{-} and Cdt1^{-}Gem^{+} populations and plating cells for 1.5 h prior to fixation. Early/mid S phase cells were obtained by plating Cdt1^{+}Gem^{-} sorted (G1) cells on coverslips for 6-8 h prior to fixation. Telomeres are detected using a FISH probe (green). DNA damage sites are marked with 53BP1 (red). DNA is counterstained with DAPI (blue). (C) Quantification of the TIF response in G1, early/mid S, and late S phase as assayed in (B). Values are the mean of three independent experiments (>60 nuclei per experiment) and SDs. p-values were determined using paired student's t-test.

Leading-strand and lagging-strand DNA synthesis generates two distinct types of telomeres that could be vulnerable to post-replicative fusions. To determine whether Apollo was important for the protection of both types of telomeres, Chromosome Orientation Fluorescent in situ Hybridization (CO-FISH; [422]) was used to distinguish between telomere ends generated by leading- and lagging-strand DNA synthesis (referred to as leading-end and lagging-end telomeres). CO-FISH analysis of the *Apollo* null cells showed that the fusions exclusively involved telomeres generated by leading-strand DNA synthesis (shown in red) (Figure 11C-E). Thus, Apollo has a specific role in protecting leading-end telomeres, resulting in chromatid-type fusions when Apollo is absent. The absence of sister fusions suggests that the lagging-end telomeres remain protected in Apollo-deficient cells. This is consistent with the contribution of Apollo to overhang generation specifically at leading end telomeres.

The function of Apollo in protecting leading-end telomeres required its localization at telomeres. The ApolloΔTRF2 mutant was unable to prevent leading-end telomere fusions (Figure 3.11C-E). Similarly, expression of TRF2-F120A resulted in a significant level of leading-end telomere fusions observed by CO-FISH while this mutant was fully capable of repressing the chromosome-type fusions associated with *TRF2* deletion (Figure 3.11C-E). Just as the overhang defect was not due to an inability for telomerase to act at telomeres, the fusions were independent of telomerase, since the cells showed the same induction of leading-end telomere fusions observed when TRF2-F120A replaced the endogenous TRF2 in telomerase-positive cells (Figure 3.11D-E).

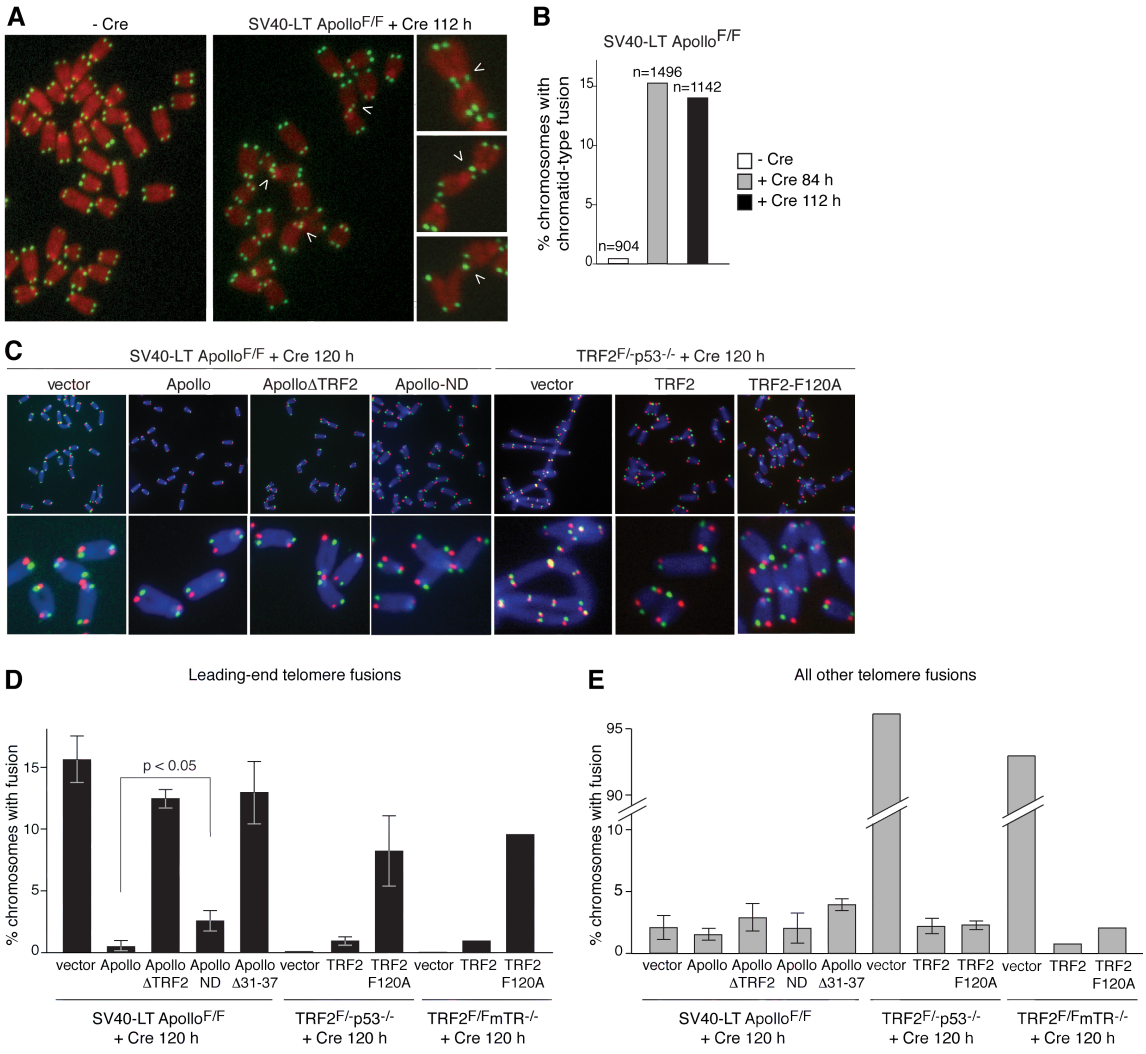

Figure 3.11. TRF2-bound Apollo prevents leading-end telomere fusions. (A) Telomere fusions in metaphase spreads from Apollo-deficient cells. Metaphase spreads were obtained from *Apollo*$^{F/F}$ MEFs before or after introduction of Cre and processed for telomeric FISH (FITC, green). DNA was stained with DAPI (false-colored in red). Arrowheads highlight chromatid-type fusion events. (B) Quantification of chromatid-type fusion events after deletion of Apollo. (C) CO-FISH analysis of leading and lagging end telomeres. Metaphases harvested from *Apollo*$^{F/F}$ MEFs or *TRF2*$^{F/-}$*p53*$^{-/-}$ MEFs expressing the indicated rescuing alleles were incubated with BrdU/BrdC and treated with ExoIII and UV to remove the newly-synthesized DNA strand. The undigested parental telomeric DNA strands were detected with TAMRA-$(TTAGGG)_3$ (red) and FITC-$(CCCTAA)_3$ (green). DNA is stained with DAPI (blue). The telomere replicated by leading-strand DNA synthesis is highlighted in red, and the telomere replicated by lagging-strand DNA synthesis is highlighted in green. (D) Quantification of leading-end telomere fusions from metaphase analyses shown in (C) at 120 hours post Cre. Values represent means of three or more experiments (chromosome number >1000 per experiment) and SDs. (E) Quantification of other telomere fusions events (lagging-to-lagging, lagging-to-leading chromatid-type fusions, and chromosome-type fusions). Values represent means of three or more experiments (>1000 chromosomes per experiment) and SDs.

Furthermore, the nuclease domain of Apollo was involved in protecting the leading-end telomeres. Cells expressing Apollo-ND instead of wild type Apollo generated a statistically significant level of leading-end telomere fusions after deletion of endogenous Apollo (Figure 3.11D). A more severe phenotype was observed with the second nuclease domain mutant (ApolloΔ31-37, removing the HxHxDH motif in the metallo β-lactamase domain and also containing the H230A mutation), which was expressed at similar levels as wild type Apollo and retained its interaction with TRF2 (Figure 3.2E) but was incapable of repressing leading-end telomere fusions (Figure 3.11D).

Although both nuclease-deficient mutants of Apollo appear to be null alleles with regard to overhang maintenance and repression of ATM signaling, it is noteworthy that Apollo-ND, containing point mutations of the HxHxDH motif in the metallo β-lactamase domain, has a reduced but still significant ability to repress the leading-end telomere fusions. In contrast, the second nuclease-deficient allele of Apollo, lacking the HxHxDH motif, completely fails to protect leading-end telomeres from fusions. One explanation for this discrepancy is that the Apollo-ND allele has residual nuclease activity that is sufficient to protect leading-end telomeres during the short time period in S/G2 when they are vulnerable to fusion. This residual nuclease activity would have to be very minor because there is no overt difference in the overhang signal compared to Apollo deletion. Another possibility is that the Apollo protein itself protects the leading-end telomeres from fusion. Such protection could conceivably involve the nuclease domain in a manner that is destroyed by deletion of amino acids 31-37 but preserved in Apollo-ND despite

the point mutations. It will therefore be of interest to study the nuclease and end-binding activities of TRF2-Apollo complexes *in vitro*.

It is worth noting that when the different Apollo alleles were overexpressed in 293T cells, wild type Apollo and Apollo-ND appeared to migrate as two forms that were both pulled down by TRF2 while only the faster migrating form was observed for ApolloΔTRF2 and ApolloΔ31-37 (3.2D-E). This has not observed in any other cell lines, so the modification that results in the slower migrating form of Apollo might be specific to the case of overexpressing Apollo in 293T cells. Nonetheless, it is interesting that the absence of the slower migrating form of Apollo correlates with the inability to suppress the telomere fusion phenotype associated with Apollo loss. It remains an open question whether Apollo is post-translationally modified, in the absence or presence of DNA damage, and whether such a modification contributes to the protection of leading end telomeres from fusions independent of the role of Apollo in overhang generation.

NHEJ between leading-end telomeres lacking Apollo are independent of Ligase IV

The leading-end associations that occur in the absence of Apollo were presumed to be NHEJ events and have since been reported by others to depend on Ku[423]. To further investigate the genetic requirements for the leading-end fusions that occur following deletion of Apollo, I analyzed the appearance of fusions in the absence of ligase IV, which is responsible for sealing the nicks between ends joined by classical NHEJ. First, I evaluated *TRF2$^{F/-}$p53$^{-/-}$Lig4$^{-/-}$* MEFs expressing TRF2-F120A following Cre-mediated deletion of endogenous TRF2. The extensive chromosome type fusions that occur after TRF2 deletion were almost completely abrogated in the absence of ligase IV, though a

low level of leading-leading and other telomere fusions remained (Figure 3.12B). Wild type TRF2 suppressed these residual fusions, while interestingly, a significant level of leading-end fusions persisted in the presence of TRF2-F120A, while other telomere fusions appeared at the same level as wild type (Figure 3.12A-B). In an alternative approach, I generated SV40LT-immortalized *Apollo*$^{F/F}$*Lig4*$^{-/-}$ MEFs. Cells lacking both Apollo and ligase IV still showed a 20-30% reduction in the telomeric overhang signal and leading end fusions at a frequency similar to that observed in the presence of ligase IV (Figure 3.12C).

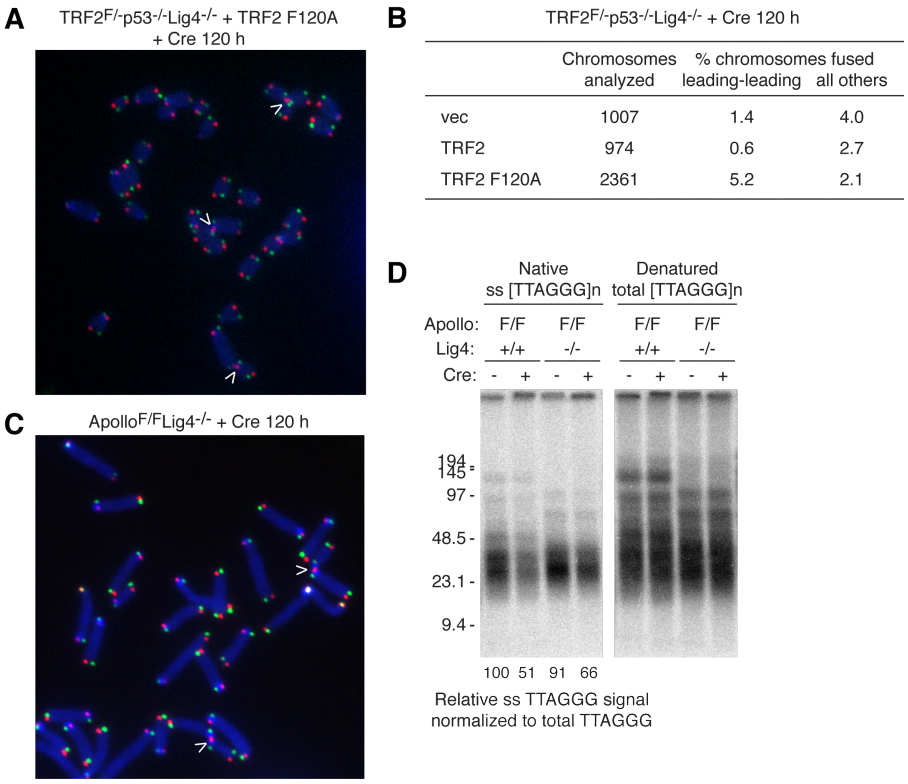

Figure 3.12. Leading-end fusions occurring in the absence of Apollo are independent of Ligase IV. (A) Representative CO-FISH analysis of leading and lagging end telomeres on metaphases harvested from *TRF2*$^{F/-}$*p53*$^{-/-}$*Lig4*$^{-/-}$ MEFs expressing TRF2-F120A. Cells were incubated with BrdU and BrdC for 16 hours and treated with colcemid prior to harvest. Metaphase spreads were prepared, treated with ExoIII and UV to remove the newly-synthesized strand. The undigested parental telomeric DNA strands were detected with TAMRA-$(TTAGGG)_3$ (red) and FITC-$(CCCTAA)_3$ (green). DNA is stained with DAPI (blue). The leading-end telomere is highlighted in red, and the lagging-end telomere is highlighted in green. (B) Quantification of leading-end telomere fusions from metaphase analyses shown in (A). (C) Representative CO-FISH analysis of leading and lagging end telomeres on metaphases harvested from *Apollo*$^{F/F}$*Lig4*$^{-/-}$ MEFs at 120 hours after Hit&Run Cre. (D) In-gel overhang analysis of *Apollo*$^{F/F}$*Lig4*$^{-/-}$ before and after Cre.

Though further investigation is required regarding the mechanism of end-joining that occurs in the absence of Apollo, it appears that these events do not strictly require ligase IV. Whether they depend on Ku requires further validation using Apollo$^{F/F}$Ku$^{-/-}$ MEFs (or TRF2/Ku DKO cells complemented with TRF2-F120A), since the study attributing Ku to the joining of Apollo-deficient telomeres used cells derived from mice containing a null (rather than conditional) allele of Apollo[423].

Studies of cells lacking classical end-joining factors have provided evidence for the existence of alternative end-joining pathways. Though Ku and ligase IV are required for V(D)J recombination[172,173,176] and contribute to class-switch recombination[424], recent studies have shown that in the absence of Ku or XRCC4/ligase IV, or in the absence of both factors, CSR can still occur at a reduced frequency[425,426]. Furthermore, when DNA DSBs are induced at specific sites on different chromosomes in mouse cells deficient for classical NHEJ factors, A-EJ gives rise to chromosome translocations[427]. Whereas classical end-joining primarily involves direct joining of non-homologous ends, A-EJ pathways have largely been reported to use microhomology, though A-EJ in the absence of microhomology has also been documented[425,427].

The aberrant repair pathway activated in the absence of Apollo, which joins unprotected leading-end telomeres in S phase, appears distinct from the NHEJ between telomeres lacking TRF2, which occurs in G1 and largely depends on ligase IV. It would be interesting to identify the factors involved in NHEJ of leading-end telomeres lacking Apollo and investigate how and why this repair pathway differs from that activated in the absence of TRF2.

Expression of TRF2-F120A does not slow the rate of telomere shortening in telomerase-deficient cells

Since the length of the telomeric overhang correlates with the rate of telomere shortening in the absence of telomerase[248], I investigated whether Apollo-mediated resection contributes to telomere shortening by monitoring telomere length in telomerase-deficient cells deficient for Apollo function. As the loss of Apollo from telomeres activates only a transient and mild DNA damage response, I attempted to monitor the long-term consequences of Apollo deficiency using the TRF2-F120A mutant, which appeared to be less detrimental to cell proliferation than complete loss of Apollo. Therefore, I propagated *TRF2*$^{F/F}$*mTR*$^{-/-}$ MEFs expressing exogenously introduced wild type TRF2 or TRF2-F120A in the absence of endogenous TRF2 for up to 60 population doublings in culture.

Growth curves of cells expressing either the wild type or mutant TRF2 were almost identical (Figure 3.13A), indicating that the proliferation of MEFs expressing TRF2-F120A was not hindered by the transient ATM-dependent DNA damage response elicited by leading-end telomeres lacking Apollo. The apparent absence of a proliferation defect in the presence of TRF2-F120A could in fact be due to overgrowth of cells that do not express the TRF2-F120A mutant at high levels or of cells from which endogenous TRF2 was not efficiently deleted. Immunoblot detection of TRF2 showed that at 30 PDs, exogenously introduced wild type and mutant TRF2 continued to be expressed at high levels, though this masked the detection of endogenous TRF2 (Figure 3.13B). Nonetheless, overhang analyses of cells expressing TRF2-F120A showed persistently

reduced overhang signals compared to wild type, suggesting that the defect in overhang generation was maintained throughout the propagation of the cells (Figure 3.13C).

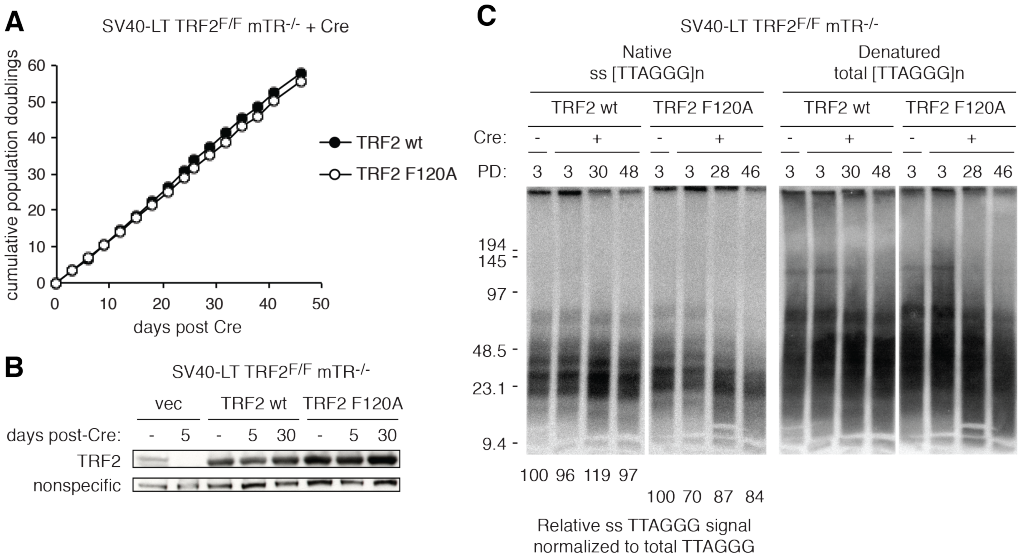

Figure 3.13. Loss of Apollo does not slow the rate of telomere shortening in telomerase-deficient cells. (A) Growth curve of *TRF2*$^{F/F}$*mTR*$^{-/-}$ MEFs expressing wild type TRF2 and TRF2-F120A in long-term culture after Cre-mediated deletion of endogenous TRF2. (B) Immunoblot detection of endogenous and exogenous TRF2 alleles in long-term cultures at 5 and 30 days after Cre. (C) Telomere length analysis of cells expressing TRF2-F120A harvested at several time points during long-term passaging to >50 population doublings. Native in-gel detection of the telomeric overhang is shown on the left, while the denatured gel is shown on the right.

Telomere length was assayed by fractionating DNA on pulsed-field gels and detecting the telomeric signal in the denatured gel by in-gel hybridization with a telomeric probe. The rate of telomere shortening in telomerase-deficient cells expressing TRF2-F120A was not significantly slower than that observed in the presence of wild type TRF2 (Figure 3.13C). In fact, the presence of TRF2-F120A slightly accelerated telomere shortening and resulted in the appearance of smeared telomeric signals of lower molecular weight that were not observed in the presence of wild type TRF2.

These experiments suggest that the loss of Apollo from telomeres does not slow the rate of telomere shortening in telomerase-deficient cells. However, the current experiments do not adequately address the contribution of resection to the rate of

telomere shortening, since the dynamics of bulk telomere length in cells lacking Apollo could reflect the DNA damage responses, albeit transient, that are activated when overhang generation is compromised. The proper assessment of whether inhibiting Apollo-mediated resection can slow telomere shortening requires a setting in which nuclease activity is compromised without abolishing the ability to initiate overhang generation, in order to monitor the rate of telomere shortening in cells with short telomeric overhangs that do not activate any DNA damage response.

SUMMARY OF FINDINGS

These data reveal that TRF2-bound Apollo functions at replicating telomeres, promoting the maintenance of the telomeric overhang, repressing S phase specific ATM signaling, and protecting leading-end telomeres from fusion. These results provide the basis for a model in which TRF2 recruits the Apollo nuclease to process leading-end telomeres immediately after their replication. If this processing does not occur or is delayed, the leading-end telomeres would remain blunt, making them vulnerable to end-joining reactions and exposing the telomere end in a manner that activates the MRN/ATM pathway. These findings establish that, as was generally assumed, maintenance of the telomeric overhang is important for the protection of mammalian telomeres.

As Apollo has been implicated in ICL repair[413,416], the appearance of S-phase TIFs in the absence of Apollo could alternatively be explained by an inability to repair lesions encountered during telomere replication. This explanation is not favored because the major phenotypes observed in the absence of Apollo are not associated with aphidicolin-induced replication stress or deletion of the shelterin component TRF1. Replication fork stalling prior to collapse is often associated with accumulation of single-stranded DNA and activation of the ATR kinase, which is not observed in Apollo null cells. Furthermore, deletion of Apollo in mouse cells does not induce the fragile telomere phenotype associated with telomere replication problems[215]. In addition, CsCl density gradient equilibrium centrifugation of BrdU-labeled telomeres from Apollo-deficient cells revealed no aberrant incorporation of BrdU that would be suggestive of replication defects. Although contributions of telomeric Apollo in repairing lesions encountered by

the replication machinery have not been formally excluded, the major phenotypes observed at telomeres lacking Apollo are inconsistent with the prevention of replication stress being a primary function of Apollo at telomeres.

It has been previously proposed that the F120 site in TRF2 not only provides a docking site for Apollo but also recruits additional shelterin accessory factors, such as Nbs1, XPF, PARP1, ATM, and ATR[28,44]. There would be no competition for this docking site because TRF2 is very abundant at telomeres, whereas most shelterin accessory factors are not[36]. The versatility of the F120 docking site was supported by the identification of two proteins, PNUTS and MCPH1, which can bind to TRF2 using the YxLxP motif[428]. However, the current data now cast doubt on the importance of the F120 docking site beyond the interaction with Apollo. The phenotype of the TRF2-F120A mutant is mild, showing the limited DNA damage response phenotype and telomere fusions associated with Apollo loss but no additional telomere dysfunction. Although it is possible that the other F120 interacting factors are dispensable for telomere protection (for instance, due to redundancy), further testing of the concept of the common F120 docking site is warranted.

The role of Apollo at replicating telomeres is distinct from previously characterized functions of the core components of shelterin. The predominance of leading-end telomere fusions in the Apollo knockout cells contrasts with both the TRF2 and POT1a/b knockout phenotypes. Although TRF2 deletion induces occasional chromatid-type fusions, most of the fusions in TRF2 null cells occur in G1 and manifest as chromosome-type fusions in the subsequent metaphase[193,197]. POT1a/b deletion results in sporadic chromosome-type fusions and post-replicative fusions involving sister

telomeres[37]. Neither chromosome-type fusions nor sister fusions are observed in Apollo null cells. Thus, whereas TRF2 and POT1a/b function at both leading- and lagging-end telomeres, Apollo acts specifically in the protection of leading-end telomeres.

CHAPTER 4:

THE MECHANISM BY WHICH THE SINGLE-STRANDED TELOMERIC BINDING PROTEIN POT1B REGULATES TERMINAL STRUCTURE

INTRODUCTION

Mouse shelterin contains two single-stranded telomeric DNA binding proteins, POT1a and POT1b, which serve distinct roles in telomere protection. POT1a represses ATR signaling at telomeres, while POT1b restricts the accumulation of excessive terminal single-stranded overhangs[37]. Deletion of POT1b results in a two- to four- fold increase in the terminal single stranded overhang, and subsequently accelerated telomere shortening[37,187]. POT1b-deficient mice are alive, but develop characteristics of the human disease, dyskeratosis congenita, which are exacerbated in the case of heterozygosity for the RNA component of telomerase[187]. POT1b has been proposed to limit degradation of the telomeric C-rich strand, but the mechanism by which POT1b serves this protective role was unknown.

Here, I evaluated the genetic requirements of the aberrant overhang phenotype that occurs in the absence of POT1b. My work revealed that POT1b limits overhang size at both newly synthesized telomeres in S phase by inhibiting Apollo and promoting the function of the Ctc1/Stn1/Ten1 (CST) complex. POT1b was found to interact physically with the CST complex through unique residues that are not conserved in POT1a (H. Takai). Based on these findings, a POT1b mutant unable to bind CST was generated and used to explore the telomere-specific functions of the CST complex as well as the aspects of POT1b function that specifically involve its interaction with CST.

RESULTS

POT1b suppresses aberrant processing of newly synthesized telomeres in S phase

To begin to elucidate the mechanism by which POT1b protects telomeres from aberrant degradation, I investigated whether the function of POT1b is required in non-cycling cells. POT1b was posited to either block the action of nucleases that do not normally act at telomeres or to regulate physiologic telomere processing events. End-processing events that normally occur at telomeres, such as the generation of single-stranded overhangs at newly synthesized leading-end telomeres, are thought to be associated with telomere replication in S phase. Thus, if POT1b negatively regulates physiologic end-processing, the overhang phenotype associated with POT1b deficiency might be predicted to occur only when POT1b is removed from telomeres in S phase.

The technical difficulties associated with arresting immortalized MEFs in G0/G1 and efficiently transducing Cre recombinase into quiescent cells were bypassed with the use of primary *POT1b*$^{F/F}$ *ROSA-Cre-ER*^{T2} MEFs generated by crossing POT1b$^{F/F}$ mice[187] with mice carrying an allele of Cre recombinase fused to a tamoxifen-responsive estrogen receptor targeted to the ubiquitously expressed ROSA26 locus[429] (Figure 4.1A). Addition of tamoxifen to these cells results in the translocation of Cre-ER from the cytoplasm to the nuclease and subsequent deletion of POT1b. Asynchronous cells treated for 12 hours with 100 nM tamoxifen showed a 5-fold reduction in POT1b protein levels within 48 hours (Figure 4.1B). The reduced POT1b protein level resulted in a reproducible 2-fold increase in the telomeric overhang signal at 120 hours following tamoxifen treatment (Figure 4.1D-E). This phenotype is weaker than that observed when POT1b is deleted in SV40LT-immortalized MEFs using retroviral transduction of Cre recombinase, which

generally results in a 3-4 fold increase in the telomeric overhang signal. However, since primary MEFs are more readily arrested in G0 than immortalized MEFs, this was the optimal system to determine whether POT1b affects the telomere terminus in quiescent cells.

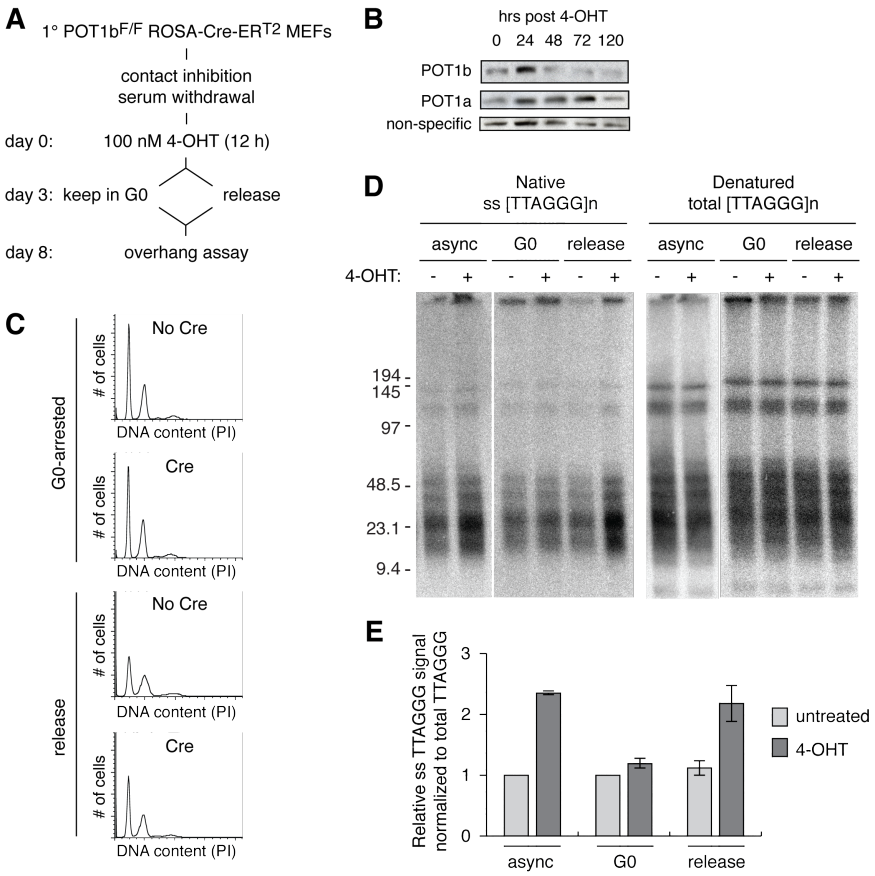

Figure 4.1. POT1b is not required in G0 to suppress accumulation of overhangs. (A) Scheme to assess the effect of deleting POT1b in non-cycling *POT1b*$^{F/F}$ *ROSA-Cre-ER*^{T2} MEFs. (B) Immunoblot detection of POT1b and POT1a in asynchronous *POT1b*$^{F/F}$ *ROSA-Cre-ER*^{T2} MEFs at successive timepoints after 12-hour incubation with 100 nM tamoxifen. (C) Cell cycle profile of cells at the time of preparation for overhang analysis. (D) In-gel overhang assay of asynchronous, G0-arrested, and released *POT1b*$^{F/F}$ *ROSA-Cre-ER*^{T2} MEFs with and without tamoxifen treatment. (E) Quanfication of overhang analysis shown in (D). Values represent the mean of two experiments with two independent *POT1b*$^{F/F}$ *ROSA-Cre-ER*^{T2} MEF lines and s.e.m.

Primary *POT1b*$^{F/F}$*ROSA-Cre-ER*^{T2} MEFs were arrested in G0 by contact inhibition and gradual serum withdrawal over several days. Following treatment with tamoxifen, the cells were either maintained under contact inhibition in serum-free media

or passaged in serum-rich media and allowed to progress through S phase (Figure 4.1A). After five days, at a time when POT1b protein levels had reached a minimum, cell cycle profiles were analyzed, and the telomeric overhang was assayed by in-gel hybridization. Flow cytometry showed that the contact-inhibited cells were mostly arrested with a 2N DNA content, and few cells had an intermediate DNA content between 2N and 4N indicative of ongoing replication (Figure 4.1C). Upon release into serum-rich media, the percentage of cells with 2N content was reduced though these cells did not proliferate well and showed a broad 4N peak, possibly indicative of G2/M arrest. The deletion of POT1b in arrested cells resulted in no increase in the telomeric overhang, whereas POT1b-deficient cells that were released accumulated increased overhang signals similar to asynchronous cells (Fig 4.1D-E). Similar results were obtained with two independent *POT1b*$^{F/F}$ *ROSA-Cre-ER*^{T2} cell lines. Thus, POT1b does not appear to be required in G0 to protect telomeres from aberrant degradation but instead suppresses aberrant processing in S phase.

Next, to evaluate the cell cycle dynamics of the aberrant overhangs in POT1b-deficient cells, I assessed the telomeric overhang in different phases of the cell cycle in the steady state after POT1b had been deleted using the FUCCI-FACS system (described in Chapter 3). The FUCCI vectors (mAG-Geminin, mKO2-Cdt1) were transduced into *POT1b*$^{F/-}$ MEFs and following Cre-mediated deletion of POT1b, cells were sorted in G1 and late S/G2 by FACS. Overhang analysis by in-gel hybridization showed that the excessive overhangs due to POT1b deletion were not restricted to a specific cell cycle phase (Figure 4.2A-B). Instead, similarly elevated overhang signals were observed in both G1 and S phase. Wild type cells undergo a two-fold increase in the telomeric

overhang in late S phase compared to G1, and this extended overhang is presumably filled in by C-strand synthesis as cells progress through mitosis. POT1b-deficient cells, on the other hand, appeared to lack any dynamic changes in overhang signal, which could reflect a defect in fill-in synthesis of the C-rich strand.

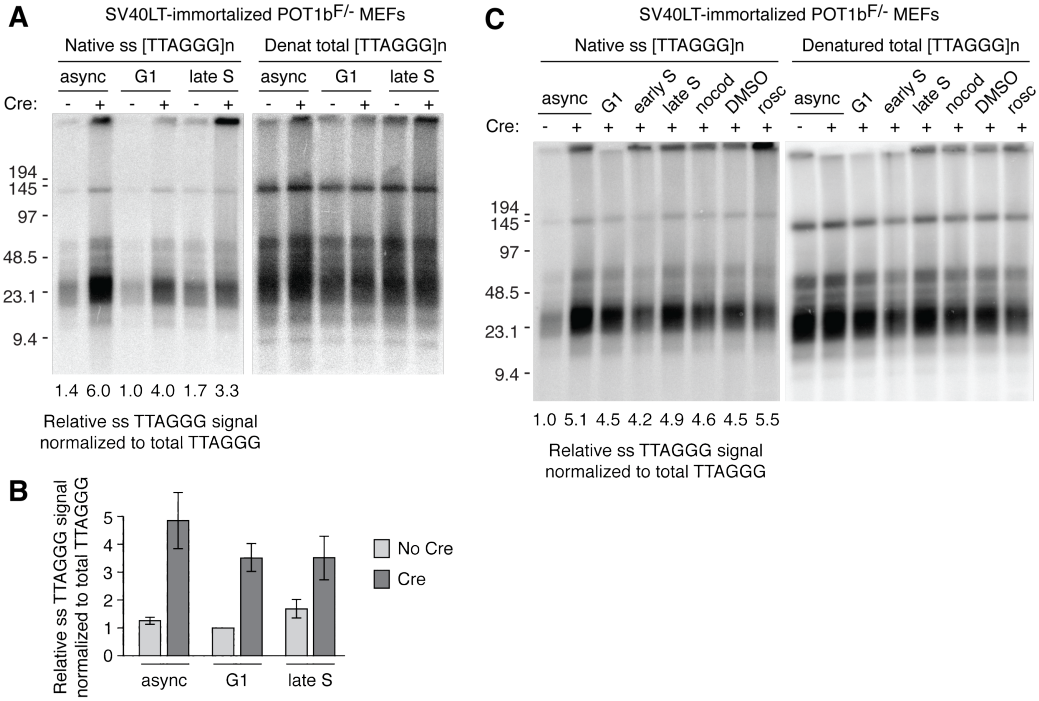

Figure 4.2. Aberrant overhangs in POT1b-deficient cells are not restricted to a specific cell cycle phase. (A) In-gel overhang analysis of POT1b$^{F/F}$ cells in G1 and late S at 120 hours post-Cre, isolated by FUCCI-FACS as previously described. The relative overhang signal normalized to the total telomeric signal was determined with the lane containing wild type cells in G1 set to 1. (B) Quantification of overhang analyses shown in (A). Values represent the mean of three independent experiments and standard deviations. (C) Overhang analyses of synchronized POT1b-deficient cells treated for the duration of S phase with nocodazole or roscovitine. Cells in G1, early S, and late S phase were sorted by FUCCI-FACS. Early S phase cells were plated and treated with drugs for 4-6 hours prior to harvesting.

As seen in Figure 4.2A-B, the overhang signal of unsorted asynchronous POT1b-deficient cells was on average greater than in either the G1 or late S phase cells, prompting a more careful investigation of whether the overhang phenotype associated with POT1b loss was more severe during a specific cell cycle phase other than G1 or late S. I evaluated the effect of different drug treatments on the aberrant overhangs in

POT1b-deficient cells. POT1b-deficient cells in early S phase were sorted by FUCCI for the $Cdt1^{+}Gem^{+}$ population. These cells were plated and treated with nocodazole for 8 hours to arrest the cells in mitosis, or with roscovitine for 4 hours, to inhibit Cdk and arrest the cells in S phase. Nocodazole treatment had very little effect on the overhang signal, indicating that the accumulation of excessive overhangs in the absence of POT1b is not affected by mitotic arrest (Figure 4.2C). Meanwhile, roscovitine treatment did not reduce the level of overhang signal, suggesting that the excess overhangs are not the result of nucleases whose activity depends on Cdk phosphorylation (Figure 4.2C). This is in contrast to the Cdk-dependent C-strand degradation that occurs in *S. cerevisiae* cdc13-1 mutant[430]. In fact, Cdk inhibition resulted in a slight increase in the overhangs, suggesting that prolonged S phase arrest could result in further accumulation of excess overhangs. Though POT1b-deficient cells do not exhibit overt signs of checkpoint activation, they may nevertheless progress slowly through G2, which may account for the slightly elevated overhang signal in asynchronous populations compared to G1 and late S cells (Figure 4.2A-B).

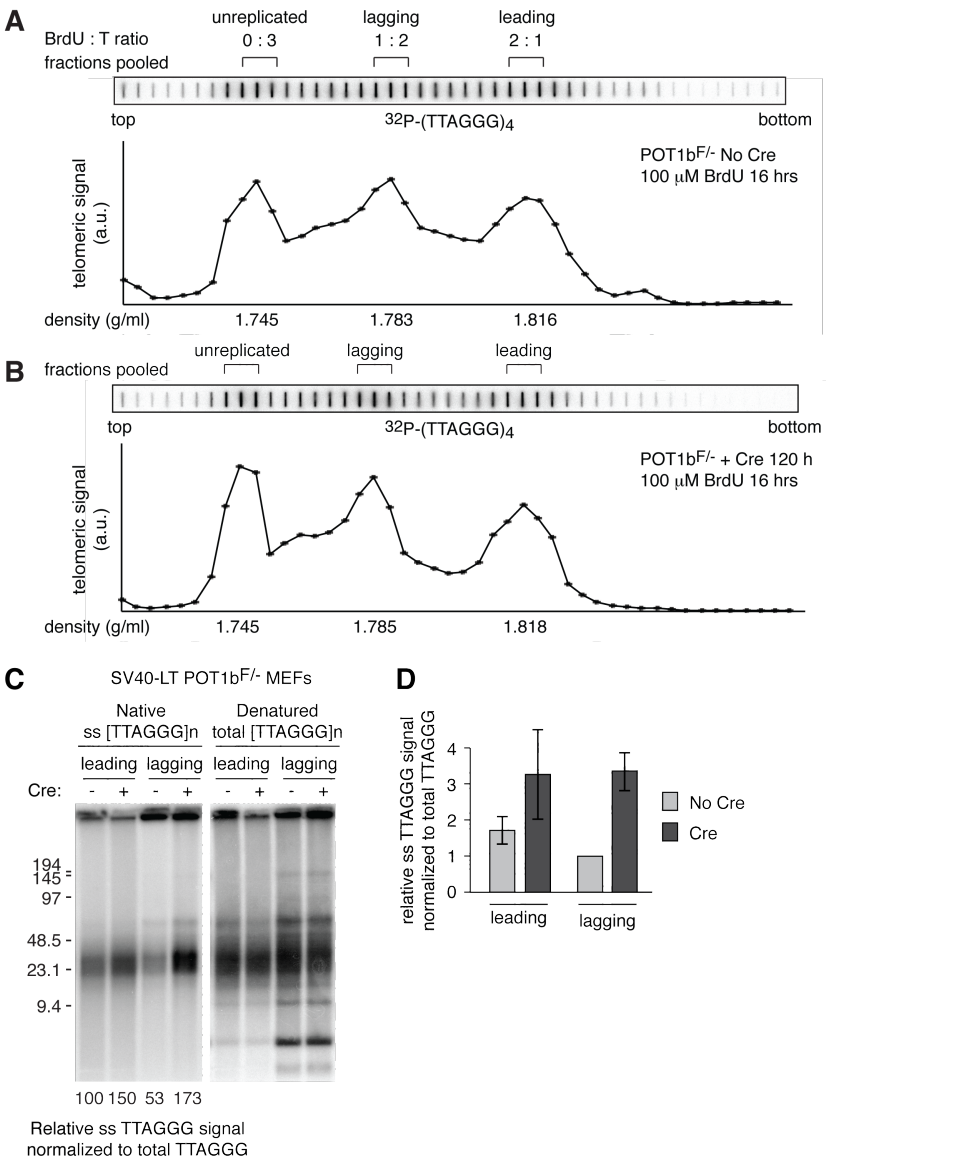

Figure 4.3. POT1b limits overhang size at both newly synthesized telomeres. (A) and (B) Representative slot blot of telomeric signal in each fraction collected from CsCl density gradient equilibrium centrifugation of telomeric DNA from *POT1b*$^{F/-}$ MEFs without Cre (A) and 120 hours after Cre (B) labeled with BrdU for one round of replication. The fractions pooled for overhang analyses are shown. (C) Representative overhang analysis of the separated leading, and lagging-end telomeres from POT1b$^{F/-}$ MEFs in the absence of Cre and 120 hours post-Cre. (D) Quantification of relative overhang signal as detected in (C). Values represent the mean of three independent experiments and standard deviations.

Next, to determine whether POT1b is differentially required at telomeres synthesized by leading- and lagging-strand DNA replication, I labeled POT1b-null cells with BrdU for one round of replication and used CsCl density gradient equilibrium centrifugation to separate the newly synthesized telomeres (as described in Chapter 3). Slot blot detection of the telomeric signal in each fraction collected from the CsCl gradient showed peaks of intensity in fractions corresponding to the leading-end, lagging-end, and unreplicated telomeres. Similar separation of the newly-synthesized telomeres was achieved for both wild type and POT1b-deficient cells (Figure 4.3A-B). In-gel hybridization to detect the telomeric overhangs in pooled fractions isolated from the CsCl gradient revealed that POT1b deletion induced a ~2 fold increase in leading-end overhangs and a ~3 fold increase in the lagging-end overhangs (Figure 4.3C-D). Thus, POT1b appears to be required to limit overhang length at both newly-synthesized telomeres. As expected based on previous work indicating that POT1b function is independent of telomerase[187], the effect of POT1b deletion on the overhangs of both newly synthesized telomeres was similar in telomerase-deficient cells (see Figure 15 for example).

DSB resection factors do not contribute to the excessive overhangs associated with POT1b deficiency

In order to identify factor(s) responsible for the excessive overhangs associated with POT1b deletion, I investigated whether the aberrant overhang phenotype could be rescued by co-depletion of a number of candidate nucleases and/or helicases. To evaluate whether POT1b deletion results in aberrant processing of telomeres by the

nucleases/helicases that act in response to a DSB, I assessed the telomeric overhang of POT1b-deficient MEFs after Nbs1, Exo1, or various RecQ helicases were depleted individually as well as in MEFs lacking POT1b, Nbs1 and Exo1. Among many tested candidates that appeared to have no role in the aberrant resection associated with POT1b loss, those whose depletion was confirmed included Nbs1, Exo1, BLM, and RecQL5. These negative results are summarized below.

Deletion of POT1b and Nbs1 in SV40LT-immortalized *POT1b*$^{F/F}$*Nbs1*$^{F/-}$ cells (generated by N. Dimitrova) with hygromycin-selectable pWzl-Cre resulted in a significant growth defect that was also observed with deletion of Nbs1 alone. Initial overhang analyses using this approach suggested that Nbs1 deficiency did not abrogate the overhang increase that occurs when POT1b is deleted. Since the growth defect could affect the ability for cells to accumulate excess overhangs, I repeated this experiment using non-selectable Hit&Run Cre, which resulted in a less severe growth defect in POT1b/Nbs1 DKO cells (Figure 4.4B-C). I assayed the overhang at 3 and 5 days after the introduction of Cre, timepoints during which POT1b/Nbs1 DKO and POT1b KO cells were still growing at similar rates. Co-deletion of Nbs1 and POT1b had no effect on the aberrant overhang signal that appears in the absence of POT1b (Figure 4.4A).

To address the possibility that MRN/CtIP and Exo1 act in a redundant manner, I generated *POT1b*$^{F/F}$*Nbs*$^{F/F}$*Exo1*$^{-/-}$ MEFs. Deletion of POT1b in the absence of both Nbs1 and Exo1 still resulted in an increase in the telomeric overhang signal at 96 hours post-Cre that was comparable to the increased overhang signal following deletion of POT1b and Nbs1, in littermate MEFs that were assessed in parallel (Fig. 4.4D).

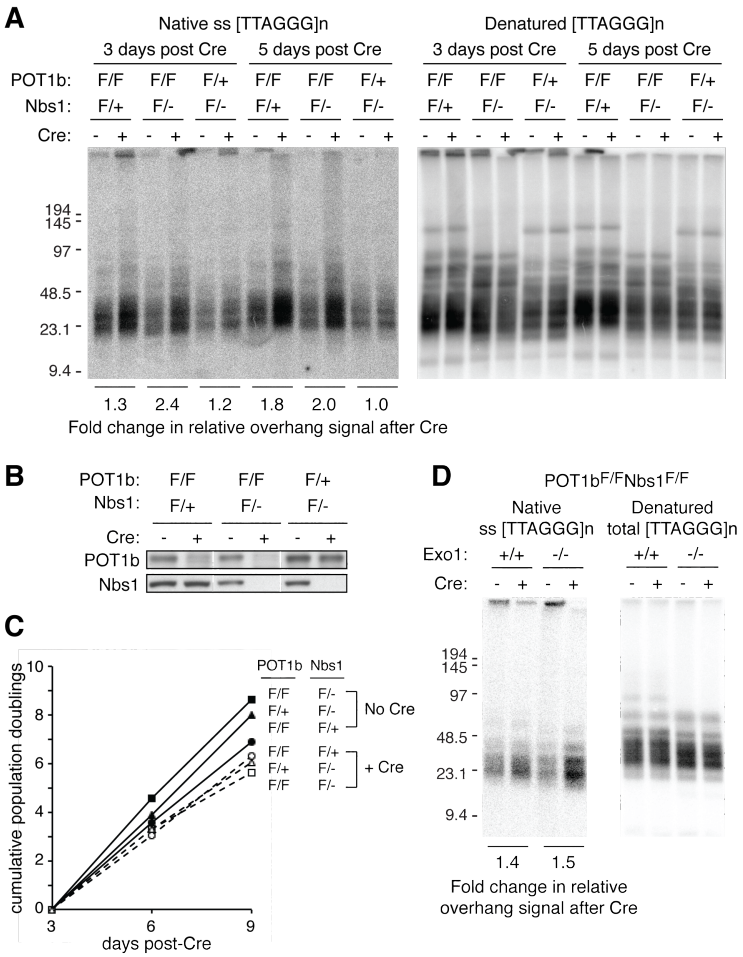

Figure 4.4. The aberrant overhang phenotype that occurs following POT1b deletion does not depend on Nbs1 and/or Exo1. (A) In-gel overhang assay on *POT1b*$^{F/F}$*Nbs1*$^{F/+}$, *POT1b*$^{F/F}$*Nbs1*$^{F/-}$ and *POT1b*$^{F/+}$*Nbs1*$^{F/-}$ MEFs at 84 hours after Hit&Run Cre. (B) Immunoblot detection of POT1b and Nbs1 in the indicated MEFs. (C) Growth curve of *POT1b*$^{F/F}$*Nbs1*$^{F/+}$, *POT1b*$^{F/F}$*Nbs1*$^{F/-}$ and *POT1b*$^{F/+}$*Nbs1*$^{F/-}$ MEFs in the absence and presence of Cre. (D) In-gel overhang assay on primary *POT1b*$^{F/F}$ *Nbs1*$^{F/F}$ *Exo1*$^{-/-}$ and *POT1b*$^{F/F}$ *Nbs1*$^{F/F}$ *Exo1*$^{+/+}$ littermate MEFs at 96 hours after Hit&Run Cre.

In addition, depleting either the BLM or RecQL5 helicase by shRNA also had no effect on the overhang phenotype associated with POT1b deletion (Figure 4.5A-C). Based on these results, it appeared unlikely that POT1b represses aberrant resection by factors involved in DSB resection. These results in themselves did not rule out the possibility that these factors might act redundantly in POT1b-deficient cells – however, subsequent experiments identifying factors that are indeed regulated by POT1b provided support that these negative results are valid.

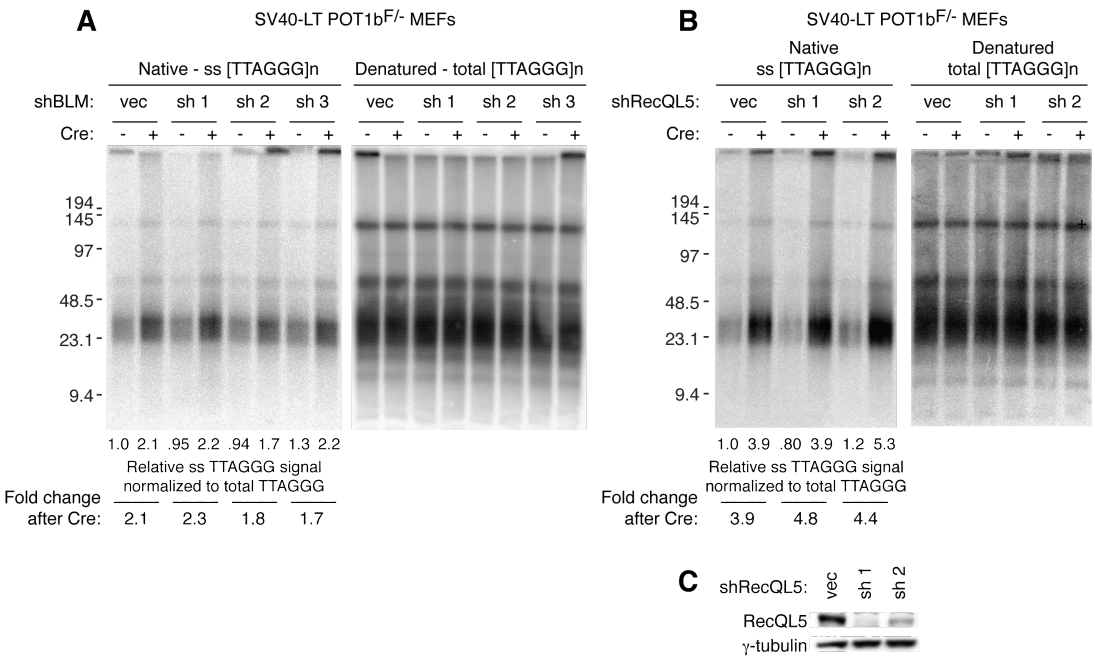

Figure 4.5. The aberrant overhang phenotype that occurs following POT1b deletion does not depend on BLM or RecQL5. A) In-gel overhang assay on *POT1b*$^{F/-}$ MEFs following depletion of BLM with three different retroviral shRNAs (puromycin-selectable) and at 96 hours after pWzl-Cre (hygromycin-selectable). (B) In-gel overhang assay on *POT1b*$^{F/-}$ MEFs following depletion of RecQL5 with two different lentiviral shRNAs (puromycin-selectable) and at 96 hours after pWzl-Cre (hygromycin-selectable). (C) Immunoblot detection of RecQL5 showing depletion with shRNAs.

POT1b inhibits the Apollo nuclease at leading- and lagging-end telomeres

Based on the previously identified role of the Apollo nuclease in the generation of overhangs at leading-end telomeres, I tested whether POT1b inhibits Apollo by generating SV40LT-immortalized *POT1b*$^{F/F}$*Apollo*$^{F/F}$ MEFs from which both POT1b and Apollo could be deleted by Cre recombinase (Figure 4.6A). Following Cre-mediated deletion of Apollo and POT1b, cells showed a mild proliferation defect similar to that observed in the absence of Apollo only (Figure 4.6B). This growth defect was partially rescued by the introduction of wild type Apollo but not by the introduction of the ApolloΔTRF2 allele (refer to Chapter 3) lacking the ability to localize to telomeres due to mutations in the TRF2-interacting YxLxP motif (Figure 4.6C-D). When the telomeric overhang signal was detected by in-gel hybridization, co-deletion of Apollo and POT1b

resulted in a ~1.5 fold increase in the telomeric overhang signal, which was approximately half that observed in the absence of POT1b alone (Figure 4.6E-F).

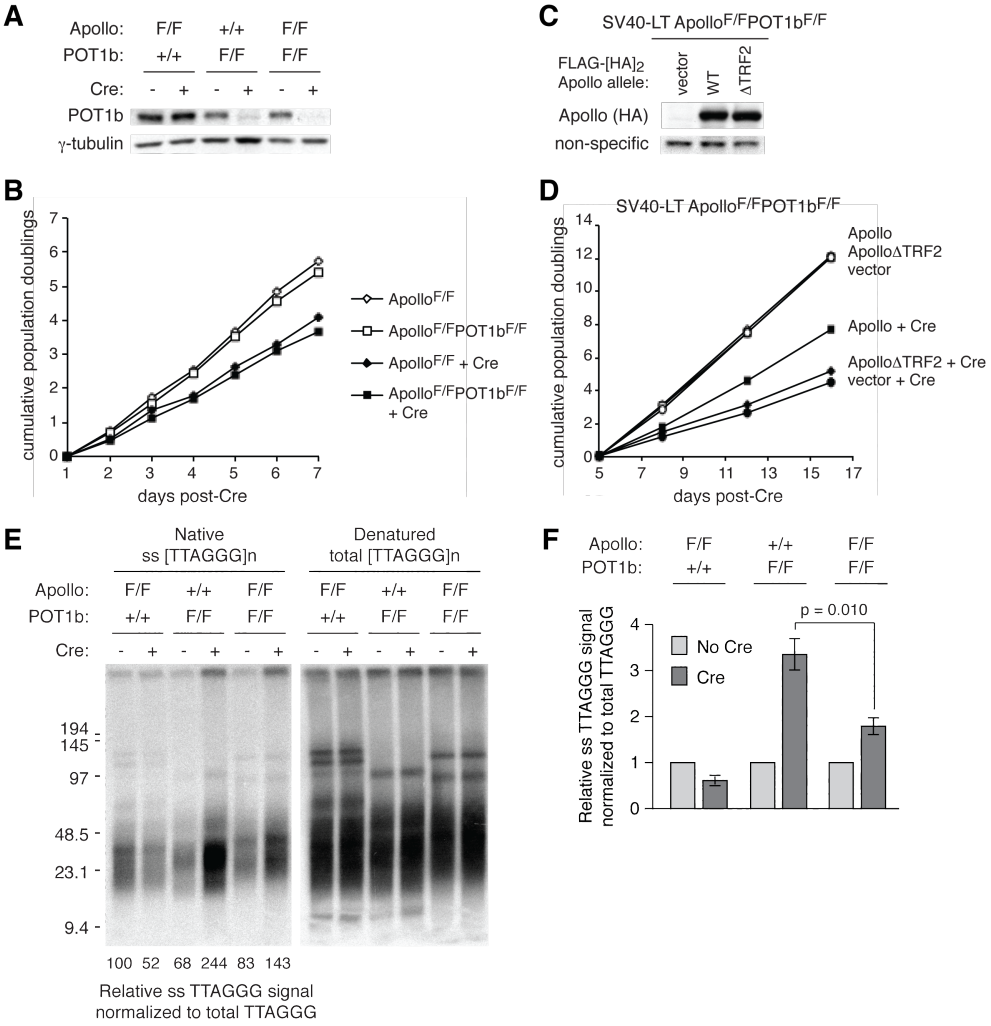

G

	Chromosomes analyzed	% chromosomes fused leading-leading	all others
Apollo$^{F/F}$ + Cre	1086	10.1	1.7
Apollo$^{F/F}$POT1b$^{F/F}$ + Cre	1367	9.2	2.9

Figure 4.6. Accumulation of excess overhangs upon POT1b deletion partially depends upon Apollo. (A) Immunoblot detection of POT1b at 120 h after Cre in SV40LT-immortalized *Apollo$^{F/F}$*, *POT1b$^{F/F}$*, and *Apollo$^{F/F}$POT1b$^{F/F}$* MEFs. (B) Growth curve of SV40LT-immortalized *Apollo$^{F/F}$* and *Apollo$^{F/F}$POT1b$^{F/F}$* MEFs after treatment with Hit&Run Cre. (C) Immunoblot detection of FLAG-[HA]$_2$-tagged Apollo alleles expressed in SV40LT-immortalized *Apollo$^{F/F}$POT1b$^{F/F}$* MEFs. HA.11 antibody was used to detect exogenously-introduced Apollo. (D) Growth curve of SV40LT-immortalized *Apollo$^{F/F}$POT1b$^{F/F}$* MEFs expressing Apollo alleles in the absence and presence of hygromycin-selectable pWzl-Cre. (E) In-gel overhang analysis of indicated MEFs without and at 120 h after Hit&Run Cre. (F) Quantification of overhang assay as shown in (E). Values indicate the mean and sd of three independent experiments. (G) Quantifiation of CO-FISH analysis to detect telomere fusions in *Apollo$^{F/F}$POT1b$^{F/F}$* MEFs after Cre.

Though the bulk overhang signal in the absence of both Apollo and POT1b was increased compared to that of wild type cells, a mild telomere dysfunction phenotype was observed, as might be expected based on the proliferation defect. Metaphase spreads of cells lacking Apollo and POT1b revealed a significant incidence of chromatid-type fusions between telomeres, at a similar level as that observed in the absence of Apollo alone (Figure 4.6G). CO-FISH analysis revealed that the fusions occurred largely between leading-end telomeres (Figure 4.6G). Thus, despite no apparent reduction in the relative overhang signal of bulk telomeres in Apollo/POT1b DKO cells, the appearance of leading-end fusions suggested that at least a subset of these telomeres become deprotected in the absence of both Apollo and POT1b.

These results suggested that POT1b might limit overhang size by inhibiting Apollo at both newly-synthesized telomeres. Alternatively, co-deletion of Apollo and POT1b could result in a reduction in overhang size at leading-end telomeres while accumulating excessive overhangs at lagging-end telomeres to the same extent as in the absence of POT1b alone. The latter scenario is plausible due the specific role of Apollo in overhang generation at leading-end telomeres, and since cells lacking both Apollo and POT1b exhibited some of the telomere dysfunction phenotypes associated with the loss of Apollo alone. To distinguish between these possibilities, I used the CsCl density gradient approach to isolate the leading- and lagging-end telomeres in cells lacking Apollo and POT1b. If POT1b inhibits Apollo at both newly synthesized telomeres, the overhang signal at both leading- and lagging-end telomeres lacking Apollo and POT1b would be less than that in the absence of POT1b alone. Meanwhile, if the excess overhangs at lagging-end telomeres lacking POT1b are generated independently of

Apollo, cells deficient for both Apollo and POT1b would have reduced overhangs at leading-end telomeres while the overhang signal at lagging-end telomeres would remain similar to that observed as in the absence of POT1b alone.

Separation of newly synthesized telomeres by the CsCl density gradient approach revealed that cells lacking both Apollo and POT1b had a reduced overhang signal at leading-end telomeres compared to wild type cells, though this defect was less severe than in cells lacking Apollo only (Figure 4.7A-E, refer to Figure 3.8 for Apollo KO data). The finding that the co-deletion of POT1b and Apollo does not result in an increase in the overhang signal at leading-end telomeres, as observed in the absence of POT1b alone (Figure 4.7C-E, refer to Figure 4.3 for POT1b KO data), suggests that POT1b inhibits Apollo at newly-synthesized leading-end telomeres. In Apollo-deficient cells, a subset of leading-end telomeres activate a DNA damage response and engage in fusions due to compromised overhang generation. At the remaining leading-end telomeres that still possess overhangs in the absence of Apollo, POT1b is dispensable for limiting overhang size.

Following deletion of Apollo and POT1b, the overhang signal at lagging-end telomeres was elevated by approximately 1.5 fold compared to wild type (Figure 4.7C-D). This phenotype was much milder than that observed in the absence of POT1b alone, which induces a ~3 fold increase in the lagging-end telomeric overhang signal (Figure 4.7E, refer to Figure 4.3 for POT1b KO data). Thus, POT1b limits overhang size at both newly-synthesized telomeres through the inhibition of Apollo. Since co-deletion of Apollo and POT1b does not completely abolish the accumulation of excessive single-stranded overhang signals at lagging-end telomeres (4.7C-E, also see Figure 4.6E-F,

4.8A,C), POT1b is likely to limit overhang size through additional mechanisms besides the inhibition of Apollo.

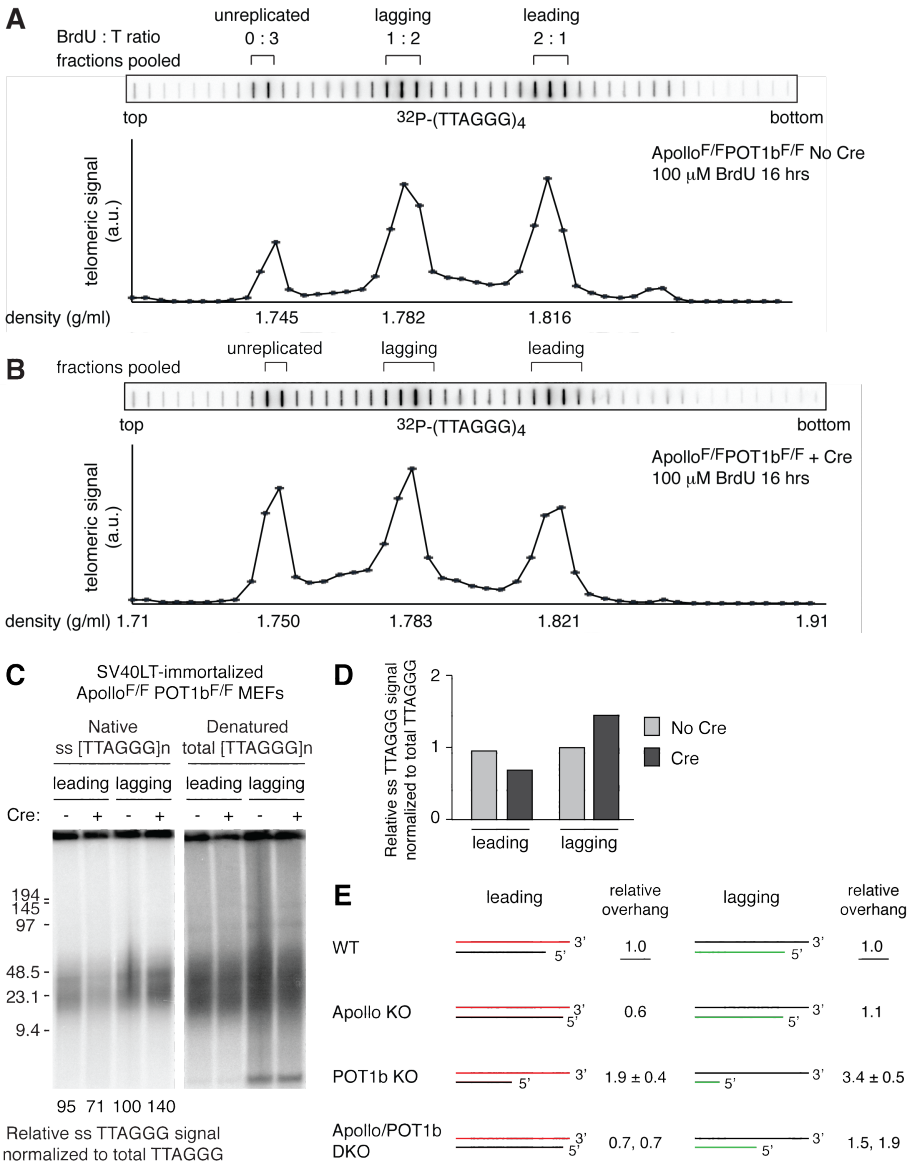

Figure 4.7. POT1b inhibits Apollo at both newly synthesized telomeres. (A) and (B) Representative slot blot of telomeric signal in each fraction collected from CsCl density gradient equilibrium centrifugation of telomeric DNA from *Apollo*$^{F/F}$*POT1b*$^{F/F}$ MEFs without Cre (A) and 120 hours after Cre (B) labeled with BrdU for one round of replication. (C) Representative overhang analysis of the separated leading- and lagging-end telomeres from *Apollo*$^{F/F}$*POT1b*$^{F/F}$ MEFs in the absence of Cre and 120 hours post-Cre. (D) Quantitation of relative overhang signal as detected in (C). Values for the leading- and lagging- end telomeres represent the mean of two independent experiments. (E) Relative overhang size in different genetic backgrounds (refer to Figs. 3.8 and 4.3 for data on Apollo KO and POT1b KO).

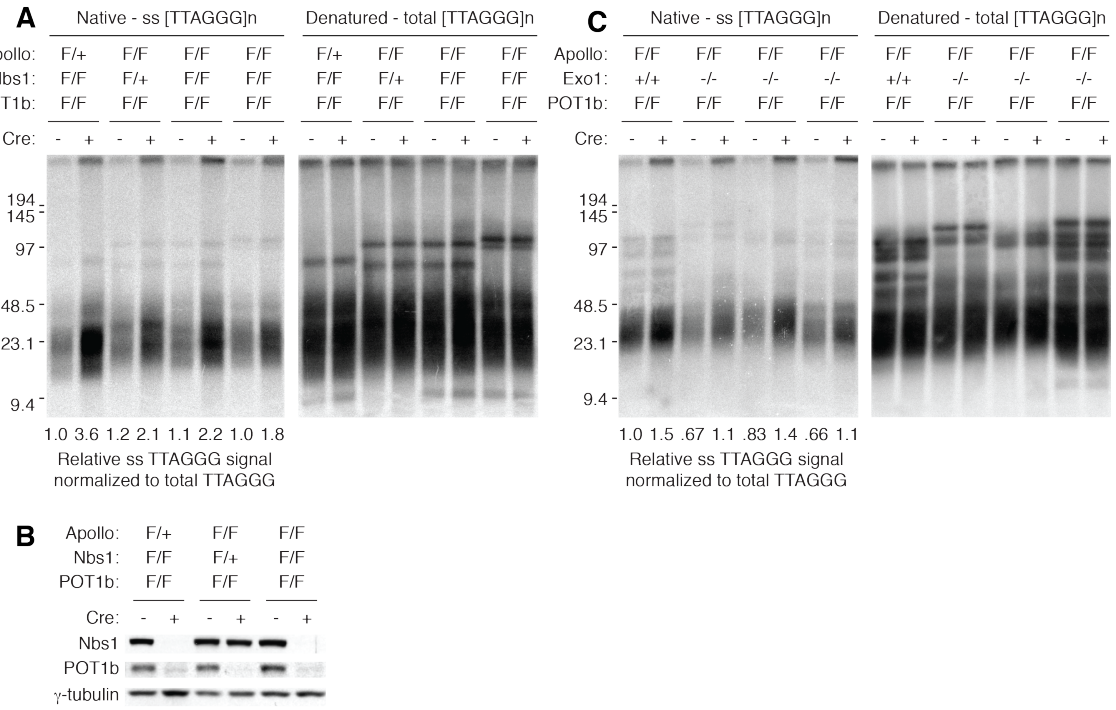

Figure 4.8. The excess telomeric overhang signal that persists in the absence of POT1b and Apollo does not depend on Nbs1 or Exo1. A) In-gel overhang assay on MEFs of the indicated genotypes at 96 hours after Hit&Run Cre. (B) Immunoblot detection of Nbs1 and POT1b in MEFs assayed in (A). (C) In-gel overhang assay on MEFs of the indicated genotypes at 96 hours after Hit&Run Cre.

To determine if other nucleases such as MRN/CtIP or Exo1 contribute to the residual accumulation of excess overhangs that occurs in the absence of POT1b and Apollo, the telomeric overhang was analyzed in *Apollo*$^{F/F}$*Nbs1*$^{F/F}$*POT1b*$^{F/F}$ and *Apollo*$^{F/F}$*Exo1*$^{-/-}$*POT1b*$^{F/F}$ MEFs treated with Cre. Co-deletion of Nbs1 in addition to Apollo and POT1b resulted in a similar level of excess overhang accumulation as in the absence of Apollo and POT1b (Figure 4.8A-B). As will be discussed in the next chapter, Exo1 contributes to the transient elongation of the telomeric overhang that occurs in wild type cells during late S phase; however, co-deletion of Exo1, Apollo, and POT1b did not abolish the accumulation of excess overhang signal observed in Apollo/POT1b DKO cells (Figure 4.8C). Thus, as suggested by previous work, POT1b does not protect telomeres from excessive degradation by Exo1[187]. Together, these results argue against a

role for POT1b in protecting telomeres from aberrant degradation by nucleases involved in DNA DSB resection. This is consistent with the fact that the absence of POT1b does not elicit any DNA damage signal that might be expected to activate nucleases involved in DSB resection[37].

POT1b promotes the activity of Stn1 at leading and lagging end telomeres

Since there was no evidence that POT1b inhibited resection by other candidate nuclease(s)/helicase(s), I tested whether POT1b has a role in promoting the telomeric function of the mammalian Ctc1/Stn1/Ten1 (CST) complex, which has recently been implicated in limiting overhang size in human cells[288,289]. Ctc1 and Stn1, also known as AAF144 and AAF42, respectively, were originally identified as accessory factors of polymerase alpha/primase that stimulate its activity *in vitro* and share structural similarities with RPA32 and RPA70[290]. Along with a third OB-fold containing protein, Ten1, this RPA-like complex binds single-stranded DNA in a sequence-independent manner and has been reported to localize to replication foci as well as telomeres[288,290]. Based on its localization to a subset of telomeres, as well as sequence homology between mammalian and yeast Stn1 and Ten1, this complex has been proposed to be the mammalian counterpart of yeast Cdc13/Stn1/Ten1 (CST)[288,289].

Corroborating previous studies on the effects of Stn1 depletion in human cells, depleting Stn1 in wild type MEFs resulted in a 2-fold increase in the single-stranded telomeric signal (Figure 4.9A-C). This single-stranded signal was completely susceptible to digestion by the *E. coli* 3'-5' exonuclease ExoI, indicating that the signal was due to terminal and not internal single-stranded telomeric DNA that might arise from

uncoupling of the replication fork and exposure of the lagging strand template (Figure 4.10A). Stn1 depletion did not affect the levels of POT1a or b (Figure 4.9A) and did not lead to the appearance of telomere dysfunction induced foci (TIFs) (see Figure 4.16C). In addition, the effect of Stn1 depletion on the telomeric overhang was independent of telomerase (Figure 4.10A-B).

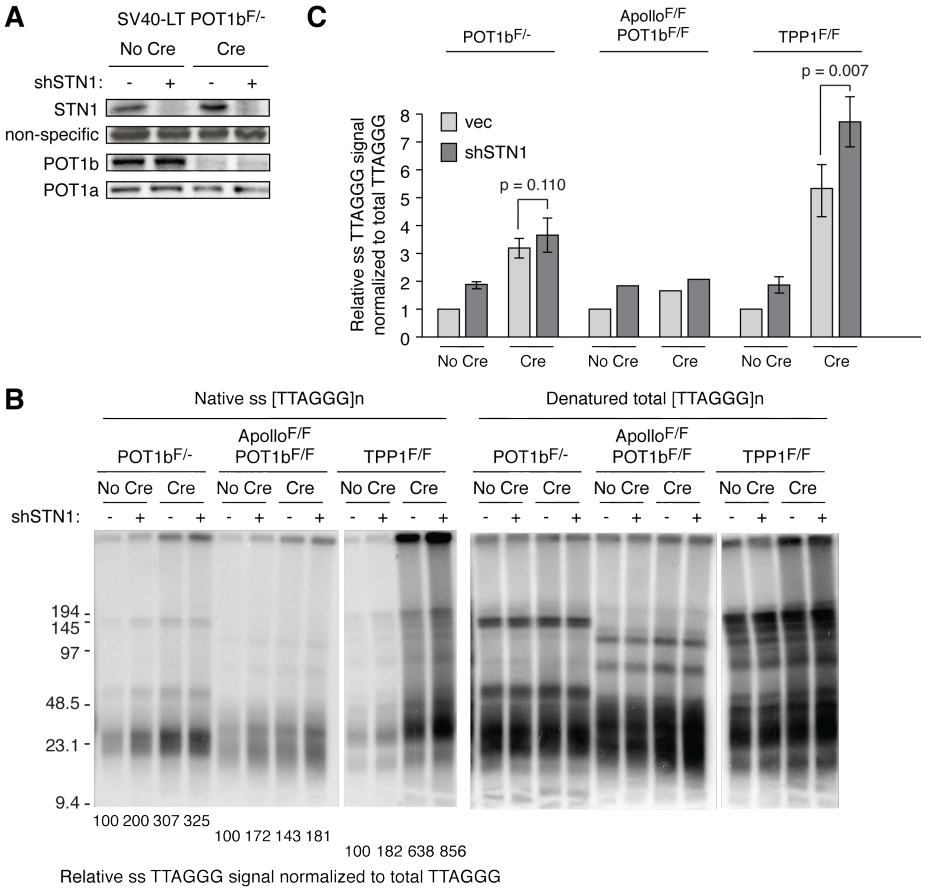

Figure 4.9. POT1b is epistatic to Stn1. A) Immunoblot detection of Stn1, POT1b, and POT1a in *POT1b*$^{F/-}$ MEFs at 96 hours following lentiviral shRNA to Stn1 and 120 hours after Cre. (B) In-gel overhang assay on MEFs of the indicated genotypes at 96 hours following lentiviral shRNA to Stn1 and 120 hours after Hit&Run Cre. For each MEF line, the relative ssTTAGGG signal is given with the first lane set to 100. (C) Quantification of overhang analyses as shown in (B).

On the other hand, depleting Stn1 in POT1b KO cells had very little additional effect on the already elevated overhang signal (Figure 4.9B-C). A similar epistatic relationship was observed when Stn1 was depleted in cells lacking both POT1b and

Apollo (Figure 4.9B-C). This suggested that Stn1 requires POT1b for its role in limiting overhang size at telomeres.

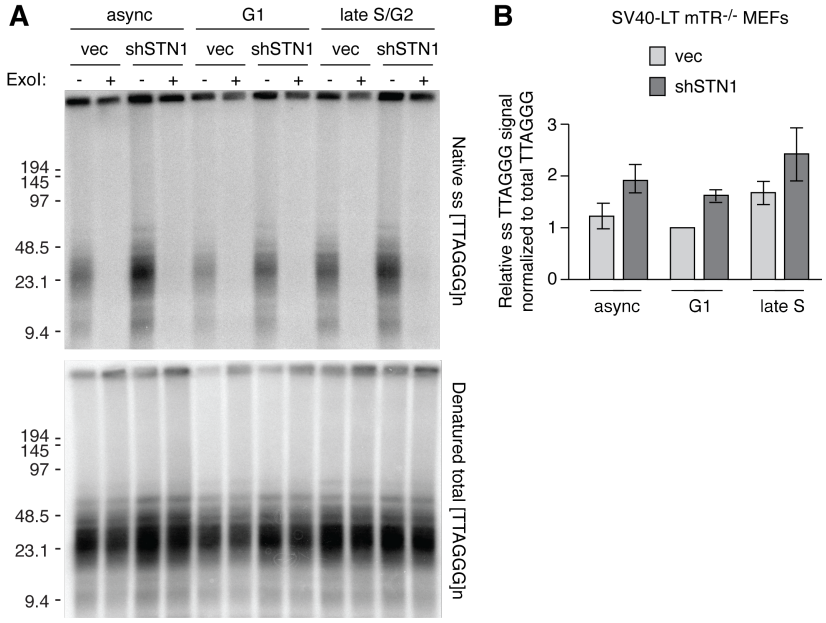

Figure 4.10. Stn1 depletion results in elevated telomeric overhangs in G1 and S phase. (A) In-gel overhang analysis of SV40LT-immortalized *mTR*$^{-/-}$ MEFs at 96 hours after retroviral shRNA to shStn1 in G1 and late S, isolated by FUCCI-FACS as previously described. (B) Quantification of overhang analyses shown in (A). Values represent the mean of three independent experiments and standard deviations.

An unexpected outcome occurred when Stn1 was depleted in TPP1-deficient cells. Since TPP1 is required for the telomeric localization of POT1b[29,188], the overhang phenotype associated with TPP1 deletion was expected to be epistatic to Stn1 depletion. However, Stn1 depletion in the absence of TPP1 resulted in a statistically significant increase in the already elevated telomeric overhang signal (Figure 4.9C). This result suggests that Stn1 may have a POT1b-independent role at telomeres in certain contexts, such as with the loss of TPP1. In contrast to deleting POT1b alone, TPP1 deletion also leads to the removal of POT1a, eliciting an ATR-dependent DNA damage signal and increased single-stranded telomeric signals greater than that observed with POT1b

deletion alone[188]. The capacity in which Stn1 may act at telomeres lacking TPP1/POT1a/POT1b remains a question for future investigation.

To further evaluate the role of Stn1 in limiting overhang size, Stn1 was depleted in telomerase-deficient cells expressing the FUCCI markers and cells G1 or late S phase cells were isolated by FACS. Stn1-depleted cells had increased overhangs in both G1 and S phase when compared to wild type cells in the same cell cycle phase (Figure 4.10A-B). These results suggest that following Stn1 depletion, not only are overhangs aberrantly increased in S phase, but fill-in synthesis of the C-rich strand is insufficient to restore overhang length to wild type levels in G1.

Next, I asked whether Stn1 acts differentially at leading and lagging end telomeres. Stn1-depleted cells incorporated BrdU into the leading and lagging end telomeres at similar ratios as wild type cells (Figure 4.11A-B), indicating that Stn1 depletion does not cause significant problems in semi-conservative replication of telomeres and that the newly synthesized telomeres in Stn1-depleted cells could be effectively separated by CsCl density gradient equilibrium centrifugation. Analyses of the overhangs at leading- and lagging-end telomeres following Stn1 depletion revealed a 2-fold increase in the overhangs at both newly synthesized telomeres (Figure 4.11C-D). Thus, Stn1 limits terminal overhang size at telomeres synthesized by both leading- and lagging-strand DNA replication. Based on its identification as an accessory factor DNA polymerase α/primase, Stn1, in complex with Ctc1 and Ten1, may promote fill-in synthesis of the telomeric C-rich strand.

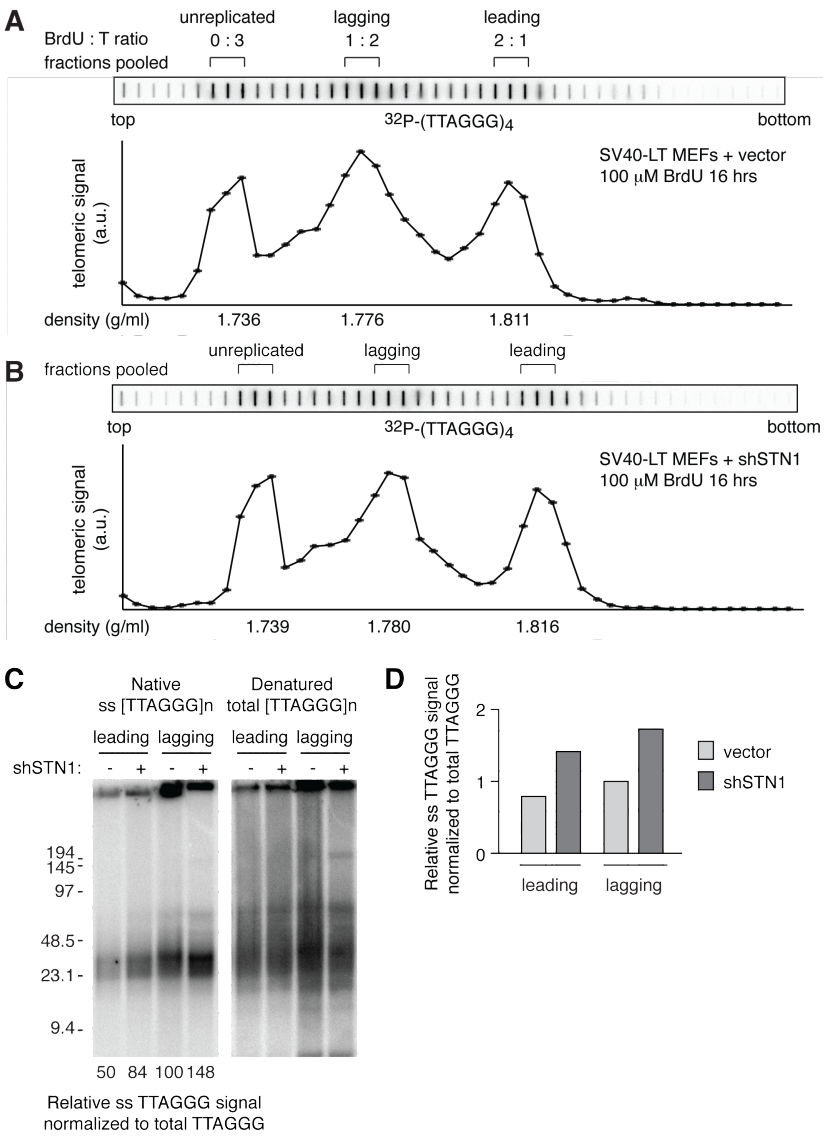

Figure 4.11. Stn1 limits overhang size at both newly synthesized telomeres. (A) and (B) Representative slot blot of telomeric signal in each fraction collected from CsCl density gradient equilibrium centrifugation of BrdU-labeled telomeric DNA from wild type MEFs at 96 hours following lentiviral transduction of vector (A) or shRNA targeting Stn1 (B). The fractions pooled for overhang analyses are shown. (C) Representative overhang analysis of the separated leading- and lagging-end telomeres from MEFs at 96 h following Stn1 depletion. (D) Quantification of relative overhang signal as detected in (C). Values represent the mean of two independent experiments.

POT1b, but not POT1a, interacts with CST

Since POT1b and CST appeared to function in the same pathway, a natural question was whether POT1b interacts physically with components of CST. Experiments performed by H. Takai (de Lange lab) showed that when myc-POT1b and FLAG-tagged

versions of all three components of mouse CST (Ctc1, Stn1, and Ten1) were co-transfected in 293T cells, co-immunoprecipitation with the myc antibody pulled down Ctc1 and Stn1. A low level of CST could also be pulled down with TPP1, but not with POT1a or any other component of mouse shelterin (Figure 4.12C). Myc-POT1b could also be detected in the reciprocal co-IP using the FLAG antibody (Figure 4.12E, right panel).

Previous studies have mapped the domain required for POT1b function using a domain-swapping approach in which chimeric constructs of POT1a, POT1b, and human POT1 were generated by interchanging the N-terminal OB-folds, C-terminal TPP1-binding domain, and an internal region spanning amino acids 300-350[39] (Figure 4.12A). These studies revealed that the C-terminal domain of POT1b was required to prevent the accumulation of single stranded telomeric DNA[39]. In relation to their ability to suppress the aberrant overhang phenotype associated with POT1b deletion, the regions spanning amino acids 300-350 of POT1b and human POT1 were functionally equivalent, while the domain C-terminal to aa 350 could not be replaced by the same region in POT1a or human POT1[39].

Figure 4.12. POT1b, but not POT1a, interacts with Ctc1/Stn1/Ten1. (A) Domain organization of mouse POT1b. Below are listed the domain requirements for suppression of aberrant overhang accumulation, as revealed from domain-swapping experiments using chimeric constructs of POT1a, POT1b, and hPOT1. (B) Sequence alignment of regions in the C-terminal domain of human POT1, mouse POT1a, and mouse POT1b. Shown in blue are residues conserved among all three POT1s. Residues conserved between hPOT1 and mPOT1b but not POT1a are shown in green and marked below with asterisks (*). Residues conserved in hPOT1 and mPOT1a but not POT1b are shown in red and marked below with arrowheads (^). Residues that were changed to generate POT1b mutants are indicated with gray boxes. (C) Co-immunoprecipitation of POT1b and Ctc1/Stn1/Ten1 (C/S/T). 293T cells were transiently co-transfected with myc-tagged mPOT1a or mPOT1b, and FLAG-tagged mCtc1, mStn1, and mTen1, in the absence or presence of myc-mTPP1. IPs were performed with the myc (9E10) antibody. Input (left) and IPs (right) were analyzed by immunoblotting for myc (top) and FLAG (bottom). (D) List of POT1b mutants tested for their ability to interact with CST in 293T co-IP. (E) Co-immunoprecipitation of POT1b mutants with C/S/T. In the left two panels, co-IP was performed as in (C). In the right panel, IPs were performed with the FLAG antibody and inputs and IPs were analyzed by immunoblotting for myc (top) and FLAG (bottom). (Experiments by H. Takai)

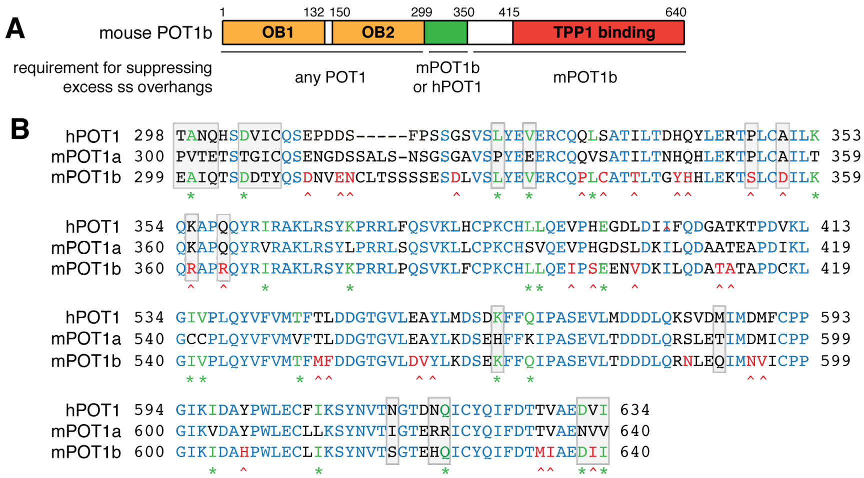

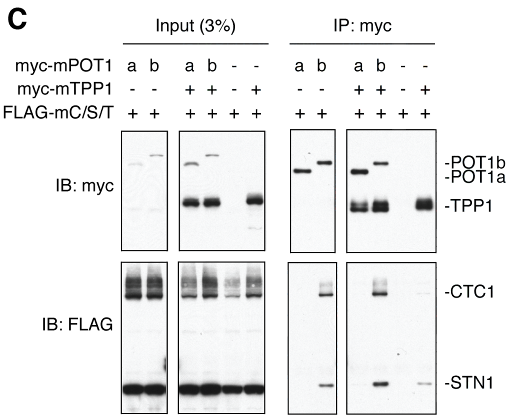

D

POT1b mutant	Site(s) of mutation
EAIQ	E299P, A300V, I301T, Q302E
DDTY	D305T, D306G, T307I, Y308C
LV	L329P, V333E
SD	S353P, D356A
RR	R361K, R364Q
K580H	K580H
Q591T	Q591T
HQ	H624R, Q625R
SHQ	S620I, H624R, Q625R
ΔC-term	Δ591-640
DII	aa1-300 replaced with POT1a aa1-301, D638N, I639V, I640V
LVDII	L329P, V332E, D638N, I639V, I640V

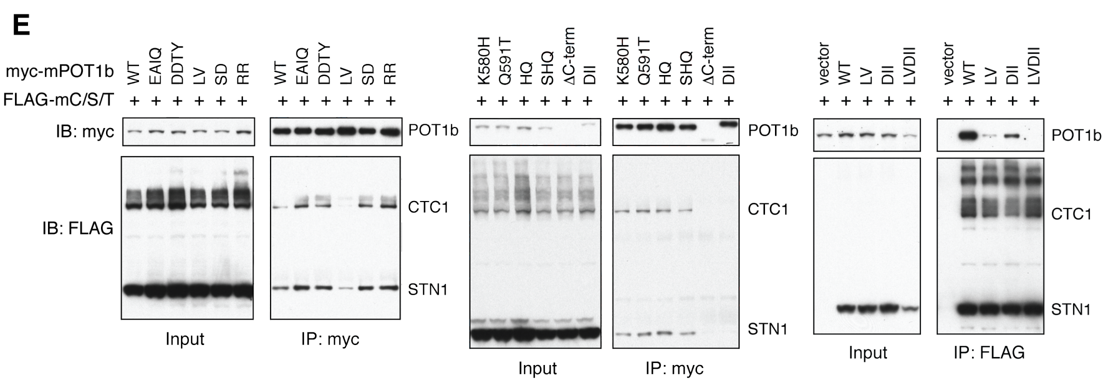

Sequence alignment of human POT1, mouse POT1a, and mouse POT1b identified a number of residues in the C-terminal domain that were conserved between human POT1 and POT1b but not found in POT1a as well as residues conserved between human POT1 and POT1a but not found in POT1b (Figure 4.12B). Based on these sequence differences, a number of POT1b mutants were generated in which the residues in POT1b were mutated to the corresponding amino acids in POT1a (Figure 4.12D). Though most of the mutations did not affect the ability of POT1b to pull down Ctc1 and Stn1 by co-immunoprecipitation in 293T cells, two POT1b mutants showed a diminished interaction with CST by 293T co-IP (Figure 4.12E). The first mutant, named POT1b-LV, contained two point mutations, L329P/V333E, of residues conserved between human POT1 and mouse POT1b in the region that was previously identified to be interchangeable between human POT1 and mouse POT1b. The second, named POT1b-DII, was generated by mutating the three residues at the C-terminus of POT1 to the corresponding amino acids in POT1a. Notably, D638 and I640 are conserved in both human POT1 and mouse POT1b, while I639 is found only in mouse POT1b (Figure 4.12B). Though these mutations comprised the interaction between POT1b and CST, a residual amount of POT1b-LV and POT1b-DII could still be detected in co-IPs with FLAG-CST (Figure 4.12E). However, the POT1b-LVDII mutant, containing mutations in all five residues, completely abolished the interaction between POT1b and CST detected by 293T co-IP (Figure 4.12E). Mutating the same residues in POT1a to the corresponding amino acids in POT1b was not sufficient to provide POT1a with the ability to interact with CST in 293T co-IPs[431].

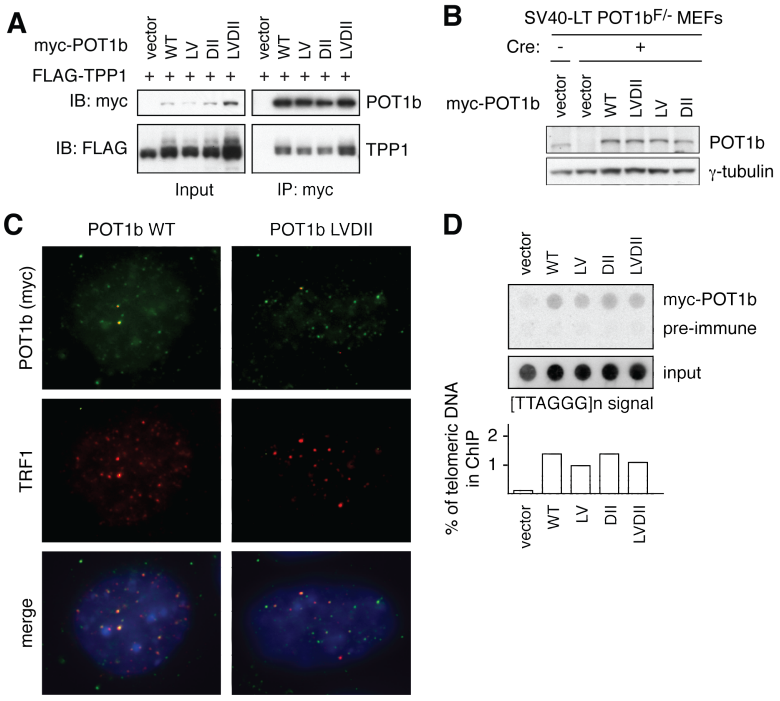

Figure 4.13. A POT1b mutant unable to interact with CST still interacts with TPP1 and localizes to telomeres. (A) Co-immunoprecipitation of POT1b mutants and TPP1. 293T cells were transiently transfected with the indicated myc-tagged POT1b alleles, and FLAG-tagged TPP1. IPs were performed with the myc (9E10) antibody. Input (left) and IPs (right) were analyzed by immunoblotting for myc (top) and FLAG (bottom). (B) Immunoblot detection of POT1b mutants expressed in *POT1b*$^{F/-}$ MEFs after Cre-mediated deletion of endogenous POT1b. (C) Immunofluorescence detection of the indicated POT1b alleles using the myc antibody. Telomeres are detected with the TRF1 antibody. (D) Telomeric DNA ChIP for POT1b mutants. ChIP was performed with myc and control (rabbit preimmune) antibodies on *POT1b*$^{F/-}$ MEFs expressing different POT1b alleles after Cre-mediated deletion of endogenous POT1b. Quantification of the % of TTAGGG repeats recovered in the IPs is shown the bar graph below. (Experiments by H. Takai)

Consistent with the preservation of most of the C-terminal TPP1-binding domain in POT1b-LVDII, 293T co-immunoprecipitation experiments showed that this mutant maintained its ability to interact with TPP1 (Figure 4.13A). When POT1b-LVDII was introduced into *POT1b*$^{F/-}$ MEFs from which endogenous POT1b was deleted by Cre recombinase, the mutant protein was detectable at telomeres by immunofluorescence for the myc tag as well as telomeric ChIP (Figure 4.13B-D). While POT1b-LVDII localized to telomeres to a similar extent as wild type POT1b, its expression reduced the telomeric localization of Stn1 as detected by immunofluorescence[431]. Thus, the POT1b-LVDII

mutant could be used not only to explore the functions of POT1b related to its interaction with CST but also to query the telomere-specific functions of CST.

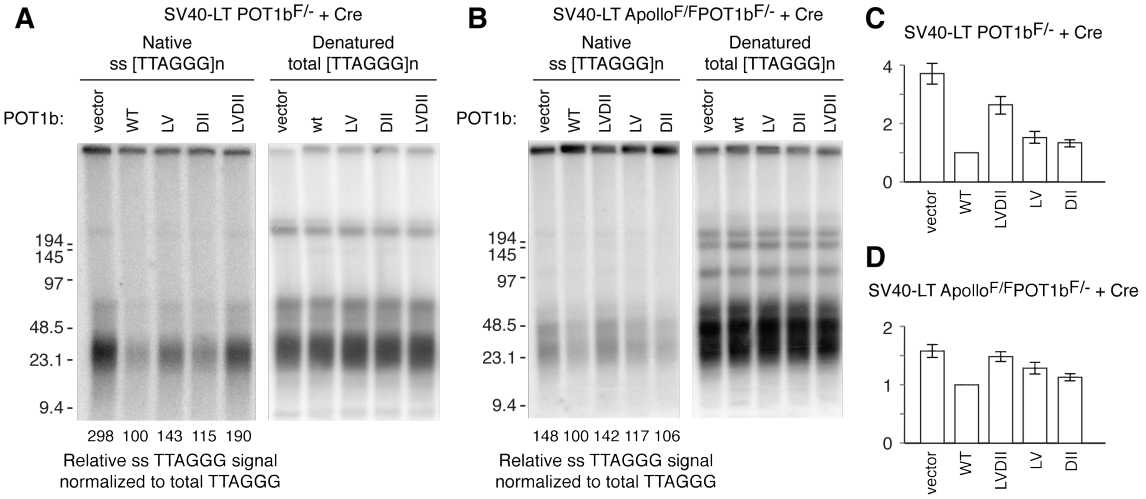

Figure 4.14. The POT1b mutant unable to interact with CST mimics depletion of Stn1. (A) Representative in-gel overhang analysis of *POT1b*$^{F/-}$ MEFs expressing the indicated POT1b alleles at 120 h after Hit&Run Cre. (B) Representative in-gel overhang analysis of *Apollo*$^{F/F}$*POT1b*$^{F/F}$ MEFs expressing the indicated POT1b alleles at 120 h after Hit&Run Cre. (C) Quantitation of overhang analysis in (A). Values indicate the mean and sd of three independent experiments. (D) Quantitation of overhang analysis in (B). Values indicate the mean and sd of three independent experiments. (Experiments by H. Takai)

In collaboration with H. Takai, I investigated the telomeric overhang signal in *POT1b*$^{F/-}$ MEFs expressing either wild type or mutant alleles of POT1b after the deletion of endogenous POT1b with Cre. Whereas wild type POT1b completely abolishes the excess overhangs associated with POT1b deletion, POT1b-LVDII mutant was unable to fully rescue this phenotype (Figure 4.14A, C). In the presence of POT1b-LVDII, the telomeric overhang signal remained elevated by ~2 fold compared to wild type, similar to the case when Stn1 was depleted by shRNA. The partial rescue of the overhang phenotype associated with POT1b deletion by the POT1b-LVDII mutant suggested that this mutant might be functional in its ability to suppress aberrant resection by Apollo while being unable to promote the telomeric function of CST.

Indeed, when *Apollo*$^{F/F}$*POT1b*$^{F/F}$ cells expressing either vector or POT1b-LVDII were treated with Cre, the resultant increase in overhang signal was identical (Figure 4.14B,D). Thus, POT1b-LVDII appears to be a dissociation-of-function mutant that inhibits Apollo while being unable to promote CST function. In the absence of both Apollo and POT1b, the accumulation of excess overhangs is due entirely to the loss of CST function at telomeres. Overhang analyses of POT1b-deficient cells complemented with the POT1b-LV and POT1b-DII mutants further confirmed that the level to which the mutants suppressed the aberrant overhang phenotype of POT1b KO cells correlated with the ability of the mutants to interact with CST. That is, the POT1b-LV and POT1b-DII mutants, which still retained some ability to interact with CST, suppressed the excessive overhangs in POT1b null cells to a greater extent than POT1b-LVDII (Figure 4.14A-D).

Next, I analyzed the overhangs of the leading- and lagging-end telomeres in cells expressing the POT1b-LVDII mutant, to corroborate the functions attributed to Stn1. Indeed, similar to what had been observed upon Stn1 depletion, POT1b-deficient cells complemented with POT1b-LVDII had increased overhangs at both the leading- and lagging-end telomeres compared to cells complemented with wild type POT1b (Figure 4.15A-F). With respect to the overhang phenotype at leading-end telomeres, POT1b-LVDII completely mimicked deletion of POT1b (Figure 4.15D-F). At the lagging-end telomeres, POT1b-LVDII partially rescued the excessive overhang signal that occurred in the absence of POT1b. These results suggest that overhang size at leading-end telomeres is limited by POT1b primarily through the recruitment of CST. At lagging-end telomeres, on the other hand, both the inhibition of Apollo and recruitment of CST are important for limiting excessive overhang accumulation.

Figure 4.15. The POT1b mutant unable to interact with CST mimics the depletion of Stn1 at at both newly synthesized telomeres. (A), (B), (C) Representative slot blots of telomeric signal in each fraction collected from CsCl density gradient equilibrium centrifugation of BrdU-labeled telomeric DNA from *POT1b*$^{F/-}$ MEFs expressing vector (A), wild type POT1b (B), or POT1b-LVDII (C) at 120 hours after Cre. (D) Overhang analysis of bulk telomeres, and the separated leading- and lagging-end telomeres from telomerase-proficient MEFs. (E) Overhang analysis of bulk telomeres, and the separated leading- and lagging-end telomeres from telomerase-deficient MEFs. (F) Compilation of results shown in (D) and (E).

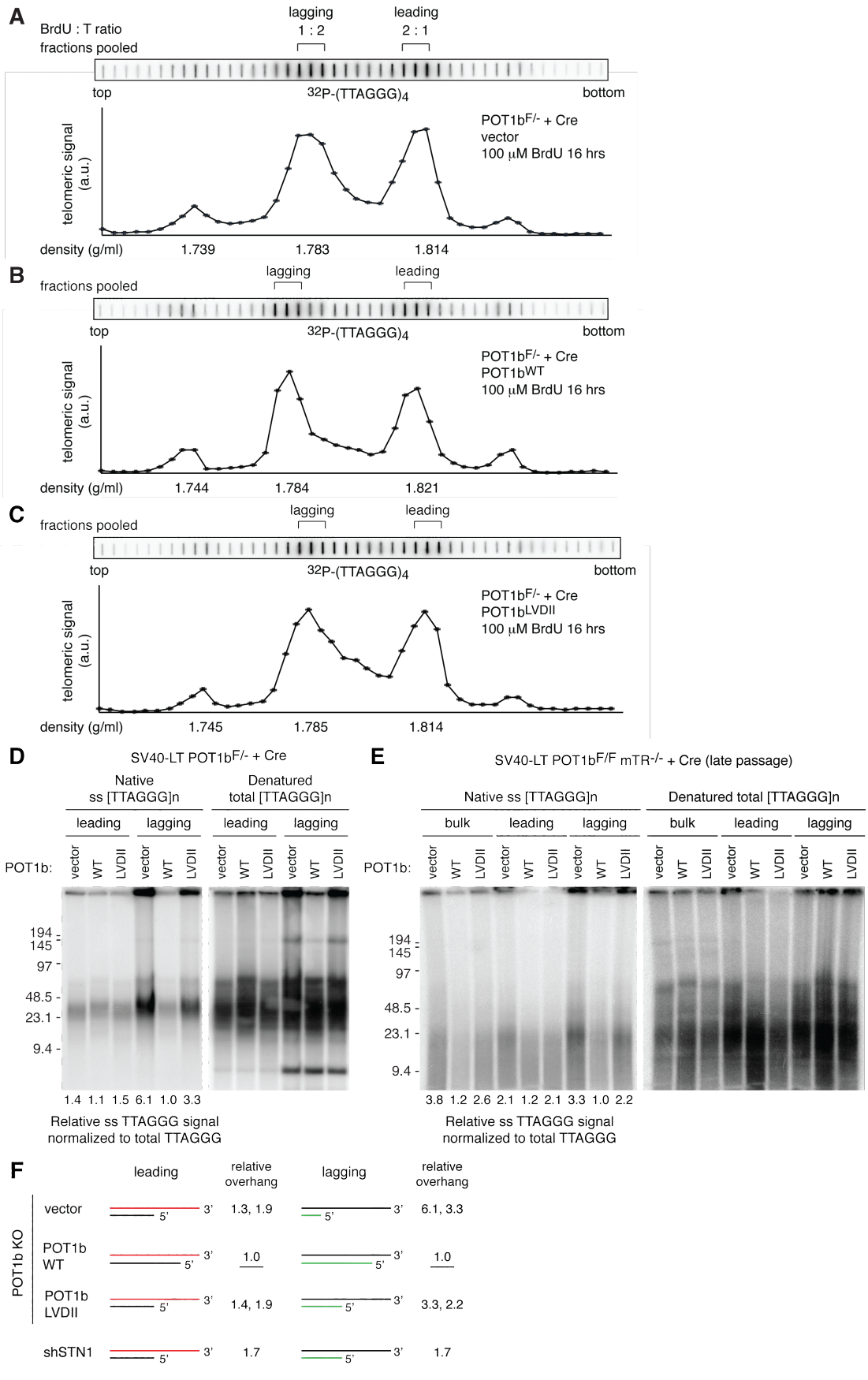
A
BrdU : T ratio
fractions pooled
lagging
1 : 2
leading
2 : 1
top
32P-(TTAGGG)4
bottom
telomeric signal (a.u.)
POT1bF/- + Cre
vector
100 μM BrdU 16 hrs
density (g/ml)
1.739
1.783
1.814
B
fractions pooled
lagging
leading
top
32P-(TTAGGG)4
bottom
telomeric signal (a.u.)
POT1bF/- + Cre
POT1bWT
100 μM BrdU 16 hrs
density (g/ml)
1.744
1.784
1.821
C
fractions pooled
lagging
leading
top
32P-(TTAGGG)4
bottom
telomeric signal (a.u.)
POT1bF/- + Cre
POT1bLVDII
100 μM BrdU 16 hrs
density (g/ml)
1.745
1.785
1.814
D
SV40-LT POT1bF/- + Cre
Native ss [TTAGGG]n
Denatured total [TTAGGG]n
leading
lagging
leading
lagging
POT1b:
vector
WT
LVDII
194
145
97
48.5
23.1
9.4
1.4 1.1 1.5 6.1 1.0 3.3
Relative ss TTAGGG signal normalized to total TTAGGG
E
SV40-LT POT1bF/F mTR-/- + Cre (late passage)
Native ss [TTAGGG]n
Denatured total [TTAGGG]n
bulk
leading
lagging
bulk
leading
lagging
POT1b:
vector
WT
LVDII
194
145
97
48.5
23.1
9.4
3.8 1.2 2.6 2.1 1.2 2.1 3.3 1.0 2.2
Relative ss TTAGGG signal normalized to total TTAGGG
F
leading
relative overhang
lagging
relative overhang
POT1b KO
vector
5'
3'
1.3, 1.9
6.1, 3.3
POT1b WT
1.0
1.0
POT1b LVDII
1.4, 1.9
3.3, 2.2
shSTN1
1.7
1.7

Similar results were observed in the presence and absence of telomerase, providing further support that the function of CST at both newly-synthesized telomeres is independent of telomerase (Figure 4.15D-F). In addition, detection of the total telomeric signal on denatured gels revealed a subtle difference in telomere length between telomerase-deficient MEFs expressing POT1b-LVDII and those expressing wild type POT1b. In the presence of wild type POT1b, telomeres were slightly longer than in cells lacking POT1b or expressing the POT1b-LVDII mutant. Since the cells in this experiment were analyzed a few weeks after endogenous POT1b had been replaced with the exogenous alleles, the observed telomere length differences might reflect the ability of wild type POT1b to rescue the accelerated telomere shortening associated with loss of POT1b, whereas the POT1b mutant unable to interact with CST appears unable to complement this function. More extensive analyses are required to explore the role of CST in telomere length homeostasis. The recruitment of CST to telomeres may be important for limiting the extent of telomere shortening that occurs in the absence of telomerase.

Additional roles of CST in telomere replication

Since Ctc1 and Stn1 were originally identified as accessory factors to DNA polymerase α[290], I further investigated whether they have additional roles in telomere replication other than at the terminus. Challenging telomere replication with the polymerase inhibitor aphidicolin or by depleting TRF1 induces the appearance of multiple telomeric signals and/or a decondensed appearance of telomeric signals detected at individual chromatid ends by telomeric FISH on metaphase spreads[215,216]. These have

been referred to as fragile telomeres, since the phenotype resembles the appearance of common fragile sites after treatment with aphidicolin. Stn1 depletion resulted in the appearance of fragile telomeres (~10%) on metaphase spreads in the absence of an apparent DNA damage response at telomeres (Figure 4.16A-C).

To investigate whether Stn1 acts in the same pathway as TRF1, I depleted Stn1 in SV40LT-immortalized *TRF1*$^{F/F}$*ROSA-Cre-ER*^{T2} MEFs from which TRF1 could be rapidly and efficiently deleted with tamoxifen (generated by A. Sfeir). At 24 hours after tamoxifen treatment of cells infected with a mock shRNA, ~60% of cells were TIF-positive, and ~30% of telomeres showed a fragile phenotype, as detected by telomeric FISH on metaphase spreads (Figure 4.16A-C). When Stn1 and TRF1 were co-depleted, the frequency of fragile telomeres increased, beyond what was observed in the absence of either factor alone (Figure 4.16B), while the percentage of TIF-positive cells remained similar to that in the absence of TRF1 (Figure 4.16C). The percentage of fragile telomeres upon depletion of both Stn1 and TRF1 was additive, while qualitatively, the telomeres appeared even more fragmented than in the absence of TRF1 alone (Figure 4.16A-B).

The severity of the fragile telomere phenotype did not correlate with the amount of single-stranded telomeric signal detectable by in-gel hybridization (Figure 4.16D). In cells lacking both Stn1 and TRF1, the single-stranded telomeric signal was not significantly elevated compared to that observed when Stn1 alone was depleted. The telomeric signal in the denatured gel also did not reveal overt telomere shortening that might be associated with chromosome breakage within the telomeres.

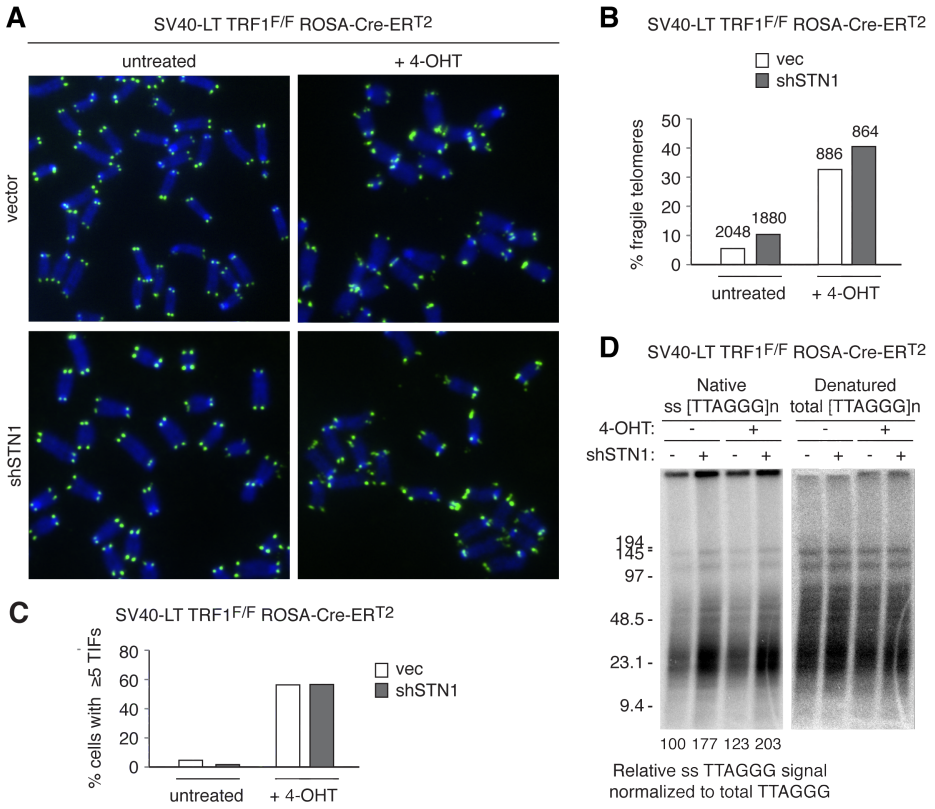

Figure 4.16. Depletion of Stn1 induces a fragile telomere phenotype that is additive with TRF1 deletion. (A) Telomeric FISH on metaphase spreads from SV40-LT *TRF1$^{F/F}$ROSA-Cre-ER^{T2}* MEFs at 96 hours after shRNA depletion of Stn1 and 24 hours after treatment with tamoxifen. (B) Quantification of fragile telomeres detected in (A). The numbers above the columns indicate the number of telomeres (long arm only) scored for each condition in one experiment. (C) Quantification of TIF assay for the colocalization of 53BP1 with telomeres detected by FISH. (D) In-gel overhang assay for cells harvested at the same timepoint as in (A).

These results suggest that Stn1 and TRF1 facilitate telomere replication through separate pathways. The phenotypes observed upon Stn1 depletion resemble those associated with aphidicolin treatment. Since Stn1 was identified as an accessory factor for DNA polymerase α, CST may be required to promote the activity of lagging-strand DNA polymerases during telomere replication. It remains to be seen whether the role of Stn1 in replication is also dependent on its interaction with POT1b. Fragile telomeres have not been reported in cells lacking TPP1/POT1b, suggesting that other mechanisms might be involved in the recruitment of CST during semi-conservative replication of

telomeres. It remains possible that the role of CST at the telomere terminus is distinct from its function at internal sites of replication.

SUMMARY OF FINDINGS

Here, I have elucidated the mechanism by which POT1b prevents aberrant degradation of the telomeric C-rich strand (Figure 4.17). POT1b functions at the termini of both newly synthesized telomeres during S phase to inhibit the nucleolytic activity of Apollo while promoting the activities of the Ctc1/Stn1/Ten1 complex.

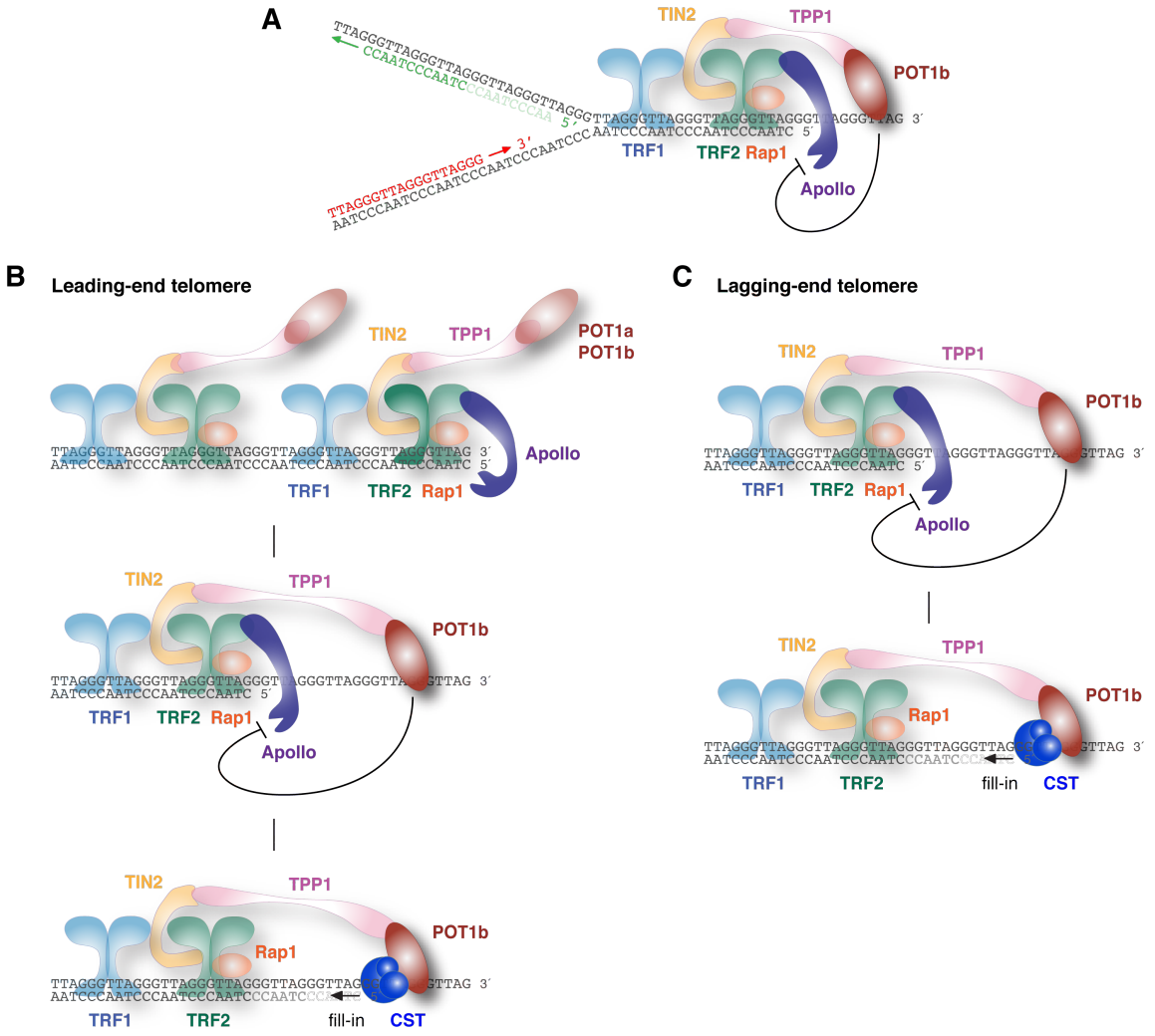

Figure 4.17. The mechanism by which POT1b protects telomeres from aberrant degradation of the C-rich strand. (A) The replication fork as its reaches the telomere terminus. Throughout S phase, POT1b loaded on the terminal overhang inhibits aberrant degradation by Apollo. (B) Apollo is required to generate the 3' overhang at leading-end telomeres. POT1b loading onto newly generated overhangs inhibits Apollo and promotes the recruitment of CST, which limits overhang size by facilitating fill-in synthesis of the C-rich strand. (C) POT1b inhibits Apollo and promotes CST function at the newly synthesized lagging-end telomere.

At newly-synthesized leading-end telomeres, Apollo initiates 5' resection, generating an overhang that binds POT1b, which in turn inhibits further degradation by Apollo. POT1b also binds the single-stranded overhangs present throughout S phase at unreplicated telomeres and newly-synthesized lagging-end telomeres, inhibiting aberrant degradation of these ends by Apollo. The results further indicate that POT1b recruits the mammalian CST complex to both newly-synthesized telomeres. Since Ctc1 and Stn1 are accessory factors of DNA polymerase α/primase, the function of CST at telomeres may be to complete fill-in synthesis of the C-rich strand, which is necessary not only following extension of the G-rich strand by telomerase but also to counteract 5' end resection by Apollo (and other nucleases that act during S phase). CST also facilitates the semi-conservative replication of telomeres and suppresses the appearance of fragile telomeres, though it is not known whether this role requires its interaction with POT1b.

CHAPTER 5:

THE TELOMERIC ROLE OF NUCLEASES THAT PERFORM 5' END RESECTION AT DNA DOUBLE STRAND BREAKS

INTRODUCTION

The aim of the research described in this section was to test the hypothesis that newly-synthesized telomeres are recognized transiently as sites of DNA damage and processed by the same factors that perform 5' end resection at a DNA double strand break. In *S. cerevisiae*, the model for DNA DSB resection involves initial processing by the Mre11/Rad50/Xrs2 complex in cooperation with the Sae2 nuclease, after which extensive resection occurs by either the Exo1 nuclease or the Dna2 nuclease in conjunction with the Sgs1 helicase[378,379]. In human cells, the RecQ helicase BLM has been found to be the helicase that acts in parallel with Exo1[380]. Here, I tested whether any of the mammalian orthologs of MRX, Sae2, Exo1, and Sgs1 contribute to the dynamics of the telomeric overhang in wild type cells. I further determined whether Exo1 and/or Nbs1 have additional functions at leading-end telomeres when overhang generation is compromised due to the absence of Apollo.

While Exonuclease 1 had previously been reported to have no contribution to telomeric structure, my experiments reveal that Exo1 contributes to an end-processing step that occurs on both newly synthesized telomeres, generating transiently elongated overhangs in late S/G2 phase. Exo1 acts at telomeres independently of Apollo, while other factors involved in resection at a DNA DSB do not appear to cooperate with Exo1. The physiologic role of this step is unclear, as it does not appear important for telomere end protection or telomere length homeostasis.

RESULTS

Exo1 contributes to 5' end resection of telomeres in late S phase

Since Exo1 has been proposed to have a major role in 5' end resection at DSBs[378-380], I evaluated the telomeric overhang in Exo1-deficient MEFs despite previous reports suggesting that Exo1 does not contribute to overhang maintenance[187,394]. *Exo1*$^{-/-}$ mice are homozygous for a mutant Exo1 allele containing a hygromycin resistance cassette inserted into exon 6, which results in alternative splicing that fuses exon 5 in-frame to exon 7, deleting amino acids 61-84 of the nuclease domain[374]. Exo1-deficient mice are sterile, develop lymphomas at a higher rate, and show reduced survival[374]. Consistent with the proposed role of Exo1 in mismatch repair, cells derived from *Exo1*$^{-/-}$ mice are impaired in the ability to repair base:base and single-base insertion/deletion mismatches in 5' and 3' nick-directed repair *in vitro* as well as increased microsatellite instability and a 30-fold increase in the mutation rate at the Hprt locus[374].

In asynchronous SV40LT-immortalized *Exo1*$^{-/-}$ MEFs, the telomeric overhang was reduced by 30-40% compared to that in wild type littermate MEFs (Figure 5.1A), in the absence of overt differences in cell cycle profile. To rule out the possibility that Exo1 loss compromises the ability of telomerase to extend the G-rich strand, I analyzed the telomeric overhang in SV40LT-immortalized *Exo1*$^{-/-}$*mTR*$^{-/-}$ MEFs generated from intercrosses of *Exo1*$^{+/-}$*mTR*$^{+/-}$ mice (Figure 5.1B). The overhang defect observed in the absence of Exo1 was independent of telomerase, consistent with a role of Exo1 in nucleolytic degradation of the telomeric C-rich strand (Figure 5.1B-C).

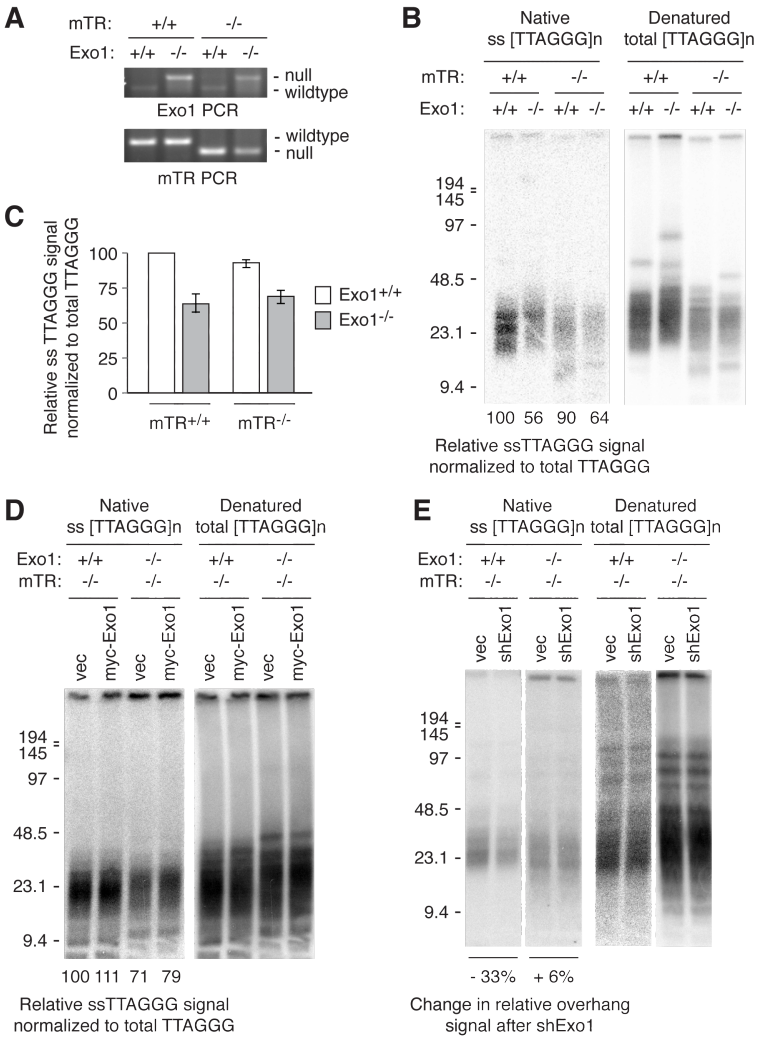

Figure 5.1. Exo1 contributes to telomerase-independent overhang dynamics. (A) Genotyping PCR of Exo1 and mTR status in MEFs generated from intercrosses between *Exo1*$^{+/-}$*mTR*$^{+/-}$ mice. (B) Representative in-gel overhang assay for MEFs genotyped in (A). The relative ssTTAGGG signal in the native gel was normalized to total TTAGGG signal in the denatured gel and lane 1 was set to 100. (C) Quantification of overhang assay shown in (B). Values shown are the means and sds from three independent experiments. (D) In-gel overhang assay on MEFs of the indicated genotypes introducing vector control or N-terminal myc-tagged Exo1 carrying the puromycin resistance marker at 3 days after selection. (E) In-gel overhang assay on MEFs of the indicated genotypes at 96 hours after retroviral shRNA targeting Exo1 (puro-resistant) at 3 days after selection.

To determine whether the overhang defect is specifically due to the loss of Exo1, I introduced N-terminal myc-tagged mouse Exo1 into Exo1-deficient MEFs. Though immunoblots for the myc tag showed a low level of Exo1 expression, the overhang signal in Exo1-deficient cells was unaffected (Figure 5.1D). The inability to rescue the

overhang defect associated with Exo1 deficiency with wild type Exo1 could be due to a dominant negative effect of the nuclease-deficient form of Exo1 (expressed in *Exo1*$^{-/-}$ MEFs) or due to haploinsufficiency, whereby exogenously introduced Exo1 is not expressed at a high enough level to achieve wild type function. In an alternative approach to evaluate the role of Exo1 in overhang generation, Exo1 was depleted in wild type MEFs by shRNA, which resulted in a similar 30% reduction in the telomeric overhang signal in the absence of changes in cell cycle profile (Figure 5.1E). Introduction of this shRNA into *Exo1*$^{-/-}$ MEFs had no effect on the telomeric overhang, suggesting that the overhang defect observed in both *Exo1*$^{-/-}$ MEFs and following Exo1 depletion by shRNA was likely due to the deficiency of the Exo1 nuclease (Figure 5.1E)

Using FUCCI-FACS, I isolated Exo1-deficient cells in G1 and late S/G2 and compared the overhang signal during different cell cycle phases. As shown previously in wild type MEFs (Chapter 3 and [213]) and human cell lines[250], a 2-fold increase in the telomeric overhang signal occurs in late S/G2 compared to G1 (Figure 5.2A). This transient increase in the single-stranded telomeric signal is due to the terminal overhang rather than internal single-stranded regions that might become exposed during replication, since the overhang signal is abolished when agarose-embedded DNA from late S phase cells is treated with the *E. coli* 3' to 5' exonuclease ExoI prior to preparation for the in-gel hybridization assay (Figure 5.2A). Since this change in overhang signal is observed in the absence of telomerase, it is likely due to 5' end resection of telomeres in late S phase, followed by fill-in synthesis of the C-rich strand as cells progress from G2 to M. In telomerase-proficient cells, Exo1 deficiency did not have a statistically significant effect on the overhang signal in G1 but specifically reduced the overhang

signal in late S/G2 (Figure 5.2B). In cells deficient for both telomerase and Exo1, the overhangs in G1 cells were ~10-20% reduced compared to telomerase-deficient cells, and the relative overhang signal remained nearly constant between G1 and late S phase (Figure 5.3C). These results are in contrast to those observed in the absence of Apollo, which induces a 40-50% reduction of the overhang signal in both G1 and late S when compared to wild type cells in the same cell cycle stages (refer to Figure 3.6E-F).

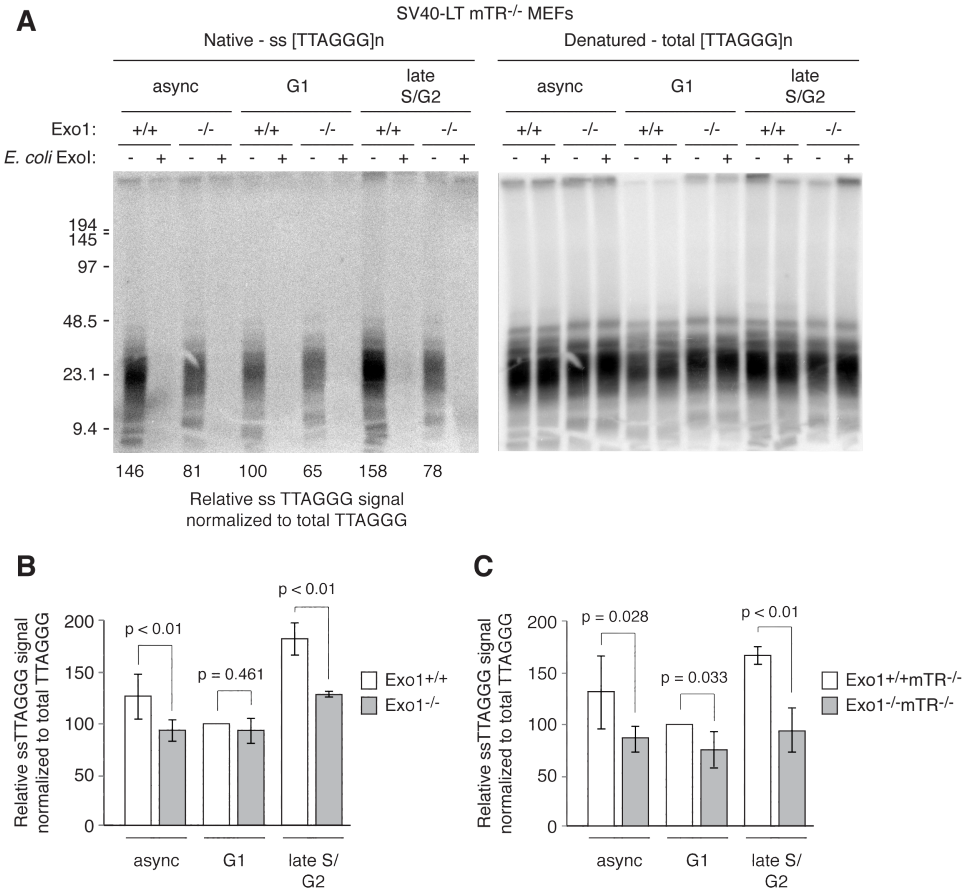

Figure 5.2. Exo1 contributes to transient overhang elongation in late S phase. (A) Representative telomeric overhang analysis of G1 and late S/G2 *Exo1*$^{+/+}$*mTR*$^{-/-}$ MEFs and *Exo1*$^{-/-}$*mTR*$^{-/-}$ isolated by FUCCI-FACS (described in Chapter 3). The relative single-stranded signal was normalized to total TTAGGG signal and determined as a percentage of the signal in the lane containing wild type G1 cells (set at 100). (B) Quantification of relative single-stranded telomeric signal in telomerase-proficient wild type and *Exo1*$^{-/-}$ cells in G1 and late S/G2. (C) Quantification of relative single-stranded telomeric signal in G1 and late S/G2 as assayed in (A).

I next determined whether Exo1 acts at both newly-synthesized telomeres using CsCl density gradient equilibrium centrifugation of BrdU-labeled telomeres to isolate the leading- and lagging-end telomeres (described in Chapter 3). Slot blots detecting the telomeric signal in each fraction collected from the CsCl gradient confirmed that similarly effective separation of the leading- and lagging-end telomeres could be achieved with BrdU-labeled DNA isolated from both wild type and Exo1-deficient cells (Figure 5.3A-B). Exo1 deficiency resulted in a 20-30% reduction in the telomeric overhang signal at both newly synthesized telomeres (Figure 5.3C-D). Thus, Exo1 contributes to the processing of both newly-synthesized telomeres in S phase.

When the CsCl gradient fractions corresponding to unreplicated telomeres were pooled and analyzed by in-gel hybridization, there was no difference in the telomeric overhang signal in the presence or absence of Exo1 (Figure 5.3C-D). This alternative method of detecting the overhangs at unreplicated telomeres did not corroborate the small reduction in the G1 overhang signal observed in $Exo1^{-/-}mTR^{-/-}$ cells compared to $Exo1^{+/+}mTR^{-/-}$ cells, when FUCCI-FACS was used to isolate non-cycling cells. To reach a more definitive conclusion as to whether Exo1 deficiency affects overhang size in G1, an additional set of littermate $Exo1^{-/-}mTR^{-/-}$ and $Exo1^{+/+}mTR^{-/-}$ MEFs may need to be generated and assessed.

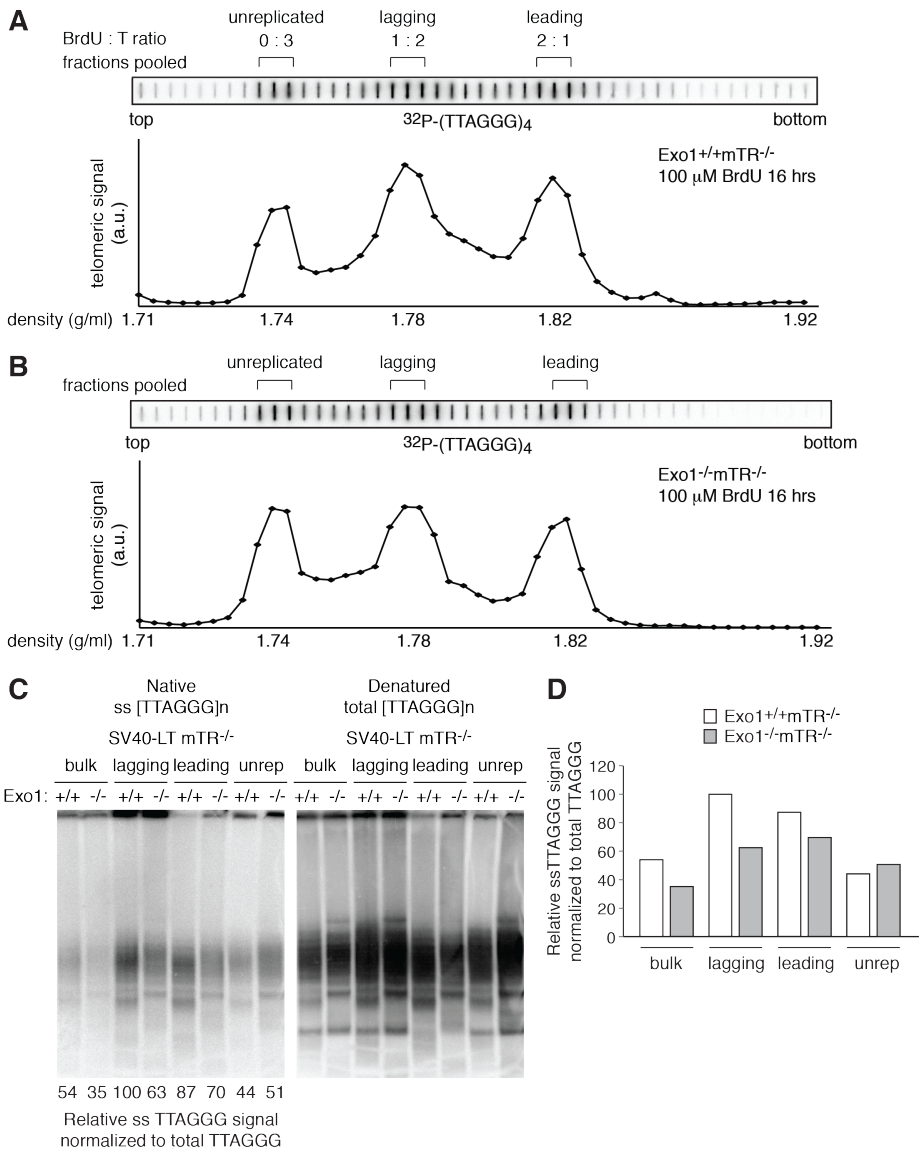

Figure 5.3. Exo1 contributes to overhang dynamics of both newly synthesized telomeres. (A) and (B) Representative slot blots of telomeric signal in each fraction collected from CsCl density gradient equilibrium centrifugation of telomeric DNA from *Exo1*$^{+/+}$*mTR*$^{-/-}$ (A) and *Exo1*$^{-/-}$*mTR*$^{-/-}$ (B) MEFs labeled with BrdU for one round of replication. The fractions pooled for overhang analyses are shown. (C) Representative overhang analysis of bulk telomeres (prior to CsCl density gradient equilibrium centrifugation), and separated leading-, lagging-end and unreplicated telomeres from *Exo1*$^{+/+}$*mTR*$^{-/-}$ and *Exo1*$^{-/-}$*mTR*$^{-/-}$ MEFs (D) Quantification of relative overhang signal as detected in (C). Values represent the mean of two independent experiments.

Exo1 is not required for telomere protection and is not responsible for the rate of telomere shortening in telomerase-deficient cells

Telomeres with blunt ends or short overhangs are expected to activate the ATM kinase signaling pathway and undergo aberrant repair as exemplified by the case of Apollo deficiency, where leading-end telomeres with short or nonexistent overhangs activate ATM and engage in end-joining reactions. However, no telomere dysfunction was observed in Exo1-deficient cells, as Exo1 deficiency did not give rise to telomere dysfunction-induced foci, downstream signs of ATM signaling such as Chk2 phosphorylation, or telomere fusions (Figure 5.4A-B). This was not due to a defect in ATM kinase signaling in the absence of Exo1, because irradiating Exo1-deficient cells still resulted in robust Chk2 phosphorylation (Figure 5.4A). These results are consistent with Exo1 acting in a late step in telomere end processing after sufficient overhangs have been generated to suppress ATM signaling and aberrant end-joining.

Consistent with Exo1 contributing to a transient step in telomere end-processing that does not significantly alter the overhang size in G1, Exo1 deficiency did not affect telomere length homeostasis. Cells lacking both Exo1 and mTR exhibited a rate of telomere shortening that was not significantly different from that of cells lacking telomerase only (Figure 5.4C-D), suggesting that Exo1-mediated processing is not responsible for the rate of telomere shortening in telomerase-deficient cells. This corroborates the previously published finding that late generation telomerase- and Exo1-deficient mice do not have longer telomeres than late generation telomerase-deficient mice[394]. Furthermore, Exo1 deficiency had no appreciable effect on telomere length in the

presence of telomerase, suggesting that the telomere end-processing step mediated by Exo1 is not required for telomerase to act at telomeres.

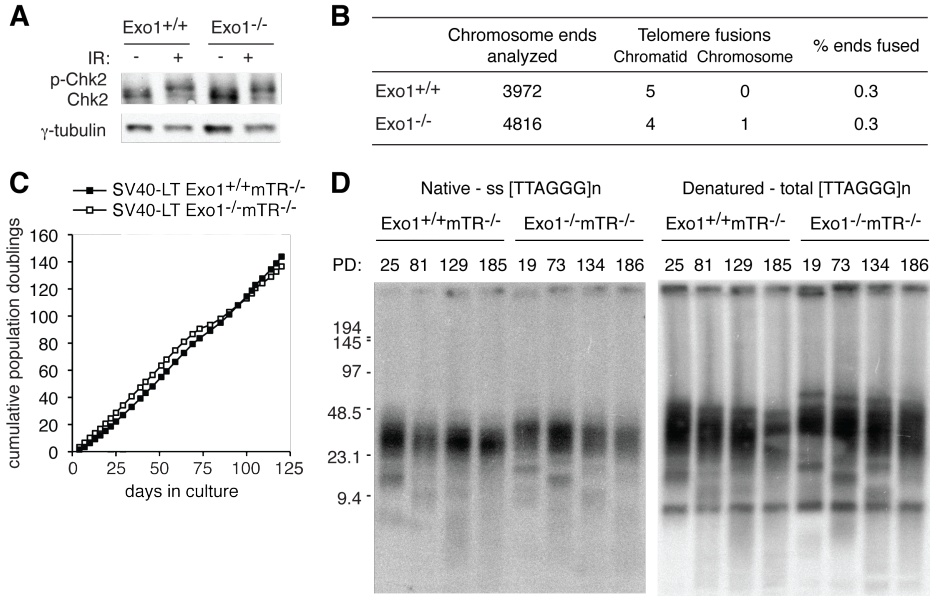

Figure 5.4. Exo1 is not required for telomere end protection. (A) Immunoblot detection of Chk2 phosphorylation status of wild type and Exo1-deficient MEFs. (B) Quantification of FISH analysis of Exo1-deficient MEFs. (C) Growth curve of SV40-LT immortalized $Exo1^{+/+}mTR^{-/-}$ and $Exo1^{-/-}mTR^{-/-}$ MEFs passaged in parallel for 120 days in culture. (D) In-gel detection of native and denatured telomeric signal in DNA from $Exo1^{+/+}mTR^{-/-}$ and $Exo1^{-/-}mTR^{-/-}$ MEFs harvested after the indicated population doublings, according to the growth curve shown in (C).

Stn1 depletion in Exo1-deficient cells still results in extended overhangs

After telomeric overhangs are transiently elongated in S phase, they must be restored to the size found in G1 cells either by fill-in synthesis of the C-rich strand or nucleolytic cleavage of the overhang. If C-strand fill-in synthesis occurs following Exo1-mediated end processing, then defects in C-strand fill-in might be expected to produce a less severe overhang phenotype in the absence of Exo1. Thus, I asked whether the accumulation of excessive overhangs associated with Stn1 depletion can be mitigated by Exo1 deficiency.

Stn1 depletion in Exo1-deficient MEFs resulted in an increase in the telomeric overhang signal, though this signal was reproducibly less than that observed when Stn1 was knocked down in wild type MEFs (Figure 5.5A-B). These results suggest that Exo1-mediated processing is not the only mechanism by which telomeres acquire long overhangs that require fill-in synthesis of the complementary strand. In the absence of Exo1, Apollo is likely to still generate long overhangs at leading-end telomeres whose length must be limited by Stn1. Meanwhile, lagging-end telomeres are likely to still require the function of Stn1 for complete synthesis of the C-rich strand even in the absence of additional processing by Exo1. Further experiments should be performed to examine the effect of depleting Stn1 in cells lacking both Apollo and Exo1.

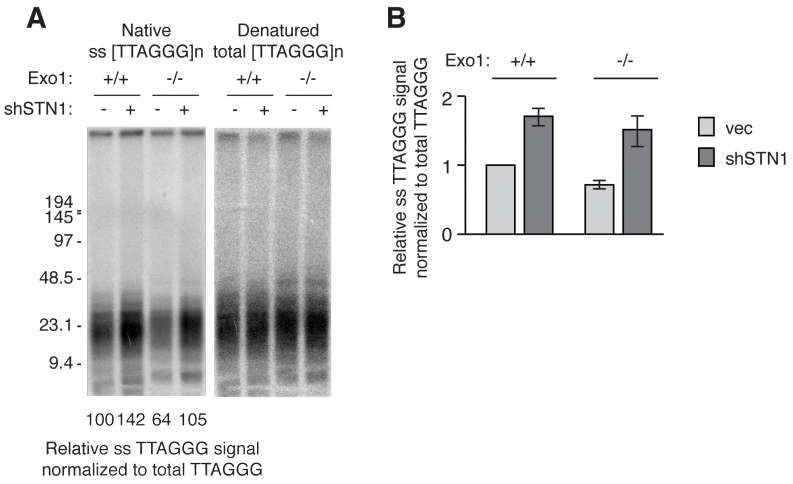

Figure 5.5. Overhang accumulation upon Stn1 depletion in Exo1-deficient cells. A) Representative overhang assay of *Exo1*$^{+/+}$ and *Exo1*$^{-/-}$ MEFs at 96 hr after lentiviral transduction of vector or shRNA targeting Stn1. (B) Quantification of overhang analyses as assayed in (A). Values represent the mean and sds of three independent experiments.

The DNA damage response to deprotected telomeres lacking TPP1/POT1 is not modulated by Exo1 deficiency

Exo1 deficiency has been reported to ameliorate the organ dysfunction observed in telomerase-deficient mice at late generations when their telomeres become critically

short[394]. In this setting, the absence of Exo1 did not rescue telomere shortening but reduced the accumulation of DNA damage foci[394]. Thus, it was proposed that Exo1-mediated resection contributes to the DNA damage responses activated in the setting of telomere dysfunction.

I therefore asked whether Exo1 deficiency mitigates the DNA damage response observed in the absence of POT1a/b, where excessive single stranded telomeric overhangs bind RPA and activate the ATR kinase pathway[37,190,213]. To address this question, I depleted TPP1 by shRNA in wild type and Exo1-deficient cells and compared the overhang signal and appearance of TIFs in both settings. As expected based on the previous finding that Exo1 is not responsible for the accumulation of excessive single stranded telomeric overhangs in the absence of POT1b[187], the aberrant increase in overhang signal induced by TPP1 depletion was not abolished in Exo1-deficient cells (Figure 5.6A-B). Nevertheless, the relative overhang signal observed when TPP1 was depleted in Exo1-deficient cells was less than that in wild type cells in which TPP1 was depleted (Figure 5.6A-B). This is likely because Exo1 deficiency abolishes the transient increase in telomeric overhang signal normally observed in S phase cells. This observation suggested that in cells depleted for both Exo1 and TPP1, the total amount of single-stranded overhangs exposed to recognition by the DNA damage response, particularly in S phase, might be less than that in the setting of TPP1 deficiency alone.

Immunofluorescence for the DNA damage factor 53BP1 at telomeres (detected by FISH) showed that Exo1 deficiency did not significantly reduce the percentage of cells with ≥5 TIFs compared to cells depleted for TPP1 alone (Figure 5.6C). However, Exo1 deficiency did result in a ~10% reduction in the percentage of cells with ≥10 TIFs (Figure

5.6C). Exo1 deficiency and the associated reduction in telomeric overhang signal may thus have a slight effect on the DNA damage response induced by TPP1 depletion by reducing the fraction of telomeres that are recognized as DNA damage.

Since the depletion of TPP1 by shRNA induces a milder phenotype than that observed when either TPP1 or POT1a and POT1b are deleted in MEFs, I investigated the contribution of Exo1 to telomere dysfunction by an alternative approach in which Exo1 was depleted with shRNA in $POT1a^{F/F}POT1b^{F/F}$ or $TPP1^{F/F}$ MEFs following Cre treatment. Similar to what was observed in the previous experiment, the aberrant overhang phenotype induced by deleting POT1a and –b or TPP1 was not abolished by the depletion of Exo1 (Figure 5.6D). In addition, Exo1 knockdown in cells deficient for POT1a and POT1b did not abolish the accumulation of 53BP1 to telomeres, though a ~10% reduction in the fraction of cells with >10 TIFs was observed (Figure 5.6E). It remains to be determined whether this small effect of Exo1 depletion on the DNA damage response to POT1a/b deletion is statistically significant, though the fact that similar trends were observed in the setting of either TPP1 depletion in Exo1-deficient cells or Exo1 depletion in POT1a/b DKO cells suggests that this may be a reproducible result.

The current studies suggest a minor (if any) contribution of Exo1 to the telomere dysfunction observed in the absence of TPP1 or POT1a/b. These results are in contrast to the previous study where the DNA damage response observed in late generation telomerase knockout mice was significantly reduced by Exo1 deficiency[394]. Since cells deficient for both POT1a and POT1b or TPP1 accumulate excessive overhangs independently of Exo1, depleting Exo1 in this setting may be insufficient to counteract

the large amount of exposed single-stranded overhangs that accumulate and activate the ATR signaling pathway. It will be of interest to determine whether the depletion of Exo1 can suppress the appearance of TIFs in cells deficient for POT1a only, which do not accumulate excess telomeric overhangs[37].

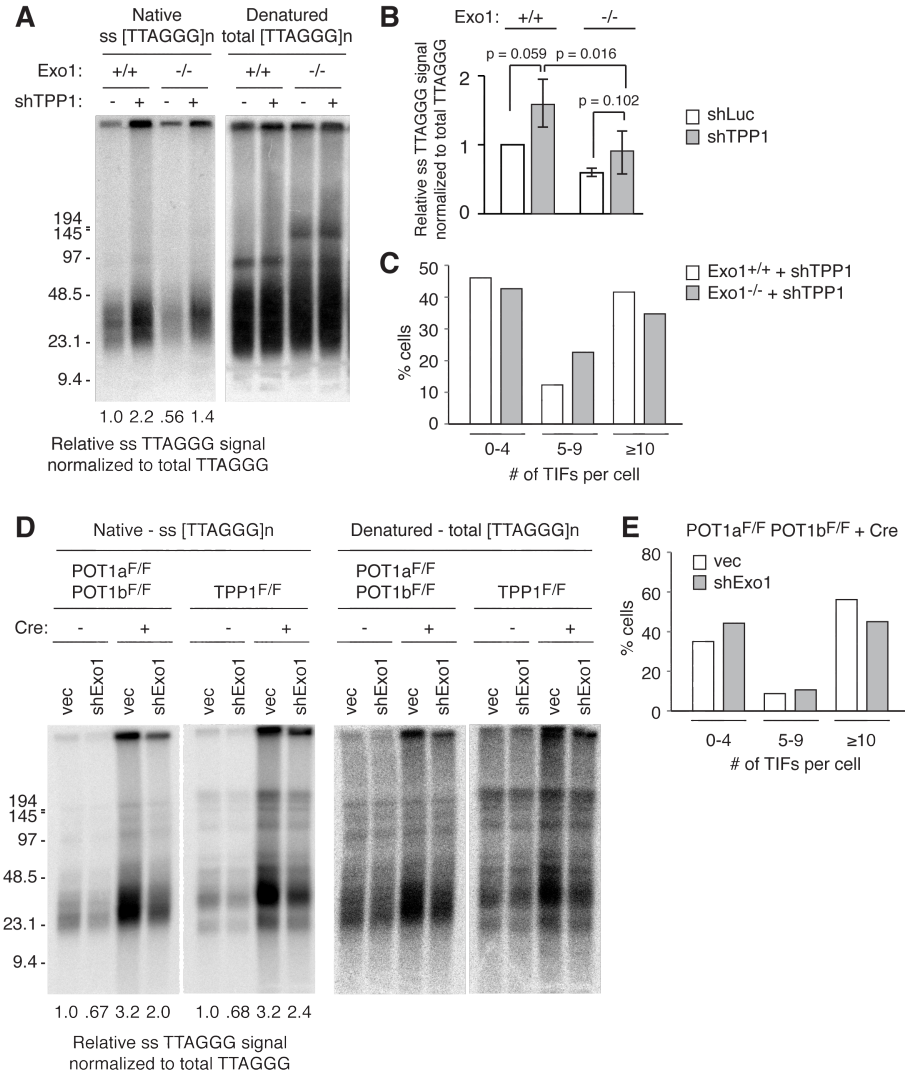

Figure 5.6. Exo1 depletion does not modulate the DNA damage response that occurs in the absence of TPP1/POT1a/b. (A) Representative overhang assay of *Exo1*$^{+/+}$ and *Exo1*$^{-/-}$ MEFs at 96 hr after retroviral introduction of vector or shRNA to TPP1. (B) Quantification of overhang analyses as assayed in (A). Values represent the mean and SDs of three independent experiments. (C) Quantification of TIFs defined as colocalization of 53BP1 detected by immunofluorescence to telomeres detected by FISH, in cells of the indicated genotype. (D) Representative overhang assay of *POT1a*$^{F/F}$*POT1b*$^{F/F}$ and *TPP1*$^{F/F}$ MEFs infected with vector control or retroviral shRNA targeting Exo1 (selected for 3 days with puromycin) at 96 hr after Hit&Run Cre. (E) Quantification of TIFs defined as colocalization of 53BP1 detected by immunofluorescence to telomeres detected by FISH, in cells of the indicated genotype.

The telomere processing step mediated by Exo1 is unaffected by the depletion of other factors involved in DSB resection

I next investigated whether the action of Exo1 at telomeres resembles the process of 5' end resection at a DNA DSB by testing whether other nucleases and helicases involved in DSB resection contribute to the telomere end-processing step mediated by Exo1. As previously shown in Chapter 4, depletion of CtIP, Nbs1, or BLM alone had no effect on the telomeric overhang signal in wild type MEFs (Figure 5.7A-F). Furthermore, depletion of CtIP in Exo1-deficient cells resulted in no further reduction in the telomeric overhang signal (Figure 5.7A-B). Co-deletion of Exo1 and Nbs1 or Exo1 and BLM also did not exacerbate the overhang defect observed in the absence of Exo1 (Figure 5.7C-F). Thus, neither the MRN complex nor BLM appear to contribute to the transient overhang elongation that occurs in late S phase, in either wild type or Exo1-deficient MEFs. This is in contrast to DSB repair in *S. cerevisiae* where resection is severely impaired in *sae2Δexo1Δ* and *sgs1Δexo1Δ* mutants[378,379] and also in human cells where the co-depletion of Exo1 and BLM reduces RPA foci formation in response to camptothecin compared to the depletion of either factor alone[380]. It has been shown in *S. cerevisiae* that in the absence of Ku, Exo1-mediated resection no longer depends on Sae2, though the Sgs1-mediated pathway still also functions in this setting[432]. The apparent differences in the action of Exo1 at telomeres and DNA DSBs could be due to differences in the factors that bind at wild type telomeres as opposed to DSBs.

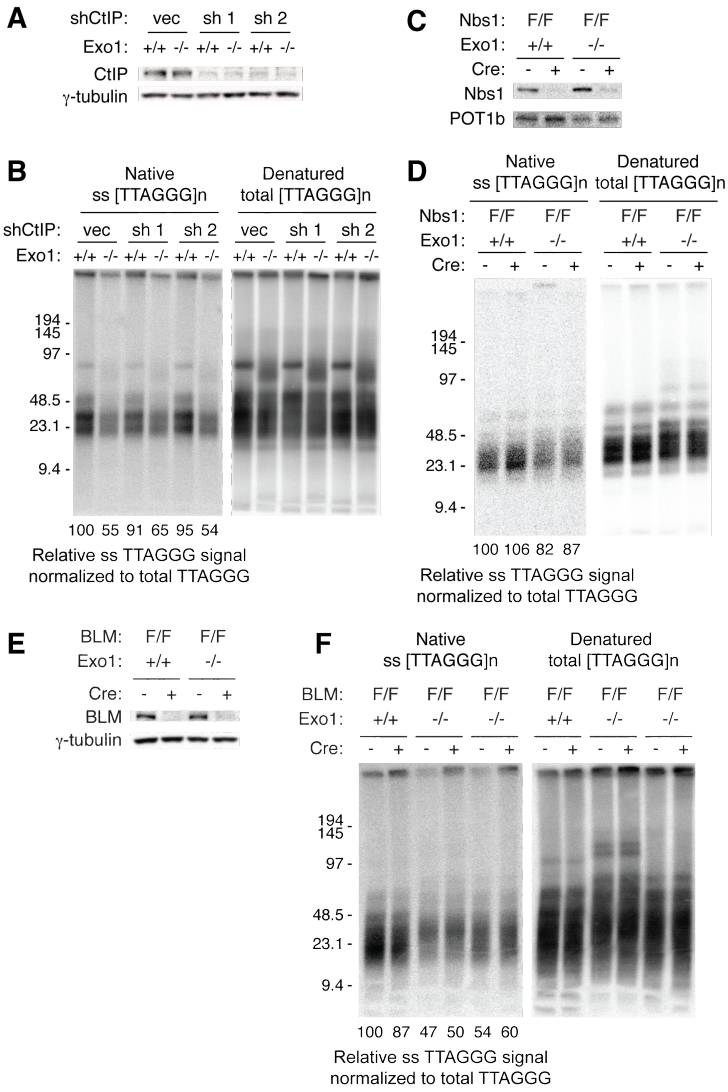

Figure 5.7. Exo1-mediated processing is not affected by depletion of CtIP, Nbs1, or BLM. (A) Immunoblot for CtIP in *Exo1*$^{+/+}$ and *Exo1*$^{-/-}$ MEFs transduced with retroviral vector or shRNA. γ-tubulin is shown as a loading control. (B) Overhang assay of cells in (A). Relative ss TTAGGG signal in each lane of the native gel was normalized to the total TTAGGG signal in the same lane of the denatured gel, with the value in lane 1 set to 100. (C) Immunoblot for Nbs1 in Exo1$^{+/+}$Nbs1$^{F/F}$ and Exo1$^{-/-}$Nbs1$^{F/F}$ MEFs without Cre and 120 hours after Hit&Run Cre. POT1b is shown as a loading control. (D) Overhang assay of cells in (C). Relative ss TTAGGG signal in each lane of the native gel was normalized to the total TTAGGG signal in the same lane of the denatured gel, with the value in lane 1 set to 100. (E) Immunoblot for BLM in *Exo1*$^{+/+}$*BLM*$^{F/F}$ and *Exo1*$^{-/-}$*BLM*$^{F/F}$ MEFs without Cre and 120 hours after Hit&Run Cre. γ-tubulin is shown as a loading control. (F) Overhang assay of cells in (E). Relative single-stranded TTAGGG signal in each lane of the native gel was normalized to the total TTAGGG signal in the same lane of the denatured gel, with the value in lane 1 set to 100.

To further examine telomere processing in S phase, I performed a number of drug treatments on cells proceeding synchronously through S phase. Using FUCCI-FACS, I

isolated $Cdt1^{+}Gem^{+}$ cells, which were confirmed to be in early S phase and progressed to late S/G2 within 6 hours after plating (Figure 5.8A). Plated cells were treated with the Cdk inhibitor, roscovitine, for 4 hours. The cell cycle profiles of roscovitine-treated cells showed that both G1 and S phase cells were arrested after 4 hours of drug treatment, indicating that Cdk activity was indeed inhibited. However, roscovitine treatment did not abolish the late S phase increase in telomeric overhang (Figure 5.8B), suggesting that the processing does not depend on factors such as CtIP that have been reported to require Cdk phosphorylation for activity[383]. A recent report has suggested that SIRT6-mediated acetylation of CtIP is also required for its nucleolytic activity, which can be inhibited by nicotinamide, a non-specific SIRT inhibitor[384]. When G1 or early S phase cells were plated and treated with nicotinamide for 4-16 h, no change in the overhang signal was observed (Figure 5.8C). Together these results suggest that resection by CtIP does not likely contribute to the telomere end-processing step that leads to transiently elongated overhangs in late S phase, though a functional assay is required to show that CtIP function is indeed impaired by these drug treatments.

Exo1 acts at newly-synthesized telomeres in the absence of Apollo

I next asked whether the action of Exo1 depends on earlier steps in end processing. Since Apollo contributes to overhang generation at leading-end telomeres, I generated $Apollo^{F/F}Exo1^{-/-}$ MEFs to determine whether Exo1 activity at leading-end telomeres requires initial processing by Apollo. Co-deletion of Apollo and Exo1 by Cre treatment resulted in an additive effect on the telomeric overhang. Whereas a deficiency in either Apollo or Exo1 alone resulted in a 30-40% reduction in the overhang signal, the

absence of both nucleases reduced the overhang signal by approximately 70% (Figure 5.9A-B). Thus, the action of Exo1 at telomeres appears to be independent of Apollo.

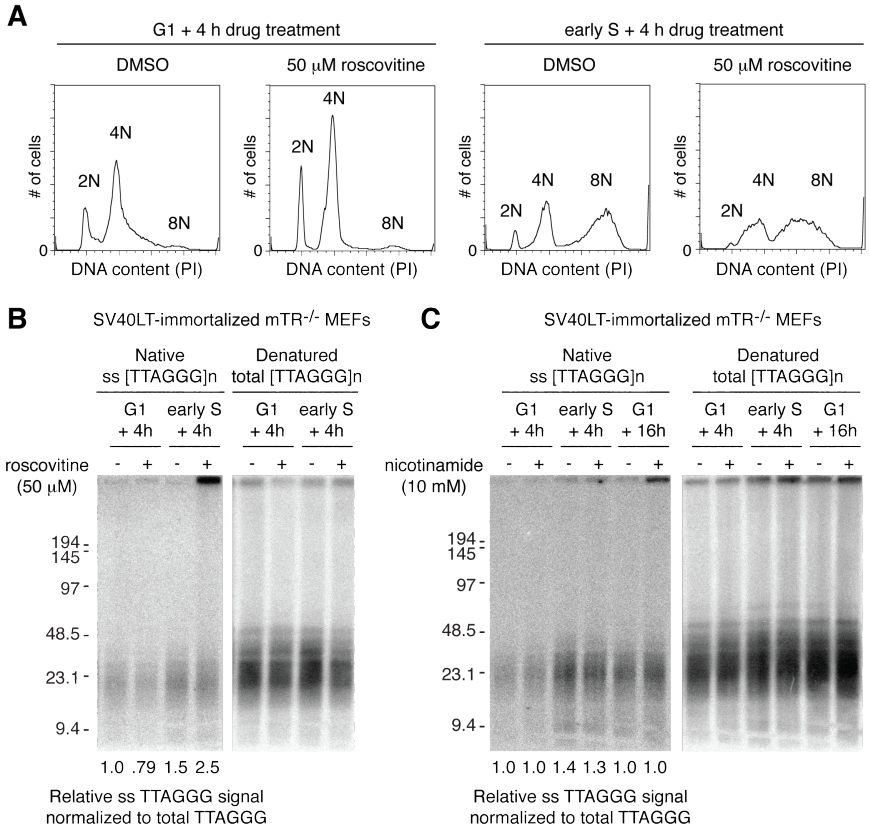

Figure 5.8. Late S phase processing of telomere ends is unaffected by roscovitine or nicotinamide treatment. (A) Cell cycle profile of cells sorted by FUCCI-FACS in G1 or early S and plated for 1.5 hours prior to addition of DMSO or 50 μM roscovitine for 4 hours. Cells were fixed with 70% ethanol, stained with PI for DNA content, and analyzed by flow cytometry. (B) Overhang assay of cells treated as in (A). (C) Overhang assay of cells sorted by FUCCI-FACS in G1 or early S and plated for 1.5 hours prior to addition of DMSO or 10mM nicotinamide for the indicated amount of time.

Overhang analyses of Apollo/Exo1 DKO cells by FUCCI-FACS were also consistent with the conclusion that Apollo and Exo1 act independently of each other. When Apollo was deleted from Exo1-deficient cells, the telomeric overhangs in G1 and S phase were reduced by ~40% compared to those of wild type cells in the same cell cycle phases. Furthermore, in the absence of both Apollo and Exo1, no increase in overhang signal was observed as cells progress from G1 to S phase (Figure 5.9C-D), whereas both

wild type and Apollo-deficient cells displayed a 2-fold increase in overhang signal in late S phase.

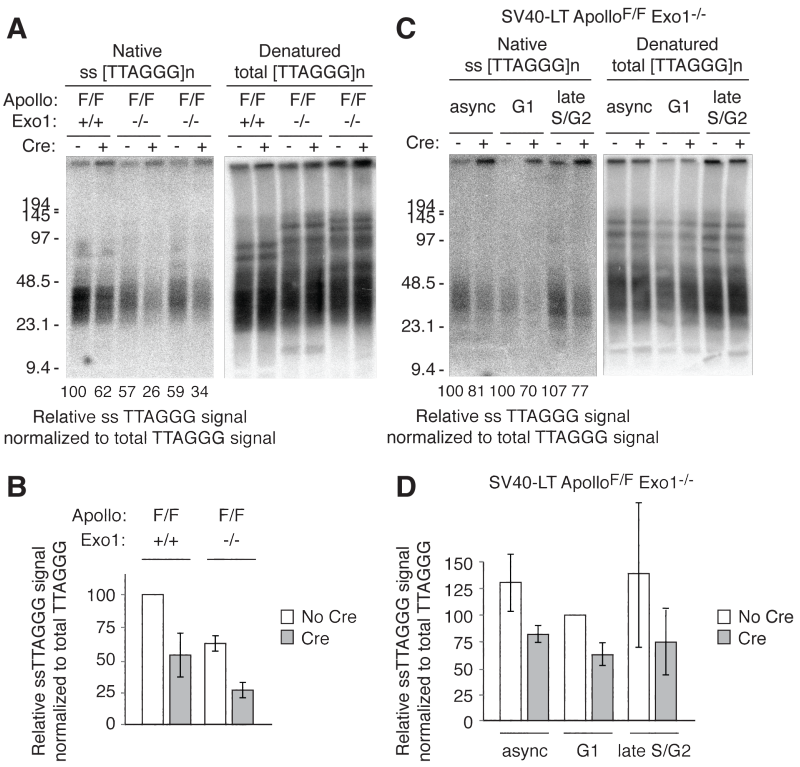

Figure 5.9. In the absence of Apollo, Exo1 contributes to extensive resection in S phase. (A) Representative overhang assay of SV40-LT immortalized Apollo$^{F/F}$ Exo1$^{+/+}$ and two independent Apollo$^{F/F}$ Exo1$^{-/-}$ MEF lines at 120 hr after Hit&Run Cre. (B) Quantification of overhang analyses as assayed in (A). Values represent the mean and sds of three independent experiments. (C) Representative telomeric overhang analysis of G1 and late S/G2 Apollo$^{F/F}$ Exo1$^{-/-}$ in the absence and 120 hour post Cre, isolated by FUCCI-FACS. The relative single-stranded signal was normalized to total TTAGGG signal and determined as a percentage of the signal in the lane containing wild type G1 cells (set at 100). (D) Quantification of relative single-stranded telomeric signal in G1 and late S/G2 as assayed in (A). The single-stranded telomeric signal was normalized to total TTAGGG signal and determined as a percentage of the signal in wild type G1 cells (set at 100). Values are the mean of three independent experiments and SDs.

When CsCl density gradient equilibrium centrifugation was used to separate the leading- and lagging-end telomeres, Cre treatment of *Apollo$^{F/F}$ Exo1$^{-/-}$* MEFs resulted in a ~60% reduction in the overhang at leading-end telomeres with no effect on lagging-end overhangs. In this experiment, the deletion of Apollo in Exo1-deficient cells appeared to cause a more severe overhang defect at leading-end telomeres than when Apollo was

deleted in Exo1-proficient cells. This result requires validation, since it may suggest that Exo1 has an even greater role in the 5' resection of leading-end telomeres in the absence of Apollo than in wild type cells. Nonetheless, these results permit the conclusion that Apollo and Exo1 act independently and differentially at newly synthesized leading- and lagging-end telomeres.

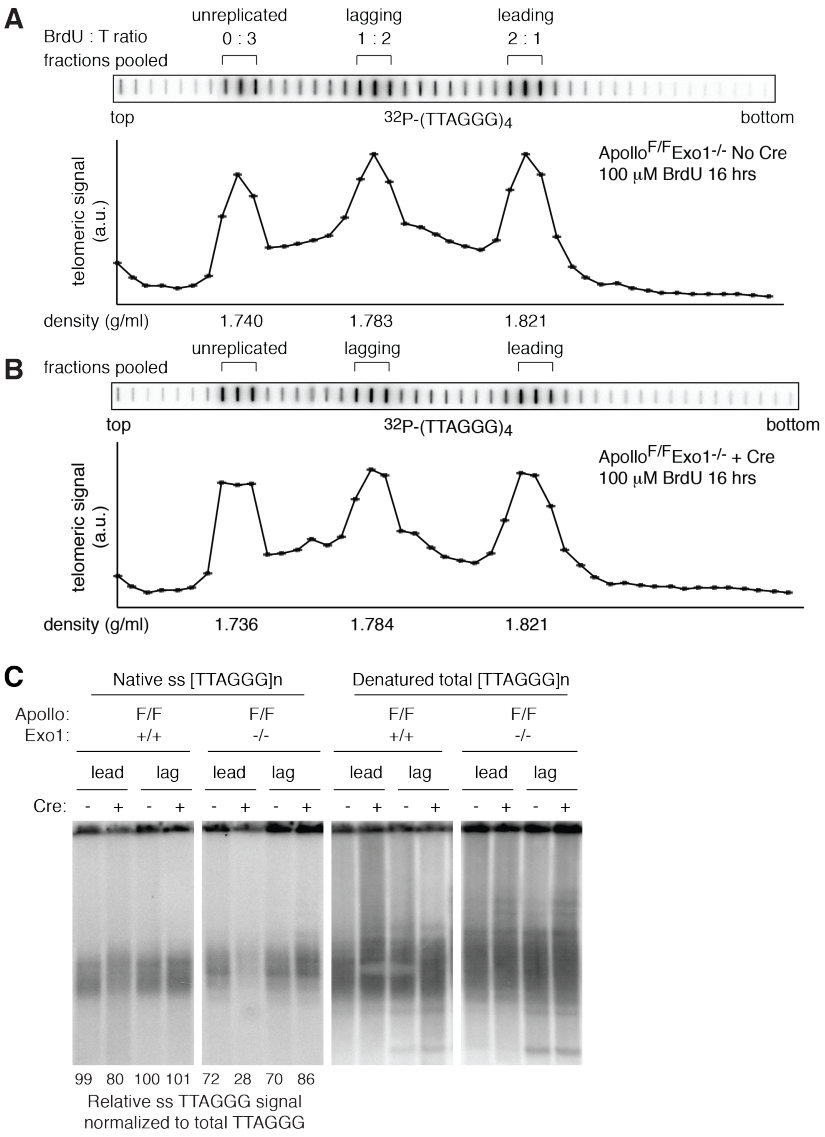

Figure 5.10. Exo1 acts at both newly-synthesized telomeres independently of Apollo. (A) and (B) Representative slot blots of telomeric signal in each fraction collected from CsCl density gradient equilibrium centrifugation of telomeric DNA from *Apollo*$^{F/F}$*Exo1*$^{-/-}$ MEFs in the absence of Cre (A) and at 120 hours after Hit&Run Cre (B), after labeling with BrdU for one round of replication. The fractions pooled for overhang analyses are shown. (C) Representative overhang analysis of leading- and lagging-end telomeres from *Apollo*$^{F/F}$ and *Apollo*$^{F/F}$*Exo1*$^{-/-}$ MEFs before and after Cre, separated in (A) and (B).

In the absence of Apollo, Exo1 and MRN contribute differentially to the processing and protection of leading-end telomeres

Though Exo1-mediated processing of telomeres in wild type cells appears to be distinct from the canonical pathway of DSB resection, in a setting such as Apollo deficiency, where the absence of a telomeric overhang elicits a DNA damage response, factors involved in DSB resection may indeed be recruited and act as a alternative method of generating overhangs at leading-end telomeres. This backup mechanism of overhang generation could explain why the DNA damage response observed in Apollo-deficient cells occurs only transiently in S phase. Since Exo1 appeared to act at leading-end telomeres even in the absence of Apollo, I asked whether Exo1 facilitates end protection at leading-end telomeres in Apollo-deficient cells. To investigate this possibility, I evaluated whether Exo1 deficiency exacerbates the telomere dysfunction phenotypes associated with the loss of Apollo. As shown previously in Chapter 3, the loss of Apollo results in a transient ATM-dependent DNA damage response at a subset of telomeres in S phase and the appearance of chromatid-type fusions between leading-end telomeres on metaphase spreads. In the absence of both Apollo and Exo1, the fraction of TIF-positive cells and the phosphorylation status of the ATM target Chk2 were comparable to what was observed in the absence of Apollo alone (Figure 5.10B-C). Exo1 deficiency also did not increase the total incidence of telomere fusion events, though there appeared to be a slight reduction in leading-leading chromatid-type fusions and a corresponding increase in fusions of other types (Figure 5.10D). Careful analyses revealed that these other fusions were mainly of the chromosome-type, which may have arisen as secondary events after chromatid-type fusions were segregated into daughter

cells and duplicated. Since there was no increased incidence in sister fusions, lagging-end telomeres appeared to remain largely protected. Consistent with the finding that Exo1 loss does not exacerbate the DNA damage response occurring at leading-end telomeres lacking Apollo, cells deficient for both Apollo and Exo1 also exhibited a similar doubling rate as cells lacking Apollo only (Figure 5.10A). Thus, in the absence of Apollo, though Exo1 mediates transient elongation of telomeric overhangs in late S phase, this process does not appear to be necessary for end protection.

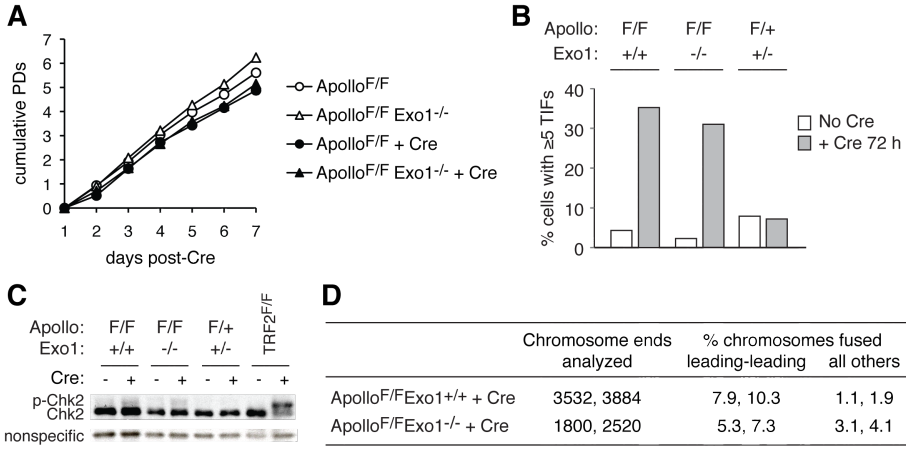

	Chromosome ends analyzed	% chromosomes fused leading-leading	% chromosomes fused all others
Apollo$^{F/F}$Exo1$^{+/+}$ + Cre	3532, 3884	7.9, 10.3	1.1, 1.9
Apollo$^{F/F}$Exo1$^{-/-}$ + Cre	1800, 2520	5.3, 7.3	3.1, 4.1

Figure 5.11. Exo1 deficiency does not exacerbate the DNA damage response associated with loss of Apollo. (A) Growth curve of *Apollo$^{F/F}$* and *Apollo$^{F/F}$Exo1$^{-/-}$* in the absence and presence of Hit&Run Cre. Open circles: *Apollo$^{F/F}$*, open triangles: *Apollo$^{F/F}$Exo1$^{-/-}$*, closed circles: *Apollo$^{F/F}$* + Cre, closed triangles: *Apollo$^{F/F}$Exo1$^{-/-}$* + Cre. (B) Quantification of TIFs defined as the co-localization of 53BP1 detected by indirect immunofluorescence to telomeres detected by FISH. (C) Immunoblot detection of Chk2 phosphorylation status. (D) Quantification of CO-FISH analysis detecting telomere fusions in *Apollo$^{F/F}$* and *Apollo$^{F/F}$Exo1$^{-/-}$* MEFs at 120 hours after Hit&Run Cre.

Based on these results, it appeared that, in the absence of Apollo, nucleases other than Exo1 were responsible for initiating resection at leading-end telomeres; thus, I next investigated the contribution of MRN/CtIP. As previously shown (refer to Figure 5.7), neither deleting Nbs1 nor depleting CtIP with two different shRNAs resulted in a defect in the telomeric overhang or a preponderance of leading-end fusions, suggesting that MRN/CtIP is not strictly required for overhang generation in wild type cells.

Nonetheless, MRN/CtIP might contribute to overhang generation at leading-ends in the absence of Apollo. Favoring this hypothesis is the observation that the level of leading end fusions in TRF2/Nbs1 DKO cells is higher than that observed in the absence of Apollo[194,195].

I determined whether the overhang phenotype and leading-end fusions observed in the absence of Apollo are exacerbated by co-deletion of Nbs1 by analyzing *Apollo*$^{F/F}$*Nbs1*$^{F/F}$ MEFs following Cre treatment. Deletion of both Apollo and Nbs1 resulted in a significant growth defect (Figure 5.12A). Experiments were performed in parallel to compare the overhang in Apollo KO vs. Apollo/Nbs1 DKO cells at 96 hours after Cre-mediated deletion. The overhang defect in the absence of both Apollo and Nbs1 was not significantly worse than in the absence of Apollo alone (Figure 5.12B). Depletion of CtIP in Apollo KO cells also resulted in no further reduction in overhang signal compared to Apollo null cells, though this result could be due to incomplete depletion of CtIP (Figure 5.12E). These experiments suggest that MRN/CtIP contribute negligibly to overhang size in the absence of Apollo.

Nonetheless, Nbs1 did appear to have a role in protecting leading-end telomeres in the absence of Apollo. Co-deletion of Apollo and Nbs1 resulted in approximately twice as many leading-end fusions as observed in the absence of Apollo alone. This level of leading-end fusion is comparable to that observed in TRF2/Nbs1 DKO cells. In analyzing the metaphases of Apollo/Nbs1 DKO cells, it appeared that roughly half of the leading-end fusions appeared as two telomeric signals juxtaposed next to each other rather than a single telomeric signal. Whether these two observed types of fusions reflect different repair pathways is not known. It is possible that the juxtaposed telomeric

signals represent a distinct class of associations between leading-end telomeres that occur only when both Apollo and Nbs1 are absent.

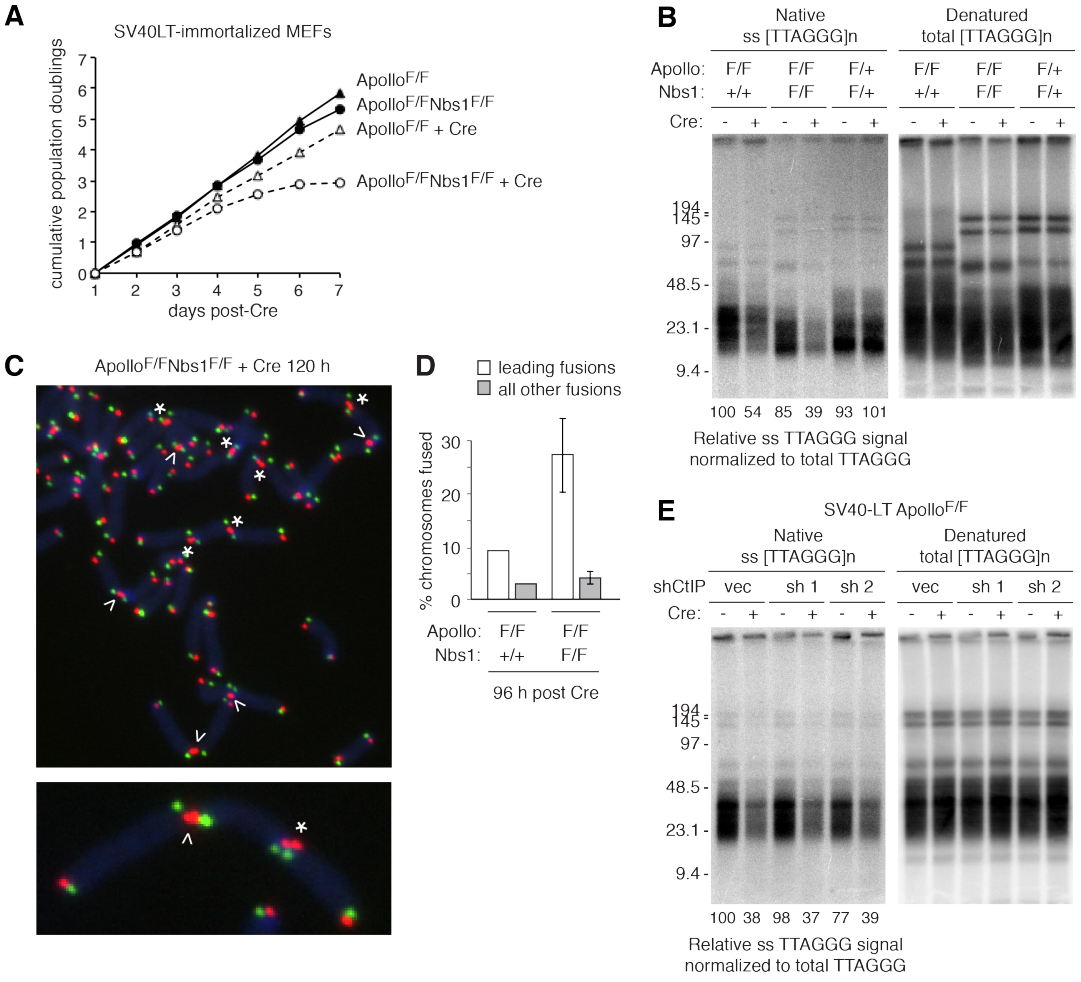

Figure 5.12. In Apollo-deficient cells, Nbs1 suppresses NHEJ of leading-end telomeres. Growth curve of SV40-LT immortalized Apollo$^{F/F}$ and Apollo$^{F/F}$ Nbs1$^{F/F}$ MEFs the absence and presence of Hit&Run Cre. Closed triangles: Apollo$^{F/F}$, closed circles: Apollo$^{F/F}$ Nbs1$^{F/F}$, open triangles: Apollo$^{F/F}$ + Cre, open circles: Apollo$^{F/F}$ Nbs1$^{F/F}$ + Cre. (B) Overhang assay of Apollo$^{F/F}$ and two independent Apollo$^{F/F}$Nbs1$^{F/F}$ MEF lines without Cre and 96 hours after Hit&Run Cre. (C) Representative CO-FISH detection of newly synthesized telomeres on metaphase spreads. ^ indicates leading-end fusions. * indicates juxtaposed leading-end signals. (D) Quantification of CO-FISH analysis detecting telomere fusions in Apollo$^{F/F}$ and Apollo$^{F/F}$ Exo1$^{-/-}$ MEFs at 120 hours after Hit&Run Cre. (E) Overhang assay of Apollo$^{F/F}$ at 96 hours after lentiviral transduction with empty vector or two different shRNAs to CtIP, without Cre or 120 hours after Hit&Run Cre.

One explanation for these results could be that in the absence of Apollo, MRN can accelerate the rate of overhang generation by other nucleases (such as Exo1) that otherwise act at a slow rate. Thus, in the absence of MRN/CtIP, the bulk overhang size

observed by in-gel hybridization is not changed but the slow rate of overhang generation results in a longer time interval during which leading-ends are vulnerable to fusion. If Exo1 is the nuclease responsible for this slow resection that occurs in the absence of Apollo and Exo1, depleting Exo1 in Apollo/Nbs1 DKO cells would be expected to further increase the leading-end fusions. The ATM-dependent DNA damage response activated at leading-ends lacking Apollo may thus recruit/activate nucleases and helicases, that act redundantly and have differential roles in protecting leading-ends from fusing.

Alternatively, the MRN complex could inhibit end-joining of Apollo-deficient telomeres in a manner that is independent of its ability to promote 5' end resection. It has been shown that in DNA-PKcs-deficient cells, MRN promotes alternative end-joining between coding ends that require hairpin-opening activity, while suppressing alternative NHEJ between signal ends. Based on the previous finding that the leading-end telomere fusions occurring in Apollo-deficient cells do not depend on ligase IV (Chapter 3), an alternative hypothesis is that the binding of these ends by the MRN complex inhibits the apparent A-EJ pathway that occurs in the absence of Apollo.

SUMMARY OF FINDINGS

The major findings of this chapter are summarized in Table 5.1. Here, I uncover a role for Exo1 in the transient elongation of telomeric overhangs in late S phase. The physiologic function of this processing step is unclear, though Exo1-mediated telomere processing does not appear to contribute to telomere end protection or the ability for telomerase to act at telomeres. Furthermore, the telomere dysfunction phenotype observed upon TPP1/POT1 deletion, whereby extensive telomeric overhangs activate an ATR-dependent DNA damage response, appeared to be largely independent of Exo1. The behavior of Exo1 at telomeres does not appear to recapitulate its activity in DNA DSB resection, since the effects of Exo1 depletion are not exacerbated by deficiencies in Nbs1, CtIP, or BLM. Exo1 acts at telomeres in Apollo-deficient cells, but its absence does not exacerbate the telomere dysfunction phenotypes associated with Apollo loss, suggesting that Exo1 is not required for initiating end resection at leading-end telomeres that lack Apollo. On the other hand, cells lacking both Apollo and Nbs1 show an increase in leading-end fusions compared to cells lacking Apollo only. This could reflect a role of the MRN complex in initiating resection at a fraction of ends in Apollo-deficient cells, though it has not been excluded that MRN might repress leading-end fusions by an alternative mechanism.

How Exo1 is recruited to telomeres remains an unanswered question. These studies suggest that a transient DNA damage response activated during telomere replication is unlikely to be the mode by which Exo1 localizes to telomeres in S phase. Investigations into the contributions of mismatch repair pathway components to telomeric overhang dynamics may shed light on whether Exo1 is recruited to telomeres through

interactions with mismatch repair proteins. Investigations into whether Exo1 interacts with shelterin proteins are also warranted.

Table 5.1. Relative overhang size and telomere fusions observed in different genetic backgrounds.

	relative normalized overhang signal					chromosomes fused	
	bulk	G1	late S	lead	lag	leading-leading	other
WT	100	100	200	90	100	<1%	<1%
mTR KO	100	100	170	100	100	-	-
Exo1 KO	60-70	95	125	70	70	<1%	<1%
Exo1/mTR DKO	60-70	80	100	70	60	-	-
Exo1/BLM DKO	50-60	-	-	-	-	-	-
Exo1/Nbs1 DKO	80	-	-	-	-	-	-
Exo1/Apollo DKO	30	60	70	30	85	5-8%	3-4%
Apollo KO	60-80	60	100	70-80	100	10%	1-2%
Apollo/Nbs1 DKO	50	-	-	-	-	25%	1-2%

Underlined values were set to 100, to which all numbers in the same column were normalized.

CHAPTER 6:

DISCUSSION

A model for the generation and maintenance of terminal telomere structure

The work described in this thesis delineates a model, based on genetic experiments in mouse cells, for the generation and maintenance of the terminal structure of mammalian telomeres (Figure 1). As replication reaches the telomere terminus, leading-strand DNA synthesis results in a blunt duplex or 5' single-stranded end that is degraded by the nuclease Apollo to generate a single-stranded 3' overhang. Apollo is dispensable for overhang generation at telomeres generated by lagging-strand DNA synthesis, which presumably contain constitutive overhangs throughout DNA replication. In the absence of Apollo, unprocessed leading-end telomeres activate a transient ATM-dependent DNA damage response in S phase and engage in fusions. This DNA damage response is not observed at all leading-end telomeres nor does it persist in G1 cells, likely due to additional pathways by which overhangs can be generated at leading-ends in the absence of Apollo. One such backup pathway appears to involve the Mre11/Rad50/Nbs1 complex, which has no apparent role in wild type cells but protects a subset of leading-end telomeres from fusing in the absence of Apollo.

In late S phase, telomeric overhangs undergo further transient elongation that depends on Exonuclease 1. Exo1 acts at both leading- and lagging-end telomeres in a step that appears to be independent of other nucleases involved in 5' end resection at a DNA DSB. Exo1 contributes to telomere end processing in the absence of Apollo, but has no apparent contribution to end protection in wild type or Apollo-deficient cells. The transient elongation of telomeric overhangs by Exo1 is thus not likely required for the initiation of 5' resection at telomeres in the presence or absence of Apollo. The loss of

Exo1 also does not affect the rate of telomere shortening in telomerase-deficient cells. Thus, the physiologic role of Exo1-mediated processing remains unclear.

At mouse telomeres, the single-stranded telomeric DNA binding protein, POT1b, regulates overhang size by inhibiting Apollo while facilitating the activities of the Ctc1/Stn1/Ten1 (CST) complex, composed of accessory factors of DNA polymerase alpha/primase. Loading of POT1b onto newly synthesized leading-end telomeres depends on Apollo, while the single-stranded overhang present on the template strand for lagging-strand DNA synthesis can presumably bind POT1b throughout S phase. In the absence of POT1b, both leading- and lagging-end telomeres accumulate significantly increased single-stranded overhangs that depend partially on Apollo. POT1b also limits overhang length by facilitating CST at both newly-synthesized telomeres. Specific residues in POT1b that are not conserved in POT1a mediate a physical interaction with members of the CST complex. A POT1b mutant that can interact with TPP1 and localize to telomeres while no longer interacting with CST is unable to fully suppress the excessive accumulation of single stranded telomeric overhangs, though this apparent dissociation-of-function mutant inhibits aberrant nucleolytic degradation by Apollo.

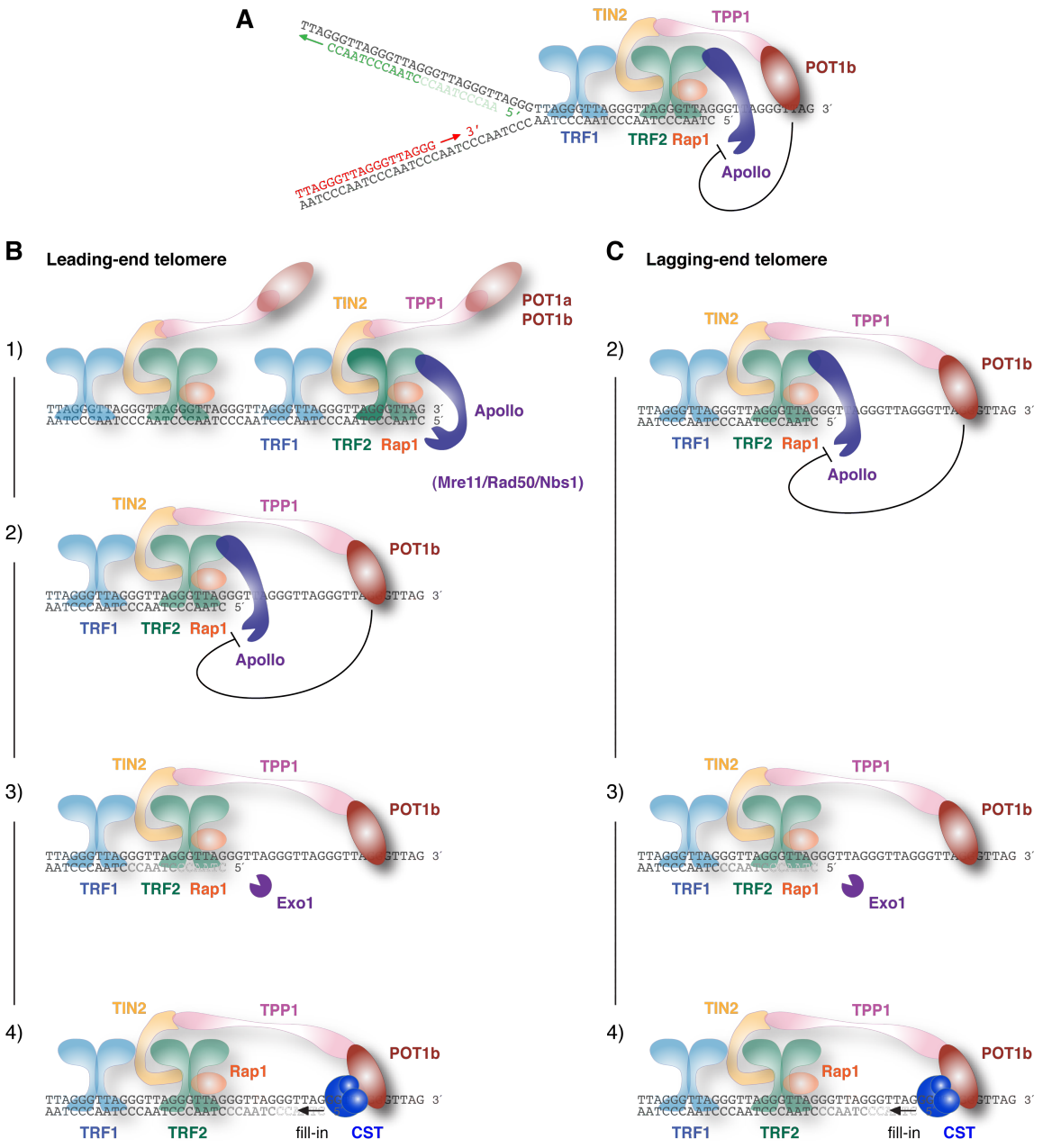

Figure 6.1. A unified model for the generation and maintenance of the terminal structure of mammalian telomeres. (A) The replication fork as it reaches the telomere terminus. Throughout S phase, POT1b loaded on the terminal overhang inhibits aberrant degradation by Apollo. (B) and (C) show the different telomere end-processing steps that occur at newly-synthesized leading- and lagging-end telomeres. 1) Apollo is required to generate the 3' overhang at leading-end telomeres. In the absence of Apollo, Nbs1 has a role in initiating 5' end resection and protecting leading-end telomeres from fusing. 2) POT1b loading onto overhangs inhibits Apollo. 3) Exo1 acts at both newly synthesized telomeres leading to transient elongation of the telomeric overhang. 4) POT1b promotes the recruitment of CST, which limits overhang size by facilitating fill-in synthesis of the C-rich strand.

Differential processing of leading- and lagging-end telomeres

My work highlights significant differences in the genetic requirements for telomere end processing at leading- and lagging-end telomeres in mammalian cells. In *S. cerevisiae*, chromatin immunoprecipitation studies have detected the single-stranded DNA binding protein Cdc13 and the Est1 and Est2 subunits of telomerase at both daughter telomeres, while deficiencies in the Mre11/Rad50/Xrs2 complex specifically compromise their ability to localize to newly synthesized leading-end telomeres[433]. However, these differences have not been linked directly to differences in overhang generation at leading- and lagging-end telomeres. In human cells, differences in overhang dynamics at leading- and lagging-end telomeres have been described[7], though the factors responsible for such differences were not identified.

The work attributing the nucleolytic activity of Apollo to overhang generation specifically at leading-end telomeres validates the long-held hypothesis that nucleases are required to generate the appropriate terminal structure at the end of leading strand DNA replication, which results in ends that are blunt or have a 5' single-stranded overhang. The only nuclease so far implicated in the protection of lagging-end telomeres is FEN1[54,392]. Nonetheless, it is likely that some nucleolytic processing is required for degradation of the terminal RNA primer. While such processing may not be critical for the protection of lagging ends from activating DNA damage responses, the finding that POT1b and CST have roles at both leading- and lagging-end telomeres suggest that regulatory mechanisms are nonetheless important to ensure the proper terminal structure at both newly-synthesized telomeres.

The differences in processing between leading- and lagging-end telomeres may be due to the different problems faced by the two newly-synthesized telomeres. Newly-synthesized leading-end telomeres must solve the unique problem of generating a single-stranded overhang in order to achieve end protection. On the other hand, lagging-end telomeres may not have a problem maintaining end protection *per se* but face the difficulties inherent in ensuring complete duplication of the template and the protection of newly-synthesized Okazaki fragments from aberrant degradation. Both newly-synthesized telomeres require a mechanism for fill-in synthesis of the C-rich strand, a process important not only after the extension of G-rich strands by telomerase but also to limit the extent of degradation by nucleases in S phase.

In the absence of POT1b, significant degradation occurs at the 5' end of newly-synthesized lagging-strand telomeres, inducing an increase in overhang size greater than what is observed at leading-end telomeres. This appears to be due to excessive degradation by Apollo since the POT1b mutant unable to bind CST partially rescues the overhang phenotype at lagging-end telomeres in POT1b-deficient cells but has no effect on the excessive overhangs that occur in Apollo/POT1b DKO cells. One explanation for why lagging-end overhangs become even longer than leading-end overhangs in the absence of POT1b could be due to the constitutive presence of a 3' overhang at lagging-end telomeres. In the absence of POT1b, if Apollo performs an equal extent of 5' exonucleolytic degradation of the C-rich strands of newly synthesized lagging- and leading-end telomeres, the lagging-end telomere would naturally accumulate longer 3' overhangs.

Recruitment and activation of telomeric nucleases

A primary mode by which nucleases localize to telomeres involves shelterin. TRF2 recruits Apollo to telomeres and mutations of the interaction sites in either TRF2 or Apollo abolishes the function of Apollo in overhang generation[44,51,53]. The absence of an antibody to detect endogenous Apollo has made it difficult to investigate the temporal and physical regulation of its recruitment. Theoretically, the activity of Apollo at newly synthesized leading-end telomeres could be due either to its specific recruitment to these sites or due to differential regulation of Apollo activity at leading- and lagging-end telomeres. The finding that POT1b inhibits aberrant degradation of lagging-end telomeres by Apollo suggests that Apollo is likely recruited to both newly-synthesized telomeres. The overhangs present at lagging-end telomeres throughout S phase likely provide a constitutive binding site for POT1b. On the other hand, the absence of a single-stranded 3' overhang immediately upon completion of leading-strand DNA synthesis may provide a window for the nucleolytic activity of Apollo until sufficient amounts of single-stranded telomeric DNA have accumulated to bind POT1b.

My investigations ruling out telomeric contributions of nucleases and helicases involved in DNA DSB resection suggests that the transient activation of a canonical DNA damage response is not likely the instigating event that normally promotes 5' end resection at telomeres. Besides Exonuclease 1, other nucleases involved in DSB resection do not appear to act at telomeres except in cases of telomere deprotection. For instance, in the absence of Apollo, the recognition of newly synthesized leading-end telomeres as DNA damage by the MRN complex appears to provide an alternate route by which to initiate overhang generation. Thus, shelterin provides a specific mode of

recruiting nucleases to telomeres under normal circumstances, while the DNA damage response provides a backup mechanism to resume end protection in settings where overhang generation is compromised. While a major function of shelterin is to protect telomeres from activating cell cycle checkpoints and aberrant repair pathways that promote genome instability, the transient localization of DNA damage factors to telomeres might be beneficial in cases when telomere function is compromised due to loss of the overhang.

How Apollo is activated at the end of leading strand DNA synthesis is unknown. It may simply be that the exposure of a blunt or single-stranded 5' end at the terminus of leading-strand DNA replication provides the preferred substrate for Apollo at leading-end telomeres. Since leading-strand DNA replication uses the telomeric C-rich strand as the template, the C-rich strand would not be expected to have discontinuities that expose a 5' end to nucleolytic activities. At the recessed 5' ends of unreplicated telomeres and newly-synthesized lagging-end telomeres, Apollo would be inhibited by the binding of POT1b to the adjacent single-stranded DNA.

Another (not mutually exclusive) possibility is that post-translational modifications of Apollo occur as the replication fork reaches the telomere terminus, promoting its nucleolytic activity. Though modifications of Apollo that modulate its nuclease activity have not been identified, the examples of Artemis and CtIP provide precedents for this mode of regulation. DNA-PK binding and phosphorylation of Artemis modulate its nucleolytic activities[337], while the phosphorylation and acetylation of CtIP by Cdk and SIRT6[383,384], respectively, promotes its activity in 5' end resection of DNA DSBs. Though not tested in this work, previous studies have suggested DNA-PK

activity is required in mouse cells to protect a subset of leading-end telomeres from fusions[422,434]. The finding that the Cdk inhibitor roscovitine does not compromise overhang generation or cause any defects in overhang dynamics suggests that Cdk activity is not required for the activities of Apollo and Exo1 at telomeres.

Regulation of nuclease activity by POT1b

The studies on POT1b indicate that the nucleolytic activity of Apollo must be well regulated during S phase to prevent extensive degradation. The possible mechanisms by which POT1b inhibits resection include physical blockade of the 5' end, direct inhibition of nuclease activity, or recruitment of factors that counteract the action of Apollo. The ability to replace the N-terminal OB folds of POT1b with the equivalent domains in POT1a or human POT1 without eliciting an aberrant overhang phenotype suggests that there are no functional differences between the DNA binding capabilities of these three POT1 proteins[39]. Furthermore, the *in vitro* binding affinities of POT1a and POT1b to both internal and terminal single-stranded telomeric DNA do not significantly differ[39].

The interaction between CST and POT1b, which requires specific residues in the C-terminal domain of POT1b, provides one mechanism by which Apollo-mediated resection is counteracted. However, in the POT1b-LVDII mutant, this function can be dissociated from the inhibition of Apollo at lagging-end telomeres. The finding that this mutant can counteract resection by Apollo while being unable to recruit CST suggests that POT1b can negatively regulate resection by additional mechanisms besides the

recruitment of CST. POT1b may interact with yet other factors that directly inhibit Apollo or it may inhibit a factor that aberrantly stimulates Apollo activity.

With regards to other mechanisms by which POT1b inhibits Apollo, no direct physical association has been identified between the two proteins. Since unique attributes of the C-terminal domain of POT1b confer the ability to suppress resection by Apollo, the interaction between TPP1 and POT1b provides another potential point of difference between the POT1 proteins. Previous studies reported no apparent differences between the interactions of POT1b and POT1a with TPP1[29,435]. Nonetheless, differences between the recruitment of POT1a and POT1b to the telomere terminus *in vivo* might allow POT1b but not POT1a to block terminal resection. In mouse cells, no gross differences in RNA or protein expression of POT1a and POT1b have been noted in different tissues or at different times during the cell cycle[37], though the inability to overexpress POT1b suggests that the protein levels are tightly regulated.

The balance between degradation and synthesis of the telomeric C-rich strand

Though aberrant nuclease degradation might accelerate telomere shortening in pathological situations, the work described in this thesis suggests that the rate of telomere shortening in telomerase-deficient cells does not depend primarily on nuclease activities. Indeed, the transient elongation of overhangs by Exo1 has no apparent effect on the rate of telomere shortening in the absence of telomerase. Furthermore, telomere shortening is not slowed when Apollo is rendered unable to localize to telomeres in telomerase-deficient cells, though the interpretation of such experiments are complicated by the transient DNA damage response that occurs at leading-end telomeres lacking Apollo.

The results show that CST is an important determinant of overhang size, and the recruitment of CST can limit the rate of telomere shortening in the absence of telomerase. The proposed model is that POT1b recruits CST to mouse telomeres subsequent to nuclease-mediated end processing. This final step likely involves the fill-in synthesis of the C-rich strand and may ultimately contribute more significantly than nucleolytic degradation to the rate of telomere shortening. The challenge will be in dissociating the various roles of CST at telomeres, since this complex appears to not only limit overhang size at the telomere terminus but also facilitates replication within internal telomeric sequences and may have roles in regulating telomerase[292].

Consequences of an aberrant structure at the telomere terminus

My work indicates that proper overhang generation is required to suppress the activation of a DNA damage response, though the protective role of Apollo appears to be limited to S phase. In the absence of Apollo, despite a persistent overhang defect throughout the cell cycle, the accumulation of DNA damage factors to a subset of telomeres is observed only in S phase cells. Furthermore, notably absent are the chromosome-type fusions that would result if leading-end telomeres continued to be vulnerable to fusion in daughter cells.

How the protected state is restored as cells progress through mitosis remains unclear. One possibility is that intrinsic properties of telomeres allow protection of unprocessed ends in G1 but not in S phase. For instance, leading-end telomeres with short overhangs might still form t-loops at a slower rate. Another possibility is that additional Apollo-independent processing could be sufficient to restore end protection. Indeed, the

overhang signal transiently increases in late S/G2 in both wild type and Apollo-deficient cells, and subsequent studies indicate that this additional processing is mediated by Exo1. However, the extensive resection of telomeres by Exo1 in the absence of Apollo does not appear to contribute to end protection. Rather, the MRN complex has a protective role in suppressing additional leading-end fusions when Apollo is absent. Finally, it is possible that the milieu of G1 and S phase exposes telomeres to different threats, requiring distinct protective measures to ensure telomere protection in different stages of the cell cycle.

The conditional deletion of Apollo in MEFs causes a proliferation defect (Chapter 3) and mice homozygous for the null allele die with developmental abnormalities in the perinatal period[436], suggesting that overhang generation is crucial for viability. On the other hand, excessive C-strand degradation in the absence of POT1b alone does not compromise cell proliferation and only when combined with telomerase deficiency does POT1b become essential for development[187]. Significant organ dysfunction reminiscent of the human disease, dyskeratosis congenita, also occurs mainly in the setting of telomerase haploinsufficiency[187,437]. The relative tolerance of mammalian cells to excessive degradation of the telomeric C-strand may explain why so many nucleases act in partially redundant ways at telomeres in order to ensure appropriate overhang generation despite an increased risk of telomere degradation if any of the nucleolytic activities are not properly regulated.

The evolution of telomere end processing

The findings described here support the accumulating evidence of significant evolutionary divergence in the pathways that modulate telomere length and function.

The preservation of the appropriate terminal structure of telomeres is achieved by multiple mechanisms involving different nucleases that do not appear to have conserved telomeric functions across organisms. For instance, whereas the MRX complex is involved in end processing at budding yeast telomeres[256-258], its role appears secondary to Apollo in mouse cells.

In addition, it has been previously established that overhangs at mammalian telomeres are almost an order of magnitude longer than those in lower eukaryotes (refer to Introduction). Since mammalian telomeres are longer than those in yeast and other unicellular organisms and single-stranded DNA binding proteins can suppress ATR activation[190], perhaps there is no inherent disadvantage to generating longer overhangs, and thus the recruitment of many nucleases to telomeres by shelterin might have resulted in the collateral effect of more nucleolytic degradation at the telomere terminus. It may also be that proper telomere function in mammalian cells requires longer overhangs. With regards to this question, it would be useful to know the minimal length of the telomeric overhang that must be present at a single telomere in order to maintain both end protection and telomere elongation by telomerase.

Additionally, the results presented here suggest that resection at least at leading-end telomeres in mouse cells may be more extensive than at human telomeres. Although I have not been able to define the length distribution of telomeric overhangs in mouse cells, the relative overhang signals at leading and lagging end telomeres are similar in mouse cells whereas, in human cells, the leading-end telomeres have shorter overhangs compared to lagging-end telomeres[7]. Though resection is regulated to some extent by POT1b in mouse cells, limiting overhang length at leading end telomeres may be

relatively less important than ensuring that overhangs of sufficient length are generated and able to facilitate end protection. On the other hand, perhaps the absence of extensive resection in the setting of shRNA depletion of human POT1[210] may be due to the presence of alternative or redundant mechanisms that protect human telomeres from extensive resection.

Whereas in human cells, the single TPP1/POT1 complex[30,31] appears to interact with telomerase[35,114], CST[291], and coordinate end protection[210], in mouse, the TPP1/POT1a complex suppresses activation of ATR[190], while the TPP1/POT1b facilitates the function of CST in telomere end processing. TPP1 is presumed to form in complexes with either POT1a or POT1b, and these two complexes reside simultaneously at telomeres. It is unclear whether evolutionary advantages are conferred by this division of labor or if these differences evolved and were retained in rodents simply due to the absence of major disadvantages.

Implications for human disease

The findings on telomere end processing are relevant to the inherited bone marrow failure syndrome, dyskeratosis congenita (DC), which has been attributed to telomere dysfunction. DC can be caused by mutations in telomerase components and the shelterin component TIN2, but shelterin accessory factors had not been implicated in the disease[241,438,439].

A recent study to understand the pathogenesis of Hoyeraal-Hreidarsson syndrome, a severe variant of DC, identified a single patient expressing a dominant negative allele of Apollo that lacks the TRF2 binding domain and induces an ATM-dependent telomere

damage signal[243]. However, the Apollo locus appeared to lack a disease-causing mutation. Our findings that Apollo deficiency is specifically associated with defective overhang maintenance and leading-end telomere fusions may facilitate the identification of additional patients with Hoyeraal-Hreidarsson syndrome or other forms of DC that are caused by defects in Apollo. The finding that defects in the telomeric function of CST can contribute to accelerated telomere shortening, which is in turn responsible for DC-like phenotypes in *POT1b*$^{-/-}$*mTR*$^{+/-}$ mice[187], provides a basis for studying whether mutations in human CST occur in DC.

Whether telomere dysfunction caused by changes in the telomeric overhang contributes to genome instability during tumorigenesis remains an important open question. A better understanding of the end processing activities that modify telomere length could also provide new avenues for the development of drugs to complement the telomerase inhibitor, imetelstat/GRN163L, currently in Phase I or II clinical trials for the treatment of several cancer types[440]. The elucidation of multiple regulatory mechanisms that govern the proper terminal structure of mammalian telomeres is hoped to provide information that may someday guide the treatment of human diseases in which the status of telomere function modifies pathogenesis or prognosis, a lofty challenge for translational medicine.

MATERIALS AND METHODS

Mammalian cell culture

Mouse embryonic fibroblasts (MEFs) were obtained from E13.5 embryos using standard techniques and cultured in Dulbecco's modified Eagle medium supplemented with 15% fetal bovine serum (Gibco), 2 mM L-glutamine, 100 U/ml penicillin (Sigma), 0.1μg/ml streptomycin (Sigma), 0.1 mM non-essential amino acids (Invitrogen), 1mM sodium pyruvate (Sigma), and 50 μM β-mercaptoethanol (Chemicon). Primary MEFs were immortalized at passage 2 with pBabe SV40-LT (gift from G. Hannon) by retroviral transduction (described below).

SV40-LT immortalized and p53-/- MEFs, Phoenix ecotropic packaging cell line (ATCC), and 293T cells were grown in DMEM supplemented with 10-15% fetal bovine serum (Gibco), 2 mM L-glutamine, 100 U/ml penicillin (Sigma), 0.1μg/ml streptomycin (Sigma), and 0.1 mMnon-essential amino acids (Invitrogen).

All cells were grown at 37C in the presence of 5% CO_2 and 95% relative humidity. Cells were passaged by pre-rinsing with room temperature phosphate-buffered saline, followed by incubation in trypsin-EDTA for 2-5 min. Trypsin was inactivated by adding serum-containing medium. Cells were counted with a Coulter Z1 Particle counter and seeded onto a new plate as desired.

Synchronization of primary MEFs in G0

Primary MEFs were grown to confluency on 10 cm dishes in DMEM supplemented with 10% fetal bovine serum (Gibco). Medium was refreshed daily according to the following serum withdrawal protocol: 10% FBS (day 1), 5% FBS (day

2-3), 1% FBS (day 4-5), 0.5% FBS (day 6 and on). Cells were considered synchronized and amenable to treatments on day 8.

Retroviral gene delivery

For infection of mouse cells, 24 h prior to transfection, $5x10^6$ Phoenix ecotropic packaging cells were plated in 10 cm dishes. Pheonix cells were transfected with 20 μg of the appropriate plasmid DNA by $CaPO_4$ precipitation (described below). The media was refreshed 6-8 h later. 36 h after transfection, media was collected and filtered through a 0.45 μm filter. Polybrene was added to a final concentration of 4 mg/mL and the virus-containing medium was used to infected target cells plated 24 h earlier at a density of 5×10^5 cells per 10 cm dish. Fresh media was added to the virus-producing cells, and the same cells were used for a total of 3-4 infections at 12 h intervals. 12 h after the last infection, cells were split into fresh media containing antibiotics for selection, as appropriate (puromycin: 2 μg/ml, hygromycin: 90 μg/ml). Selection was maintained for 3 days in the presence of puromycin or 5 days in the presence of hygromycin, until uninfected control cells had died. Experimental timepoints were counted as hours or days from t=0 set at 12 h after the first infection.

Lentiviral gene delivery

24 h prior to transfection, $5x10^6$ 293T cells were plated in 10 cm dishes. 293T cells were transfected with 10 μg of the appropriate plasmid DNA, along with packaging plasmids (5 μg pVSVg, 3 μg pMDLg, 2.5 μg pRSV) by $CaPO_4$ precipitation (described below). The media was refreshed 6-8 h later. The first infection was performed at 36 h

after transfection. Target cells were infected for a total of 3-4 infections at 4-6 h intervals. Experimental timepoints were counted as hours or days from t=0 set at 12 h after the first infection.

Retroviral introduction of Cre recombinase

Cre recombinase was introduced using the retroviral transduction protocol described above. MEFs were infected 4 times at 12 h intervals with pMMP Hit&Run Cre retrovirus. Mock infection was used as a negative control. No selection was applied. Experimental timepoints were counted as hours or days from t=0 set at 12 h after the first infection.

For long-term analyses requiring selectable Cre expression, retroviral infection of pWzl-hygro-Cre or empty vector, as a negative control, was performed, followed by selection with hygromycin.

Tamoxifen-inducible Cre-ER system

Cells in 10 cm dishes were treated for 6-12 hours with 500 nM 4-OH tamoxifen. Cells were washed with PBS and media was replaced. Experimental timepoints were counted as hours from the time of media change.

Temperature-sensitive TRF2ts cell line

The temperature sensitive TRF2ts DNA ligase IV deficient cell line[197] contains the TRF2ts allele (mouse TRF2-I468A) in the context of $TRF2^{F/-}p53^{-/-}Lig4^{-/-}$ MEFs from which the endogenous TRF2 allele was deleted with Cre. The cells were grown at the

permissive temperature of 32°C and shifted to 37°C to induce the release of TRFts from telomeres.

Growth analysis

For growth curves, 1 x 10^6 and 5 x 10^5 cells were plated on 10 cm dishes at 24 h post-retroviral infection and counted, respectively, at 48 and 72 h post-infection. Cells were harvested, counted, and replated at 5 x 10^5 per 10 cm dish, and counted every 48 h afterward. Growth curves were presented as population doublings plotted over time. PDs were determined by the following formula: PD = original PD + [ln(# cells at passage/# cells seeded)/ln(2)].

Calcium phosphate transfection of 293T and Phoenix cells

16-24 h prior to transfection, 3-4 x 10^6 cells were plated in 10 cm dishes. For each plate, 428 µl H_2O, 62 µl 2 M $CaCl_2$ and 10 µl total plasmid DNA were mixed with an equal amount of 2 x HBS (50 mM HEPES pH 7.05, 10 mM KCl, 12 mM dextrose, 280 mM NaCl, 1.5 mM Na_2PO_4). During the process of mixing, the solution was aerated by blowing air through a 10 mL pipette with a Pipet-aid (Drummond). Medium was refreshed 6-8 h after transfection.

Whole cell lysates and immunoblotting

Cells were lysed in 2 x Laemmli buffer (100 mM Tris-HCl, pH 6.8, 200 mM DTT, 3% SDS, 20% glycerol, 0.05% bromophenol blue) at 10^4 cells per µl, denatured for 7 min at 100°C, and sheared with a 28 gauge insulin needle before loading the equivalent

of 1 x 10^5 per lane. Protein samples were separated by SDS-PAGE and blotted on nitrocellulose membranes. Membranes were blocked in 5% milk in PBST (0.5% Tween-20 in PBS) for 30 min at RT and nutated with primary antibodies in 5% or 0.1% milk in PBST overnight at 4°C. Membranes were washed 3 times with PBST, nutated in secondary antibody in 5% milk in PBST for 1 h at RT, and washed 3 times with PBST. Blots were developed with enhanced chemiluminescence (Amersham).

Co-immunoprecipitation of overexpressed proteins in 293T cells

For immunoprecipitation of proteins transiently expressed in 293T cells, transfection was performed as decribed above. 48 h after transfection, cells were harvested, washed with PBS, and resuspended in 200-500 µl of lysis buffer (50 mM Tris-HCl pH 7.4, 1% Triton X-100, 0.1% SDS, 150 mM NaCl, 1 mM EDTA, 1 mM DTT, 100 µM PMSF, with a complete mini-protease inhibitor tablet [Roche] per 10 ml). The NaCl concentration was raised to 400 mM, and the lysate was incubated on ice for 5 min. The NaCl concentration was reduced to 200 mM with an equal volume of cold water, and cell debris was removed by centrifugation at 13000 rpm for 10 min at 4°C. 50 µl of 2x Laemmli buffer was added to 50 µl of lysate and set aside as input. 5 µl of anti-myc antibody (9E10, oncogene) was added to 800 µl of lysate. Samples were nutated at 4°C for 5 h. 60 µl of a Protein G sepharose slurry (50% (v/v) Protein-G sepharose [Amersham] in PBS in 1 mg/ml BSA) was added, and the sampled were nutated at 4°C for an additional 60 min. Beads were washed 4 times at 4°C with lysis buffer, and immunoprecipitated protein was eluted with 60 µl of 2x Laemmli buffer. Samples were boiled for 5 min before loading onto SDS-PAGE gels.

Immunofluorescence

Cells grown on coverslips were rinsed with PBS, fixed with 2% paraformaldehyde in PBS for 10 min at room temperature and washed twice with PBS for 5 min. Cells were either stored in PBS with the addition of 0.02% azide or processed immediately. If extraction was required, prior to fixation, cells were treated for 1-2 min with Triton X-100 extraction buffer (0.5% Triton X-100, 20 mM HEPES-KOH pH 7.9, 50 mM NaCl, 3 mM MgCl2, 300 mM sucrose). Extracted cells were fixed with 3% paraformaldehyde/2% sucrose for 10 min at room temperature, and washed twice with PBS. Cells were permeabilized with Triton X-100 buffer after fixation. After permeabilization, cells were washed three times with PBS and blocked with PBG (0.2% (w/v) cold water fish gelatin (Sigma), 0.5% (w/v) BSA (sigma) in PBS) for 1 h at RT. Cells were incubated with primary antibody, diluted in PBG for 2 h at RT or overnight at 4°C, washed 3 times with PBG at RT, incubated with secondary antibody 1:250 in PBG for 1 h at RT, and washed 3 times with PBS. To the second PBS wash 0.1 μg/ml 4,6-diamidino-2-phenylindole (DAPI) was added. Coverslips were sealed onto glass slides with embedding media (ProLong Gold Antifade Reagent, Invitrogen). Digital images were captured with a Zeiss Axioplan II microscope with a Hamamatsu C4742-95 camera using Improvision OpenLab software.

Telomere fluorescence in situ hybridization (FISH)

MEFs were grown to approximately 80% confluence on 10-cm dishes and incubated for 90 min in 0.2 μg/ml colecmide (Sigma). Cells were harvested by trypsinization, centrifuged at 1000 rpm for 5 min, and resuspended in 0.075 M KCl

prewarmed to 37°C. Cells were incubated at 37°C for 15-30 min with occasional inversion. Cells were centrifuged at 1000 rpm for 5 min and the supernatant was decanted. 500 µl of cold 3:1 methanol:glacial acetic acid fixative was added dropwise while cells were mixed gently on a vortexer (<1000 rpm). Another 500 µl fixative was added slowly with mixing. Tubes were then filled to 10 ml with fixative and fixed at 4°C for at least 24 h. To prepare metaphase spreads, cells were centrifuged at 1000 rpm for 5 min and the supernatant was decanted. Cells were resuspended in 1 ml remaining fixative and 100 µl was dropped onto glass slides in a temperature- and humidity-controlled chamber set at 4°C and 50% humidity (Thermotron). Slides were washed with fixative and dried overnight.

For peptide nucleic acid (PNA) FISH, slides were washed in PBS once and fixed in 4% formaldehyde for 2 min at room temperature. After three PBS washes for 5 min each, spreads were digested for 10 min at 37°C with 1 mg/ml pepsin dissolved in 10 mM glycine, pH 2.2. Slides were then washed in PBS, fixed again in 4% formaldehyde for 2 min at room temperature, and washed in PBS before dehydration by 5 min incubation with 70%, 95%, and 100% ethanol. After air-drying, hybridizing solution (70% formamide, 1 mg/ml blocking reagent (Roche), 10 mM Tris-HCl, pH 7.2) containing FITC-OO-$(AATCCC)_3$ PNA probe (Applied Biosystems) was added, and spreads were denatured by heating for 3 min at 80°C on a heating block. Spreads were then allowed to hybridize in the dark for 2 h at room temperature or overnight at at 4°C. Two 15-min washes were performed in a mixture containing 70% formamide, 10 mM Tris-HCl, pH 7.2, followed by three washes in a mixture containing 0.1 M Tris, HCl, pH 7.2, 0.15 M NaCl, and 0.08% Tween-20, with DAPI added to the second wash to counter-stain the

chromosomal DNA. Slides were mounted in embedding medium (ProLong Gold Antifade Reagent, Invitrogen), and digital images were captured with a Zeiss Axioplan II microscope with a Hamamatsu C4742-95 camera using Improvision OpenLab software.

CO-FISH

Cells were incubated in the presence of BrdU:BrdC (3:1, final concentration: 10 μM) for 16 hours with the addition of 0.2 μg/ml (Sigma) for the last 90 min. Cell fixation and preparation of metaphase spreads was performed as described above for FISH. Slides were treated with 0.5 mg/ml RNase A (in PBS, DNase free) for 10 min at 37°C. Slides were stained with 0.5 μg/ml Hoechst 33258 (Sigma) in 2xSSC for 15 min at RT. Slides were then exposed to 365-nm UV light (Stratalinker 1800 UV irradiator) for 30 min (equivalent to $5.4x10^3$ J/m^2). The slides were digested twice with 80 μl of 10 U/ μl Exonuclease III (Promega) in buffer supplied by the manufacturer (50 mM Tris-HCl, 5 mM MgCl2, and 5 mM DTT, pH 8.0) at RT for 10 min each. The slides were washed with PBS and dehydrated with 70%, 95%, 100% ethanol at RT. After air-drying, spreads were incubated for 2 hours at RT with hybridizing solution (70% formamide, 1 mg/ml blocking reagent (Roche), 10 mM Tris-HCl, pH 7.2) containing TAMRA-OO-$(TTAGGG)_3$ PNA probe (Applied Biosystems). Slides were rinsed for a few seconds in a wash containing 10 mM Tris-HCl pH 72, 70% formamide, then hybridized for 2 hours at RT with hybridizing solution containing FITC-OO-$(AATCCC)_3$ PNA probe (Applied Biosystems). Slides were washed and mounted as for FISH.

Southern blotting and detection of telomeric DNA

Digested genomic DNA in solution was electrophoresed in 1% agarose in 0.5x TBE at 1 V/cm for at least 2 hours, followed by raising the voltage to 3-4 V/cm until the Orange-G dye in the loading buffer ran off the gel. The DNA was denatured (1.5 M NaCl, 0.5 M NaOH – 2 times 30 min), neutralized (3 M NaCl, 0.5 M Tris-HCl, pH 7.0 – 2 times 30 min), then transferred to a Hybond-N membrane in 20x SSC (3 M NaCl, 300 mM Na3-citrate, pH 7). The DNA was UV-crosslinked to the membrane, which was then pre-hybridized in Church mix (0.5 M Na phosphate buffer [pH 7.2], 1 mM EDTA [pH 8], 7% w/v SDS, 1% w/v BSA) for 1 h followed by hybridization with an end-labeled [^{32}P](CCCTAA)$_4$ oligonucleotide at 50°C for at least 4 hours. The membrane was washed at 55°C, three times for 30 min in 4x SSC and once for 15 min in 4x SSC/0.1% SDS.

Analysis of telomeric DNA by in-gel hybridization

For the analysis of mouse genomic DNA, cells were suspended in PBS and mixed 1:1 (v/v) with 2% agarose (SeaKem) in PBS to obtain between 5x10^5 to 1x10^6 cells per plug. Plugs were digested overnight with 1 mg/ml Proteinase K (in buffer containing 10 mM Tris-HCl pH 8.0, 250 mM EDTA, 0.2% sodium deoxycholate, 1% sodium lauryl sarcosine), washed four times for 1 h each with TE buffer (10 mM Tris-HCl, pH 8.0, 1 mM EDTA), including 1 mM PMSF in the last wash. Plugs were washed once more with H_2O and digestion buffer. Plugs were incubated overnight at 37°C with 60 U *Mbo*I and 60 U *Alu*I. The following day, the plugs were washed once in TE, and once in 0.5x TBE, and loaded onto a 1% agarose/0.5x TBE gel. Samples were run for 24 h on a CHEF-DRII PFGE apparatus (BioRad) in 0.5 x TBE running buffer. The settings were as

follows: initial pulse, 5 s; final pulse, 5 s; 6 V/cm; 14°C. The gels were dried and prehybridized in Church mix for 1 h at 50°C. Hybridization was performed overnight at 50°C in Church mix with 4 ng of a γ-^{32}P-ATP end-labeled $(AACCCT)_4$ probe (labeling protocol described below). The gel was washed at 55°C three times for 30 min each in 4x SSC and once for 30 min in 4x SSC/0.1% SDS. The gel was exposed to a PhosphoImager screen overnight. After the image was captured, the gel was denatured in 0.5 M NaOH, 1.5 M NaCl for 30 min, neutralized with two 15-min washes in 0.5 M Tris-HCl pH 7.5, 3 M NaCl, prehybridized in Church mix for 1 h at 55°C, and hybridized overnight with the same probe at 55°C. The gel was washed and exposed as above. The single-stranded G-rich overhang signal in the native gel was quantified with ImageQuant software and normalized to the total telomeric DNA quantified after the gel had been denatured and re-hybridized with the telomeric probe.

γ-^{32}P-ATP end-labeling of oligonucleotides with T4 polynucleotide kinase (PNK)

2 µl H2O, 1 µl 10x T4 DNA PNK buffer (NEB), 1 µl 10 U/ µl T4 DNA PNK (NEB), 1 µl 50 ng/µl $(AACCCT)_4$ oligonucleotide and 5 µl 10.0 mCi/ml γ-^{32}P-ATP (NEN) were mixed and incubated for 45 min at 37°C. 80 µl TES (10 mM Tris-HCl pH 8.0, 10 mM EDTA pH 8.0, 0.01% SDS) were added to stop the reaction. The probe was loaded onto a 3 ml G25 Sephadex column equilibrated with TNES (10 mM Tris-HCl pH 7.4, 10 mM EDTA, 100 mM NaCl, 1% SDS). The column was washed with 700 µl TNES, and the probe was eluted with 600 µl TNES and diluted in 25 ml Church mix.

Exonuclease I digestion in solution or in plugs

Fragments recovered after MNase digestion were subjected to treatment with E. coli exonuclease I. Approximately 2 µg MNase-treated DNA was incubated with ExoI (1 U/µl, New England Biolabs) in reaction buffer (New England Biolabs) at 37°C overnight. DNA fragments were recovered by phenol- chloroform extraction followed by precipitation with isopropanol in the presence of 0.2 M sodium acetate (pH 5.5).

FACS

Cell cycle analyses were performed using standard techniques to evaluate BrdU incorporation and propidium iodide (PI) staining of DNA content. Cells were pulsed with 10 mM BrdU for 30 minutes, then fixed and stained with FITC-conjugated anti-BrdU antibody (BD Biosciences) and PI. Flow cytometry was performed on FACSCalibur-1 (Becton Dickinson), and data were analyzed using FlowJo 8.7.1 software.

FUCCI-FACS to isolate cells in different cell cycle phases

For the FUCCI sort experiments, MEFs were transduced with three infections of mKO2-Cdt1 30/120 (lentiviral) followed by three infections of mAG-Geminin 1/110 (lentiviral) at 6 hour intervals (gift from A. Miyawaki, [421]). $Cdt1^{+}Gem^{+}$ cells were collected by FACS, replated, and infected with two rounds of Hit&Run Cre. Sorting of G1 and S phase cells according to levels of Cdt1 and Geminin was performed on BD FACSAria-1 and Aria-2 cell sorters (BD Biosciences) with excitation by the 488 nm and

561 nm lasers. Cells were collected in PBS and immediately plated on coverslips or embedded in agarose for DNA analysis.

Separation of leading- and lagging- daughter telomere DNA

MEFs were cultured in the presence of 100 μM of BrdU for 16 hours. To prevent nicking of DNA after BrdU incorporation, all steps were performed with minimal exposure to light. Cells were harvested, and genomic DNA was extracted by with phenol-chloroform, precipitated with isopropanol in the presence of 0.2 M sodium acetate (pH 5.5), and resuspended in TE (10 mM Tris, 1 mM EDTA [pH 8.0]). 250 μg DNA was digested overnight with 200 U *Mbo*I and 200 U *Alu*I and loaded uniformly onto CsCl solution (density of 1.800 g/ml) in a total volume of 5 mL. Samples were ultracentrifuged at 55,000 rpm for 20 hr at 25°C. 100 μL fractions were collected from the bottom of the centrifuge tube. Aliquots of DNA from each fraction were denatured in 0.1 M NaOH for 20-30 min at 37°C. An equal volume of 12× SSC was added to neutralize the samples. Samples were loaded on a Minifold® II Slot Blot (Schleicher & Schuell, Inc.) onto Hybond-N+ nylon transfer membrane (GE Healthcare/Amersham). The membrane was washed twice with 20x SSC, dried, and baked in a drying oven for 2 h at 80°C. The membrane was pre-hybridized at 55°C with Church mix, and hybridized at 55°C with a ^{32}P-$(TTAGGG)_4$ probe (end-labeled as described) in Church mix. The membrane was washed three times with 4x SSC for 30 min each, and once with 4x SSC/0.1% SDS. The membrane was exposed to a PhosphorImager screen to detect fractions containing telomeric DNA. Pooled DNA from each peak was then surface dialyzed by rocking the solution on a layer of 2% agarose in a 50 ml tube for 30 min at

room temperature to reduce the CsCl concentration. The DNA was ethanol precipitated and resuspended in TE.

MNase digestion of nuclei

Nuclei were prepared for digestion with micrococcal nuclease (MNase). Briefly, cells were trypsinized, suspended in growth medium, and harvested by centrifugation in a RT6000 centrifuge at 1,500 rpm for 5 min. Cells were suspended at 2 x 106 cells/ml in buffer A (100 mM KCl, 10 mM Tris [pH 7.5], 3 mM MgCl2, 1 mM CaCl2, 0.5 mM PMSF), washed twice with buffer A, then resuspended at 5 x 106 cells/ml in buffer A with 0.6% Nonidet P-40 to lyse cells. After gently mixing and incubating on ice for 5 min, nuclei were harvested at 2,000 rpm for 5 min and resuspended in buffer A without NP-40 at 2.5 x 107 cells/ml. Nuclei were homogenized in a dounce with 10 strokes with a tight B-type pestle. Aliquots of 150 µl were digested for 5 min at 30°C with MNase (Roche Diagnostics) at concentrations ranging from 5 – 600 U/ml. Reactions were stopped by adding one volume of TEES/protK (10 mM Tris HCl [pH 7.5], 10 mM EDTA, 10 mM EGTA, 1% SDS, 50 µg/ml proteinase K) and incubating at 37°C for 2 hours to overnight. DNA was extracted with phenol-chloroform, precipitated with isopropanol in the presence of 0.2 M sodium acetate (pH 5.5), and resuspended in 500 µl TE (10 mM Tris, 1 mM EDTA [pH 8.0]).

MNase digestion of DNA in agarose plugs

Agarose-embedded DNA plugs were prepared as described above. Plugs were washed extensively with TE, then equilibrated in buffer A for 1 hour at 4°C. Digestions

were performed by incubating plugs for 10 min at 30°C with MNase in buffer A at concentrations ranging from 0 – 8 U/ml in a total volume of 500 µl. Reactions were stopped by adding an equal volume of TEES/protK and incubating overnight at 37°C. Plugs were washed in TE in preparation for PFGE.

Assay for the last nucleosomes

DNA associated with the last nucleosome was isolated by a variation on the previously described telomere purification protocol (44). Following MNase digestion of nuclei, the recovered DNA fragments were annealed to a biotinylated oligonucleotide in a 50 µl reaction containing ~40 µg MNase-digested DNA, 0.25 pmol biotin-(CCCTAA)6, 1x SSC, and 1.0% Triton X-100 was incubated for 30 min each at 37°C, 30°C, 25°C, 15°C, 10°C, and 4°C. The mixture was rotated overnight at 4°C with 0.5 mg/ml streptavidin-coupled Dynabeads (Dynal, Invitrogen), which were pre-washed with 1xSSC, pre-coated with 5x Denhardt's solution (0.1% Ficoll 400, 0.1% polyvinylpyrrolidone, 0.1% BSA) for 30 min at room temperature, and resuspended in cold 1x SSC.

To isolate the annealed DNA, a magnet (Dynal Magnetic Particle Concentrator) was used to concentrate the beads, and the supernatant was removed. The beads were washed twice with 150 µl 1x SSC, once with 150 µl 0.2x SSC, and once with 50 µl TE. All washes were performed on ice. The beads were then resuspended in 20 µl TE and heated to 65°C for 10 min. The supernatant was recovered, fractionated on 1% agarose, and the telomeric signal was detected by Southern blot hybridization as described above.

Construction of model telomeric fragments

A 226 bp *Bgl*II/*Kpn*I fragment containing 25 TTAGGG repeats was excised from pSXneo.25(T_2AG_3), dephosphorylated with calf intestinal phosphatase, and purified by gel extraction. The *Bgl*II end of the double stranded telomeric fragment was ligated overnight at 16°C to the phosphorylated oligonucleotide 5'-GATC$(T_2AG_3)_{12}$-3' with T4 DNA ligase. Reactions lacking either the double stranded fragment or the single stranded oligonucleotide were used as controls.

Apollo gene targeting

The targeting vector for modification of the mouse *Apollo* locus was generated in pSL301 by standard cloning techniques using Bac-derived DNA fragments extending from the *Nhe*I site upstream of the Apollo gene to the *Sac*I site in the 3' UTR. A TK-neomycin cassette flanked by FRT sites and carrying one loxP site was inserted into the *Pac*I site in the third intron of the *Apollo* gene. A second loxP site was introduced into the *Nse*I site in intron 1 by insertion of a loxP oligonucleotide that also contained an *Nsi*I site used in genomic analysis of targeted ES cells. ES clones with the correct integration were identified by genomic blotting of *Nsi*I-digested DNA using a probe upstream of the *Nhe*I site and the presence of a single neo integration was confirmed. Targeted ES cells were used to generate chimeras and offspring with the targeted genotype. The neo cassette was removed using the FLPe deleter mouse strain (Jackson labs). The resulting $Apollo^{F/+}$ genotype was maintained on a mixed background (129/C57Bl/6J).

RT-PCR transcript analysis

RT-PCR was performed with the oligo-dT ThermoScript RT-PCR system (Invitrogen). RNA was isolated from approximately 10^6 cells with the Qiagen RNAeasy kit. Two to three micrograms RNA was reverse transcribed with the ThermoScript RT-PCR system (Invitrogen) by using oligo dT priming and the protocol provided by the manufacturer. The primers used for PCR after cDNA synthesis are as follows:

Apollo RT1:

Forward: CACGGTGGGTTTGTCTAGC

Reverse: GTTGCTCCAGCAGTGATTC

Apollo RT2:

Forward: CTCCCATCACTGCTTGCCTC

Reverse: GCAACTGTACCAACTCCAGG

GAPDH:

Forward: TGAAGGTCGGTGTGAACGGATTTGGC

Reverse: CATGTAGGCCATGAGGTCCACCAC

Ap4b1 RT1:

Forward: GACGATGCCATACCTTGGCTC

Reverse: GTTCAGTACTTCAGCCTG

Ap4b1 RT2:

Forward: GACGATGCCATACC TTGGCTC

Reverse: CTGCTCTTGAGATAGCTGTC

Plasmid constructs

N-terminal FLAG-$[HA]_2$-tagged Apollo alleles were generated by PCR-mediated mutagenesis and expressed using the pLPC puromycin-selectable retroviral vector. N-terminal myc-tagged TRF2-F120A was generated by site-directed mutagenesis and cloned in a pLPC puromycin-selectable retroviral expression vector.

LIST OF CELL LINES

Mouse embryonic fibroblasts

Apollo$^{F/F}$	SV40-LT	this work
BLM$^{F/F}$	SV40-LT	this work, mice from P. Leder
Exo1$^{-/-}$	SV40-LT	this work, mice from W. Edelman
mTR$^{-/-}$	SV40-LT	this work, mice from C. Greider
Nbs1$^{F/F}$	SV40-LT	this work, mice from A. Nussenzweig
POT1a$^{S/F}$	SV40-LT	D. Hockemeyer, ref. 37
POT1b$^{S/F}$	SV40-LT	D. Hockemeyer, ref. 37
POT1b$^{F/-}$	SV40-LT	D. Hockemeyer
TRF2$^{F/F}$	SV40-LT	this work, mice generated by G. Celli
TRF2ts	SV40-LT	A. Konishi, ref. 194
Apollo$^{F/F}$Exo1$^{-/-}$	SV40-LT	this work
Apollo$^{F/F}$Lig4$^{-/-}$	SV40-LT	this work
Apollo$^{F/F}$Nbs1$^{F/F}$	SV40-LT	this work
Apollo$^{F/F}$POT1b$^{F/F}$	SV40-LT	this work
Exo1$^{-/-}$BLM$^{F/F}$	SV40-LT	this work
Exo1$^{-/-}$mTR$^{-/-}$	SV40-LT	this work
Exo1$^{-/-}$Nbs1$^{F/F}$	SV40-LT	this work
POT1a$^{S/F}$POT1b$^{S/F}$	SV40-LT	D. Hockemeyer, ref. 37
POT1a$^{F/F}$POT1b$^{F/F}$	SV40-LT	T. Davoli
POT1b$^{F/F}$Nbs1$^{F/-}$	SV40-LT	N. Dimitrova, ref. 191
POT1b$^{F/F}$ROSA-Cre-ERT2	primary	this work

LIST OF CELL LINES (cont.)

Mouse embryonic fibroblasts

TRF1$^{F/F}$ROSA-Cre-ERT2	SV40-LT	A. Sfeir
TRF2$^{F/F}$Ku$^{-/-}$	SV40-LT	G. Celli, ref. 197
TRF2$^{F/F}$mTR$^{-/-}$	SV40-LT	this work
TRF2$^{F/F}$Nbs1$^{F/F}$	SV40-LT	N. Dimitrova, ref.
TRF2$^{F/-}$p53$^{-/-}$	SV40-LT	G. Celli, ref. 190
Apollo$^{F/F}$Exo1$^{-/-}$POT1b$^{F/F}$	SV40-LT	this work
Apollo$^{F/F}$Nbs1$^{F/F}$ POT1b$^{F/F}$	SV40-LT	this work
Exo1$^{-/-}$Nbs1$^{F/F}$POT1b$^{F/F}$	SV40-LT	this work
TRF2$^{F/-}$Lig4$^{-/-}$p53$^{-/-}$	SV40-LT	G. Celli, ref. 190

Human cell lines

293T embryonic kidney	SV40-LT
Phoenix, ecotropic	SV40-LT

LIST OF GENOTYPING PCR PRIMERS

Gene	Alleles	Primer sequences (5' – 3')
mApollo	WT, FL	3' loxP2: ACATCTCCTCATCTTGTCTG 5' loxP: CCTATCATGATAATCCCAGC 5' neo: CTTGAGGGTTTCTTTTGGAG
mBLM	WT, FL	1: AGGTTGTCTGGCCTAGACATAAGG 2:TGGTGGGTAAACATTCCTCAGTGG 3: TCTACTGCTCAGTAAAGGCTC 5: ATTTAGGCTTCCATTCTGAGG
mExo1	WT, Δ	A: CTCTTGTCTGGGCTGATATGC B: ATGGCGTGCGTGATGTTGATA C: AGGAGTAGAAGTGGCGCGAAGG
mLigase 4	WT, Δ	WT1: CTCTGTAGGGCTTAGTGACATCTC WT2: GCGCTCACCATCAAGCGCAGTTTCGATGTAG MUT1: GACTCTTTTTACCCTGCAATGAGACTCATTC MUT2: ACCGCTATCAGGACATAGCGTTGG
mTR	WT, Δ	Common: TTCTGACCACCACCAACTTCAAT WT: CTAAGCCGGCACTCCTTACAAG KO: GGGGCTGCTAAAGCGCAT
mPOT1b	WT, FL, Δ	Common2: ATGGTTCCCCAGTGCTTTGAC WT2: CACTGGAAAGAAAGGGCTTTGTG Delta2: TCCTTCCCCAAGTTGCTTTTG
mNbs1	WT, FL, Δ	com: GCGTAAATGGTTGATTGTCC wt: GATTGTCAGCACAGAAATCTTCCC mut: GCGCCTCCCCTACCCGGTAGAATT LoxP-5N: CGTATAATGTATGCTATACGAAG LoxP-R: TTCCCACTGTATCCTGAGTG
mTRF2	WT, FL, Δ	Common2: TTGGCACTATCTCAGCACTGCAAC P4A: ATCCGTAGTTCCTCTTGTGTCTG Delta: CATGCAAACCAGGCATTTAATCTC

LIST OF SHRNAS

Target	Vector	Target sequence (5' – 3')
mATM	pSuperior (retro)	GGAAGTCAAGGAACAACTA
mATR	pSuperior (retro)	GGAGATGCAACTCGTTTAA
mBLM-1	pSuperior (retro)	GCATCCTAATAAAGAGTTA
mBLM-2	pSuperior (retro)	GGAGGGTTATTATCAAGAA
mBLM-3	pSuperior (retro)	GGACCTGCTGGAAGATTTA
mCtIP-1	pSuperior (retro)	GCAGACCTTTCTCAGTATA
mCtIP-2	pSuperior (retro)	GCATTAACCGGCTACGAAA
mExo1	pSuperior (retro)	GCATTTGGCACAAGAATTA
mRecQL5-1	pLKO.1 (lenti)	CCTAGATGAGAAGGTCCAGAT
mRecQL5-2	pLKO.1 (lenti)	GCCATAACGAAGAAGCTGGAT
mStn1	pLKO.1 (lenti)	GATCCTGTGTTTCTAGCCTTT
mTPP1	pSuperior (retro)	GGACACATGGGCTGACGGA

LIST OF ANTIBODIES

Antigen	ID	Type	Source	Use(s)
HA	HA.11	M, mono	Covance	IB 1:1000
				IF 1:1000
Myc	9B11	M, mono	Cell Signaling	IB 1:1000
Myc	9E10	M, mono	Sigma	IB 1:1000, IP
FLAG	M2	M, mono	Sigma	IB 1:1000
γ-tubulin	GTU88	M, mono	Sigma	IB 1:5000
mPOT1a	1221	Rb, poly	de Lange lab	IB 1:1000
mPOT1b	1223	Rb, poly	de Lange lab	IB 1:1000
hRap1	765	Rb, poly	de Lange lab	IB 1:2000
hTRF2	647	Rb, poly	de Lange lab	IB 1:2000
53BP1	100-304	Rb, poly	Novus	IF 1:1000
ATM	Mat3	M, mono	Sigma	IB 1:1000
ATR	N-19	FRP goat	Santa Cruz	1:1000
Chk2	Chk2	M, mono	BD Transduction	IB 1:250
mCtIP	H-300	Rb, poly	SC Biotech	IB 1:250
γ-H2AX	γ-H2AX	M, mono	Upstate	IB 1:1000
mNbs1	93’6	Rb, poly	gift, J. Petrini	IB 1:5000
mRecQL5		Rb, poly	gift	IB 1:1000
mStn1		M, poly	de Lange lab	IB 1:250

REFERENCES

1. Brown, W. R. Molecular cloning of human telomeres in yeast. *Nature* **338**, 774-776 (1989).
2. Cross, S. H., Allshire, R. C., McKay, S. J., McGill, N. I. & Cooke, H. J. Cloning of human telomeres by complementation in yeast. *Nature* **338**, 771-774 (1989).
3. Meyne, J., Ratliff, R. L. & Moyzis, R. K. Conservation of the human telomere sequence (TTAGGG)n among vertebrates. *Proc Natl Acad Sci USA* **86**, 7049-7053 (1989).
4. de Lange, T. et al. Structure and variability of human chromosome ends. *Mol Cell Biol* **10**, 518-527 (1990).
5. Makarov, V. L., Hirose, Y. & Langmore, J. P. Long G tails at both ends of human chromosomes suggest a C strand degradation mechanism for telomere shortening. *Cell* **88**, 657-666 (1997).
6. McElligott, R. & Wellinger, R. J. The terminal DNA structure of mammalian chromosomes. *EMBO J* **16**, 3705-3714 (1997).
7. Chai, W., Du, Q., Shay, J. W. & Wright, W. E. Human telomeres have different overhang sizes at leading versus lagging strands. *Mol Cell* **21**, 427-435 (2006).
8. Blackburn, E. H. & Gall, J. G. A tandemly repeated sequence at the termini of the extrachromosomal ribosomal RNA genes in Tetrahymena. *J Mol Biol* **120**, 33-53 (1978).
9. Klobutcher, L. A., Swanton, M. T., Donini, P. & Prescott, D. M. All gene-sized DNA molecules in four species of hypotrichs have the same terminal sequence and an unusual 3' terminus. *Proc Natl Acad Sci USA* **78**, 3015-3019 (1981).

10. Pluta, A. F., Dani, G. M., Spear, B. B. & Zakian, V. A. Elaboration of telomeres in yeast: recognition and modification of termini from Oxytricha macronuclear DNA. *Proc Natl Acad Sci USA* **81**, 1475-1479 (1984).

11. Shampay, J., Szostak, J. W. & Blackburn, E. H. DNA sequences of telomeres maintained in yeast. *Nature* **310**, 154-157 (1984).

12. Lejnine, S., Makarov, V. L. & Langmore, J. P. Conserved nucleoprotein structure at the ends of vertebrate and invertebrate chromosomes. *Proc Natl Acad Sci USA* **92**, 2393-2397 (1995).

13. Gomes, N. M. et al. Comparative biology of mammalian telomeres: hypotheses on ancestral states and the roles of telomeres in longevity determination. *Aging Cell* **10**, 761-768 (2011).

14. Griffith, J. D. et al. Mammalian telomeres end in a large duplex loop. *Cell* **97**, 503-14. (1999).

15. Nikitina, T. & Woodcock, C. L. Closed chromatin loops at the ends of chromosomes. *J Cell Biol* **166**, 161-165 (2004).

16. Stansel, R. M., de Lange, T. & Griffith, J. D. T-loop assembly in vitro involves binding of TRF2 near the 3' telomeric overhang. *EMBO J* **20**, 5532-5540 (2001).

17. de Lange, T. How telomeres solve the end-protection problem. *Science* **326**, 948-952 (2009).

18. Bianchi, A., Smith, S., Chong, L., Elias, P. & de Lange, T. TRF1 is a dimer and bends telomeric DNA. *Embo J* **16**, 1785-1794 (1997).

19. Bilaud, T. et al. Telomeric localization of TRF2, a novel human telobox protein. *Nat Genet* **17**, 236-239 (1997).

20. Broccoli, D., Smogorzewska, A., Chong, L. & de Lange, T. Human telomeres contain two distinct Myb-related proteins, TRF1 and TRF2. *Nat Genet* **17**, 231-235 (1997).

21. Bianchi, A. et al. TRF1 binds a bipartite telomeric site with extreme spatial flexibility. *Embo J* **18**, 5735-5744 (1999).

22. Chong, L. et al. A human telomeric protein. *Science* **270**, 1663-1667 (1995).

23. Broccoli, D. et al. Comparison of the human and mouse genes encoding the telomeric protein, TRF1: chromosomal localization, expression and conserved protein domains. *Hum Mol Genet* **6**, 69-76 (1997).

24. Sfeir, A., Kabir, S., van Overbeek, M., Celli, G. B. & de Lange, T. Loss of Rap1 induces telomere recombination in the absence of NHEJ or a DNA damage signal. *Science* **327**, 1657-1661 (2010).

25. Li, B., Oestreich, S. & de Lange, T. Identification of human Rap1: implications for telomere evolution. *Cell* **101**, 471-483 (2000).

26. Martinez, P. et al. Mammalian Rap1 controls telomere function and gene expression through binding to telomeric and extratelomeric sites. *Nat Cell Biol* **12**, 768-780 (2010).

27. Yang, D. et al. Human telomeric proteins occupy selective interstitial sites. *Cell Res* **21**, 1013-1027 (2011).

28. Palm, W. & de Lange, T. How shelterin protects mammalian telomeres. *Annu Rev Genet* **42**, 301-334 (2008).

29. Hockemeyer, D. et al. Telomere protection by mammalian POT1 requires interaction with TPP1. *Nat Struct Mol Biol* **14**, 754-761 (2007).

30. Liu, D. et al. PTOP interacts with POT1 and regulates its localization to telomeres. *Nat Cell Biol* **6**, 673-680 (2004).

31. Ye, J. Z. et al. POT1-interacting protein PIP1: a telomere length regulator that recruits POT1 to the TIN2/TRF1 complex. *Genes Dev* **18**, 1649-1654 (2004).

32. Baumann, P. & Cech, T. R. Pot1, the putative telomere end-binding protein in fission yeast and humans. *Science* **292**, 1171-115. (2001).

33. Lei, M., Podell, E. R. & Cech, T. R. Structure of human POT1 bound to telomeric single-stranded DNA provides a model for chromosome end-protection. *Nat Struct Mol Biol* **11**, 1223-1229 (2004).

34. Loayza, D., Parsons, H., Donigian, J., Hoke, K. & de Lange, T. DNA binding features of human POT1: A nonamer 5'-TAGGGTTAG-3' minimal binding site, sequence specificity, and internal binding to multimeric sites. *J Biol Chem* **279**, 13241-13248 (2004).

35. Wang, F. et al. The POT1-TPP1 telomere complex is a telomerase processivity factor. *Nature* **445**, 506-510 (2007).

36. Takai, K. K., Hooper, S., Blackwood, S., Gandhi, R. & de Lange, T. In vivo stoichiometry of shelterin components. *J Biol Chem* **285**, 1457-1467 (2010).

37. Hockemeyer, D., Daniels, J. P., Takai, H. & de Lange, T. Recent expansion of the telomeric complex in rodents: Two distinct POT1 proteins protect mouse telomeres. *Cell* **126**, 63-77 (2006).

38. Wu, L. et al. Pot1 deficiency initiates DNA damage checkpoint activation and aberrant homologous recombination at telomeres. *Cell* **126**, 49-62 (2006).

39. Palm, W., Hockemeyer, D., Kibe, T. & de Lange, T. Functional dissection of human and mouse POT1 proteins. *Mol Cell Biol* **29**, 471-482 (2009).

40. Ye, J. Z. et al. TIN2 binds TRF1 and TRF2 simultaneously and stabilizes the TRF2 complex on telomeres. *J Biol Chem* **279**, 47264-47271 (2004).

41. O'Connor, M. S., Safari, A., Xin, H., Liu, D. & Songyang, Z. A critical role for TPP1 and TIN2 interaction in high-order telomeric complex assembly. *Proc Natl Acad Sci USA* **103**, 11874-11879 (2006).

42. Kim, S. H., Kaminker, P. & Campisi, J. TIN2, a new regulator of telomere length in human cells. *Nat Genet* **23**, 405-412 (1999).

43. Kim, S. H., Han, S., You, Y. H., Chen, D. J. & Campisi, J. The human telomere-associated protein TIN2 stimulates interactions between telomeric DNA tracts in vitro. *EMBO Rep* **4**, 685-691 (2003).

44. Chen, Y. et al. A shared docking motif in TRF1 and TRF2 used for differential recruitment of telomeric proteins. *Science* **319**, 1092-1096 (2008).

45. Frescas, D. & de Lange, T. (unpublished).

46. Smith, S., Giriat, I., Schmitt, A. & de Lange, T. Tankyrase, a poly(ADP-ribose) polymerase at human telomeres. *Science* **282**, 1484-1487 (1998).

47. Lillard-Wetherell, K. et al. Association and regulation of the BLM helicase by the telomere proteins TRF1 and TRF2. *Hum Mol Genet* **13**, 1919-1932 (2004).

48. Hsu, H. L. et al. Ku acts in a unique way at the mammalian telomere to prevent end joining. *Genes Dev* **14**, 2807-212. (2000).

49. Zhu, X. D., Kuster, B., Mann, M., Petrini, J. H. & de Lange, T. Cell-cycle-regulated association of RAD50/MRE11/NBS1 with TRF2 and human telomeres. *Nat Genet* **25**, 347-352 (2000).

50. Zhu, X. D. et al. ERCC1/XPF Removes the 3' Overhang from Uncapped Telomeres and Represses Formation of Telomeric DNA-Containing Double Minute Chromosomes. *Mol Cell* **12**, 1489-1498 (2003).

51. van Overbeek, M. & de Lange, T. Apollo, an Artemis-related nuclease, interacts with TRF2 and protects human telomeres in S phase. *Curr Biol* **16**, 1295-1302 (2006).

52. Lenain, C. et al. The Apollo 5' exonuclease functions together with TRF2 to protect telomeres from DNA repair. *Curr Biol* **16**, 1303-1310 (2006).

53. Freibaum, B. D. & Counter, C. M. hSnm1B is a novel telomere-associated protein. *J Biol Chem* **281**, 15033-15036 (2006).

54. Saharia, A. et al. Flap endonuclease 1 contributes to telomere stability. *Curr Biol* **18**, 496-500 (2008).

55. Zeng, S. et al. Telomere recombination requires the MUS81 endonuclease. *Nat Cell Biol* **11**, 616-623 (2009).

56. Makarov, V. L., Lejnine, S., Bedoyan, J. & Langmore, J. P. Nucleosomal organization of telomere-specific chromatin in rat. *Cell* **73**, 775-787 (1993).

57. Tommerup, H., Dousmanis, A. & de Lange, T. Unusual chromatin in human telomeres. *Mol Cell Biol* **14**, 5777-5785 (1994).

58. Blackburn, E. H. & Chiou, S. S. Non-nucleosomal packaging of a tandemly repeated DNA sequence at termini of extrachromosomal DNA coding for rRNA in Tetrahymena. *Proc Natl Acad Sci USA* **78**, 2263-2267 (1981).

59. Gottschling, D. E. & Cech, T. R. Chromatin structure of the molecular ends of Oxytricha macronuclear DNA: phased nucleosomes and a telomeric complex. *Cell* **38**, 501-510 (1984).

60. Wright, J. H., Gottschling, D. E. & Zakian, V. A. Saccharomyces telomeres assume a non-nucleosomal chromatin structure. *Genes Dev* **6**, 197-210 (1992).

61. Benetti, R., Garcia-Cao, M. & Blasco, M. A. Telomere length regulates the epigenetic status of mammalian telomeres and subtelomeres. *Nat Genet* **39**, 243-250 (2007).

62. Garcia-Cao, M., O'Sullivan, R., Peters, A. H., Jenuwein, T. & Blasco, M. A. Epigenetic regulation of telomere length in mammalian cells by the Suv39h1 and Suv39h2 histone methyltransferases. *Nat Genet* **36**, 94-99 (2004).

63. Gonzalo, S. et al. DNA methyltransferases control telomere length and telomere recombination in mammalian cells. *Nat Cell Biol* **8**, 416-424 (2006).

64. Watson, J. D. Origin of concatemeric T7 DNA. *Nat New Biol* **239**, 197-201 (1972).

65. Olovnikov, A. M. A theory of marginotomy. The incomplete copying of template margin in enzymic synthesis of polynucleotides and biological significance of the phenomenon. *J Theor Biol* **41**, 181-190 (1973).

66. Li, J. J. & Kelly, T. J. Simian virus 40 DNA replication *in vitro*. *PNAS* **81**, 6973-6977 (1984).

67. Li, J. J. & Kelly, T. J. Simian virus 40 DNA replication *in vitro*: specificity of initiation and evidence for bidirectional replication. *Mol Cell Biol* **5**, 1238-1246 (1985).

68. Stillman, B. W. & Gluzman, Y. Replication and supercoiling of simian virus 40 DNA in cell extracts from human cells. *Mol Cell Biol* **5**, 2051-2060 (1985).

69. Wobbe, C. R., Dean, F., Weissbach, L. & Hurwitz, J. *In vitro* replication of duplex circular DNA containing the simian virus 40 DNA origin site. *PNAS* **82**, 5710-5714 (1985).

70. Murakami, Y., Wobbe, C. R., Weissbach, L., Dean, F. B. & J, H. Role of DNA polymerase alpha and DNA primase in simian virus 40 DNA replication *in vitro*. *PNAS* **83**, 2869-2873 (1986).

71. Tsurimoto, T., Melendy, T. & Stillman, B. Sequential initiation of lagging and leading strand synthesis by two different polymerase complexes at the SV40 DNA replication origin. *Nature* **346**, 534-539 (1990).

72. Wold, M. S., Weinberg, D. H., Virshup, D. M., Li, J. J. & Kelly, T. J. Identification of cellular proteins required for simian virus 40 DNA replication. *J Biol Chem* **264**, 2801-2809 (1989).

73. Weinberg, D. H. et al. Reconstitution of simian virus 40 DNA replication with purified proteins. *PNAS* **87**, 8692-8696 (1990).

74. Ohki, R., Tsurimoto, T. & Ishikawa, F. In vitro reconstitution of the end replication problem. *Mol Cell Biol* **21**, 5753-5766 (2001).

75. Lingner, J., Cooper, J. P. & Cech, T. R. Telomerase and DNA end replication: no longer a lagging strand problem? *Science* **269**, 1533-1534 (1995).

76. Biessmann, H. et al. Addition of telomere-associated HeT DNA sequences "heals" broken chromosome ends in Drosophila. *Cell* **61**, 663-673 (1990).

77. Levis, R. W., Ganesan, R., Houtchens, K., Tolar, L. A. & Sheen, F. M. Transposons in place of telomeric repeats at a Drosophila telomere. *Cell* **75**, 1083-1093 (1993).

78. Danilevskaya, O. N., Slot, F., Traverse, K. L., Hogan, N. C. & Pardue, M. L. Drosophila telomere transposon HeT-A produces a transcript with tightly bound protein. *Proc Natl Acad Sci USA* **91**, 6679-6682 (1994).

79. Bryan, T. M., Englezou, A., Dalla-Pozza, L., Dunham, M. A. & Reddel, R. R. Evidence for an alternative mechanism for maintaining telomere length in human tumors and tumor-derived cell lines. *Nat Med* **3**, 1271-1274 (1997).

80. Dunham, M. A., Neumann, A. A., Fasching, C. L. & Reddel, R. R. Telomere maintenance by recombination in human cells. *Nat Genet* **26**, 447-450 (2000).

81. Szostak, J. W. & Blackburn, E. H. Cloning yeast telomeres on linear plasmid vectors. *Cell* **29**, 245-255 (1982).

82. Greider, C. W. & Blackburn, E. H. Identification of a specific telomere terminal transferase activity in Tetrahymena extracts. *Cell* **43**, 405-413 (1985).

83. Greider, C. W. & Blackburn, E. H. The telomere terminal transferase of Tetrahymena is a ribonucleoprotein enzyme with two kinds of primer specificity. *Cell* **51**, 887-898 (1987).

84. Greider, C. W. & Blackburn, E. H. A telomeric sequence in the RNA of Tetrahymena telomerase required for telomere repeat synthesis. *Nature* **337**, 331-337 (1989).

85. Yu, G. L., Bradley, J. D., Attardi, L. D. & Blackburn, E. H. In vivo alteration of telomere sequences and senescence caused by mutated Tetrahymena telomerase RNAs. *Nature* **344**, 126-32. (1990).

86. Blasco, M. A. et al. Telomere shortening and tumor formation by mouse cells lacking telomerase RNA. *Cell* **91**, 25-34. (1997).

87. Lundblad, V. & Szostak, J. W. A mutant with a defect in telomere elongation leads to senescence in yeast. *Cell* **57**, 633-643 (1989).

88. Lingner, J. et al. Reverse transcriptase motifs in the catalytic subunit of telomerase. *Science* **276**, 561-567 (1997).

89. Lendvay, T. S., Morris, D. K., Sah, J., Balasubramanian, B. & Lundblad, V. Senescence mutants of Saccharomyces cerevisiae with a defect in telomere replication identify three additional EST genes. *Genetics* **144**, 1399-1412 (1996).

90. Lingner, J., Cech, T. R., Hughes, T. R. & Lundblad, V. Three Ever Shorter Telomere (EST) genes are dispensable for in vitro yeast telomerase activity. *Proc Natl Acad Sci USA* **94**, 11190-11195 (1997).

91. Counter, C. M., Meyerson, M., Eaton, E. N. & Weinberg, R. A. The catalytic subunit of yeast telomerase. *Proc Natl Acad Sci USA* **94**, 9202-9207 (1997).

92. Cohen, S. et al. Protein Composition of Catalytically Active Human Telomerase from Immortal Cells. *Science* **315**, 1850-1853 (2007).

93. Jady, B. E., Bertrand, E. & Kiss, T. Human telomerase RNA and box H/ACA scaRNAs share a common Cajal body-specific localization signal. *J Cell Biol* **164**, 647-652 (2004).

94. Venteicher, A. S., Meng, Z., Mason, P. J., Veenstra, T. D. & Artandi, S. E. Identification of ATPases pontin and reptin as telomerase components essential for holoenzyme assembly. *Cell* **132**, 945-957 (2008).

95. Venteicher, A. S. et al. A human telomerase holoenzyme protein required for Cajal body localization and telomere synthesis. *Science* **323**, 644-648 (2009).

96. Kim, N. W. et al. Specific association of human telomerase activity with immortal cells and cancer. *Science* **266**, 2011-205. (1994).

97. Diede, S. J. & Gottschling, D. E. Telomerase-mediated telomere addition in vivo requires DNA primase and DNA polymerases alpha and delta. *Cell* **99**, 723-733 (1999).

98. Marcand, S., Brevet, V., Mann, C. & Gilson, E. Cell cycle restriction of telomere elongation. *Curr Biol* **10**, 487-490 (2000).

99. Teixeira, M. T., Arneric, M., Sperisen, P. & Lingner, J. Telomere Length Homeostasis Is Achieved via a Switch between Telomerase- Extendible and -Nonextendible States. *Cell* **117**, 323-335 (2004).

100. Marcand, S., Brevet, V. & Gilson, E. Progressive cis-inhibition of telomerase upon telomere elongation. *Embo J* **18**, 3509-3519 (1999).

101. Zhao, Y. et al. Telomere extension occurs at most chromosome ends and is uncoupled from fill-in in human cancer cells. *Cell* **138**, 463-475 (2009).

102. Fan, X. & Price, C. M. Coordinate regulation of G- and C strand length during new telomere synthesis. *Mol Biol Cell* **8**, 2145-2155 (1997).

103. Adams Martin, A., Dionne, I., Wellinger, R. J. & Holm, C. The function of DNA polymerase alpha at telomeric G tails is important for telomere homeostasis. *Mol Cell Biol* **20**, 786-796 (2000).

104. Harley, C. B., Futcher, A. B. & Greider, C. W. Telomeres shorten during ageing of human fibroblasts. *Nature* **345**, 458-460 (1990).

105. Prowse, K. R. & Greider, C. W. Developmental and tissue-specific regulation of mouse telomerase and telomere length. *Proc Natl Acad Sci USA* **92**, 4818-4822 (1995).

106. Marcand, S., Gilson, E. & Shore, D. A protein-counting mechanism for telomere length regulation in yeast. *Science* **275**, 986-990 (1997).

107. van Steensel, B. & de Lange, T. Control of telomere length by the human telomeric protein TRF1. *Nature* **385**, 740-743 (1997).

108. Loayza, D. & de Lange, T. POT1 as a terminal transducer of TRF1 telomere length control. *Nature* **424**, 1013-1018 (2003).

109. Houghtaling, B. R., Cuttonaro, L., Chang, W. & Smith, S. A dynamic molecular link between the telomere length regulator TRF1 and the chromosome end protector TRF2. *Curr Biol* **14**, 1621-1631 (2004).

110. Taggart, A. K., Teng, S. C. & Zakian, V. A. Est1p as a cell cycle-regulated activator of telomere-bound telomerase. *Science* **297**, 1023-1026 (2002).

111. Fisher, T. S., Taggart, A. K. & Zakian, V. A. Cell cycle-dependent regulation of yeast telomerase by Ku. *Nat Struct Mol Biol* **11**, 1198-1205 (2004).

112. Stellwagen, A. E., Haimberger, Z. W., Veatch, J. R. & Gottschling, D. E. Ku interacts with telomerase RNA to promote telomere addition at native and broken chromosome ends. *Genes Dev* **17**, 2384-2395 (2003).

113. Evans, S. K. & Lundblad, V. Est1 and Cdc13 as comediators of telomerase access. *Science* **286**, 117-120 (1999).

114. Xin, H. et al. TPP1 is a homologue of ciliate TEBP-beta and interacts with POT1 to recruit telomerase. *Nature* **445**, 559-562 (2007).

115. Abreu, E. et al. TIN2-tethered TPP1 recruits human telomerase to telomeres in vivo. *Mol Cell Biol* **30**, 2971-2982 (2010).

116. Tejera, A. M. et al. TPP1 is required for TERT recruitment, telomere elongation during nuclear reprogramming, and normal skin development in mice. *Dev Cell* **18**, 775-789 (2010).

117. Tomlinson, R. L., Ziegler, T. D., Supakorndej, T., Terns, R. M. & Terns, M. P. Cell cycle-regulated trafficking of human telomerase to telomeres. *Mol Biol Cell* **17**, 955-965 (2006).

118. Zhu, Y., Tomlinson, R. L., Lukowiak, A. A., Terns, R. M. & Terns, M. P. Telomerase RNA accumulates in Cajal bodies in human cancer cells. *Mol Biol Cell* **15**, 81-90 (2004).

119. McClintock, B. The stability of broken ends of chromosomes in Zea mays. *Genetics* **26**, 234-282 (1941).

120. Muller, H. J. The remaking of chromosomes. *The Collecting Net, Woods Hole* **8**, 182-195 (1938).

121. Ciccia, A. & Elledge, S. J. The DNA damage response: making it safe to play with knives. *Mol Cell* **40**, 179-204 (2010).

122. Sancar, A., Lindsey-Boltz, L. A., Unsal-Kacmaz, K. & Linn, S. Molecular mechanisms of mammalian DNA repair and the DNA damage checkpoints. *Annu Rev Biochem* **73**, 39-85 (2004).

123. Sanchez, Y. et al. Conservation of the Chk1 checkpoint pathway in mammals: linkage of DNA damage to Cdk regulation through Cdc25. *Science* **277**, 1497-1501 (1997).

124. Liu, Q. et al. Chk1 is an essential kinase that is regulated by Atr and required for the G(2)/M DNA damage checkpoint. *Genes Dev* **14**, 1448-1459 (2000).

125. Matsuoka, S., Huang, M. & Elledge, S. J. Linkage of ATM to cell cycle regulation by the Chk2 protein kinase. *Science* **282**, 1893-1897 (1998).

126. Chaturvedi, P. et al. Mammalian Chk2 is a downstream effector of the ATM-dependent DNA damage checkpoint pathway. *Oncogene* **18**, 4047-4054 (1999).

127. Mailand, N. et al. Rapid destruction of human Cdc25A in response to DNA damage. *Science* **288**, 1425-149. (2000).

128. Matsuoka, S. et al. Ataxia telangiectasia-mutated phosphorylates Chk2 in vivo and in vitro. *Proc Natl Acad Sci U S A* **97**, 10389-10394 (2000).

129. Falck, J., Mailand, N., Syljuasen, R. G., Bartek, J. & Lukas, J. The ATM-Chk2-Cdc25A checkpoint pathway guards against radioresistant DNA synthesis. *Nature* **410**, 842-847 (2001).

130. Costanzo, V. et al. Reconstitution of an ATM-dependent checkpoint that inhibits chromosomal DNA replication following DNA damage. *Mol Cell* **6**, 649-659 (2000).

131. Walter, J. & Newport, J. Initiation of eukaryotic DNA replication: origin unwinding and sequential chromatin association of Cdc45, RPA, and DNA polymerase alpha. *Mol Cell* **5**, 617-627 (2000).

132. Agami, R. & Bernards, R. Distinct initiation and maintenance mechanisms cooperate to induce G1 cell cycle arrest in response to DNA damage. *Cell* **102**, 55-66 (2000).

133. Shieh, S. Y., Ahn, J., Tamai, K., Taya, Y. & Prives, C. The human homologs of checkpoint kinases Chk1 and Cds1 (Chk2) phosphorylate p53 at multiple DNA damage-inducible sites. *Genes Dev* **14**, 289-300 (2000).

134. Hirao, A. et al. DNA damage-induced activation of p53 by the checkpoint kinase Chk2. *Science* **287**, 1824-1827 (2000).

135. Tibbetts, R. S. et al. A role for ATR in the DNA damage-induced phosphorylation of p53. *Genes Dev* **13**, 152-17. (1999).

136. Lakin, N. D., Hann, B. C. & Jackson, S. P. The ataxia-telangiectasia related protein ATR mediates DNA-dependent phosphorylation of p53. *Oncogene* **18**, 3989-395. (1999).

137. el-Deiry, W. S. et al. WAF1, a potential mediator of p53 tumor suppression. *Cell* **75**, 817-825 (1993).

138. Harper, J. W., Adami, G. R., Wei, N., Keyomarsi, K. & Elledge, S. J. The p21 Cdk-interacting protein Cip1 is a potent inhibitor of G1 cyclin-dependent kinases. *Cell* **75**, 805-816 (1993).

139. Harper, J. W. et al. Inhibition of cyclin-dependent kinases by p21. *Mol Biol Cell* **6**, 387-400 (1995).

140. Buscemi, G. et al. Chk2 activation dependence on Nbs1 after DNA damage. *Mol Cell Biol* **21**, 5214-5222 (2001).

141. Falck, J., Coates, J. & Jackson, S. P. Conserved modes of recruitment of ATM, ATR and DNA-PKcs to sites of DNA damage. *Nature* **434**, 605-611 (2005).

142. Morales, M. et al. The Rad50S allele promotes ATM-dependent DNA damage responses and suppresses ATM deficiency: implications for the Mre11 complex as a DNA damage sensor. *Genes Dev* **19**, 3043-3054 (2005).

143. de Jager, M. et al. Human Rad50/Mre11 is a flexible complex that can tether DNA ends. *Mol Cell* **8**, 1129-1135 (2001).

144. Hopfner, K. P. et al. The Rad50 zinc-hook is a structure joining Mre11 complexes in DNA recombination and repair. *Nature* **418**, 562-566 (2002).

145. Williams, R. S. et al. Mre11 dimers coordinate DNA end bridging and nuclease processing in double-strand-break repair. *Cell* **135**, 97-109 (2008).

146. Williams, R. S. et al. Nbs1 flexibly tethers Ctp1 and Mre11-Rad50 to coordinate DNA double-strand break processing and repair. *Cell* **139**, 87-99 (2009).

147. Lloyd, J. et al. A supramodular FHA/BRCT-repeat architecture mediates Nbs1 adaptor function in response to DNA damage. *Cell* **139**, 100-111 (2009).

148. Adelman, C. A., Petrini, J. H. & Attwooll, C. L. Modeling disease in the mouse: lessons from DNA damage response and cell cycle control genes. *J Cell Biochem* **97**, 459-473 (2006).

149. Zou, L. & Elledge, S. J. Sensing DNA damage through ATRIP recognition of RPA-ssDNA complexes. *Science* **300**, 1542-1548 (2003).

150. Kumagai, A., Lee, J., Yoo, H. Y. & Dunphy, W. G. TopBP1 activates the ATR-ATRIP complex. *Cell* **124**, 943-955 (2006).

151. Lee, J., Kumagai, A. & Dunphy, W. G. The Rad9-Hus1-Rad1 checkpoint clamp regulates interaction of TopBP1 with ATR. *J Biol Chem* **282**, 28036-28044 (2007).

152. Delacroix, S., Wagner, J. M., Kobayashi, M., Yamamoto, K. & Karnitz, L. M. The Rad9-Hus1-Rad1 (9-1-1) clamp activates checkpoint signaling via TopBP1. *Genes Dev* **21**, 1472-1477 (2007).

153. Mordes, D. A., Glick, G. G., Zhao, R. & Cortez, D. TopBP1 activates ATR through ATRIP and a PIKK regulatory domain. *Genes Dev* **22**, 1478-1489 (2008).

154. Namiki, Y. & Zou, L. ATRIP associates with replication protein A-coated ssDNA through multiple interactions. *Proc Natl Acad Sci U S A* **103**, 580-585 (2006).

155. Ball, H. L., Myers, J. S. & Cortez, D. ATRIP binding to replication protein A-single-stranded DNA promotes ATR-ATRIP localization but is dispensable for Chk1 phosphorylation. *Mol Biol Cell* **16**, 2372-2381 (2005).

156. Maser, R. S., Monsen, K. J., Nelms, B. E. & Petrini, J. H. hMre11 and hRad50 nuclear foci are induced during the normal cellular response to DNA double-strand breaks. *Mol Cell Biol* **17**, 6087-6096 (1997).

157. Carney, J. P. et al. The hMre11/hRad50 protein complex and Nijmegen breakage syndrome: linkage of double-strand break repair to the cellular DNA damage response. *Cell* **93**, 477-486 (1998).

158. Rogakou, E. P., Pilch, D. R., Orr, A. H., Ivanova, V. S. & Bonner, W. M. DNA double-stranded breaks induce histone H2AX phosphorylation on serine 139. *J Biol Chem* **273**, 5858-5868 (1998).

159. Rogakou, E. P., Boon, C., Redon, C. & Bonner, W. M. Megabase chromatin domains involved in DNA double-strand breaks in vivo. *J Cell Biol* **146**, 905-916 (1999).

160. Schultz, L. B., Chehab, N. H., Malikzay, A. & Halazonetis, T. D. p53 binding protein 1 (53BP1) is an early participant in the cellular response to DNA double-strand breaks. *J Cell Biol* **151**, 1381-1390 (2000).

161. Lou, Z., Minter-Dykhouse, K., Wu, X. & Chen, J. MDC1 is coupled to activated CHK2 in mammalian DNA damage response pathways. *Nature* **421**, 957-961 (2003).

162. Goldberg, M. et al. MDC1 is required for the intra-S-phase DNA damage checkpoint. *Nature* **421**, 952-956 (2003).

163. Stewart, G. S., Wang, B., Bignell, C. R., Taylor, A. M. & Elledge, S. J. MDC1 is a mediator of the mammalian DNA damage checkpoint. *Nature* **421**, 961-966 (2003).

164. Meier, A. et al. Spreading of mammalian DNA-damage response factors studied by ChIP-chip at damaged telomeres. *EMBO J* **26**, 2707-2718 (2007).

165. Wang, B. & Elledge, S. J. Ubc13/Rnf8 ubiquitin ligases control foci formation of the Rap80/Abraxas/Brca1/Brcc36 complex in response to DNA damage. *Proc Natl Acad Sci U S A* **104**, 20759-20763 (2007).

166. Kolas, N. K. et al. Orchestration of the DNA-damage response by the RNF8 ubiquitin ligase. *Science* **318**, 1637-1640 (2007).

167. Huen, M. S. et al. RNF8 transduces the DNA-damage signal via histone ubiquitylation and checkpoint protein assembly. *Cell* **131**, 901-914 (2007).

168. Mailand, N. et al. RNF8 ubiquitylates histones at DNA double-strand breaks and promotes assembly of repair proteins. *Cell* **131**, 887-900 (2007).

169. Stewart, G. S. et al. The RIDDLE syndrome protein mediates a ubiquitin-dependent signaling cascade at sites of DNA damage. *Cell* **136**, 420-434 (2009).

170. Nakada, S. et al. Non-canonical inhibition of DNA damage-dependent ubiquitination by OTUB1. *Nature* **466**, 941-946 (2010).

171. Doil, C. et al. RNF168 binds and amplifies ubiquitin conjugates on damaged chromosomes to allow accumulation of repair proteins. *Cell* **136**, 435-446 (2009).

172. Gu, Y. et al. Growth retardation and leaky SCID phenotype of Ku70-deficient mice. *Immunity* **7**, 653-665 (1997).

173. Zhu, C., Bogue, M. A., Lim, D. S., Hasty, P. & Roth, D. B. Ku86-deficient mice exhibit severe combined immunodeficiency and defective processing of V(D)J recombination intermediates. *Cell* **86**, 379-389 (1996).

174. Moshous, D. et al. Artemis, a novel DNA double-strand break repair/V(D)J recombination protein, is mutated in human severe combined immune deficiency. *Cell* **105**, 177-186 (2001).

175. Gao, Y. et al. A targeted DNA-PKcs-null mutation reveals DNA-PK-independent functions for KU in V(D)J recombination. *Immunity* **9**, 367-376 (1998).

176. Frank, K. M. et al. Late embryonic lethality and impaired V(D)J recombination in mice lacking DNA ligase IV. *Nature* **396**, 173-17. (1998).

177. Gao, Y. et al. A critical role for DNA end-joining proteins in both lymphogenesis and neurogenesis. *Cell* **95**, 891-902 (1998).

178. Baumann, P. & West, S. C. DNA end-joining catalyzed by human cell-free extracts. *Proc Natl Acad Sci U S A* **95**, 14066-14070 (1998).

179. Yan, C. T. et al. IgH class switching and translocations use a robust non-classical end-joining pathway. *Nature* **449**, 478-482 (2007).

180. Corneo, B. et al. Rag mutations reveal robust alternative end joining. *Nature* **449**, 483-486 (2007).

181. Weinstock, D. M. & Jasin, M. Alternative pathways for the repair of RAG-induced DNA breaks. *Mol Cell Biol* **26**, 131-139 (2006).

182. Benson, F. E., Baumann, P. & West, S. C. Synergistic actions of Rad51 and Rad52 in recombination and DNA repair. *Nature* **391**, 401-404 (1998).

183. Davies, A. A. et al. Role of BRCA2 in control of the RAD51 recombination and DNA repair protein. *Mol Cell* **7**, 273-282 (2001).

184. Xia, F. et al. Deficiency of human BRCA2 leads to impaired homologous recombination but maintains normal nonhomologous end joining. *Proc Natl Acad Sci U S A* **98**, 8644-8649 (2001).

185. Moynahan, M. E., Chiu, J. W., Koller, B. H. & Jasin, M. Brca1 controls homology-directed DNA repair. *Mol Cell* **4**, 511-518 (1999).

186. Essers, J. et al. Disruption of mouse RAD54 reduces ionizing radiation resistance and homologous recombination. *Cell* **89**, 195-204 (1997).

187. Hockemeyer, D., Palm, W., Wang, R. C., Couto, S. S. & de Lange, T. Engineered telomere degradation models dyskeratosis congenita. *Genes Dev* **22**, 1773-1785 (2008).

188. Kibe, T., Osawa, G. A., Keegan, C. E. & de Lange, T. Telomere Protection by TPP1 Is Mediated by POT1a and POT1b. *Mol Cell Biol* **30**, 1059-1066 (2010).

189. Takai, K. K., Kibe, T., Donigian, J. R., Frescas, D. & de Lange, T. Telomere protection by TPP1/POT1 requires tethering to TIN2. *Mol Cell* **44**, 647-659 (2011).

190. Denchi, E. L. & de Lange, T. Protection of telomeres through independent control of ATM and ATR by TRF2 and POT1. *Nature* **448**, 1068-1071 (2007).

191. Karlseder, J., Broccoli, D., Dai, Y., Hardy, S. & de Lange, T. p53- and ATM-dependent apoptosis induced by telomeres lacking TRF2. *Science* **283**, 1321-1325 (1999).

192. Takai, H., Smogorzewska, A. & de Lange, T. DNA damage foci at dysfunctional telomeres. *Curr Biol* **13**, 1549-1556 (2003).

193. Celli, G. B. & de Lange, T. DNA processing is not required for ATM-mediated telomere damage response after TRF2 deletion. *Nat Cell Biol* **7**, 712-718 (2005).

194. Dimitrova, N. & de Lange, T. Cell cycle dependent role of MRN at dysfunctional telomeres: ATM signaling-dependent induction of NHEJ in G1 and resection-mediated inhibition of NHEJ in G2. *Mol Cell Biol* **29**, 5552-5563 (2009).

195. Attwooll, C. L., Akpinar, M. & Petrini, J. H. The mre11 complex and the response to dysfunctional telomeres. *Mol Cell Biol* **29**, 5540-5551 (2009).

196. Dimitrova, N. & de Lange, T. MDC1 accelerates nonhomologous end-joining of dysfunctional telomeres. *Genes Dev* **20**, 3238-3243 (2006).

197. Konishi, A. & de Lange, T. Cell cycle control of telomere protection and NHEJ revealed by a ts mutation in the DNA-binding domain of TRF2. *Genes Dev* **22**, 1221-1230 (2008).

198. Celli, G. B., Lazzerini Denchi, E. & de Lange, T. Ku70 stimulates fusion of dysfunctional telomeres yet protects chromosome ends from homologous recombination. *Nat Cell Biol* **8**, 885-890 (2006).

199. Dimitrova, N., Chen, Y. C., Spector, D. L. & de Lange, T. 53BP1 promotes non-homologous end joining of telomeres by increasing chromatin mobility. *Nature* **456**, 524-528 (2008).

200. Ward, I. M. et al. 53BP1 is required for class switch recombination. *J Cell Biol* **165**, 459-464 (2004).

201. Manis, J. P. et al. 53BP1 links DNA damage-response pathways to immunoglobulin heavy chain class-switch recombination. *Nat Immunol* **5**, 481-487 (2004).

202. Reina-San-Martin, B., Chen, J., Nussenzweig, A. & Nussenzweig, M. C. Enhanced intra-switch region recombination during immunoglobulin class switch recombination in 53BP1-/- B cells. *Eur J Immunol* **37**, 235-239 (2007).

203. Difilippantonio, S. et al. 53BP1 facilitates long-range DNA end-joining during V(D)J recombination. *Nature* **456**, 529-533 (2008).

204. Deng, Y., Guo, X., Ferguson, D. O. & Chang, S. Multiple roles for MRE11 at uncapped telomeres. *Nature* **460**, 914-918 (2009).

205. Fouche, N. et al. The basic domain of TRF2 directs binding to DNA junctions irrespective of the presence of TTAGGG repeats. *J Biol Chem* **281**, 37486-37495 (2006).

206. Poulet, A. et al. TRF2 promotes, remodels and protects telomeric Holliday junctions. *EMBO J* **28**, 641-651 (2009).

207. Wang, R. C., Smogorzewska, A. & de Lange, T. Homologous recombination generates T-loop-sized deletions at human telomeres. *Cell* **119**, 355-368 (2004).

208. Cesare, A. J. & Griffith, J. D. Telomeric DNA in ALT cells is characterized by free telomeric circles and heterogeneous t-loops. *Mol Cell Biol* **24**, 9948-9957 (2004).

209. Guo, X. et al. Dysfunctional telomeres activate an ATM-ATR-dependent DNA damage response to suppress tumorigenesis. *EMBO J* **26**, 4709-4719 (2007).

210. Hockemeyer, D., Sfeir, A. J., Shay, J. W., Wright, W. E. & de Lange, T. POT1 protects telomeres from a transient DNA damage response and determines how human chromosomes end. *EMBO J*. **24**, 2667-2678 (2005).

211. Veldman, T., Etheridge, K. T. & Counter, C. M. Loss of hPot1 function leads to telomere instability and a cut-like phenotype. *Curr Biol* **14**, 2264-2270 (2004).

212. Davoli, T., Denchi, E. L. & de Lange, T. Persistent telomere damage induces bypass of mitosis and tetraploidy. *Cell* **141**, 81-93 (2010).

213. Gong, Y. & de Lange, T. A Shld1-controlled POT1a provides support for repression of ATR signaling at telomeres through RPA exclusion. *Mol Cell* **40**, 377-387 (2010).

214. Flynn, R. L. et al. TERRA and hnRNPA1 orchestrate an RPA-to-POT1 switch on telomeric single-stranded DNA. *Nature* (2011).

215. Sfeir, A. et al. Mammalian telomeres resemble fragile sites and require TRF1 for efficient replication. *Cell* **138**, 90-103 (2009).

216. Martinez, P. et al. Increased telomere fragility and fusions resulting from TRF1 deficiency lead to degenerative pathologies and increased cancer in mice. *Genes Dev* **23**, 2060-2075 (2009).

217. Ye, J. et al. TRF2 and Apollo Cooperate with Topoisomerase 2alpha to Protect Human Telomeres from Replicative Damage. *Cell* **142**, 230-242 (2010).

218. Hanada, K. et al. The structure-specific endonuclease Mus81 contributes to replication restart by generating double-strand DNA breaks. *Nat Struct Mol Biol* **14**, 1096-1104 (2007).

219. Petermann, E., Orta, M. L., Issaeva, N., Schultz, N. & Helleday, T. Hydroxyurea-stalled replication forks become progressively inactivated and require two different RAD51-mediated pathways for restart and repair. *Mol Cell* **37**, 492-502 (2010).

220. Hayflick, L. The limited in vitro lifetime of human diploid cell strains. *Exp Cell Res* **37**, 614-636 (1965).

221. Dimri, G. P. et al. A biomarker that identifies senescent human cells in culture and in aging skin in vivo. *Proc Natl Acad Sci USA* **92**, 9363-937. (1995).

222. Bodnar, A. G. et al. Extension of life-span by introduction of telomerase into normal human cells. *Science* **279**, 349-352 (1998).

223. Wright, W. E. & Shay, J. W. The two-stage mechanism controlling cellular senescence and immortalization. *Exp Gerontol* **27**, 383-389 (1992).

224. Shay, J. W., Pereira-Smith, O. M. & Wright, W. E. A role for both RB and p53 in the regulation of human cellular senescence. *Exp Cell Res* **196**, 33-39 (1991).

225. Shay, J. W., Van Der Haegen, B. A., Ying, Y. & Wright, W. E. The frequency of immortalization of human fibroblasts and mammary epithelial cells transfected with SV40 large T-antigen. *Exp Cell Res* **209**, 45-52 (1993).

226. Greenberg, R. A. et al. Short dysfunctional telomeres impair tumorigenesis in the INK4a(delta2/3) cancer-prone mouse. *Cell* **97**, 515-525 (1999).

227. Feldser, D. M. & Greider, C. W. Short telomeres limit tumor progression in vivo by inducing senescence. *Cancer Cell* **11**, 461-469 (2007).

228. Rudolph, K. L. et al. Longevity, stress response, and cancer in aging telomerase-deficient mice. *Cell* **96**, 701-712 (1999).

229. Chin, L. et al. p53 deficiency rescues the adverse effects of telomere loss and cooperates with telomere dysfunction to accelerate carcinogenesis. *Cell* **97**, 527-538 (1999).

230. Artandi, S. E. et al. Telomere dysfunction promotes non-reciprocal translocations and epithelial cancers in mice. *Nature* **406**, 641-65. (2000).

231. Lin, T. T. et al. Telomere dysfunction and fusion during the progression of chronic lymphocytic leukemia: evidence for a telomere crisis. *Blood* **116**, 1899-1907 (2010).

232. Savage, S. A. & Bertuch, A. A. The genetics and clinical manifestations of telomere biology disorders. *Genet Med* **12**, 753-764 (2010).

233. Dokal, I. Dyskeratosis congenita in all its forms. *Br J Haematol* **110**, 768-779 (2000).

234. Marrone, A. et al. Telomerase reverse-transcriptase homozygous mutations in autosomal recessive dyskeratosis congenita and Hoyeraal-Hreidarsson syndrome. *Blood* **110**, 4198-4205 (2007).

235. Armanios, M. et al. Haploinsufficiency of telomerase reverse transcriptase leads to anticipation in autosomal dominant dyskeratosis congenita. *Proc Natl Acad Sci USA* **102**, 15960-15964 (2005).

236. Vulliamy, T. et al. The RNA component of telomerase is mutated in autosomal dominant dyskeratosis congenita. *Nature* **413**, 432-435 (2001).

237. Heiss, N. S. et al. X-linked dyskeratosis congenita is caused by mutations in a highly conserved gene with putative nucleolar functions. *Nat Genet* **19**, 32-8. (1998).

238. Mitchell, J. R., Wood, E. & Collins, K. A telomerase component is defective in the human disease dyskeratosis congenita. *Nature* **402**, 551-55. (1999).

239. Walne, A. J. et al. Genetic heterogeneity in autosomal recessive dyskeratosis congenita with one subtype due to mutations in the telomerase-associated protein NOP10. *Hum Mol Genet* **16**, 1619-1629 (2007).

240. Vulliamy, T. et al. Mutations in the telomerase component NHP2 cause the premature ageing syndrome dyskeratosis congenita. *PNAS* **105**, 8073-8078 (2008).

241. Savage, S. A. et al. TINF2, a component of the shelterin telomere protection complex, is mutated in dyskeratosis congenita. *Am J Hum Genet* **82**, 501-509 (2008).

242. Savage, S. A. et al. Sequence analysis of the shelterin telomere protection complex genes in dyskeratosis congenita. *J Med Genet* **48**, 285-288 (2011).

243. Touzot, F. et al. Function of Apollo (SNM1B) at telomere highlighted by a splice variant identified in a patient with Hoyeraal-Hreidarsson syndrome. *Proc Natl Acad Sci U S A* **107**, 10097-10102 (2010).

244. Armanios, M. Y. et al. Telomerase mutations in families with idiopathic pulmonary fibrosis. *N Engl J Med* **356**, 1317-1326 (2007).

245. Vulliamy, T., Marrone, A., Dokal, I. & Mason, P. J. Association between aplastic anaemia and mutations in telomerase RNA. *Lancet* **359**, 2168-2170 (2002).

246. Yamaguchi, H. et al. Mutations of the human telomerase RNA gene (TERC) in aplastic anemia and myelodysplastic syndrome. *Blood* **102**, 916-918 (2003).

247. Lingner, J. & Cech, T. R. Purification of telomerase from Euplotes aediculatus: requirement of a primer 3' overhang. *Proc Natl Acad Sci USA* **93**, 10712-10717 (1996).

248. Huffman, K. E., Levene, S. D., Tesmer, V. M., Shay, J. W. & Wright, W. E. Telomere shortening is proportional to the size of the G-rich telomeric 3'-overhang. *J Biol Chem* **275**, 19719-19722 (2000).

249. Chai, W., Shay, J. W. & Wright, W. E. Human telomeres maintain their overhang length at senescence. *Mol Cell Biol* **25**, 2158-2168 (2005).

250. Dai, X. et al. Molecular steps of G-overhang generation at human telomeres and its function in chromosome end protection. *EMBO J* **29**, 2788-2801 (2010).

251. Vermeesch, J. R. & Price, C. M. Telomeric DNA sequence and structure following de novo telomere synthesis in Euplotes crassus. *Mol Cell Biol* **14**, 554-566 (1994).

252. Wellinger, R. J., Wolf, A. J. & Zakian, V. A. Saccharomyces telomeres acquire single-strand TG1-3 tails late in S phase. *Cell* **72**, 51-60 (1993).

253. Dionne, I. & Wellinger, R. J. Cell cycle-regulated generation of single-stranded G-rich DNA in the absence of telomerase. *Proc Natl Acad Sci USA* **93**, 13902-13907 (1996).

254. Wellinger, R. J., Ethier, K., Labrecque, P. & Zakian, V. A. Evidence for a new step in telomere maintenance. *Cell* **85**, 423-433 (1996).

255. Dionne, I. & Wellinger, R. J. Processing of telomeric DNA ends requires the passage of a replication fork. *Nucleic Acids Res* **26**, 5365-5371 (1998).

256. Tsukamoto, Y., Taggart, A. K. & Zakian, V. A. The role of the Mre11-Rad50-Xrs2 complex in telomerase- mediated lengthening of Saccharomyces cerevisiae telomeres. *Curr Biol* **11**, 1328-135. (2001).

257. Diede, S. J. & Gottschling, D. E. Exonuclease activity is required for sequence addition and Cdc13p loading at a de novo telomere. *Curr Biol* **11**, 1336-140. (2001).

258. Larrivée, M., LeBel, C. & Wellinger, R. J. The generation of proper constitutive G-tails on yeast telomeres is dependent on the MRX complex. *Genes Dev* **18**, 1391-1396 (2004).

259. Bonetti, D., Martina, M., Clerici, M., Lucchini, G. & Longhese, M. P. Multiple pathways regulate 3' overhang generation at *S. cerevisiae* telomeres. *Mol Cell* **35**, 70-81 (2009).

260. Zhao, Y., Hoshiyama, H., Shay, J. W. & Wright, W. E. Quantitative telomeric overhang determination using a double-strand specific nuclease. *Nucleic Acids Res* **36**, e14 (2008).

261. Sfeir, A. J., Chai, W., Shay, J. W. & Wright, W. E. Telomere-end processing the terminal nucleotides of human chromosomes. *Mol Cell* **18**, 131-138 (2005).

262. Chai, W., Sfeir, A. J., Hoshiyama, H., Shay, J. W. & Wright, W. E. The involvement of the Mre11/Rad50/Nbs1 complex in the generation of G-overhangs at human telomeres. *EMBO Rep* **7**, 225-230 (2006).

263. Calado, R. T., Regal, J. A., Kajigaya, S. & Young, N. S. Erosion of telomeric single-stranded overhang in patients with aplastic anaemia carrying telomerase complex mutations. *Eur J Clin Invest* **39**, 1025-1032 (2009).

264. Lamm, N. et al. Diminished telomeric 3' overhangs are associated with telomere dysfunction in Hoyeraal-Hreidarsson syndrome. *PLoS One* **4**, e5666 (2009).

265. Lee, J. E., Oh, B. K., Choi, J. & Park, Y. N. Telomeric 3' overhangs in chronic HBV-related hepatitis and hepatocellular carcinoma. *Int J Cancer* **123**, 264-272 (2008).

266. Mitton-Fry, R. M., Anderson, E. M., Hughes, T. R., Lundblad, V. & Wuttke, D. S. Conserved structure for single-stranded telomeric DNA recognition. *Science* **296**, 145-147 (2002).

267. Gottschling, D. E. & Zakian, V. A. Telomere proteins: specific recognition and protection of the natural termini of Oxytricha macronuclear DNA. *Cell* **47**, 195-205 (1986).

268. Price, C. M. & Cech, T. R. Properties of the telomeric DNA-binding protein from Oxytricha nova. *Biochemistry* **28**, 769-774 (1989).

269. Price, C. M. Telomere structure in Euplotes crassus: characterization of DNA-protein interactions and isolation of a telomere-binding protein. *Mol Cell Biol* **10**, 3421-3431 (1990).

270. Gray, J. T., Celander, D. W., Price, C. M. & Cech, T. R. Cloning and expression of genes for the Oxytricha telomere-binding protein: specific subunit interactions in the telomeric complex. *Cell* **67**, 807-814 (1991).

271. Lin, J. J. & Zakian, V. A. The Saccharomyces CDC13 protein is a single-strand TG1-3 telomeric DNA- binding protein in vitro that affects telomere behavior in vivo. *Proc Natl Acad Sci USA* **93**, 13760-13765 (1996).

272. Nugent, C. I., Hughes, T. R., Lue, N. F. & Lundblad, V. Cdc13p: a single-strand telomeric DNA-binding protein with a dual role in yeast telomere maintenance. *Science* **274**, 249-252 (1996).

273. Grandin, N., Reed, S. I. & Charbonneau, M. Stn1, a new Saccharomyces cerevisiae protein, is implicated in telomere size regulation in association with Cdc13. *Genes Dev* **11**, 512-27. (1997).

274. Chandra, A., Hughes, T. R., Nugent, C. I. & Lundblad, V. Cdc13 both positively and negatively regulates telomere replication. *Genes Dev* **15**, 404-14. (2001).

275. Grandin, N., Damon, C. & Charbonneau, M. Cdc13 prevents telomere uncapping and Rad50-dependent homologous recombination. *Embo J* **20**, 6127-6139 (2001).

276. Garvik, B., Carson, M. & Hartwell, L. Single-stranded DNA arising at telomeres in cdc13 mutants may constitute a specific signal for the RAD9 checkpoint. *Mol Cell Biol* **15**, 6128-6138 (1995).

277. Pennock, E., Buckley, K. & Lundblad, V. Cdc13 delivers separate complexes to the telomere for end protection and replication. *Cell* **104**, 387-96. (2001).

278. Grossi, S., Puglisi, A., Dmitriev, P. V., Lopes, M. & Shore, D. Pol12, the B subunit of DNA polymerase alpha, functions in both telomere capping and length regulation. *Genes Dev* **18**, 992-1006 (2004).

279. Martin, V., Du, L. L., Rozenzhak, S. & Russell, P. Protection of telomeres by a conserved Stn1-Ten1 complex. *Proc Natl Acad Sci U S A* **104**, 14038-14043 (2007).

280. Gao, H., Cervantes, R. B., Mandell, E. K., Otero, J. H. & Lundblad, V. RPA-like proteins mediate yeast telomere function. *Nat Struct Mol Biol* **14**, 208-214 (2007).

281. Polotnianka, R. M., Li, J. & Lustig, A. J. The yeast Ku heterodimer is essential for protection of the telomere against nucleolytic and recombinational activities. *Curr Biol* **8**, 831-834 (1998).

282. Gravel, S., Larrivee, M., Labrecque, P. & Wellinger, R. J. Yeast Ku as a regulator of chromosomal DNA end structure. *Science* **280**, 741-744 (1998).

283. Baumann, P. & Cech, T. R. Protection of telomeres by the Ku protein in fission yeast. *Mol Biol Cell* **11**, 3265-375. (2000).

284. Bonetti, D. et al. Shelterin-like proteins and Yku inhibit nucleolytic processing of Saccharomyces cerevisiae telomeres. *PLoS Genet* **6**, e1000966 (2010).

285. Vodenicharov, M. D., Laterreur, N. & Wellinger, R. J. Telomere capping in non-dividing yeast cells requires Yku and Rap1. *EMBO J* **ePub ahead of print**, (2010).

286. Anbalagan, S., Bonetti, D., Lucchini, G. & Longhese, M. P. Shelterin-like proteins and Yku inhibit nucleolytic processing of *Saccharomyces cerevisiae* telomeres. *PLoS Genet* **6**, e1000966 (2010).

287. Pitt, C. W. & Cooper, J. P. Pot1 inactivation leads to rampant telomere resection and loss in one cell cycle. *Nucl Acids Res* **38**, 6968-6975 (2010).

288. Miyake, Y. et al. RPA-like mammalian Ctc1-Stn1-Ten1 complex binds to single-stranded DNA and protects telomeres independently of the Pot1 pathway. *Mol Cell* **36**, 193-206 (2009).

289. Surovtseva, Y. V. et al. Conserved telomere maintenance component 1 interacts with STN1 and maintains chromosome ends in higher eukaryotes. *Mol Cell* **36**, 207-218 (2009).

290. Casteel, D. E. et al. A DNA polymerase-{alpha}{middle dot}primase cofactor with homology to replication protein A-32 regulates DNA replication in mammalian cells. *J Biol Chem* **284**, 5807-5818 (2009).

291. Wan, M., Qin, J., Songyang, Z. & Liu, D. OB fold-containing protein 1 (OBFC1), a human homolog of yeast Stn1, associates with TPP1 and is implicated in telomere length regulation. *J Biol Chem* **284**, 26725-26731 (2009).

292. Lingner, J. personal communication.

293. Sfeir, A. & de Lange, T. (unpublished).

294. Tom, H. I. & Greider, C. W. A sequence-dependent exonuclease activity from *Tetrahymena thermophila*. *BMC Biochem* **11**, 45 (2010).

295. Freibaum, B. D. & Counter, C. M. The protein hSnm1B is stabilized when bound to the telomere-binding protein TRF2. *J Biol Chem* **283**, 23671-23676 (2008).

296. Opresko, P. L. et al. Telomere binding protein TRF2 binds to and stimulates the Werner and Bloom syndrome helicases. *J Biol Chem* **277**, 41110-41119 (2002).

297. Machwe, A., Xiao, L. & Orren, D. K. TRF2 recruits the Werner syndrome (WRN) exonuclease for processing of telomeric DNA. *Oncogene* **23**, 149-156 (2004).

298. Karlseder, J. et al. The telomeric protein TRF2 binds the ATM kinase and can inhibit the ATM-dependent DNA damage response. *PLoS Biol* **2**, E240 (2004).

299. Svendsen, J. M. et al. Mammalian BTBD12/SLX4 assembles a Holliday junction resolvase and is required for DNA repair. *Cell* **138**, 63-77 (2009).

300. Verdun, R. E. & Karlseder, J. The DNA damage machinery and homologous recombination pathway act consecutively to protect human telomeres. *Cell* **127**, 709-720 (2006).

301. Verdun, R. E., Crabbe, L., Haggblom, C. & Karlseder, J. Functional human telomeres are recognized as DNA damage in G2 of the cell cycle. *Mol Cell* **20**, 551-561 (2005).

302. Chan, S. H., Stoddard, B. L. & Xu, S. Y. Natural and engineered nicking endonucleases--from cleavage mechanism to engineering of strand-specificity. *Nucl Acids Res* **39**, 1-18 (2011).

303. Strathern, J. N. et al. Homothallic switching of yeast mating type cassettes is initiated by a double-stranded cut in the MAT locus. *Cell* **1982**, 183-192 (1982).

304. Nickoloff, J. A., Chen, E. Y. & Heffron, F. A 24-base-pair DNA sequence from the MAT locus stimulates intergenic recombination in yeast. *PNAS* **83**, 7831-7835 (1986).

305. Nickoloff, J. A., Singer, J. D. & Heffron, F. *In vivo* analysis of the *Saccharomyces cerevisiae* HO nuclease recognition site by site-directed mutagenesis. *Mol Cell Biol* **10**, 1174-1179 (1990).

306. Plessis, A., Perrin, A., Haber, J. E. & Dujon, B. Site-specific recombination determined by I-SceI, a mitochondrial group I intron-encoded endonuclease expressed in the yeast nucleus. *Genetics* **130**, 451-460 (1992).

307. Colleaux, L. et al. Universal code equivalent of a yeast mitochondrial intron reading frame is expressed into *E. coli* as a specific double strand endonuclease. *Cell* **44**, 521-533 (1986).

308. Tomlinson, C. G., Atack, J. M., Chapados, B., Tainer, J. A. & Grasby, J. A. Substrate recognition and catalysis by flap endonucleases and related enzymes. *Biochem Soc Trans* **38**, 433-437 (2010).

309. Hosfield, D. J., Mol, C. D., Shen, B. & Tainer, J. A. Structure of the DNA repair and replication endonuclease and exonuclease FEN-1: coupling DNA and PCNA binding to FEN-1 activity. *Cell* **95**, 135-146 (1998).

310. Harrington, J. J. & Lieber, M. R. The characterization of a mammalian DNA structure-specific endonuclease. *EMBO J* **13**, 1235-1246 (1994).

311. Lee, B. I. & Wilson, D. M. r. The RAD2 domain of human exonuclease 1 exhibits 5' to 3' exonuclease and flap structure-specific endonuclease activities. *J Biol Chem* **274**, 37763-37769 (1999).

312. O'Donovan, A., Davies, A. A., Moggs, J. G., West, S. C. & Wood, R. D. XPG endonuclease makes the 3' incision in human DNA nucleotide excision repair. *Nature* **371**, 432-435 (1994).

313. Ip, S. C. et al. Identification of Holliday junction resolvases from humans and yeast. *Nature* **456**, 357-361 (2008).

314. Habraken, Y., Sung, P., Prakash, L. & Prakash, S. A conserved 5' to 3' exonuclease activity in the yeast and human nucleotide excision repair proteins RAD2 and XPG. *J Biol Chem* **269**, 31342-33145 (1994).

315. Hwang, K. Y., Baek, K., Kim, H. Y. & Cho, Y. The crystal structure of flap endonuclease-1 from *Methanococcus jannaschii*. *Nat Struct Biol* **5**, 707-713 (1998).

316. Tsutakawa, S. E. et al. Human flap endonuclease structures, DNA double-base flipping, and a unified understanding of the FEN1 superfamily. *Cell* **145**, 198-211 (2011).

317. Orans, J. et al. Structures of human exonuclease 1 DNA complexes suggest a unified mechanism for nuclease family. *Cell* **145**, 212-223 (2011).

318. Brookman, K. W. et al. ERCC4 (XPF) encodes a human nucleotide excision repair protein with eukaryotic recombination homologs. *Mol Cell Biol* **16**, 6553-6562 (1996).

319. Boddy, M. N. et al. Damage tolerance protein Mus81 associates with the FHA1 domain of checkpoint kinase Cds1. *Mol Cell Biol* **20**, 8758-8766 (2000).

320. Interthal, H. & Heyer, W. D. MUS81 encodes a novel helix-hairpin-helix protein involved in the response to UV- and methylation-induced DNA damage in *Saccharomyces cerevisiae*. *Mol Gen Genet* **263**, 812-827 (2000).

321. de Laat, W. L., Sijbers, A. M., Odijk, H., Jaspers, N. G. & Hoeijmakers, J. H. Mapping of interaction domains between human repair proteins ERCC1 and XPF. *Nucleic Acids Res* **26**, 4146-4152 (1998).

322. Boddy, M. N. et al. Mus81-Eme1 are essential components of a Holliday junction resolvase. *Cell* **107**, 537-548 (2001).

323. Kaliraman, V., Mullen, J. R., Fricke, W. M., Bastin-Shanower, S. A. & Brill, S. J. Functional overlap between Sgs1-Top3 and the Mms4-Mus81 endonuclease. *Genes Dev* **15**, 2730-2740 (2001).

324. de Laat, W. L., Appeldoorn, E., Jaspers, N. G. & Hoeijmakers, J. H. DNA structural elements required for ERCC1-XPF endonuclease activity. *J Biol Chem* **273**, 7835-7842 (1998).

325. Park, C. H., Bessho, T., Matsunaga, T. & Sancar, A. Purification and characterization of the XPF-ERCC1 complex of human DNA repair excision nuclease. *J Biol Chem* **270**, 22657-22660 (1995).

326. Matsunaga, T., Park, C. H., Bessho, T., Mu, D. & Sancar, A. Replication protein A confers structure-specific endonuclease activities to the XPF-ERCC1 and XPG subunits of human DNA repair excision nuclease. *J Biol Chem* **271**, 11047-11050 (1996).

327. de Laat, W. L. et al. DNA-binding polarity of human replication protein A positions nucleases in nucleotide excision repair. *Genes Dev* **12**, 2598-2609 (1998).

328. Chen, X. B. et al. Human Mus81-associated endonuclease cleaves Holliday junctions *in vitro*. *Mol Cell* **8**, 1117-1127 (2001).

329. Fricke, W. M. & Brill, S. J. Slx1-Slx4 is a second structure-specific endonuclease functionally redundant with Sgs1-Top3. *Genes Dev* **17**, 1768-1778 (2003).

330. Coulon, S. et al. Slx1-Slx4 are subunits of a structure-specific endonuclease that maintains ribosomal DNA in fission yeast. *Mol Biol Cell* **15**, 71-80 (2004).

331. Fekairi, S. et al. Human SLX4 is a Holliday junction resolvase subunit that binds multiple DNA repair/recombination endonucleases. *Cell* **138**, 78-89 (2009).

332. Munoz, I. M. et al. Coordination of structure-specific nucleases by human SLX4/BTBD12 is required for DNA repair. *Mol Cell* **35**, 116-127 (2009).

333. Callebaut, I., Moshous, D., Mornon, J. P. & de Villartay, J. P. Metallo-beta-lactamase fold within nucleic acids processing enzymes: the beta-CASP family. *Nucleic Acids Res* **30**, 3592-3601 (2002).

334. Carfi, A. et al. The 3-D structure of a zinc metallo-beta-lactamase from *Bacillus cereus* reveals a new type of protein fold. *EMBO J* **14**, 4914-4921 (1995).

335. Ishikawa, H., Nakagawa, N., Kuramitsu, S. & Masui, R. Crystal structure of TTHA0252 from *Thermus thermophilus* HB8, a RNA degradation protein of the metallo-beta-lactamase superfamily. *J Biochem* **140**, 535-542 (2006).

336. Mandel, C. R. et al. Polyadenylation factor CPSF-73 is the pre-mRNA 3'-end-processing endonuclease. *Nature* **444**, 953-956 (2006).

337. Ma, Y., Pannicke, U., Schwarz, K. & Lieber, M. R. Hairpin opening and overhang processing by an Artemis/DNA-dependent protein kinase complex in nonhomologous end joining and V(D)J recombination. *Cell* **108**, 781-794 (2002).

338. Sekiguchi, J. personal communication.

339. Balakrishnan, L. & Bambara, R. A. Eukaryotic lagging strand DNA replication employs a multi-pathway mechanism that protects genome integrity. *J Biol Chem* **286**, 6865-6870 (2011).

340. Kozu, T., Yagura, T. & Seno, T. De novo DNA synthesis by a novel mouse DNA polymerase associated with primase activity.

341. Gronostajski, R. M., Field, J. & Hurwitz, J. Purification of a primase activity associated with DNA polymerase alpha from HeLa cells. *J Biol Chem* **259**, 9479-9486 (1984).

342. Matsumoto, T., Eki, T. & Hurwitz, J. Studies on the initiation and elongation reactions in the simian virus 40 DNA replication system. *PNAS* **87**, 9712-9716 (1990).

343. Goulian, M. & Heard, C. J. Intact DNA polymerase alpha/primase from mouse cells. Purification and structure. *J Biol Chem* **264**, 19407-19415 (1989).

344. Waga, S. & Stillman, B. Anatomy of a DNA replication fork revealed by reconstitution of SV40 DNA replication *in vitro*. *Nature* **369**, 207-212 (1994).

345. Nick McElhinny, S. A., Gordenin, D. A., Stith, C. M., Burgers, P. M. & Kunkel, T. A. Division of labor at the eukaryotic replication fork. *Mol Cell* **30**, 137-144 (2008).

346. Pursell, Z. F., Isoz, I., Lundstrom, E. B., Johansson, E. & Kunkel, T. A. Yeast DNA polymerase epsilon participates in leading-strand DNA replication. *Science* **317**, 127-130 (2007).

347. Lindahl, T., Gally, J. A. & Edelman, G. M. Deoxyribonuclease IV: a new exonuclease from mammalian tissues. *PNAS* **62**, 597-603 (1969).

348. Goulian, M., Richards, S. H., Heard, C. J. & Bigsby, B. M. Discontinuous DNA synthesis by purified mammalian proteins. *J Biol Chem* **265**, 18461-18471 (1990).

349. Ishimi, Y., Claude, A., Bullock, P. & Hurwitz, J. Complete enzymatic synthesis of DNA containing the SV40 origin of replication. *J Biol Chem* **263**, 19723-19733 (1988).

350. Kenny, M. K., Balogh, L. A. & Hurwitz, J. Initiation of adenovirus DNA replication. I. Mechanism of action of a host protein required for replication of adenovirus DNA templates devoid of the terminal protein. *J Biol Chem* **263**, 9801-9808 (1988).

351. Murante, R. S., Henricksen, L. A. & Bambara, R. A. Junction ribonuclease: an activity in Okazaki fragment processing. *PNAS* **95**, 2244-2249 (1998).

352. Qiu, J., Qian, Y., Frank, P., Wintersberger, U. & Shen, B. *Saccharomyces cerevisiae* RNase H(35) functions in RNA primer removal during lagging-strand DNA synthesis, most efficiently in cooperation with Rad27 nuclease. *Mol Cell Biol* **19**, 8361-8371 (1999).

353. Budd, M. E. & Campbell, J. L. A yeast gene required for DNA replication encodes a protein with homology to DNA helicases. *PNAS* **92**, 7642-7646 (1995).

354. Budd, M. E. & Campbell, J. L. A yeast replicative helicase, Dna2 helicase, interacts with yeast FEN-1 nuclease in carrying out its essential function. *Mol Cell Biol* **17**, 2136-2142 (1997).

355. Rossi, M. L. & Bambara, R. A. Reconstituted Okazaki.

356. Stewart, J. A., Miller, A. S., Campbell, J. L. & Bambara, R. A. Dynamic removal of replication protein A by Dna2 facilitates primer cleavage during Okazaki fragment processing in *Saccharomyces cerevisiae*. *J Biol Chem* **283**, 31356-31365 (2008).

357. Barnes, D. E. & Lindahl, T. Repair and genetic consequences of endogenous DNA base damage in mammalian cells. *Annu Rev Genet* **38**, 445-476 (2004).

358. Kane, C. M. & Linn, S. Purification and characterization of an apurinic/apyrimidinic endonuclease from HeLa cells. *J Biol Chem* **256**, 3405-3414 (1981).

359. Mosbaugh, D. W. & Linn, S. Further characterization of human fibroblast apurinic/apyrimidinic DNA endonucleases. The definition of two mechanistic classes of enzyme. *J Biol Chem* **255**, 11743-11752 (1980).

360. Petermann, E., Keil, C. & Oei, S. L. Roles of DNA ligase III and XRCC1 in regulating the switch between short patch and long patch BER. *DNA Repair (Amst)* **5**, 544-555 (2006).

361. Pascucci, B., Stucki, M., Jonsson, Z. O., dogliotti, E. & Hubscher, U. Long patch base excision repair with purified human proteins. DNA ligase I as patch size mediator for DNA polymerases delta and epsilon. *J Biol Chem* **274**, 33696-33702 (1999).

362. Prigent, C., Satoh, M. S., Daly, G., Barnes, D. E. & Lindahl, T. Aberrant DNA repair and DNA replication due to an inherited enzymatic defect in human DNA ligase I. *Mol Cell Biol* **14**, 310-317 (1994).

363. Aboussekhra, A. et al. Mammalian DNA nucleotide excision repair reconstituted with purified protein components. *Cell* **80**, 859-868 (1995).

364. Venema, J. et al. Xeroderma pigmentosum complementation group C cells remove pyrimidine dimers selectively from the transcribed strand of active genes. *Mol Cell Biol* **11**, 4128-4134 (1991).

365. Mellon, I., Spivak, G. & Hanawalt, P. C. Selective removal of transcription-blocking DNA damage from the transcribed strand of the mammalian DHFR gene. *Cell* **51**, 241-249 (1987).

366. Sugasawa, K. et al. Xeroderma pigmentosum group C protein complex is the initiator of global genome nucleotide excision repair. *Mol Cell* **2**, 223-232 (1998).

367. Matsunaga, T., Mu, D., Park, C. H., Reardon, J. T. & Sancar, A. Human DNA repair excision nuclease. Analysis of the roles of the subunits involved in dual incisions by using anti-XPG and anti-ERCC1 antibodies. *J Biol Chem* **270**, 20862-20869 (1995).

368. Constantin, N., Dzantiev, L., Kadyrov, F. A. & Modrich, P. Human mismatch repair: reconstitution of a nick-directed bidirectional reaction. *J Biol Chem* **280**, 39752-39761 (2005).

369. Modrich, P. Mechanisms in eukaryotic mismatch repair. *J Biol Chem* **281**, 30305-30309 (2006).

370. Genschel, J., Bazemore, L. R. & Modrich, P. Human exonuclease I is required for 5' and 3' mismatch repair. *J Biol Chem* **277**, 13302-13311 (2002).

371. Kadyrov, F. A., Dzantiev, L., Constantin, N. & Modrich, P. Endonucleolytic function of MutLalpha in human mismatch repair. *Cell* **126**, 297-308 (2006).

372. de Wind, N., Dekker, M., Berns, A., Radman, M. & te Riele, H. Inactivation of the mouse Msh2 gene results in mismatch repair deficiency, methylation tolerance, hyperrecombination, and predisposition to cancer. *Cell* **82**, 321-330 (1995).

373. Reitmair, A. H. et al. MSH2 deficient mice are viable and susceptible to lymphoid tumours. *Nat Genet* **11**, 64-70 (1995).

374. Wei, K. et al. Inactivation of Exonuclease 1 in mice results in DNA mismatch repair defects, increased cancer susceptibility, and male and female sterility. *Genes Dev* **17**, 603-614 (2003).

375. Rooney, S. et al. Leaky Scid phenotype associated with defective V(D)J coding end processing in Artemis-deficient mice. *Mol Cell* **10**, 1379-1390 (2002).

376. Rooney, S. et al. Defective DNA repair and increased genomic instability in Artemis-deficient murine cells. *J Exp Med* **197**, 553-565 (2003).

377. Ma, Y. et al. The DNA-dependent protein kinase catalytic subunit phosphorylation sites in human Artemis. *J Biol Chem* **280**, 33839-33846 (2005).

378. Mimitou, E. P. & Symington, L. S. Sae2, Exo1 and Sgs1 collaborate in DNA double-strand break processing. *Nature* **455**, 770-774 (2008).

379. Zhu, Z., Chung, W. H., Shim, E. Y., Lee, S. E. & Ira, G. Sgs1 helicase and two nucleases Dna2 and Exo1 resect DNA double-strand break ends. *Cell* **134**, 981-994 (2008).

380. Gravel, S., Chapman, J. R., Magill, C. & Jackson, S. P. DNA helicases Sgs1 and BLM promote DNA double-strand break resection. *Genes Dev* **22**, 2767-2772 (2008).

381. Cejka, P. et al. DNA end resection by Dna2-Sgs1-RPA and its stimulation by Top3-Rmi1 and Mre11-Rad50-Xrs2. *Nature* **467**, 112-116 (2010).

382. Niu, H. et al. Mechanism of the ATP-dependent DNA end-resection machinery from *Saccharomyces cerevisiae*. *Nature* **467**, 108-111 (2010).

383. Huertas, P. & Jackson, S. P. Human CtIP mediates cell cycle control of DNA end resection and double strand break repair. *J Biol Chem* **284**, 9558-9565 (2009).

384. Kaidi, A., Weinert, B. T., Choudhary, C. & Jackson, S. P. Human SIRT6 promotes DNA end resection through CtIP deacetylation. *Science* **329**, 1348-1353 (2010).

385. Svendsen, J. M. & Harper, J. W. GEN1/Yen1 and the SLX4 complex: Solutions to the problem of Holliday junction resolution. *Genes Dev* **24**, 521-536 (2010).

386. Wechsler, T., Newman, S. & West, S. C. Aberrant chromosome morphology in human cells defective for Holliday junction resolution. *Nature* **471**, 642-646 (2011).

387. Raschle, M. et al. Mechanism of replication-coupled DNA interstrand crosslink repair. *Cell* **134**, 969-980 (2008).

388. Kratz, K. et al. Deficiency of FANCD2-associated nuclease KIAA1018/FAN1 sensitizes cells to interstrand crosslinking agents.

389. MacKay, C. et al. Identification of KIAA1018/FAN1, a DNA repair nuclease recruited to DNA damage by monoubiquitinated FANCD2. *Cell* **142**, 65-76 (2010).

390. Smogorzewska, A. et al. A genetic screen identifies FAN1, a Fanconi anemia-associated nuclease necessary for DNA interstrand crosslink repair. *Mol Cell* **39**, 36-47 (2010).

391. Liu, T., Ghosal, G., Yuan, J., Chen, J. & Huang, J. FAN1 acts with FANCI-FANCD2 to promote DNA interstrand cross-link repair. *Science* **329**, 693-696 (2010).

392. Sampathi, S., Bhusari, A., Shen, B. & Chai, W. Human flap endonuclease I is in complex with telomerase and is required for telomerase-mediated telomere maintenance. *J Biol Chem* **284**, 3682-3690 (2009).

393. Rooney, S. & de Lange, T. (unpublished).

394. Schaetzlein, S. et al. Exonuclease-1 deletion impairs DNA damage signaling and prolongs lifespan of telomere-dysfunctional mice. *Cell* **130**, 863-877 (2007).

395. Wu, P. & de Lange, T. No overt nucleosome eviction at deprotected telomeres. *Mol Cell Biol* **28**, 5724-5735 (2008).

396. Wu, P., van Overbeek, M., Rooney, S. & de Lange, T. Apollo Contributes to G Overhang Maintenance and Protects Leading-End Telomeres. *Mol Cell* **39**, 1-12 (2010).

397. Bakkenist, C. J. & Kastan, M. B. DNA damage activates ATM through intermolecular autophosphorylation and dimer dissociation. *Nature* **421**, 499-506 (2003).

398. Kruhlak, M. J. et al. Changes in chromatin structure and mobility in living cells at sites of DNA double-strand breaks. *J Cell Biol* **172**, 823-834 (2006).

399. van Attikum, H., Fritsch, O., Hohn, B. & Gasser, S. M. Recruitment of the INO80 complex by H2A phosphorylation links ATP-dependent chromatin remodeling with DNA double-strand break repair. *Cell* **119**, 777-788 (2004).

400. Tsukuda, T., Fleming, A. B., Nickoloff, J. A. & Osley, M. A. Chromatin remodelling at a DNA double-strand break site in Saccharomyces cerevisiae. *Nature* **438**, 379-383 (2005).

401. Berkovich, E., Monnat, R. J. J. & Kastan, M. B. Roles of ATM and NBS1 in chromatin structure modulation and DNA double-strand break repair. *Nat Cell Biol* **9**, 683-690 (2007).

402. Chai, B., Huang, J., Cairns, B. R. & Laurent, B. C. Distinct roles for the RSC and Swi/Snf ATP-dependent chromatin remodelers in DNA double-strand break repair. *Genes Dev* **19**, 1656-1661 (2005).

403. Morrison, A. J. et al. INO80 and gamma-H2AX interaction links ATP-dependent chromatin remodeling to DNA damage repair. *Cell* **119**, 767-775 (2004).

404. Shim, E. Y. et al. RSC mobilizes nucleosomes to improve accessibility of repair machinery to the damaged chromatin. *Mol Cell Biol* **27**, 1602-1613 (2007).

405. Shim, E. Y., Ma, J. L., Oum, J. H., Yanez, Y. & Lee, S. E. The yeast chromatin remodeler RSC complex facilitates end joining repair of DNA double-strand breaks. *Mol Cell Biol* **25**, 3934-3944 (2005).

406. van Attikum, H., Fritsch, O. & Gasser, S. M. Distinct roles for SWR1 and INO80 chromatin remodeling complexes at chromosomal double-strand breaks. *EMBO J* **26**, 4113-4125 (2007).

407. Noll, M. Subunit structure of chromatin. *Nature* **251**, 249-251 (1974).

408. Wright, W. E., Tesmer, V. M., Huffman, K. E., Levene, S. D. & Shay, J. W. Normal human chromosomes have long G-rich telomeric overhangs at one end. *Genes Dev* **11**, 2801-2809 (1997).

409. Kacian, D. L. & Spiegelman, S. Use of micrococcal nuclease to monitor hybridization reactions with DNA. *Analytical Biochem* **58**, 534-540 (1974).

410. Hanish, J. P., Yanowitz, J. L. & de Lange, T. Stringent sequence requirements for the formation of human telomeres. *Proc Natl Acad Sci USA* **91**, 8861-8865 (1994).

411. Galati, A. et al. The human telomeric protein TRF1 specifically recognizes nucleosomal binding sites and alters nucleosome structure. *J Mol Biol* **360**, 377-385 (2006).

412. Pisano, S. et al. Telomeric nucleosomes are intrinsically mobile. *J Mol Biol* **369**, 1153-1162 (2007).

413. Demuth, I., Digweed, M. & Concannon, P. Human SNM1B is required for normal cellular response to both DNA interstrand crosslink-inducing agents and ionizing radiation. *Oncogene* **23**, 8611-8618 (2004).

414. Dronkert, M. L. et al. Disruption of mouse SNM1 causes increased sensitivity to the DNA interstrand cross-linking agent mitomycin C. *Mol Cell Biol* **20**, 4553-4561 (2000).

415. Dronkert, M. L. & Kanaar, R. Repair of DNA interstrand cross-links. *Mutat Res* **486**, 217-247 (2001).

416. Bae, J. B. et al. Snm1B/Apollo mediates replication fork collapse and S Phase checkpoint activation in response to DNA interstrand cross-links. *Oncogene* **27**, 5045-5056 (2008).

417. Kurosawa, A. et al. The requirement of Artemis in double-strand break repair depends on the type of DNA damage. *DNA Cell Biol* **27**, 55-61 (2008).

418. Beucher, A. et al. ATM and Artemis promote homologous recombination of radiation-induced DNA double-strand breaks in G2. *EMBO J* **28**, 3413-3427 (2009).

419. Pannicke, U. et al. Functional and biochemical dissection of the structure-specific nuclease ARTEMIS. *EMBO J* **23**, 1987-1997 (2004).

420. de Villartay, J. P. et al. A histidine in the beta-CASP domain of Artemis is critical for its full in vitro and in vivo functions. *DNA Repair (Amst)* **8**, 202-208 (2009).

421. Sakaue-Sawano, A. et al. Visualizing spatiotemporal dynamics of multicellular cell-cycle progression. *Cell* **132**, 487-498 (2008).

422. Bailey, S. M., Cornforth, M. N., Kurimasa, A., Chen, D. J. & Goodwin, E. H. Strand-specific Postreplicative Processing of Mammalian Telomeres. *Science* **293**, 2462-2465 (2001).

423. Lam, Y. C. et al. SNMIB/Apollo protects leading-strand telomeres against NHEJ-mediated repair. *EMBO J* **29**, 2230-2241 (2010).

424. Manis, J. P. et al. Ku70 is required for late B cell development and immunoglobulin heavy chain class switching. *J Exp Med* **187**, 2081-2089 (1998).

425. Boboila, C. et al. Alternative end-joining catalyzes class switch recombination in the absence of both Ku70 and DNA ligase 4. *J Exp Med* **207**, 417-427 (2010).

426. Boboila, C. et al. Alternative end-joining catalyzes robust IgH locus deletions and translocations in the combined absence of ligase 4 and Ku70. *Proc Natl Acad Sci U S A* **107**, 3034-3039 (2010).

427. Simsek, D. & Jasin, M. Alternative end-joining is suppressed by the canonical NHEJ component Xrcc4-ligase IV during chromosomal translocation formation. *Nat Struct Mol Biol* **17**, 410-416 (2010).

428. Kim, H. et al. TRF2 functions as a protein hub and regulates telomere maintenance by recognizing specific peptide motifs. *Nat Struct Mol Biol* **16**, 372-379 (2009).

429. Lo, A. W. et al. Chromosome Instability as a Result of Double-Strand Breaks near Telomeres in Mouse Embryonic Stem Cells. *Mol Cell Biol* **22**, 4836-4850 (2002).

430. Vodenicharov, M. D. & Wellinger, R. J. DNA degradation at unprotected telomeres in yeast is regulated by the CDK1 (Cdc28/Clb) cell-cycle kinase. *Mol Cell* **24**, 127-137 (2006).

431. Takai, H. personal communication.

432. Mimitou, E. P. & Symington, L. S. Ku prevents Exo1 and Sgs1-dependent resection of DNA ends in the absence of a functional MRX complex or Sae2. *EMBO J* **29**, 3358-3369 (2010).

433. Faure, V., Coulon, S., Hardy, J. & Geli, V. Cdc13 and telomerase bind through different mechanisms at the lagging- and leading-strand telomeres. *Mol Cell* **38**, 842-852 (2010).

434. Bailey, S. M. et al. The kinase activity of DNA-PK is required to protect mammalian telomeres. *DNA Repair (Amst)* **3**, 225-233 (2004).

435. He, H. et al. POT1b protects telomeres from end-to-end chromosomal fusions and aberrant homologous recombination. *Embo J* **25**, 5180-5190 (2006).

436. Akhter, S., Lam, Y. C., Chang, S. & Legerski, R. J. The telomeric protein SNM1B/Apollo is required for normal cell proliferation and embryonic development. *Aging Cell* **9**, 1047-1056 (2010).

437. He, H. et al. Pot1b deletion and telomerase haploinsufficiency in mice initiate an ATR-dependent DNA damage response and elicit phenotypes resembling dyskeratosis congenita. *Mol Cell Biol* **29**, 229-240 (2009).

438. Mason, P. J., Wilson, D. B. & Bessler, M. Dyskeratosis congenita -- a disease of dysfunctional telomere maintenance. *Curr Mol Med* **5**, 159-170 (2005).

439. Walne, A. J., Vulliamy, T., Beswick, R., Kirwan, M. & Dokal, I. TINF2 mutations result in very short telomeres: analysis of a large cohort of patients with dyskeratosis congenita and related bone marrow failure syndromes. *Blood* **112**, 3594-3600 (2008).

440. http://clinicaltrials.gov/ct2/results?term=imetelstat. Accessed: June 23, 2010.